



Rossi, Giovanni E. (2018) *Phosgene formation over an activated carbon catalyst*. PhD thesis.

<https://theses.gla.ac.uk/16187/>

Copyright and moral rights for this work are retained by the author

A copy can be downloaded for personal non-commercial research or study, without prior permission or charge

This work cannot be reproduced or quoted extensively from without first obtaining permission from the author

The content must not be changed in any way or sold commercially in any format or medium without the formal permission of the author

When referring to this work, full bibliographic details including the author, title, awarding institution and date of the thesis must be given

Enlighten: Theses

<https://theses.gla.ac.uk/>
research-enlighten@glasgow.ac.uk

Phosgene formation over an activated carbon catalyst

Giovanni E

Rossi

XXXXXXXX

For the degree of Doctor of Philosophy

Department of Chemistry



September 2017

Declaration

The work contained in this thesis, submitted for the degree Doctor of Philosophy is my own original work, except where due reference is made to other individuals and has not been previously submitted for a degree at this or any other university.

Giovanni E. Rossi

Acknowledgments

I would first of all like to thank my supervisor Prof David Lennon for all his help and guidance throughout my time at the University of Glasgow. I would also like to thank Professor John Winfield for sharing his immense knowledge and for all the help provided throughout this project. I would also like to thank Dr Cristopher Mitchell for his help and guidance in the early stages of the project. Dr Rob Carr, Dr Don Jones and Dr Nathalie Meyer from Huntsman Polyurethanes are thanked for the insightful discussions and guidance throughout the project.

I would also like to thank Ross Slavin and Cedric Boulho for their technical support throughout the project. I am very grateful to everyone I have worked with in the Lennon group. Especially Clement Morisse, and Robbie Warringham who in the early days helped me to get started; thank you for the great times in and out of the laboratory. I would also like to thank Alisha Davidson a final year project student who assisted in the first year of my PhD.

Furthermore, I would also like to thank the technical team at the University of Glasgow without your support none of the work would have been possible. In particular James Gallagher for helping with the SEM and EDX analysis. I would also like to thank Andrew Monaghan for helping with the Raman spectroscopy. I would also like to thank Dr Claire Wilson for help with the XRD and John Lidell (glass blowing) and Paul Agnew (engineering workshops).

I would also like to give a special thanks to my parents and family; for their patience and support throughout the years. Thanks to Mhairi Clydesdale for being by my side every step of the way through the last year.

The work in this thesis was undertaken in the Chemistry Process Fundamentals Laboratory. This facility was commissioned with assistance from the following parties: School of Chemistry, College of Science and Engineering, the University of Glasgow Knowledge Transfer Account, Huntsman Polyurethanes. Huntsman Polyurethanes are thanked for the provision of project support and technical guidance.

Abstract

The production of phosgene typically involves the gas phase reaction between carbon monoxide (CO) and dichlorine (Cl₂) in the presence of an activated carbon catalyst. The first stage of the study investigated the kinetics of phosgene formation over a high surface area carbon catalyst. This included determining a rate law and an activation energy for the reaction. A reaction mechanism is proposed based on the experimental observations. The second stage of the study investigated the influence of a small quantity of bromine in the reaction feed-stream. This involved modifying the apparatus and examining the possibility of a role for bromine in the phosgene formation process

Contents

Abstract	3
----------------	---

Chapter 1 Introduction

1.0 Introduction.....	15
1.1.1..... Activated Carbon	16
1.1.2 Adsorption on Activated Carbons.....	16
1.1.3 Applications of Phosgene	21
1.1.4 Polyurethanes	22
1.1.5 Chloroformates	23
1.1.6. Polycarbonates	24
1.2. Phosgene Synthesis.....	25
1.2.1 Photo-chemical Synthesis	25
1.2.2 Thermal Synthesis.....	27
1.2.3 Thermodynamics of phosgene	29
1.2.4. Catalytic (Industrial) Synthesis.....	31
1.2.5. Oxy-chlorination	37
1.2.6 Eckert cartridge.....	38
1.2.7 Alternative routes to phosgene.....	40
1.2.8 Interhalogen species.....	40
1.2.9 Mechanisms of Adsorption	41
1.3 Analytical techniques.....	42
1.3.1. Infrared Spectroscopy	42
1.3.2. Ultraviolet and Visible Absorption Spectroscopy	42
1.3.3 Electronic Transitions	43
1.4. Characterising Catalysts.....	44
1.4.1 X-Ray Diffraction	44
1.4.2 BET	45

1.4.4. Scanning Electron Microscopy	46
1.4.5 Energy Dispersive X-ray spectroscopy.....	46
1.4.6 Raman Spectroscopy.....	48
1.5.0 Aims and Relevance	49

Chapter 2 Experimental

2.0 Introduction.....	51
2.1 Conventional phosgene synthesis test apparatus	51
2.1.2 Safety	54
2.1.3 Gas Cells	56
2.2 Spectroscopy	57
2.2.1 Carbon monoxide (Infrared)	57
2.2.2 Chlorine (UV visible)	58
2.2.3 Phosgene	59
2.2.4 Calibrations.....	62
2.1.6 Space velocity	66
2.1.7 Catalyst preparation	67
2.2 Bromine Co-feed Apparatus	67
2.2.2 Quantification of bromine (Beer Lambert validation)	72
2.2.3 Mass spectrometric determination of Br ₂	74
2.2.4 Baseline bromine content in the chlorine.....	75
2.3 Summary	76

Chapter 3 Characterisation of the Donau Supersorbon K40

3.1 Introduction.....	78
3.2 Scanning Electron Microscopy (SEM)	79
3.3 XRD	81
3.4 BET	82

3.5 Raman Spectroscopy.....	83
3.6 Summary	86

Chapter 4 Kinetic Measurements

4.1.0 Introduction.....	88
4.1.1 Temperature Studies	88
4.2 Homogeneous reaction.....	93
4.3 Activation Energy	96
4.5.1 Time on Stream.....	101
4.5.2 Mass Balance	104
4.6 Rate Law	108
4.7 Summary	120

Chapter 5 Kinetic Validation- Mass Transport Considerations

5.1 Mass transport considerations.....	122
5.2 Reynolds Numbers and Flow Regimes.....	122
5.2 Plug Flow Reactors	123
5.4 Mass Transport.....	124
5.5 Thiele Modulus	126
5.6 Methods for determining the presence of mass transport	127
5.6.1 Intrapphase Mass Transport Test Results	130
5.6.2 Interphase Limitations	132
5.7 Order dependence on changing catalyst mass	133
5.8 Discussion.....	135

Chapter 6 Mechanistic Studies

6.0 Introduction.....	137
6.1 Breakthrough Measurements	137
6.2 Time on Stream (extended).....	143
6.3.1 Desorption post-reaction.....	148

6.3.2 Desorption fresh catalyst.....	152
6.4 Post reaction catalyst analysis.....	155
6.5 Summary	157
6.5 Discussion.....	158

Chapter 7 Influence of bromine on the reaction chemistry

7.1 Introduction.....	164
7.2.1 Spectroscopic Issues	165
7.2.2 Calculating the bromochloride equilibrium constant.....	167
7.2.3 Determining BrCl in the Flow	169
7.3.1 Preliminary Bromine Experiments	170
7.3.2 Reaction with Br ₂ and CO.....	175
7.3.3 Reaction with varying concentration of Bromine at a reaction temperature of 303 K.	176
7.4.1 Reactions with varying dibromine concentration 323 K	182
7.5 Bromine Desorption.....	190
7.6 Post reaction catalyst analysis (bromine).....	191
7.7 Summary	194
7.8 Discussion	195

Chapter 8- Conclusions

8.1 Conclusions.....	199
8.2 Future work.....	200
References.....	201
Appendix 1.....	206

Chapter 1 Introduction

Figure 1 Example of oxygen and nitrogen surface groups contained within activated carbons ^{10,14}	17
Figure 2 Categories of activated carbon modification techniques ¹⁰	18
Figure 3 The principal commercial applications of phosgene ¹	21
Figure 4 Reaction 1 (top line) showing synthesis of TDI and Reaction 2 and three showing (middle and bottom lines) the synthesis of MDI and PMDI ¹	23
Figure 5 Synthesis of bisphenol A polycarbonate ¹	24
Figure 6 Formation of phosgene vs. reactor temperature for Donau catalyst in crushed and pellet form ²	33
Figure 7 (i) and (ii): (i) Catalysts Donau K40, Norit RX3extra and Picatal G201 centreline temperature profiles in industrial phosgene reactor. (ii) Varying throughput on the centreline temperature profile and its effect using the Donau K40 catalyst ²	34
Figure 8 Arrhenius dependence of oxidation rate of carbon ²	35
Figure 9 Proposed mechanism for Cl ₂ /C60 T catalysed COCl ₂ formation following an Eley–Rideal mechanism. The potentially dormant off-cycle species are shown in the dashed rectangle, while alternative paths for the regeneration of the catalytic species Cl ₂ /C60 A and B ⁴⁰	36
Figure 10 Theorised Oxychlorination mechanism ¹	37
Figure 11 The mechanism for (1) phosgene synthesis, (2) and (3) regeneration of the catalyst in two steps ⁴³	38
Figure 12 First step of triphosgene breakdown to produce phosgene ⁴⁷	39
Figure 13 Release of phosgene from the Eckert cartridge ⁴⁷	39
Figure 14 Mechanisms of adsorption (left Langmuir- Hinshelwood and right Eley- Rideal) ⁵⁶	41
Figure 15 Schematic of X-Ray Diffractometer ⁶⁰	44
Figure 16 Excitation of a characteristic X-ray photon or an Auger electron by a high energy X-ray photon or electron ⁶⁰	47
Figure 17 Optics of a Raman spectrometer	48
<u>Chapter 2 Experimental</u>	
Figure 18 Phosgene synthesis apparatus	52
Figure 19 Chemical scrubber design	54

Figure 20 Gas Cell designs	56
Figure 21 : Example spectrum taken at room temperature with a flow rate of CO of 5 cm ³ min ⁻¹ in a total flow of 159 cm ³ min ⁻¹ , i.e. 5 cm ³ min ⁻¹ CO, 154 cm ³ min ⁻¹ N ₂	57
Figure 22 Example spectrum taken at room temperature with a flow rate of Cl ₂ of 3 cm ³ min ⁻¹ in a total flow of 159 cm ³ min ⁻¹ , i.e. 3 cm ³ min ⁻¹ Cl ₂ , 156 cm ³ min ⁻¹ N ₂	58
Figure 23 The fundamental vibrations of phosgene ¹	59
Figure 24 Example IR spectra of phosgene taken from calibrations at a phosgene flow of 4 cm ³ min ⁻¹ . ^{1 29,72-74} , i.e. 3 cm ³ min ⁻¹ phosgene, 156 cm ³ min ⁻¹ N ₂	60
Figure 25 Example UV spectrum of phosgene taken from calibrations at a phosgene flow of 4 cm ³ min ⁻¹ . ^{1 29,72-74} , i.e. 3 cm ³ min ⁻¹ phosgene, 156 cm ³ min ⁻¹ N ₂	61
Figure 26 Calibration of CO gas cell 1	63
Figure 27 Calibration of CO gas cell 2	63
Figure 28 Calibration of Phosgene gas cell 1 (flow rate of phosgene in 10% phosgene in He)	64
Figure 29 Calibration of phosgene gas cell 2 (flow rate of phosgene in 10% phosgene in He)	64
Figure 30 Calibration of chlorine.....	65
Figure 31 Bromine doser design	68
Figure 32 Apparatus design (the red box indicates solid bromine)	69
Figure 33 Theoretically calculated vapour pressure of bromine as a function of temperature ⁷⁸	70
Figure 34 UV-visible spectrum of dibromine. The flow rate of bromine was varied by varying the temperature of the Dewar (allowing to cool from 298-77 K) in N ₂ flow of 159 cm ³ min ⁻¹ (Drive 50 cm ³ min ⁻¹ and dilution 109 cm ³ min ⁻¹)	71
Figure 35 Chlorine calibration consistency check with measured concentration as a function of the calculated from the extinction coefficient at 330 nm	72
Figure 36 Calibration graph for dibromine (peak area against calculated flow)	73
Figure 37 Mass spectrum of bromine at room temperature in a total flow of 159 cm ³ min ⁻¹ ..	74
Figure 38 Mass spectra of chlorine at different flow rates of chlorine	75
<u>Chapter 3 Characterisation of the Donau Supersorbon K40</u>	
Figure 39 SEM Images of the Donau k40 catalyst (size indicated in the bar).....	79
Figure 40 EDX of the fresh Donau catalyst.....	80

Figure 41 XRD of the fresh Donau K40 carbon catalyst (red line indicates the reflection of graphite ⁴¹)	81
Figure 42 Raman spectrum of the fresh Donau K40 carbon catalyst	83
Figure 43 Multi-peak fitted Raman spectrum of the Donau Supersorbion K40 carbon	84
3.6 Summary	86

Chapter 4 Kinetic Measurements

Figure 44 IR Spectra of reaction between CO and Cl ₂ over the catalyst as a function of temperature with flow rates of 5 cm ³ min ⁻¹ and 4 cm ³ min ⁻¹ in a total flow of 159 cm ³ min ⁻¹ , respectively, over a temperature range of 298-433K K (gas cell 1).....	89
Figure 45 Overlay of UV Spectra of reaction between CO and Cl ₂ over the catalyst as a function of temperature with flow rates of 5 cm ³ min ⁻¹ and 4 cm ³ min ⁻¹ , respectively, over a temperature range of 298-433K.....	90
Figure 46 Temperature for the reaction of CO and Cl ₂ over the catalyst with flow rates of 5 cm ³ min ⁻¹ and 4 cm ³ min ⁻¹ , respectively, over a temperature range of 298-433K.....	91
Figure 47 Mass balance for the reaction of CO and Cl ₂ over the catalyst with flow rates of 5 cm ³ min ⁻¹ and 4 cm ³ min ⁻¹ , respectively, over a temperature range of 298-433K.....	92
Figure 48 Overlay of IR Spectra of reaction between CO and Cl ₂ over bypass as a function of temperature with flow rates of 5 cm ³ min ⁻¹ and 4 cm ³ min ⁻¹ over a temperature range of 298-663 K.....	93
Figure 49 Overlay of UV Spectra of reaction between CO and Cl ₂ over the bypass as a function of temperature with flow rates of 5 cm ³ min ⁻¹ and 4 cm ³ min ⁻¹ over a temperature range of 298-663 K.....	94
Figure 50 Infrared Spectra of the Arrhenius experiment for the reaction between CO and Cl ₂ over the catalyst with flow rates of 5 cm ³ min ⁻¹ and 4 cm ³ min ⁻¹ over a temperature range of 298-323 (gas cell 2)	96
Figure 51 Overlay of UV spectra of the Arrhenius experiment for the reaction between CO and Cl ₂ over the catalyst with flow rates of 5 cm ³ min ⁻¹ and 4 cm ³ min ⁻¹ over a temperature range of 298-323 K.....	97
Figure 52 Arrhenius temperature dependence of phosgene formation (error bars represent standard deviation of three repeat experiments)	100

Figure 53 IR Spectra of reaction between CO and Cl ₂ over the catalyst as a function of temperature with flow rates of 5 cm ³ min ⁻¹ and 4 cm ³ min ⁻¹ in a total flow of 159 cm ³ min ⁻¹ at 323 K over a period of 5 hours	101
Figure 54 UV Spectra of reaction between CO and Cl ₂ over the catalyst as a function of temperature with flow rates of 5 cm ³ min ⁻¹ and 4 cm ³ min ⁻¹ in a total flow of 159 cm ³ min ⁻¹ at 323 K over a period of 5 hours	102
Figure 55 Reaction profile for the reaction between CO and Cl ₂ over the catalyst as a function of temperature with flow rates of 5 cm ³ min ⁻¹ and 4 cm ³ min ⁻¹ in a total flow of 159 cm ³ min ⁻¹ at 323 K over a period of 5 hours	103
Figure 56 CO mass balance profile for the reaction between CO and Cl ₂ over the catalyst as a function of temperature with flow rates of 5 cm ³ min ⁻¹ and 4 cm ³ min ⁻¹ in a total flow of 159 cm ³ min ⁻¹ at 323 K over a period of 5 hours	105
Figure 57 Cl ₂ mass balance plot profile for the reaction between CO and Cl ₂ over the catalyst as a function of temperature with flow rates of 5 cm ³ min ⁻¹ and 4 cm ³ min ⁻¹ in a total flow of 159 cm ³ min ⁻¹ at 323 K over a period of 5 hours	106
Figure 58 Overall mass balance plot profile for the reaction between CO and Cl ₂ over the catalyst as a function of temperature with flow rates of 5 cm ³ min ⁻¹ and 4 cm ³ min ⁻¹ in a total flow of 159 cm ³ min ⁻¹ at 323 K over a period of 5 hours	107
Figure 59 Infrared for the rate law determination with Cl ₂ fixed at a flow rate of 15 cm ³ min ⁻¹ and the flow rate of the CO indicated in the box of each spectrum at 323 K gas cell 1	109
Figure 60 UV for the rate law determination with Cl ₂ fixed at a flow rate of 15 cm ³ min ⁻¹ and the flow rate of the CO indicated in the box of each spectrum at 323 K	110
Figure 61 Infrared for the rate law determination with Cl ₂ fixed at a flow rate of 15 cm ³ min ⁻¹ and the flow rate of the CO indicated in the box of each spectrum at 323 K gas cell 1	111
Figure 62 UV for the rate law determination with Cl ₂ fixed at a flow rate of 15 cm ³ min ⁻¹ and the flow rate of the CO indicated in the legend at 323 K	112
Figure 63 Infrared for the rate law determination of phosgene with CO and Cl ₂ fixed at a flow rate of 15 cm ³ min ⁻¹ and the flow rate of the phosgene indicated in the box of each spectrum at 323 K (Gas Cell 1)	113
Figure 64 Infrared for the rate law determination of phosgene with CO and Cl ₂ fixed at a flow rate of 15 flow rate of the phosgene indicated in the box of each spectrum at 323 K	114
Figure 65 Plot of the log of the concentration dependence of CO on phosgene production .	116
Figure 66 Plot of the log of the concentration dependence of Cl ₂ on phosgene production .	117

Figure 67 Plot of the log of the concentration dependence of COCl_2 on CO consumption .118

[Chapter 5 Kinetic Validation- Mass Transport Considerations](#)

Figure 68 Plug flow (tubular) reactor⁹².....123

Figure 69 Possible reaction regimes for a gas phase reaction occurring on a porous solid catalyst. A is the reaction operating under kinetic control, B is the reaction operating with pore diffusion, C is the reaction limited by external diffusion and D is the homogeneous reaction⁵⁶125

Figure 70 External diffusion test conversion vs flow rate. F is the flow rate and V is the volume of catalyst.⁹⁷127

Figure 71 External diffusion test conversion vs space time. F is the flow rate, V is the volume of catalyst and τ is the space time.⁹⁷128

Figure 72 Evaluation of the influence of particle diameter on reaction rate. F is the flow rate, V is the volume of catalyst and d_p is the particle size of the catalyst.⁹⁷.....129

Figure 73 Reaction rate vs particle size at steady state for 2 hours a reaction temperature of 323 K in a total flow of $159 \text{ cm}^3 \text{ min}^{-1}$ (CO at $5 \text{ cm}^3 \text{ min}^{-1}$, Cl_2 at $4 \text{ cm}^3 \text{ min}^{-1}$ and N_2 at $150 \text{ cm}^3 \text{ min}^{-1}$). The dotted line represents phosgene production over the pelleted catalyst.....130

Figure 74 Reaction rate of powder vs at steady state for 2 hours a reaction temperature of 323 K in a total flow of $159 \text{ cm}^3 \text{ min}^{-1}$ (CO at $5 \text{ cm}^3 \text{ min}^{-1}$, Cl_2 at $4 \text{ cm}^3 \text{ min}^{-1}$ and N_2 at $150 \text{ cm}^3 \text{ min}^{-1}$).....131

Figure 75 Phosgene production vs space time at 323 K. The squares are the drive flow at $20 \text{ cm}^3 \text{ min}^{-1}$, the circles are the drive flow at $30 \text{ cm}^3 \text{ min}^{-1}$, and the triangles are the drive flow at $50 \text{ cm}^3 \text{ min}^{-1}$ (CO at $5 \text{ cm}^3 \text{ min}^{-1}$, Cl_2 at $4 \text{ cm}^3 \text{ min}^{-1}$ and total N_2 at $150 \text{ cm}^3 \text{ min}^{-1}$).....132

Figure 76 Plot of the log of the catalyst mass dependence of CO on phosgene production (CO at $5 \text{ cm}^3 \text{ min}^{-1}$, Cl_2 at $4 \text{ cm}^3 \text{ min}^{-1}$ and total N_2 at $150 \text{ cm}^3 \text{ min}^{-1}$).....133

[Chapter 6 Mechanistic Studies](#)

Figure 77 Schematic of 2-reactor system. Reactor 1 contains ground quartz and reactor 2 contains the catalyst137

Figure 78 Time response of switching the flow of CO over the catalyst at 323 K in a total flow of $159 \text{ cm}^3 \text{ min}^{-1}$ 138

Figure 79 Time response of Switching the flow of chlorine over the catalyst at 323 K in a total flow of $159 \text{ cm}^3 \text{ min}^{-1}$ 139

Figure 80 Time response of Switching the flow from quartz to catalyst of repeated chlorine at 323 K in a total flow of 159 cm ³ min ⁻¹	140
Figure 81 Time response of Switching phosgene flow between quartz to catalyst at 323 K in a total flow of 159 cm ³ min ⁻¹	141
Figure 82 Concentration profile for the reaction between CO and Cl ₂ over the catalyst as a with flow rates of 5 cm ³ min ⁻¹ and 4 cm ³ min ⁻¹ in a total flow of 159 cm ³ min ⁻¹ over a period of 54 hours at 353 K.....	143
Figure 83 Concentration profile for the reaction between CO and Cl ₂ over the catalyst with flow rates of 5 cm ³ min ⁻¹ and 4 cm ³ min ⁻¹ in a total flow of 159 cm ³ min ⁻¹ a period of 74 hours at 323 K over.....	144
Figure 84 Overall mass balance plot for the reaction at 353 K for 54 Hours	145
Figure 85 Overall mass balance plot for the reaction a 323 K for 74 Hours	145
Figure 86 Cumulative missing mass as a function of time at a reaction temperature of 323 K (from fig 85)	146
Figure 87 Reaction profile for reaction at 298 K for 120 mins using a mass spectrometer with flow rates of CO and Cl ₂ of 5 cm ³ min ⁻¹ and 4 cm ³ min ⁻¹ in a total flow of 159 cm ³ min ⁻¹ ..	148
Figure 88 Temperature ramp 298-633 K in 5 K steps post reaction monitoring mass 28 for CO (159 cm ³ min ⁻¹ He).....	149
Figure 89 Temperature ramp 298-633 K in 5 K steps post reaction monitoring mass 63 and 98 for COCl ₂ (159 cm ³ min ⁻¹ He).....	150
Figure 90 Temperature ramp 298-633 K in 5 K steps post reaction monitoring mass 70 for Cl ₂ (159 cm ³ min ⁻¹ He)	151
Figure 91 Temperature ramp 298-633 K in 5 K steps on fresh catalyst monitoring mass 28 for CO (159 cm ³ min ⁻¹ He).....	152
Figure 92 Temperature ramp 298-633 K in 5 K steps on fresh catalyst monitoring mass 98 for COCl ₂ (159 cm ³ min ⁻¹ He).....	153
Figure 93 Temperature ramp 298-633 K in 5 K steps on fresh catalyst monitoring mass 70 for Cl ₂ (159 cm ³ min ⁻¹ He)	154
Figure 94 SEM image of the Donau Supersorbon K40 catalyst post reaction (4 hours at 323 K, CO 5 cm ³ min ⁻¹ and Cl ₂ cm ³ min ⁻¹) showing the area of which an EDX was taken	155
Figure 95 EDX of the Donau Supersorbon K40 catalyst (4 hours at 323 K, CO 5 cm ³ min ⁻¹ and Cl ₂ 4 cm ³ min ⁻¹).....	156

Figure 96 Proposed reaction mechanism for phosgene production over the Donau Supersorbon K40 catalyst	161
---	-----

[Chapter 7 Influence of bromine on the reaction chemistry](#)

Figure 97 UV -visible spectrum of dibromine co-fed with dichlorine (bromine doser at room temperature) and chlorine at 4 cm ³ min ⁻¹ at a fixed flow 159 cm ³ min ⁻¹ (The red line shows obtained spectrum and the black line shows the linear addition of the spectra of following (i) Cl ₂ and (ii) Br ₂)	165
--	-----

Figure 98 Example UV of Cl ₂ , Br ₂ and BrCl.....	166
---	-----

Figure 99 UV visible spectra of bromine doser at 293 K, chlorine at 4 cm min and both halogens isolated simultaneously in the gas cell after 30 minutes, i.e. spectra not acquired under flow conditions.	167
--	-----

Figure 100 UV Vis Spectra of bromine at room temperature and varying chlorine flow in a total flow of 159 cm ³ min ⁻¹ at a reaction temperature of 298 K (bromine doser at room temperature at an estimated flow rate of 0.12 mmol min ⁻¹).....	169
---	-----

Figure 101 Mass balance for the reaction of Cl ₂ and Br ₂ , the Br ₂ flow was kept constant at room temperature and the flow rate of chlorine was varied 2-5 cm ³ min ⁻¹ in a total flow rate of 159 cm ³ min ⁻¹	170
---	-----

Figure 102: IR spectra for the reaction of CO and Cl introducing the bromine co-feed(0.0016 mmol min ⁻¹) over the catalyst with flow rates of 5 cm ³ min ⁻¹ and 4 cm ³ min ⁻¹ over at a temperature of 353 K	171
--	-----

Figure 103 Phosgene production rate at 353 K as a function of reaction conditions (i) normal reaction (CO+Cl ₂) and (ii) normal reaction with bromine present (0.0016 mmol min ⁻¹ , doser temperature of 195 K)	172
--	-----

Figure 104 UV-vis spectra for the reaction of CO and Cl ₂ introducing the bromine (bromine doser temperature of 195K, 0.0016 mmol min ⁻¹) over the catalyst with flow rates of 5 cm ³ min ⁻¹ and 4 cm ³ min ⁻¹ respectively over at a temperature of 353 K.....	173
--	-----

Figure 105 Reaction profile for the reaction of CO and Cl ₂ over the catalyst with flow rates of 5 cm ³ min ⁻¹ and 4 cm ³ min ⁻¹ , over at a temperature of 353 K with bromine co-feed (bromine doser at 195 K, 0.0016 mmol min ⁻¹).....	174
---	-----

Figure 106 Example IR spectra of carbonyl bromide at a reaction temperature of 298 K , bromine doser at room temperature	175
--	-----

Figure 107 IR spectra for the reaction of CO and Cl ₂ introducing the bromine cofeed over the catalyst with flow rates of 5 cm ³ min ⁻¹ and 4 cm ³ min ⁻¹ over at a temperature of 303 K	177
Figure 108 Reaction rate as a function of bromine flow rate calculated based on the v ₁ mode of phosgene, COClBr, and COBr ₂	178
Figure 109 IR spectra for the reaction of CO and Cl introducing the bromine at room temperature co-feed over the catalyst with flow rates of 5 cm ³ min ⁻¹ and 4 cm ³ min ⁻¹ over at a catalyst temperature of 303 K	179
Figure 110 : IR spectra for the reaction of CO and Cl ₂ introducing the bromine cofeed over the catalyst with flow rates of 5 cm ³ min ⁻¹ and 4 cm ³ min ⁻¹ , respectively, over increasing the temperature from 303 K to 353 K.....	180
Figure 111 Initial bromine signal obtained over the bypass and signal on increasing the reaction temperature to 353 K in a total flow of 159 cm ³ min ⁻¹	181
Figure 112 Reaction profile of the reaction between CO and Cl ₂ at 323 K with a bromine flow rate of 3.6x10 ⁻⁴ mmol min ⁻¹ (Br ₂ doser T = 113 K) at 1 hour.....	184
Figure 113 Reaction profile of the reaction between CO and Cl ₂ at 323 K with a bromine flow rate of 6.9 x10 ⁻⁴ mmol min ⁻¹ (Br ₂ doser T = 143 K) at 1 hour (error bars are the standard deviation of 3 spectra).....	184
Figure 114 Reaction profile of the reaction between CO and Cl ₂ at 323 K with a bromine flow rate of 0.0016 mmol min ⁻¹ (Br ₂ doser T = 196 K) at 1 hour	185
Figure 115 Reaction profile of the reaction between CO and Cl ₂ at 323 K with a bromine flow rate 0.0024 mmol min ⁻¹ (Br ₂ doser T = 223 K) at 1 hour	185
Figure 116 Infrared Spectra of the reaction between CO and Cl ₂ operating at 323 K at different bromine flow rates.....	186
Figure 117 UV-Vis Spectra of the reaction between CO and Cl ₂ operating at 323 K at different bromine flow rates.....	187
Figure 118 Phosgene production as a function of bromine flow rate in the feedstream. The dotted line is the reaction operating with only CO and Cl ₂ . The error bars represent the standard deviation of the reaction operated at steady state for 2 hours. The red line represents a linear fit to all five data points [slope= 202.92 ± 4.15 mmol COCl ₂ min ⁻¹ g ⁻¹ _{cat} (mmol Br ₂ min ⁻¹) ⁻¹]	188

Figure 119 Phosgene production as a function of % bromine in the feedstream. The dotted line is the reaction operating with only CO and Cl₂. The red line represents a linear fit to all five data points [slope= 0.313 ± .018 mmol COCl₂ min⁻¹g⁻¹_{cat}(% Br₂/Cl₂)⁻¹]188

Figure 120 Relative enhancement in phosgene production rate as a function of % bromine in the feedstream. The dotted line is the reaction operating with only CO and Cl₂.The red line represents a linear fit to all five data points [slope= 1.30 ± 0.06 enhancement(% Br/Cl₂)⁻¹]189

Figure 121 Bromine desorption from the fresh Donau k40 catalyst with a temperature ramp 298-673 K at 5 K/min in a total flow of 159 cm³ min⁻¹190

Figure 122 SEM image of the Donau Supersorbon K40 catalyst post reaction (4 hours at 323 K) showing the area of which an EDX was taken192

Figure 123 EDX of the Donau Supersorbon K40 catalyst after 4 hours of reaction at 323 K (3 hours + 1 hour with bromine).....192

Figure 124 Schematic for the proposed reaction mechanism in the presence of bromine..197

[Appendix](#)

Figure A1 Phosgene synthesis and oxy-chlorination apparatus.....206

Figure A2 IR Spectra of reaction between CO and Cl₂ over the catalyst as a function of temperature with flow rates of 5 cm³ min⁻¹ and 4 cm³ min⁻¹ in a total flow of 159 cm³ min⁻¹ over a temperature range of 298-433 K (CaF₂ gas cell 2).....207

Figure A3 Infrared for the rate law determination with Cl₂ fixed at a flow rate of 15 cm³ min⁻¹ and the flow rate of the CO indicated in the box of each spectrum at 323 K (CaF₂ windows).....208

Figure A4 Infrared for the rate law determination with Cl₂ fixed at a flow rate of 15 cm³ min⁻¹ and the flow rate of the CO indicated in the box of each spectrum at 323 K (CaF₂ windows).....209

Figure A5 Infrared for the rate law determination with CO and Cl₂ fixed at a flow rate of 15 cm³ min⁻¹ and the flow rate of the COCl₂ indicated in the box of each spectrum at 323 K (CaF₂ windows).....210

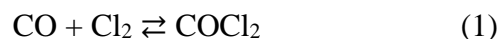
Figure A6 Infrared spectra for the reaction of CO and Cl₂ introducing the bromine over the

catalyst with flow rates of $5 \text{ cm}^3 \text{ min}^{-1}$ and $4 \text{ cm}^3 \text{ min}^{-1}$ over at a temperature of 353 K
.....211

Figure A7 Infrared spectra for the reaction of CO and Cl₂ introducing the bromine over the
catalyst with flow rates of $5 \text{ cm}^3 \text{ min}^{-1}$ and $4 \text{ cm}^3 \text{ min}^{-1}$ increasing the temperature of 303K
to 353 K.....212

1.0 Introduction

Phosgene (COCl₂) is an important chemical intermediate used in the manufacturing of polyurethanes, polycarbonates pharmaceuticals and agrochemicals. The production of phosgene in the industrial setting typically involves the gas phase reaction between carbon monoxide and chlorine in the presence of an activated carbon catalyst (Equation 1)^{1,2}.



Phosgene was discovered in 1812 by Dr John Davy when he investigated the reaction between carbon monoxide and chlorine in daylight³. It was more than 50 years after its discovery that the production of phosgene was achieved catalytically by Schützenberger⁴. The first application of phosgene was in the 1880's for the preparation of crystal violet and the dye precursor, Michler's ketone^{1,5,6}. Phosgene, due to its toxic nature, was also used in the First World War as a chemical weapon; this raised the production of phosgene significantly and thereby making this gas one of the few chemicals recognised by the general public by name¹.

Phosgene is mainly used today in the manufacture of polyurethanes. It is used in the production of isocyanates which are the starting material for the synthesis of polyurethanes. The global demand for polyurethane products continues to grow and so the production of phosgene has also increased in demand¹. Polyurethanes are produced globally with production exceeding 9 million tonnes in 2009⁷.

There have been surprisingly few open literature investigations into the kinetics and the surface chemistry of the catalytic production of phosgene over the last 50 years. Potter and Baron^{5,6} investigated the catalytic formation of phosgene production over a poorly defined carbon catalyst^{2,5,6}. In 2012 a paper was published by Mitchell and co-worker on the selection of carbon catalysts for the industrial manufacture of phosgene. In 2016 Gupta *et al* published a paper on the formation of phosgene over fullerene, as a model catalyst. Due to the paucity of literature on this topic, there is a need to develop an improved understanding of phosgene formation over a commercial grade carbon catalyst. This project aims to address that need.

Activated carbon, also known as activated charcoal, is the most commonly known form of carbon as a catalyst or a catalyst support⁸. Activated carbon is an amorphous carbon that has been processed to make it extremely porous and have a large surface area (*e.g.* >500 m²/g). Over the last 20 years activated carbons application as catalysts/supports have become popular

in heterogeneous catalysis because (i) they can be prepared economically from natural raw materials, (ii) they have high and tuneable specific surface areas, and (iii) they have a variety of surface groups⁹.

1.1.1 Activated Carbon

Activated carbons (AC) are materials that contain space (porosity) enclosed by carbon atoms. Activated carbons have been proven to be an effective adsorbent for the removal of a wide variety of organic and inorganic pollutants dissolved in aqueous media, or from gaseous environment. Activated carbon is a member of a family of carbons ranging from carbon blacks to nuclear graphites, carbon fibres, composites, electrode graphites, and many more^{8,10-12}.

Activated carbons are widely used as adsorbents in the treatment of wastewaters due to their exceptionally high surface areas which range from 500 to 1500m² g⁻¹, well-developed internal microporosity structure as well as the presence of a wide spectrum of surface functional groups.^{11,13} All activated carbons come from an organic parent source but with different carbonization and manufacturing processes. All activation reactions are heterogeneous using either carbon dioxide, or steam, or mixtures of these two gases. Carbon atoms can be removed from within porous carbons by gasification using carbon dioxide or water vapor, usually at 800-900 °C. The reaction equation is simple enough, e.g.



In addition to the main processes of activation by carbon dioxide or steam, three other techniques of chemical activation are used, involving co-carbonization with (a) zinc chloride, (b) phosphoric acid and (c) with potassium hydroxide. Mechanisms for these activations are all different, with zinc chloride promoting the extraction of water molecules from the lignocellulosic structures of parent materials, and phosphoric acid combining chemically within the lignocellulosic structures. There is no selective removal of carbon atoms as during physical activation and carbonization yields are improved. The mechanisms by which potassium hydroxide activates an existing carbon are more complex and involve the disintegration (almost explosively) of structure following intercalation as well as some gasification by the oxygen of the hydroxide. The presence of oxygen is not essential (but may be helpful) to this form of activation. The predominant types of surface functional group on activated carbons are surface oxygen complexes such as carbonyl groups. The surface oxygen

complexes of activated carbon can be created via two major oxidation methods, namely, dry and wet oxidations.

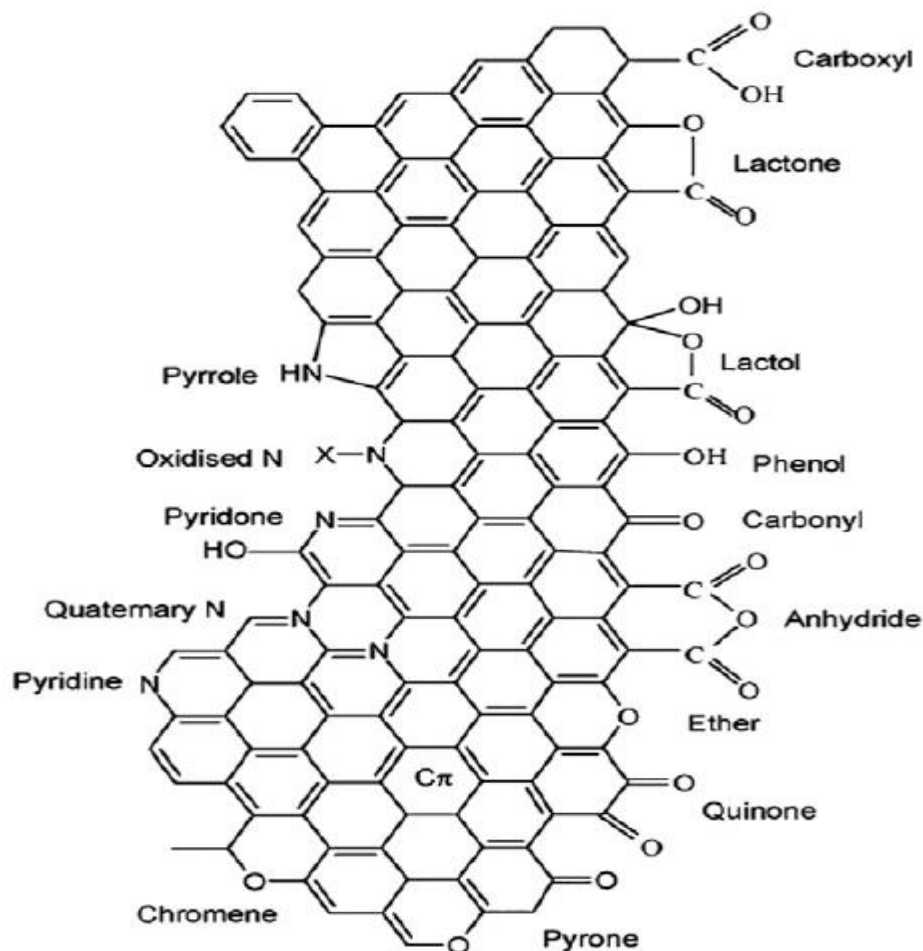


Figure 1 Example of oxygen and nitrogen surface groups contained within activated carbons^{10,14}

The chemical characteristics of activated carbons are largely determined by a certain degree of surface chemical heterogeneity, which is related to the presence of heteroatoms, i.e. atoms present in the carbon structure that are not carbon, such as oxygen, nitrogen, hydrogen, sulfur, and phosphorus. The type and quantity of these elements are derived either from the nature of starting material or introduced during the activation process. The surface functional groups (which are formed from these heteroatoms) and the delocalized electrons of the carbon structure determine the acidic or basic character of the activated carbon surface. The acidic character of activated carbon surfaces is closely related to the oxygen containing surface groups. Basicity of activated carbon can be associated with: (i) resonating π -electrons of

carbon aromatic rings that attract protons, and (ii) basic surface functionalities (e.g. nitrogen containing groups) that are capable of binding with protons^{8,10,11}

AC modification is gaining prominence due to the need to enable ACs to develop affinity for certain contaminants to cater for their removal from varying types of wastewater in the industries.

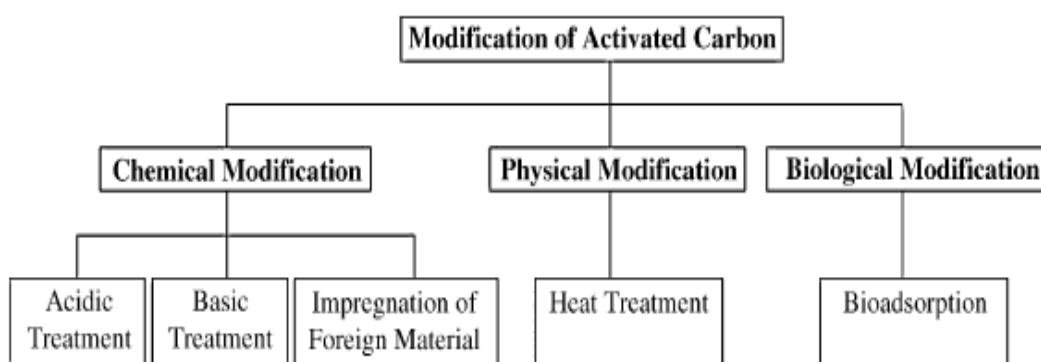


Figure 2 Categories of activated carbon modification techniques¹⁰

There are various factors that influence the adsorption capacity of AC prior to their modification. They can be tailored to their specific physical and chemical attributes to enhance their affinities toward metal, inorganic and/or organic species present in aqueous solutions. These factors include specific surface area, pore-size distribution, pore volume and presence of surface functional groups. The adsorption capacity increases with specific surface area due to the availability of adsorption site while pore size, and micropore distribution are closely related to the composition of the AC, which arises from the type of raw material used, the degree of activation during production stage and the frequency of regeneration.¹⁵

It is an established fact that the AC surface can display acidic, basic and/or neutral characteristics depending on the presence of surface functional groups¹⁶. As such, modification of chemical characteristics is taken to mean treatment to modify the inherent surface functional groups of AC. It has been widely recognized that chemical species removal by AC adsorption is due predominantly to the surface complex formation between the species and the surface functional groups. This is especially significant in the case of removing inorganics and metals from aqueous solutions where ACs are generally less effective as compared to removing organic compounds.

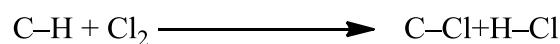
Acidic treatment of AC displays beneficial effects on adsorption of metal ions, it is, however, detrimental to the physical aspects of AC such as BET surface area and pore volume. In most cases, treatment with oxidizing agents produces modification of the textural characteristics of the original AC, which can be a drawback in carbon materials with a narrow microporosity or a well-defined porosity¹⁷. Maroto-Valer et al reported that treatment with nitric acid reduced the BET surface area and total pore volume by 9.2% and 8.8%, respectively¹⁸. This reduction in BET surface area is widely observed in the literature.^{19,20}

There were studies carried out to determine the effect of basic treatment of ACs on metal adsorption capacity. Park and Jang²¹ reported that adsorption of Cr(VI) reduced by a factor of about 2 at a contact time between NaOH-treated AC and the metal ion at over 170 min. They suggested that this reduction may be due to the decrease of specific surface area or micropore volume. Under alkaline environment (basic components in aqueous solutions), it is expected that OH⁻ ion will react with the surface functional groups of AC. This was verified in the study conducted by Chiang et al.²² where AC treated with NaOH showed major increase in concentration of phenolic functional groups on the surface. Basic treatments of AC's are beneficial in enhancing uptake of organic-based substances from aqueous solutions.

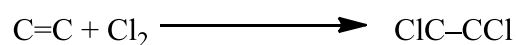
1.1.2 Adsorption on Activated Carbons

The behaviour of different types of carbon in the presence of halogens has been studied²³⁻²⁶. The interactions between chlorine and carbon surfaces can be classified into two types of adsorption phenomena, physical, and chemical. The latter are the most important ones since they provide information about the carbon material surface. Most of these chemical interactions involve atoms other than carbon present in the carbon surface, resulting in reactions with a strong bonding energy, which makes it possible to consider them as thermodynamically irreversible. Some of them are²³:

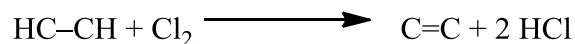
(1) substitution reactions:



(2) Addition reactions in non-conjugated double bonds:



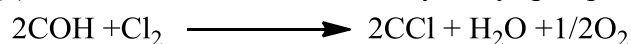
(3) Dehydrogenation reactions:



(4) Substitution reactions in the carboxyl group:



(5) Substitution reactions of the hydroxyl group:



The first three reactions, constitute the most important reactions taking place between the chlorine and the carbon. These reactions were deduced from a study by Tobias *et al.*,²⁶ on a mass balance between the chlorine uptake on the carbon surface and the formed hydrogen chloride. They observed that reactions (1) and (2) were predominant and also, by means of hydrogenation and chlorination cycles, that they were chemically reversible. Reactions (4) and (5) are due to the presence of carboxyl and hydroxyl groups on the carbon surface, the amount of which depends on the carbon characteristics. These substitution reactions have been studied considering the polarity decrease caused by chlorine on the carbon surface. All the above reactions, with the exception of (3), involve carbon mass gain. The amount of mass gained in chlorine atmosphere by chemisorption on the carbon surface should therefore be related to the availability of hydrogen atoms, non-conjugated double bonds and carboxyl and hydroxyl groups. Hence, the reactivity of carbons in the presence of chlorine, due to chemisorption, is not related to the surface area determined by BET but to the presence and number of the groups with which chlorine can react. The relative importance of the reactions between chlorine and the surface of a given carbon will therefore depend on the surface reactivity of the carbon, which varies with the carbon characteristics, the thermal treatments to which it is subjected, and with the type of precursor, among other factors.

1.1.3 Applications of Phosgene

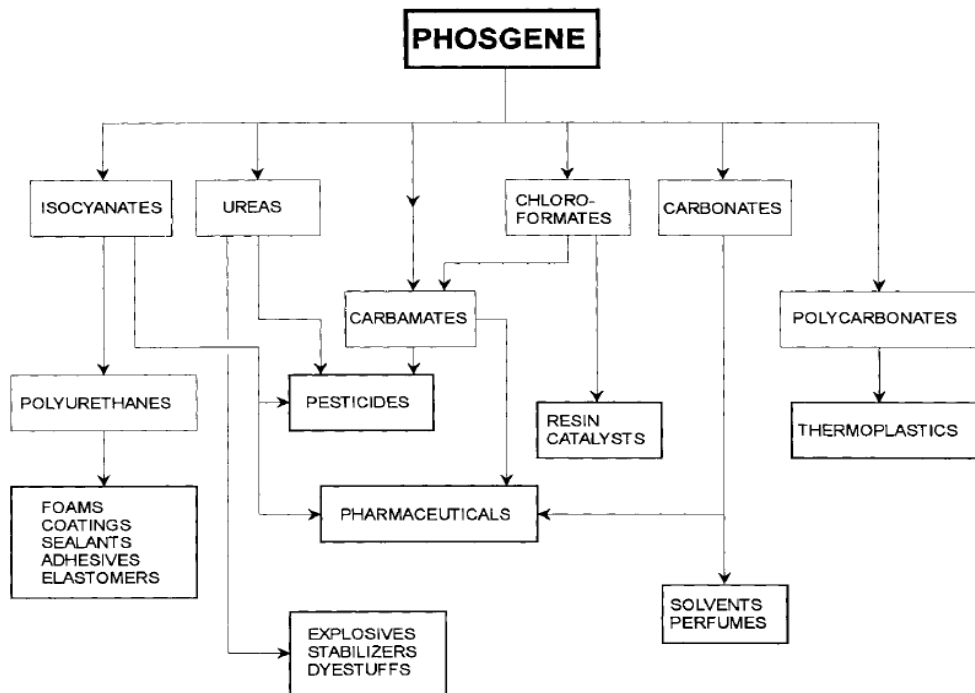
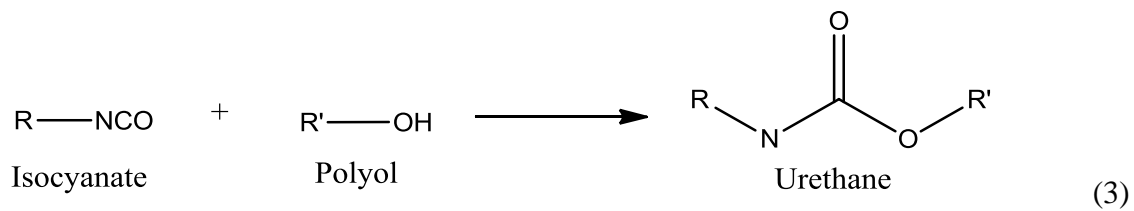


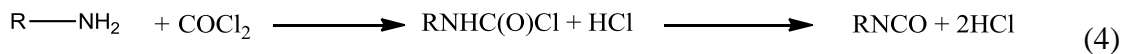
Figure 3 The principal commercial applications of phosgene¹

1.1.4 Polyurethanes

Polyurethanes are important materials used in everyday life that are formed by the reaction between an isocyanate and polyol compounds to form a urethane link (Equation 3). Today polyurethanes are manufactured by companies such as Huntsman Polyurethanes, Bayer, BASF, Wanhua, *etc*, for use in products such as adhesives, footwear, mattresses, car bumpers and refrigerators^{1,27}. Increasingly, polyurethanes are being used as insulating materials used in the construction industry.



Phosgene is used in the synthesis of the isocyanate starting material; from the reaction between amines and phosgene (Equation 3).



Many isocyanate groups are manufactured this way. The two most important isocyanates (Figure 4) in terms of amounts produced are toluene diisocyanate (TDI) and the increasingly more important diphenylmethane-4, 4'-diisocyanate (MDI) that are produced by a wide range of manufacturers^{1,27,28}.

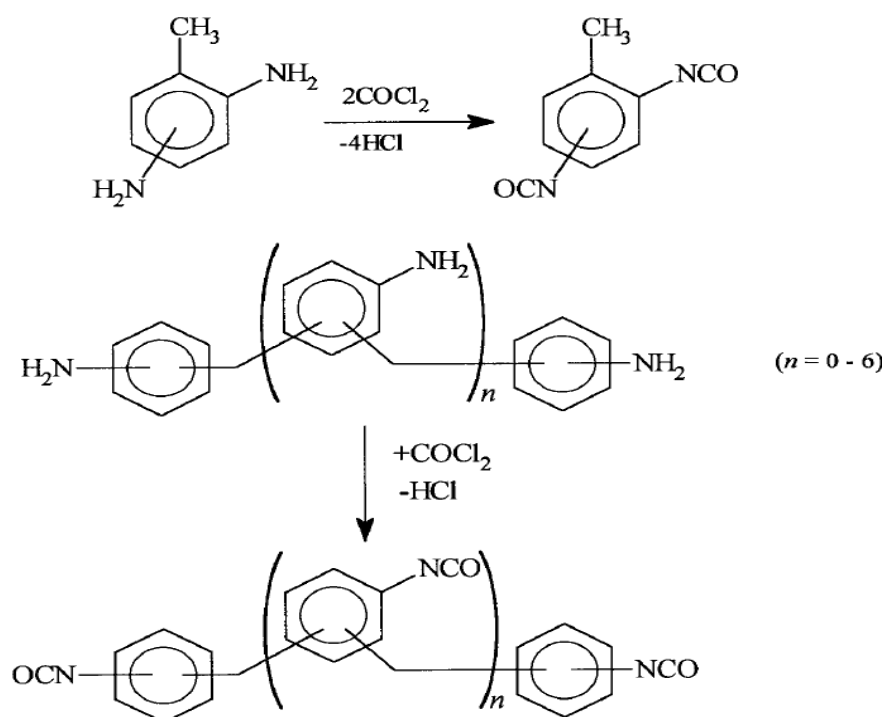


Figure 4 Reaction 1 (top line) showing synthesis of TDI and Reaction 2 and three showing (middle and bottom lines) the synthesis of MDI and PMDI¹

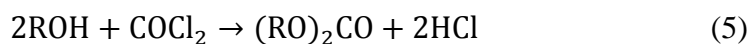
1.1.5 Chloroformates

Alkyl chloroformates are generally synthesised by the anhydrous reaction of alcohols with excess dry phosgene in a corrosion resistant reactor. To make small chloroformates, the reaction temperatures are kept low (usually between 0 and 5°C) and the phosgene is added to the alcohol to avoid the formation of carbonates. For larger chloroformates, reactions require gentle heating and acid acceptors are added to remove HCl as it forms. Chloroformates are traditionally formed in a batch process but a method to produce them as a continuous flow process has recently been developed¹

Chloroformates have a wide range of applications; for example, they are used as an intermediate for organic synthesis. However, chloroformates are also important intermediates in the synthesis of many commercial materials, pesticides, dyes, polymers, perfumes and drugs^{1,27}.

1.1.6. Polycarbonates

Carbonates are synthesised in a similar way (Equation 5) to chloroformates in either a one or two step process. The one step reaction process requires longer reaction times and extra quantities of alcohol are usually required¹.



Carbonates have application as synthetic intermediates for pharmaceuticals, dyes, and agricultural chemicals^{1,29}. However, possibly the most important carbonate reaction with phosgene is the synthesis of bisphenol A polycarbonate (Figure 3). That is made by the reaction between phosgene and bisphenol A. Bisphenol A polycarbonate is widely used in gear wheels, refrigerator parts and electrical components^{1,27}.

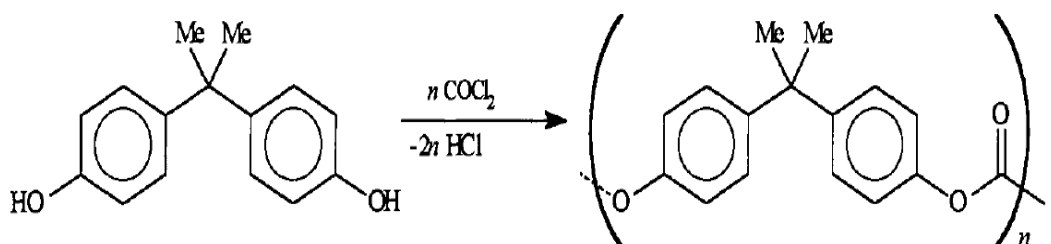


Figure 5 Synthesis of bisphenol A polycarbonate¹

1.2. Phosgene Synthesis

1.2.1 Photo-chemical Synthesis

Historically phosgene was originally formed using carbon monoxide and chlorine under UV light. It was this method which ultimately led to the discovery of phosgene in 1812^{1,3}. In many studies it was shown that the reaction is promoted by UV light under anhydrous conditions¹. However, it was also shown that the reaction takes place under visible light^{1,30}. It was reported in 1907 that the effect of the light on the reaction equilibrium was purely catalytic^{35,48}.

The first study to really begin to understand the reaction kinetics of the photo-chemical synthesis of phosgene was performed by Bodenstein et al³⁰⁻³³. The reaction rate at room temperature was found to be given by Equation 6:

$$[\text{COCl}_2]/dt = kI [\text{Cl}_2][\text{CO}] \quad (6)$$

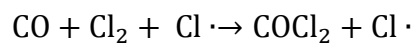
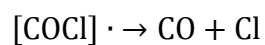
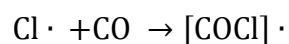
Where I = intensity of absorbed light and k is a rate coefficient

The reaction was reported to be air sensitive as the presence of di-oxygen was found to have an inhibitive effect on the reaction, resulting in the production of CO₂ in a di-chlorine sensitized reaction. The reactions were also performed at low pressure indicating that the reaction is slowed by the recombination of the chlorine radicals at the reactor walls. At lower temperatures 260-300°C the rate expression for the reaction rate is simpler as there was no formation of CO₂. At higher temperatures it was found that the thermal production of phosgene competes with the photochemical step^{1,30} (Equation 7);

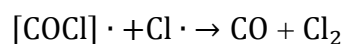
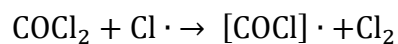
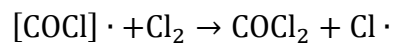
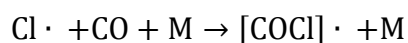
$$d[\text{COCl}_2]/dt = [\text{Cl}]\{k_1[\text{Cl}_2][\text{CO}] - k_2[\text{COCl}_2]\} \quad (7)$$

where k₁ and k₂ are rate coefficients

The procedure for the photochemical synthesis has changed and developed with time. Christiansen showed that the reaction proceeded via the formation of the [COCl] radical (Equation 8)³⁴. The simplest mechanism for the photochemical synthesis of phosgene was found to occur under atmospheric pressure, room temperature and normal pressures of phosgene and was proposed by Bodenstein and colleagues³⁰⁻³⁴.



It was not until 1965^{35,55} that the key step was identified as the reaction between the chlorine atom and CO, the radical was trapped in a low temperature matrix. The currently accepted mechanism for the photochemical production of phosgene is as follows (Equation 9);



Where M refers to the reactor walls

1.2.2 Thermal Synthesis

Phosgene can also be synthesised by the reaction of carbon monoxide and di-chlorine using only thermal energy. However, the reaction proceeds via equilibrium at high temperature, and due to the slow reaction rate the thermal equilibrium can only be measured at high temperatures (>350°C)^{1,32}

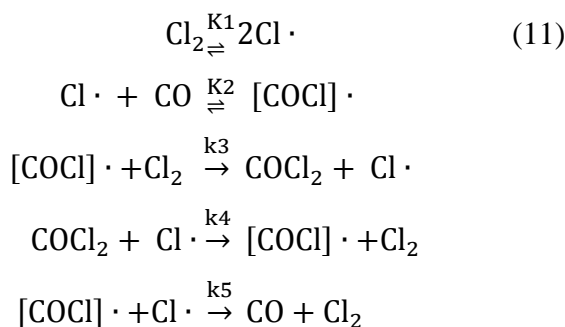


From the reaction equation the reaction equilibria would involve a reduction in pressure. The pressure effects of the dissociation of phosgene have been studied at 0.5, 1 and 10 Bar³¹. From experiments over a range of temperatures, the enthalpy of formation has been calculated by measuring the equilibrium constant (K) at a range of different temperatures. It was found that at higher temperatures the equilibrium lies on the left hand side. Useful notation (Equation 10) has been developed for the rate of formation of phosgene for temperatures between 349- 452°C at 1 bar pressure^{1,31}.

$$\frac{d[COCl_2]}{dt} = x_1[CO][Cl_2]^{\frac{3}{2}} - x_2[COCl_2][Cl_2]^{\frac{1}{2}} \quad (10)$$

$$\text{Where } x_1/x_2 = K = \frac{[CO][Cl_2]}{[COCl_2]}$$

The mechanism for the reaction that was originally proposed proceeded via Cl₃ and Cl as the radical chain carriers. However, the currently accepted mechanism proceeds via Cl· and [COCl]· as the chain carrier, and can be expressed with the following equations (Equation 11)^{1,32};



For this mechanism (Equation 12)

$$\begin{aligned}x_1 &= k_3 K_2 K_1^{\frac{1}{2}} \\x_2 &= k_4 K_1^{\frac{1}{2}}\end{aligned}\tag{12}$$

The equilibrium constants calculated agree with the experimental measurements of the equilibrium constants. For the decomposition of phosgene the reaction rate is similar, just that the sign is reversed^{1,32}.

1.2.3 Thermodynamics of phosgene

There have been several investigations to determine the standard energy of formation of phosgene by many different methods³⁵. The results are summarised in Table 1

Table 1 Enthalpy of formation of phosgene summary³⁵ (where a is hydrolysis in alkaline solution, b is combustion enthalpy in O₂ and H₂, c is the thermal synthesis of phosgene, d is the photochemical synthesis of phosgene and e is the dissociation of phosgene).

Year	Experimental method	$\Delta H_{f(298)}^0(\text{g})/\text{kJ mol}^{-1}$
1878	Calorimetry ^a	-189
1882	Calorimetry ^a	-228 ± 1
1882	Calorimetry ^b	-216 ± 2
1924	Equilibria ^c	-218.9 ± 0.6
1967	Calorimetry ^d	-224 ± 1
1970	Equilibria ^e	-219 ± 0.6
1972	Calorimetry ^f	-220 ± 1

The standard free energy of formation can be expressed by the following equation¹:

$$\Delta G_f = -221.67 \text{ kJ mol}^{-1} + 0.0392T \text{ kJ mol}^{-1}$$

The calculated thermodynamic functions for phosgene are shown in table 2 over an extended temperature range 0- 6000 K

Table 2 Thermodynamic properties of phosgene in the ideal gas state¹

T/K	C_p° ^a	S° ^a	$-(G^{\circ}-H_{298}^{\circ})/T^a$	$(H^{\circ}-H_{298}^{\circ})^b$	ΔH_f° ^b	ΔG_f° ^b	$\log_{10}(K_f)$
0	0.000	0.000	∞	-12.867	-218.372	-218.372	∞
100	36.537	233.747	328.453	-9.471	-219.399	-215.113	112.363
200	48.362	262.618	288.800	-5.236	-219.985	-210.551	54.990
250	53.603	273.992	284.724	-2.683	-220.075	-208.180	43.497
298.15	57.695	283.796	283.796	0.000	-220.078	-205.887	36.071
300	57.835	284.153	283.797	0.107	-220.077	-205.799	35.833
350	61.211	293.332	284.514	3.086	-220.026	-203.423	30.359
400	63.938	301.689	286.147	6.217	-219.945	-201.056	26.255
450	66.184	309.354	288.305	9.472	-219.853	-198.701	23.065
500	68.068	316.427	290.768	12.830	-219.760	-196.356	20.513
600	71.048	329.115	296.127	19.793	-219.587	-191.691	16.688
700	73.282	340.242	301.650	27.014	-219.438	-187.054	13.958
800	74.993	350.144	307.105	34.432	-219.309	-182.437	11.912
900	76.324	359.057	312.390	42.000	-219.198	-177.835	10.321
1000	77.373	367.155	317.468	49.687	-219.102	-173.244	9.049
1100	78.210	374.570	322.327	57.468	-219.020	-168.662	8.009
1200	78.886	381.406	326.969	65.324	-218.952	-164.087	7.143
1300	79.437	387.742	331.403	73.241	-218.898	-159.517	6.409
1400	79.891	393.646	335.641	81.208	-218.859	-154.951	5.781
1500	80.270	399.172	339.694	89.217	-218.836	-150.387	5.237
2000	81.455	422.448	357.605	129.686	-219.018	-127.559	3.331
2500	82.040	440.694	372.464	170.575	-219.846	-104.614	2.186
3000	82.368	455.683	385.122	211.684	-221.515	-81.425	1.418
3500	82.570	468.397	396.133	252.922	-224.076	-57.887	0.864
4000	82.703	479.432	405.871	294.243	-227.366	-33.927	0.443
4500	82.794	489.178	414.596	335.618	-231.079	-9.528	0.111
5000	82.860	497.905	422.498	377.033	-234.905	15.295	-0.160
5500	82.909	505.805	429.718	418.476	-238.620	40.496	-0.385
6000	82.946	513.020	436.364	459.940	-242.119	66.026	-0.575

^a Units of $J\ mol^{-1}\ K^{-1}$. ^b Units of $kJ\ mol^{-1}$.

From Table 2 it is clear that the formation of phosgene is thermodynamically favourable and is not equilibrium limited until temperatures $\geq 4500\ K$

1.2.4. Catalytic (Industrial) Synthesis

Phosgene is made industrially by the gas phase reaction between carbon monoxide and dichlorine in the presence of an activated carbon catalyst^{1,2,5,6,36-38}. The reaction can easily be performed in the laboratory by passing equimolar flows of the mixed reactants through a glass reactor packed with the carbon catalyst (charcoal). The kinetics of the catalytic formation of phosgene was reported for temperatures between 31-99°C and the rate (r_m) can be given in moles per gram catalyst per hour by the expression (Equation 13)^{1,6}

$$r_m = \frac{kK_{CO}K_{Cl_2}p_{CO}p_{Cl_2}}{(1 + K_{Cl_2}p_{Cl_2} + K_{COCl_2}p_{COCl_2})^2} \quad (13)$$

Where p is the partial pressures and K ($K = k_{ad}/k_{des}$ of the reagent) relates to the adsorption of the reactants on the catalyst surface³⁵. The reaction has been reported to show Langmuir-Hinshelwood kinetics⁵. The equation can be simplified to (Equation 14)⁵;

$$r_m = kp_{CO}p_{Cl_2}^{\frac{1}{2}} \quad (14)$$

The simplified expression does not take into consideration the slowing effect of the formation of phosgene. Using similar conditions to the industrial synthesis^{1,5} of phosgene, the reaction rate can be expressed as (Equation 15);

$$r_m = p_{CO} \left(\frac{p_{Cl_2}}{Ap_{CO} + p_{COCl_2}} \right)^m \quad (15)$$

where A and k are constants and $m = 1/4$

Although the kinetics for the catalytic formation of phosgene has been investigated by Potter and Baron⁶, there are relatively few studies that relate to commercially available carbon catalysts today. An exception is an investigation by Mitchell *et al*² that looked at the rate of phosgene formation for a number of commercially available carbon catalysts.

Ajmera *et al.*¹⁸ studied the synthesis of phosgene using a silicon based micro-fabricated packed-bed reactor. Micro-fabricated chemical systems, in particular silicon-based with sub-millimetre length scales, have a safety advantage over larger systems due to the design of the reactor system. The surface area to volume ratio is increased and the length of reactor is decreased, increasing the area for heat transfer. This reduces thermal gradients and, for an exothermic reaction, reduces the production of hot spots which in turn prevents a reaction runaway. By preventing possible reaction runaway, it allows the system to be run under aggressive conditions, which could be unsafe in larger reactor systems. This method can be particularly beneficial for phosgene synthesis as the development of multi-stage reactor systems involving subsequent processing steps such as the production of isocyanates using phosgene can be carried out within the one reactor device. This prevents the need for storage and/or transportation of phosgene, which has many restrictions and safety precautions that must be adhered to. The results of this experiment showed chlorine was corroding the silicon in the reactors, particularly at elevated temperatures. To overcome this, the silicon was coated with silicon oxide. Results had also shown no by-products were formed, such as silicon tetrachloride, which would form if chlorine reacted with silicon. This was confirmed using a mass spectrometer. It was also confirmed there was complete conversion of chlorine at elevated temperatures, and a significant volume of phosgene produced: 1.1 g/h. Overall, this experiment showed that this could be a potential method used in industry for phosgene production, though further research is needed to determine if the multi-stage reactor system is possible for the addition of the synthesis of isocyanates.⁷

Mitchell *et al.* (2012)² investigated the catalytic production of phosgene over a range of commercially available carbon catalysts. Effects of impurities such as oxygen on catalytic activity, catalyst loading and how this reaction could be scaled up to work in industrial phosgene reactors was investigated. It was shown the temperature of the reactor increases to ~55°C and the rate of phosgene formation increases for all of the catalysts tested, with a direct comparison of the rate of formation at 40°C with the relative catalytic activity of results by Potter and Baron.⁸

Table 3 Different carbon catalysts and their reactivity (a) activity relative to that reported by Potter and Baron^{2,5,6}

Catalyst	COCl ₂ formation rate at 40 °C (mmol min ⁻¹ (g cat) ⁻¹)	Relative activity ^a
Chemviron Solcarb 208C DM	0.62	3.9
Chemviron Solcarb 208C DR-P	0.52	3.2
Donau Supersorbon K40	0.60	3.8
DuPont IPC	0.19	1.2
Norit RB4C	0.61	3.8
Norit RX3 extra	0.76	4.4
Picatal G201	0.48	3.0

^a Relative to results of Potter and Baron.²

The catalysts tested showed Arrhenius temperature dependence and activation energies were calculated to lie within the range of 42-50 kJ mol⁻¹. The Norit RX3 extra catalyst is most active and DuPoint IPC the least. However, there was no correlation with the physical properties of the IPC catalyst and its catalytic activity; it was proposed that the mesoporous nature of the catalyst resulted in its poor activity. The catalyst particle size is an important physical property in the rate of formation of phosgene. A few catalysts (Norit RX3extra, Donau Supersorbon K40 and Picatal G201) were selected to study this. It was shown that pellets had a slower rate of formation of phosgene than that of ground catalyst as shown in figure 6.

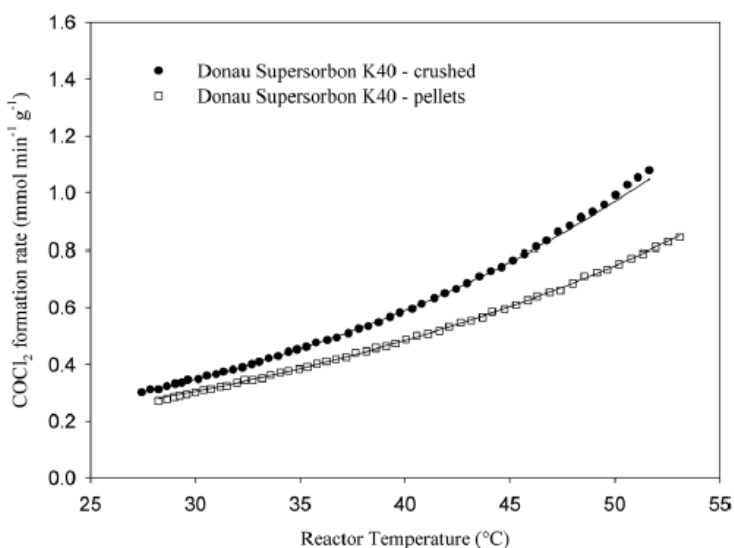


Figure 6 Formation of phosgene vs. reactor temperature for Donau catalyst in crushed and pellet form²

This data was used to determine the catalyst effectiveness of the Donau Supersorbon K40 carbon. This is determined by the ratio of the rate of formation of phosgene on the pellet catalyst

vs. crushed catalyst. Using this data and the reactor model developed by re-parametrising the work by Potter and Barron, an estimate of the effective diffusivity (D_{eff}) of the reactants within the pores of the catalyst was made. This was used to make scale-up predictions of how the catalyst would behave in an industrial sized reactor and to estimate peak temperatures of the catalyst which lie between 547-565°C, an outcome comparable to conditions observed in industry. This is observed in the centreline temperature profiles (Figure 7). The results from this paper show they can also predict how an industrial phosgene reactor will be affected by changing conditions in which they are operated. An example is varying throughput on the centreline temperature profile and its effect using the Donau K40 catalyst. (Figure 7(ii))

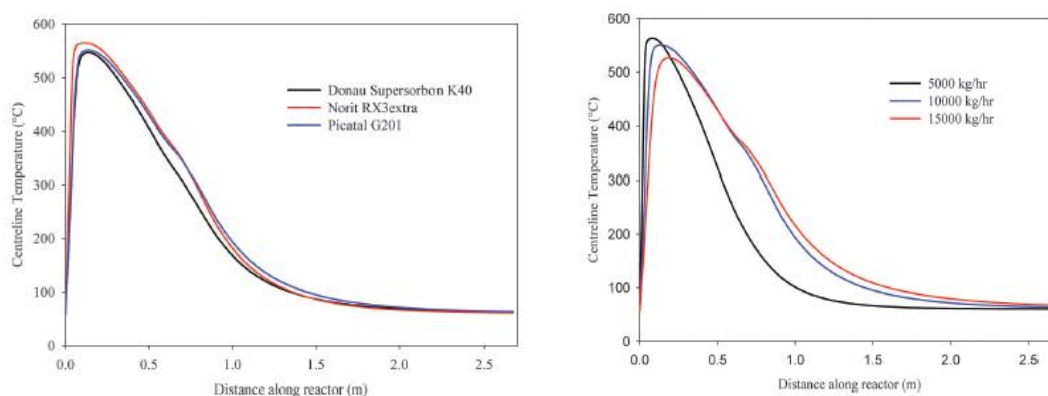


Figure 7 (i) and (ii): (i) Catalysts Donau K40, Norit RX3extra and Picatal G201 centreline temperature profiles in industrial phosgene reactor. (ii) Varying throughput on the centreline temperature profile and its effect using the Donau K40 catalyst²

Analysis into the oxidative stability of the catalyst in the presence of small volumes of oxygen present within the system was also carried out. From this it was shown the range of activation energies of the catalysts agreed with those in literature, (120-170 kJ mol⁻¹), showing the oxidation of carbons to be highly sensitive to temperature. Of the seven catalysts tested, the Norit RX3extra and Donau Supersorbon K40 catalysts are the most stable and thus could be the best catalysts for use in a phosgene manufacturing facility when oxygen is present in the chlorine.

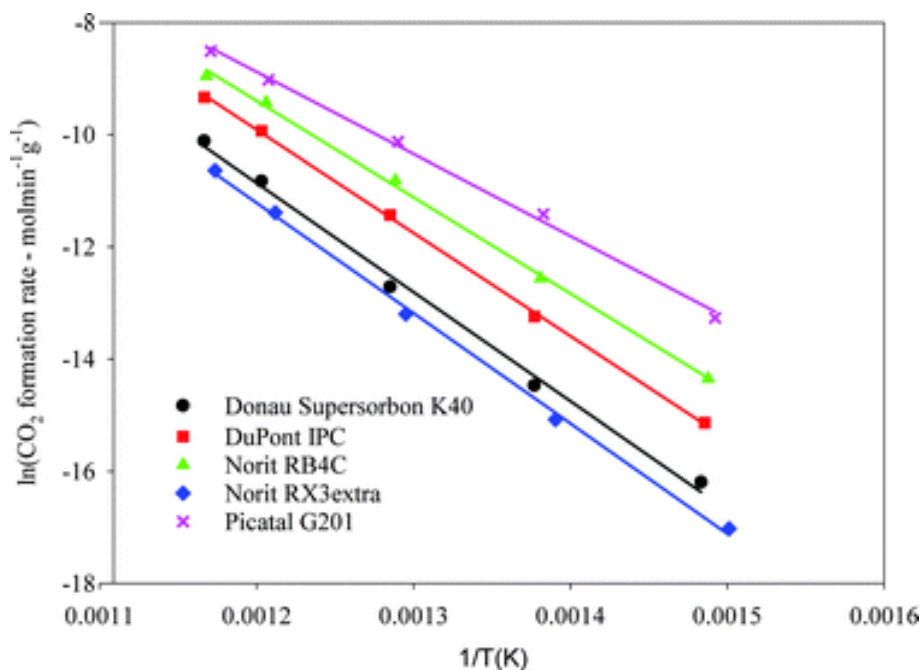


Figure 8 Arrhenius dependence of oxidation rate of carbon²

It was concluded that the Donau K40 catalyst would be the preferred catalyst for a process that contained small traces of oxygen due to a narrower peak in the centreline profile (figure 7ii) and from the oxidation rates calculated.²

Both the Ajmera and Mitchell studies have their own method of phosgene production. The first used micro-bed reactors, which had a safety advantage however, the problem is scaling to meet industrial specification. To produce industrially significant volumes of phosgene, a huge quantity of micro-bed reactors would be required, which is not economically viable.¹⁸ The work carried out by Mitchell *et al.*³ is the basis of the work currently underway in this project. This method can be a highly efficient means of phosgene production if the right catalyst is selected and can be used to model the industrial scale production of phosgene. Sufficient quantities of phosgene are available with a reasonable rate for use industrially with reported conversion rates.

In 2013 an apparatus was commissioned at the University of Glasgow to test the kinetics of phosgene formation³⁹. The study showed that the process operated under a closed mass balance and the activation energy for phosgene formation over the Donau K40 catalyst was 28.4 ± 1 kJ mol⁻¹. The rate law for the process was found to be:

$$r_m = k[CO]^{0.82}[Cl_2]^{0.32} \quad (16)$$

where k is a rate coefficient

This is consistent with early literature^{5,6} and it was concluded that the reaction involving the Donau Supersorbon K40 carbon was an efficient process. This investigation was the foundation for the work discussed in the present study. Indeed, the work documented here makes use of the apparatus commissioned during the Masters by Research studies³⁹ building on these efforts. In particular, this would seek to develop a mechanistic understanding of the surface chemistry leading to phosgene formation. Subsequent kinetic work considers the situation when small quantities of halogen contaminants are present in the feedstream.

In 2016, Gupta et al^{40,41} released a communication which investigated phosgene formation using fullerenes as a model catalysts as they have no defects or other surface functional groups. The reaction was first tested over C₆₀ to check the suitability as a model phosgene catalyst. Once reversible adsorption of chlorine was established the steady production of phosgene was observed. They propose that the reaction precedes via a two-step Eley-Rideal mechanism.

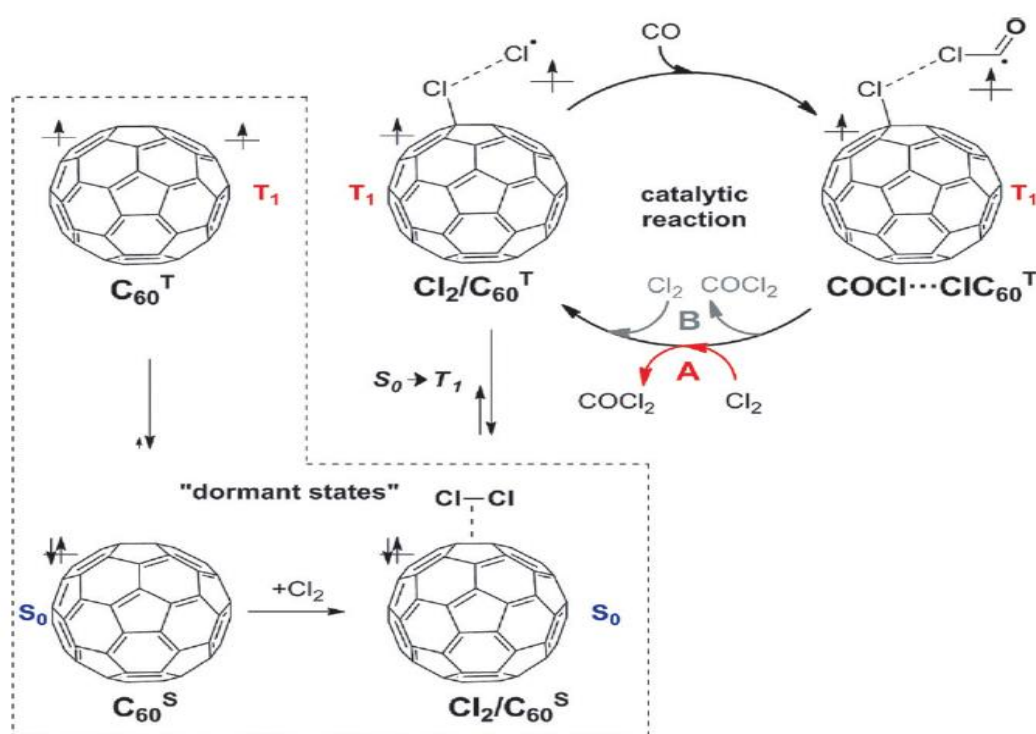


Figure 9 Proposed mechanism for Cl₂/C₆₀ T catalysed COCl₂ formation following an Eley-Rideal mechanism. The potentially dormant off-cycle species are shown in the dashed rectangle, while alternative paths for the regeneration of the catalytic species Cl₂/C₆₀ A and B⁴⁰

The reaction scheme was deduced from the order of reaction, which was reported as being first order in chlorine and CO. The activation energy over the fullerene catalyst was significantly lower (18 kJ mol⁻¹) than that of conventional carbon catalyst, indicating the effects of local surface environment on the active sites.

1.2.5. Oxy-chlorination

In industry, phosgene is used to make isocyanates, however, the chlorine atoms are usually partitioned as HCl as a by-product. It would be economically beneficial to recycle the chlorine from the HCl by-product and use it to perform chlorinating processes, for example, during phosgene synthesis^{1,42-44}. The direct transformation of HCl to H₂ and Cl₂ is thermodynamically unfeasible. However, coupled with a thermodynamically favourable reaction, the reaction becomes possible via a Deacon catalytic oxidation process. The process combines the oxidation of Cl⁻ and reduction of oxygen to produce Cl₂ and water. The process requires high temperatures (400-450°C) and typically uses a copper chloride catalyst⁴³.

Oxy-chlorination could be used as a novel way of producing phosgene using the HCl as the chlorine source in the presence of a copper catalyst. The mechanism is catalytic; however, it is a three step process, two of which are regeneration of the catalyst to a copper (II) species. The mechanistic scheme is as follows (Figure 10)^{42,43,45};

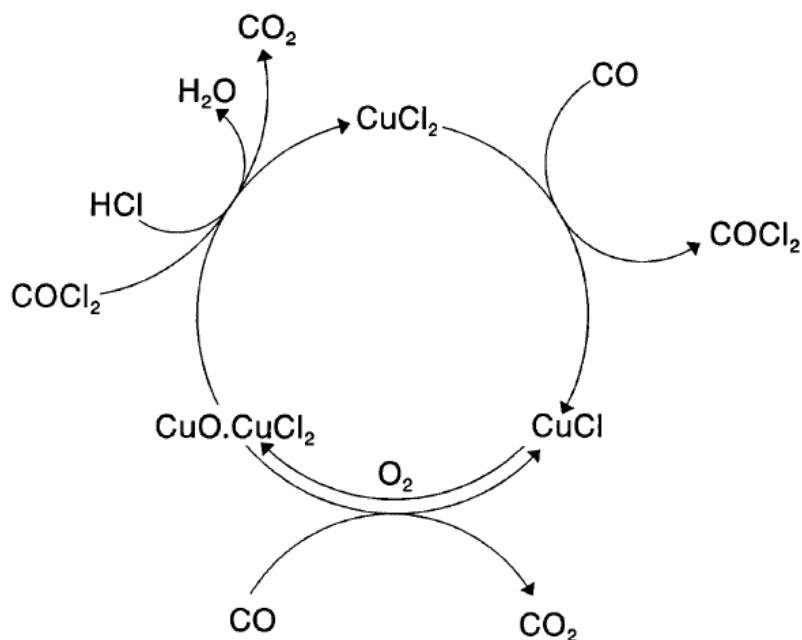


Figure 10 Theorised Oxychlorination mechanism¹

This reaction could be performed on the same location site as the production of isocyanates. However, the reaction rates of this process are found to be slow and have low conversions.

Recent studies carried out by Weber and colleagues^{42,43,45} investigated the chemistry of silica supported CuCl_2/KCl . These investigations concluded that performing the catalyst regeneration in two steps (Figure 11), avoids unwanted side reactions such as the Deacon reaction and the disproportionation reaction. These studies highlight a renewed interest in the chemical industry for this valuable type of process. Oxychlorination is beyond the scope of the current work but, nevertheless, this recently initiated a parallel research project to this investigation that examined aspects of an alternative route to phosgene production⁴⁶. Such recent activity reflects a dynamic in this profitable area of the chemical manufacturing industry.

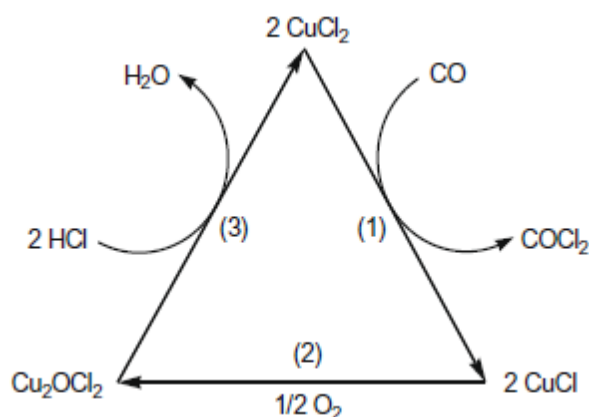


Figure 11 The mechanism for (1) phosgene synthesis, (2) and (3) regeneration of the catalyst in two steps⁴³

1.2.6 Eckert cartridge

A method for the safe production of phosgene has been developed by Eckert⁴⁷. The cartridges (purchased from Sigma-Aldrich) produce phosgene from solid triphosgene to produce three moles of phosgene using an amine or imine based catalyst^{47,48}. The reaction is activated at the temperature when triphosgene begins to melt ($\sim 353 \text{ K}$) (Figure 12).

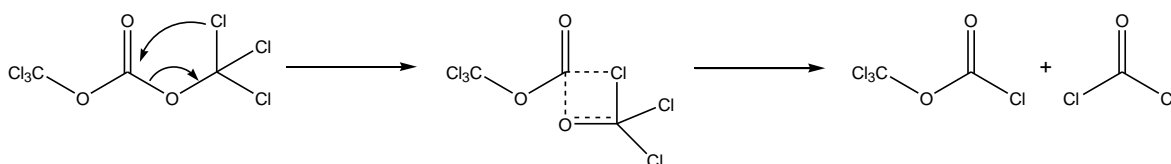


Figure 12 First step of triphosgene breakdown to produce phosgene⁴⁷

The reaction rate for phosgene production is a function of reaction temperature (Figure 13) as these have been calculated and can be manipulated to carry out laboratory studies using gas phase phosgene.

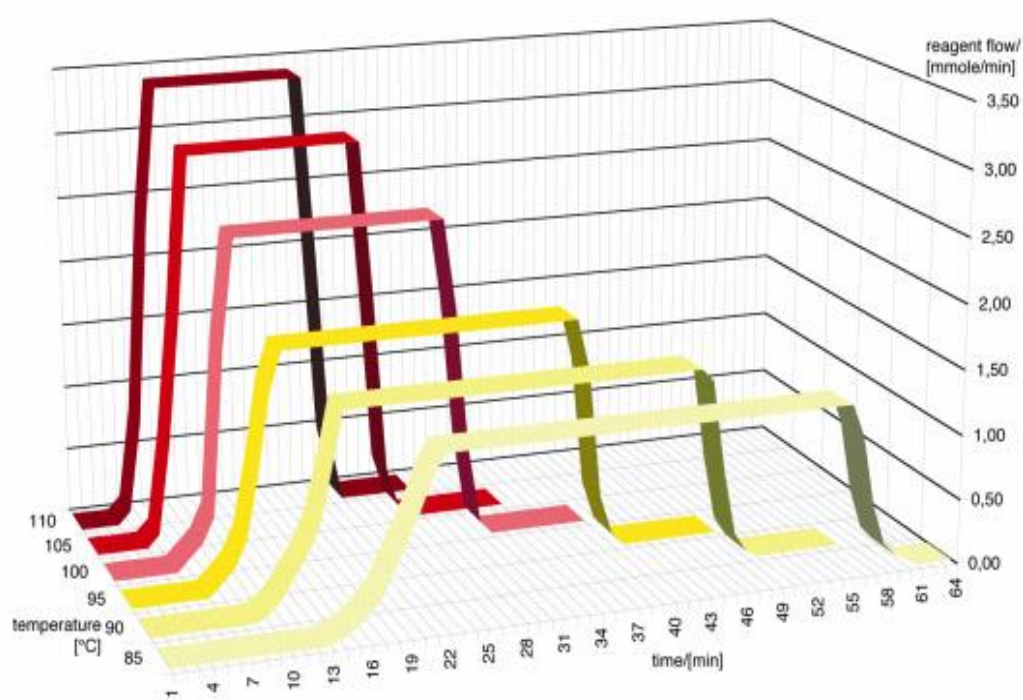


Figure 13 Release of phosgene from the Eckert cartridge⁴⁷

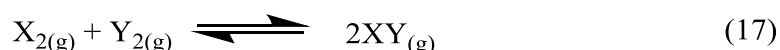
1.2.7 Alternative routes to phosgene

There are several different routes to phosgene other than the conventional catalytic, oxychlorination and light/thermal synthesis. Phosgene is reported to be formed at a gas diffusion anode when electrolysing a sodium chloride solution while CO is supplied to the anode^{1,49}. Carbon monoxide reacts with a number of inorganic chlorides to produce phosgene. The reaction with CCl₄ and CO is reported to produce considerable quantities of phosgene⁵⁰. Phosgene can be made by reacting CO with other inorganic chlorides *i.e* NOCl, SCl₂, SbCl₅, PbCl₂, NiCl₂, AuCl₃, AgCl, RuCl₃, PtCl₂ and PtCl₄.⁵¹

1.2.8 Interhalogen species

The halogens or group 17 elements can form compounds among themselves creating interhalogens which are unique to this group of elements. The binary interhalogens usually molecular compounds with a formula of XY, XY₃, XY₅ and XY₇.⁵² All the interhalogen species are strong oxidising agents with intermediate properties of their parent halogens.

The diatomic halogens readily form in the gas phase



In all cases the interhalogen species is the favoured product. However, the tendency is weakest for BrCl, where K is only ~ 10 .⁵³ Therefore, appreciable amounts of Br₂ and/or Cl₂ are always present along with BrCl for any mixing ratio of the parent gases. In a recent study, the UV visible spectra of Br₂, Cl₂ and BrCl were used and the equilibrium constant for the interhalogen reaction was found to be 6.4.⁵⁴

1.2.9 Mechanisms of Adsorption

There are two main mechanisms by which species reacts on the surface of heterogeneous catalysts. The first of which is the Langmuir-Hinshelwood (LH) mechanism (figure 14) where both of the reactants are adsorbed onto the surface of the catalyst and react. The reaction takes place on the surface of the catalyst. The rate law is expected to be second order with respect to the adsorbed species⁵⁵.

The second of the two mechanisms is the Eley-Rideal (ER) mechanism, where one of the species adsorbs onto the surface of the catalyst whilst the other collides with the adsorbed molecule before the product is desorbed for the surface (Figure 14). Almost all catalytic reactions are believed to proceed via the LH mechanism and only a few reactions have been identified as utilising the ER mechanism.

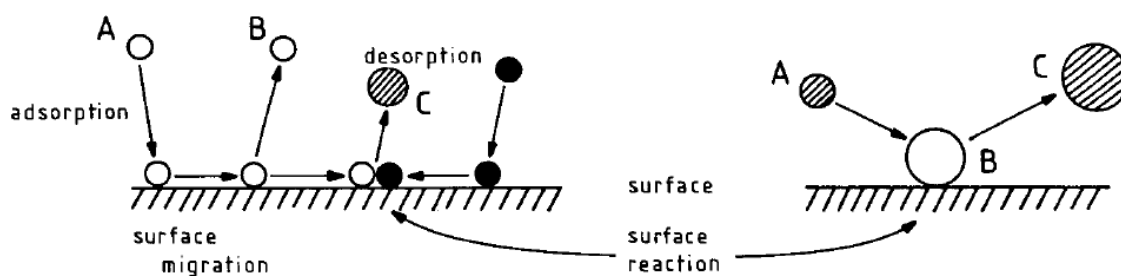


Figure 14 Mechanisms of adsorption (left Langmuir- Hinshelwood and right Eley- Rideal)⁵⁶

However, these mechanisms are considered to be ideal cases and the mechanisms of any reaction should lie in between the two limits⁵⁶.

1.3 Analytical techniques

1.3.1. Infrared Spectroscopy

Infrared spectroscopy is an important technique that is used to measure molecular vibrations. The infrared region of the electromagnetic spectrum is sub-divided into 3 ranges, the near infrared (1 – 2.5 μm), the mid infrared (2.5 – 50 μm), and the far infrared (beyond 25 μm).⁵⁷ The most useful vibrations within an organic compound occur in the range of 2.5 – 16 μm .⁵⁷ with an infrared spectrometer normally recording in the range 4000 – 500 cm^{-1} . Each functional group has a specific vibrational frequency, providing a method of identification. The frequency at which a group vibrates is determined by interatomic distances, bond angles and force constants within the molecule^{29,57}. The simplicity, accuracy and versatility of IR spectroscopy make it one of the most popular techniques for identification of organic compounds⁵⁸.

Infrared can also be across all states liquids, gases and solids; the application of the infrared in this project is gaseous. Gases have densities several orders of magnitude smaller than liquids, so the path length of the cell needs to be longer, typically 10 cm or longer. The gas cell can be filled by flushing or connecting directly to a gas line⁵⁹. This makes infrared a powerful tool for following molecules with distinct vibrational modes in the gas phase, *i.e.* phosgene.

1.3.2. Ultraviolet and Visible Absorption Spectroscopy

Ultraviolet-visible (UV/Vis) spectroscopy is concerned with measuring electronic transitions in compounds in the region between 180 and 1100 nm. Similar to the IR, the spectral region is split into three sections, near UV (185 – 400 nm), visible (400 – 700 nm), near infrared (700 – 1100 nm).⁷ It is difficult to distinguish between different functional groups in UV/Vis spectroscopy. However, this technique is a useful tool for quantitative measurements. This type of spectroscopy is based on two laws; Beer's law states that absorption is proportional to the number of absorbing molecules; Lambert's law states that the fraction of the incident light adsorbed is independent of the intensity of the source.⁵⁸ These laws are combined to give the equation 18 below⁵⁸:

$$\text{Absorbance} = \log_{10} \frac{I_0}{I} = \epsilon c l \quad (18)$$

Where:

I_0 = incident monochromatic light intensity

I = transmitted monochromatic light intensity

ϵ = molar extinction coefficient ($M^{-1}L \text{ cm}^{-1}$)

c = concentration ($M L^{-1}$)

l = path length (cm)

In order to measure the absorbance of a compound the gas/liquid is flowed through a transparent gas cell in which a beam of light is passed through. A second beam of light is passed through a nitrogen atmosphere as a reference. The difference in transmission is used to create the absorbance spectrum.

1.3.3 Electronic Transitions

A number of transitions can be measured in UV/Vis spectrometry. These include $\sigma \rightarrow \sigma^*$, $n \rightarrow \sigma^*$, $n \rightarrow \pi^*$, $\pi \rightarrow \pi^*$ and $d \rightarrow d$ transitions. These transitions appear at different wavelengths with different intensities. Therefore it is useful to look at different regions of the spectrum with different concentrations of the sample solution. This technique can also be used to look at molecules in the gas and liquid phase.⁵⁴

1.4. Characterising Catalysts

1.4.1 X-Ray Diffraction

X-Ray Diffraction (XRD) is a non-destructive technique which can be used to obtain structural information on crystalline materials⁶⁰. More specifically it can be used to investigate and identify a various number of parameters: identification of phases and compounds, determination of crystalline structures and lattice parameters, degree of crystallinity, orientation and size of single crystals, and the analysis of phases and surface texture.

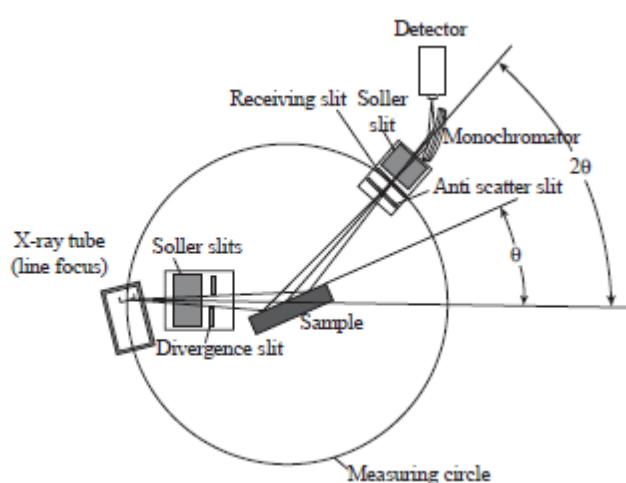


Figure 15 Schematic of X-Ray Diffractometer⁶⁰

Solids can be described as amorphous or crystalline. In crystalline solids the atoms are arranged in a highly ordered pattern which extends in all spatial directions. Amorphous structures have random arrangements of atoms that lack long range order. Materials used in heterogeneous catalysis usually consist of a mixture of different phases. Separation of these phases can result in loss of activity or complete deactivation of the catalyst^{61,62}.

A monochromatic x-ray beam is projected into the sample. The wavelength of x-rays is equal to the magnitude of the spacing between atoms. This allows x-rays to be diffracted in crystalline lattices. By varying the angle 2θ (see Figure 15) plot of the angle position vs. intensity of the resulting peaks creates a diffractogram characteristic of the sample analysed. If multiple phases are present the diffractogram will contain a combination of all phase patterns⁶².

One advantage of using XRD in the study of catalysis is that samples can be studied *in situ*¹. The strength of XRD for catalyst characterization is that it gives clear structural information

on crystallites that are sufficiently large, along with an estimate of their size, and it can reveal this information under reaction conditions.

1.4.2 BET

BET is named after Brunauer, Emmett and Teller who developed this technique in 1938⁵⁵. BET was the first method used to measure the specific surface of finely divided and porous solids. It is used mainly to give specific surface areas by analysing gas adsorption data. Pore size and pore distribution can also be calculated using the BJH method^{55,63}.

BET theory is an extension of Langmuir theory, which is a theory of adsorption for monolayers to multilayers. It makes the assumptions that the first layer of adsorbate is taken up with a specific heat of adsorption (H_1) whereas the second and subsequent layers are characterised by heats of adsorption equal to the latent heat of evaporation (H_L). On considering the equilibrium with adsorbate and each layer the BET equation can be written as^{55,64}:

$$\frac{p}{V(p_0-p)} = \frac{1}{V_m c} + \frac{c-1}{V_m c} \cdot \frac{p}{p_0} \quad (19)$$

Where V is the volume of gas adsorbed, p is the pressure of the gas, p_0 is the saturated vapour pressure of the liquid at the operation temperature, V_m is the volume equivalent of an adsorbed monolayer. The BET constant is given by:

$$c = e^{\left(\frac{H_1-H_L}{RT}\right)} \quad (20)$$

A plot of $p/V(p_0-p)$ versus p/p_0 is usually linear within the range 0.05 to 0.35. The slope and intercept allow values for c and V_m to be calculated³. Before analysis, the sample must be purged of all impurities bound to the surface. This is generally done under vacuum or constant flowing inert gas⁶⁵. The BET method is ideally suited to determine the surface area of porous materials *e.g.*, activated carbon.

1.4.4. Scanning Electron Microscopy

Scanning electron microscopes (SEM) are the most commonly used equipment for electron microscopy. An SEM is able to examine the microscopic structure by scanning the surface of materials. An SEM image is formed by a focused electron beam that scans over the surface area of a specimen. An SEM can be used to obtain chemical information from a specimen and examine the surface microstructure and morphology^{60,62}.

A scanning electron microscope consists of an electron gun and a series of electromagnetic lenses and apertures. The electron beam emitted is condensed to a fine probe for surface scanning. The probe scanning is operated by a beam deflection system contained within the instrument. The deflection system scans the sample line by line and the signal electrons emitted by the sample are detected, amplified and used to generate the image⁶⁰.

1.4.5 Energy Dispersive X-ray spectroscopy

Energy Dispersive X-ray spectroscopy (EDX) is a technique which can be used to identify the presence and quantities of chemical elements by detecting characteristic X-rays that are irradiated from a high energy beam⁶⁰. The most commonly used spectrometers for X-ray spectroscopy include X-ray fluorescence spectrometers and microanalyzers in electron microscopes. When a high energy particle, such as an X-ray photon, an electron or a neutron, strikes an electron in the inner shell of an atom, the energy of the particle can be high enough to knock an electron out of its original position in an atom. The knocked-out electron leaves the atom as a 'free' electron and the atom becomes ionized. Because ionization is an excited state, the atom will quickly return to its normal state after refilling the inner electron vacancy by an outer shell electron. In the meantime, the energy difference between an outer shell electron and an inner shell electron will generate either an X-ray photon (characteristic X-ray) or another characteristic free electron that is emitted from the atom. The latter is called as the Auger electron, which also can be used for elemental analysis

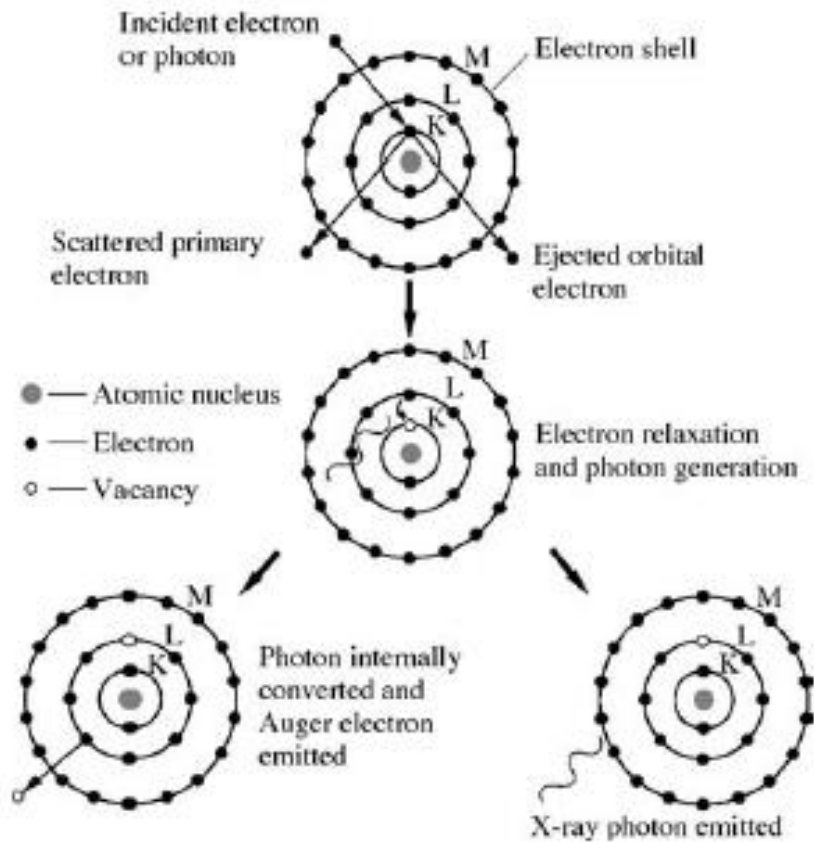


Figure 16 Excitation of a characteristic X-ray photon or an Auger electron by a high energy X-ray photon or electron⁶⁰

The energy of characteristic X-rays is the energy difference between two electrons in different shells. It is well defined and dependent on the atomic number of the atom. For example, the energy of the X-ray $K\alpha$ line is the energy difference between a K shell electron and L shell electron. Thus, we can identify a chemical element from the characteristic X-rays that it emits. Moseley's Law defines the relationship between wavelength of characteristic X-rays (λ) and atomic number (Z).

$$B \lambda = \frac{1}{(Z - \sigma)^2} \quad (21)$$

B and σ are constants that depend upon the specific shells. This relationship can also be expressed as the energy of characteristic X-rays and atomic number using the energy–wavelength relationship (Equation 21)

1.4.6 Raman Spectroscopy

Raman spectroscopy is an alternative, and often a complementary method to measure vibrational spectra compared to infrared. Raman spectroscopy relies on inelastic scattering, or Raman scattering, of monochromatic light, usually from a laser in the visible, near infrared, or near ultraviolet range. The laser light interacts with molecular vibrations, and other excitations in the system, resulting in the energy of the laser photons being shifted up or down. The shift in energy gives information about the vibrational modes in the system. The intensity of bands in the Raman spectrum of a compound are governed by the change in polarizability, that occurs during the vibration. A Raman spectrometer may consist of a light source usually a Nd:YAG laser, a charge-coupled-device (CCD) array detector, and a polychromator⁵⁷.

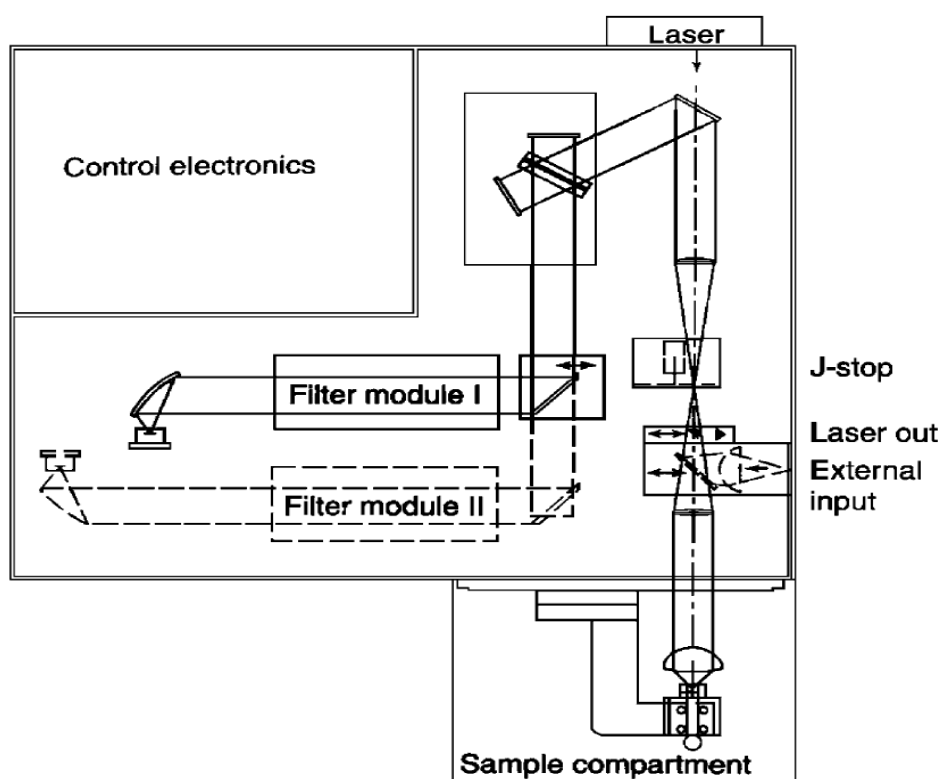


Figure 17 Optics of a Raman spectrometer

Raman spectroscopy can identify the S-S, and C=C stretching bands, that are often so weak as to be essentially unrecognizable in the IR spectrum. This makes Raman ideal for studying activated carbons⁶⁶⁻⁷⁰.

1.5.0 Aims and Relevance

Phosgene is a widely used chemical intermediate and can be synthesised in many ways. Due to the toxic nature of the gas there are academic interests in using non-phosgene synthesis routes. An example of this 'green' approach to synthesize polyurethane precursors was demonstrated by work originating from Avelino Corma's group in Valencia⁷¹. Here, gold nanoparticles supported on nano-particulated ceria catalyze the selective N-carbamoylation of 2,4-diaminotoluene, an important aromatic amine for polyurethane production⁷¹.

However despite these academic reports, phosgene is predominantly synthesized industrially by the gas phase reaction of carbon monoxide and chlorine in the presence of an activated carbon catalyst^{1,2,40,41}. Surprisingly for such an important process, there have been relatively few studies to investigate the kinetics of this process for modern activated carbon catalysts. This work is an extension of a Masters by Research submitted in 2014. That work primarily involved the commissioning of an experiential apparatus housed within the school of chemistry's Chemical Process Fundamentals Laboratory³⁹.

This investigation aims to:

- Explore the kinetics over an activated carbon catalyst (Donau Supersorbon K40).
- Determine the rate law, activation energy, and the adsorption coefficients over the Donau K40 carbon catalyst.
- Propose a reaction mechanism for the phosgene production process.
- Once the understanding of the phosgene synthesis kinetics have been developed, the effects of a bromine impurity in the feed stream on the rate of phosgene production will then be investigated.

Chapter 2-Experimental

2.0 Introduction

This chapter will describe the apparatus developed in the Chemical Process Fundamentals Laboratory to test the kinetics of the gas phase reaction between CO and Cl₂ to form phosgene. The apparatus, safety features and operational conditions will be described in the first section. The present description includes advances incorporated into the hardware and experimental protocols that go beyond those reported in the Masters by Research thesis³⁹

The spectroscopic tools used for the analysis and quantification procedures will be described. The spectroscopic features of all the reagents and products will be described and the operational preparation of the catalyst defined.

The second section of this chapter will describe how the apparatus was modified to accommodate a bromine co-feed. Also, the quantification procedures to accommodate the bromine co-feed are defined.

2.1 Conventional phosgene synthesis test apparatus

The conventional phosgene synthesis test apparatus was developed further from the apparatus used in the Masters work³⁹. The apparatus was modified to include a source of phosgene (BOC 10% in He) allowing quantification for all reagents in the process. The apparatus was constructed out of 1/8" stainless steel Swagelok tubing and the schematic of the test facility is shown in Figure 16.

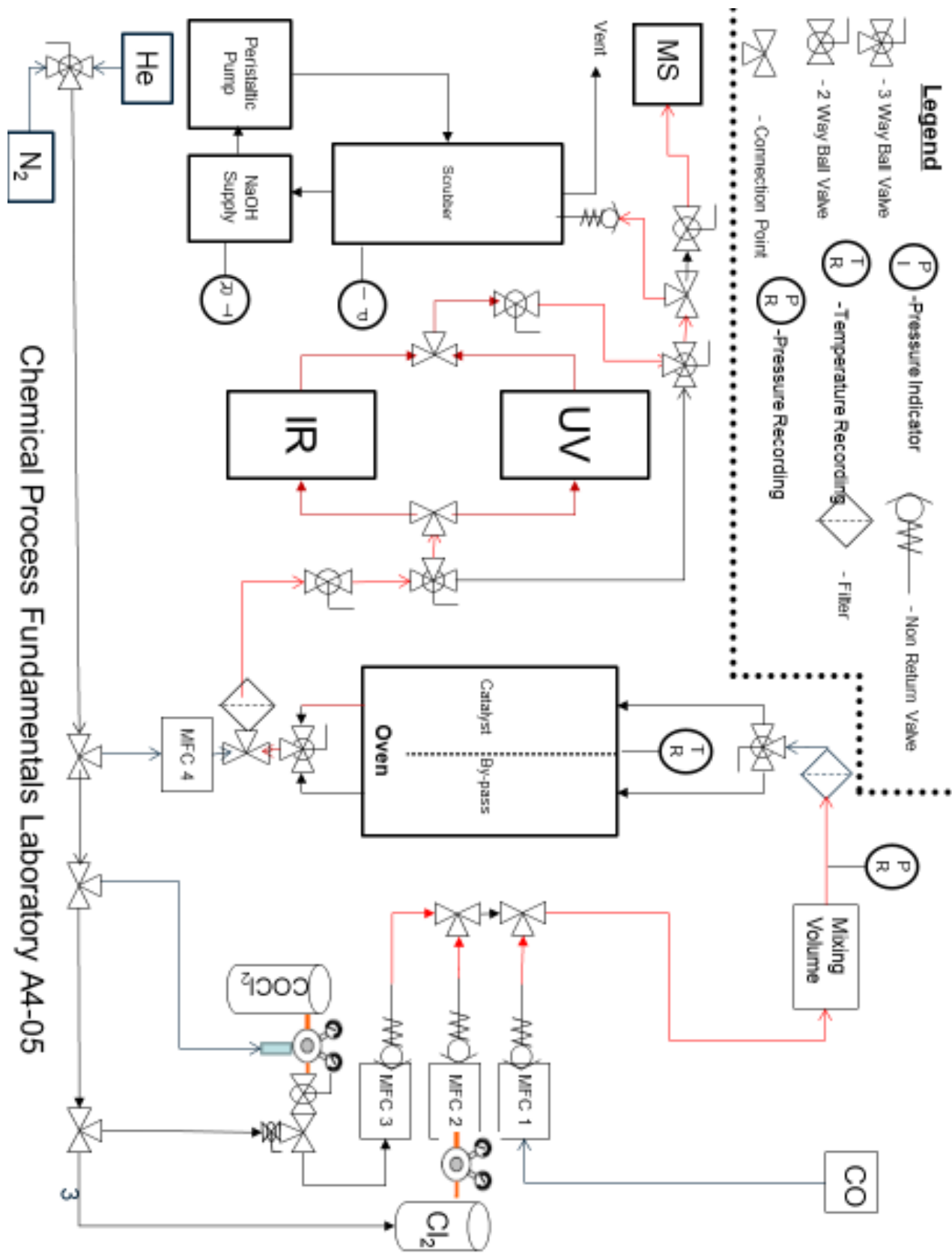


Figure 18 Phosgene synthesis apparatus

The total flow through the system was kept constant at $159 \text{ cm}^3 \text{ min}^{-1}$, with standard flows being set at:

CO (BOC CP Grade) : $5 \text{ cm}^3 \text{ min}^{-1}$

Cl₂ (Sigma purity $\geq 99.5\%$): $4 \text{ cm}^3 \text{ min}^{-1}$

N₂ (BOC 99.998%) dilution (post-reactor): $100 \text{ cm}^3 \text{ min}^{-1}$

N₂ (BOC 99.998%) drive(pre-reactor): $50 \text{ cm}^3 \text{ min}^{-1}$

The lines of the apparatus were constructed of stainless steel 1/8" Swagelok tubing. Mass flow controllers (Hastings HFC-202) and control box (Chell 1.04) were used to control the flows of gases through the system, with non-return valves positioned after each in order to ensure the flow is in one direction. The control box was operated remotely using Display-X software. The spectrometers housed in Perspex boxes and are purged with nitrogen using a Peak Scientific NitroGen N118LA. The total flow through the gas cells was kept constant at $159 \text{ cm}^3 \text{ min}^{-1}$ during the majority of the experiments.

The initial flow rate (A_0) was determined by passing the flow over the bypass containing ground quartz (250-500 μm) of comparable volume to the reactor containing catalyst. The oven was a converted GC oven (Shimadzu GC-14A) which has a temperature range of 20-400°C. On exiting the oven, the reactants are diluted further before passing through all the spectrometers, and/or over a bypass which just uses the mass spectrometer in order to maintain detection linearity and avoid saturation of the detectors. The reactor exit gases are then analysed by mass spectrometry, a quadrupole mass spectrometer (MKS Spectra Microvision Plus RGA) that sampled the eluting gas stream via a fine control valve. The infrared spectrometer used is a Thermo Nicolet Is10 spectrometer which has an optimal spectral range of 7800-350 cm^{-1} and is controlled using the OMNIC 8 software. The UV-visible spectrometer used is a Shimadzu UV-1800 which has a wavelength range of 190-1100 nm and is controlled using the UV Probe software. Both spectrometers connect to the computer via USB allowing the entire system to be controlled remotely

2.1.2 Safety

As this project involves the use and production of highly toxic and harmful gases, a chemical scrubber is used at the end of the line to ensure a zero-emission facility. It is mainly in position to destroy any phosgene that is produced but it also efficient at destroying chlorine. The scrubber contained sodium hydroxide (10 % NaOH) which reacts with the phosgene to produce sodium chloride (NaCl), carbon dioxide (CO₂) and water (H₂O). All experiments are carried out in a walk in fume hood.

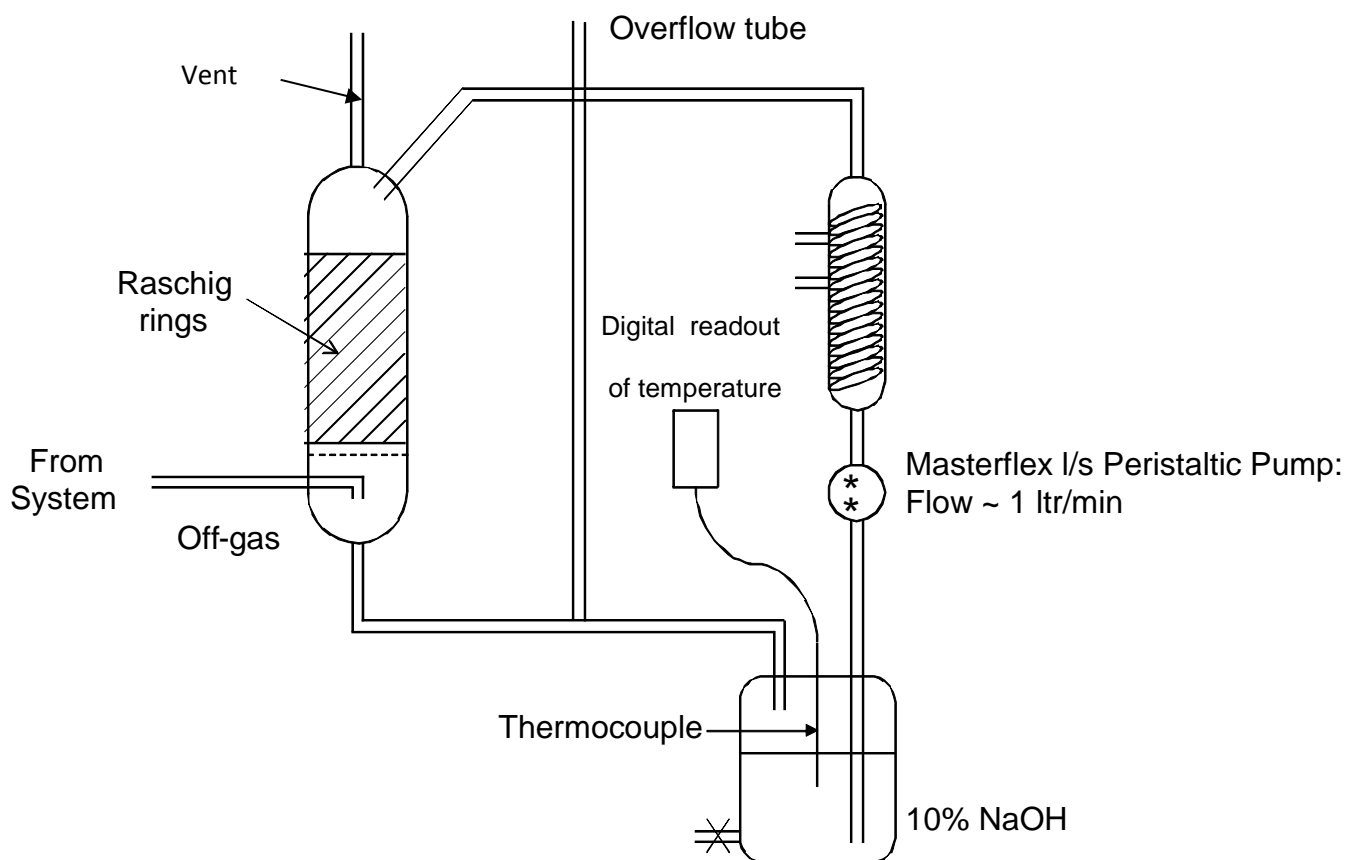
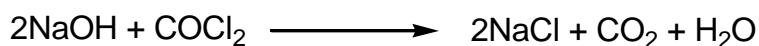


Figure 19 Chemical scrubber design

Also, the laboratory is equipped with two phosgene and one carbon monoxide (Crowcon Xgard) sensors controlled by a Crowcon Gasmaster which detects any releases of the hazardous gases into the lab. Another safety system in place is a handheld phosgene and chlorine sensor (Drager X-AM 5000) detectors to test the air in the lab before entering. Another precaution is phosgene detection badges (Compur) and personal carbon monoxide detectors (Honeywell Gas Alert Clip Extreme) worn by all occupants of the lab as well as detection tape (Honeywell Analytics) which changes colour in the presence of phosgene which was placed beside the experiment. The spectrometers are also a vulnerable point in the experiment, so they are placed in Perspex boxes which are purged by a constant flow of nitrogen (PEAK). The laboratory operated a lone worker policy and a walkie talkie system was available when operating for extended time periods. The apparatus can be operated remotely i.e for extended runs, the only time personal intervention into the walk in fume cupboard was to load and discharge the catalyst in the reactor.

2.1.3 Gas Cells

There were two gas cell designs used throughout this project both were made in the Glassblowing workshops of the University of Glasgow. Gas cell 2 was based on the design of commercially available gas cell from PIKE Technologies used in the Masters work³⁹

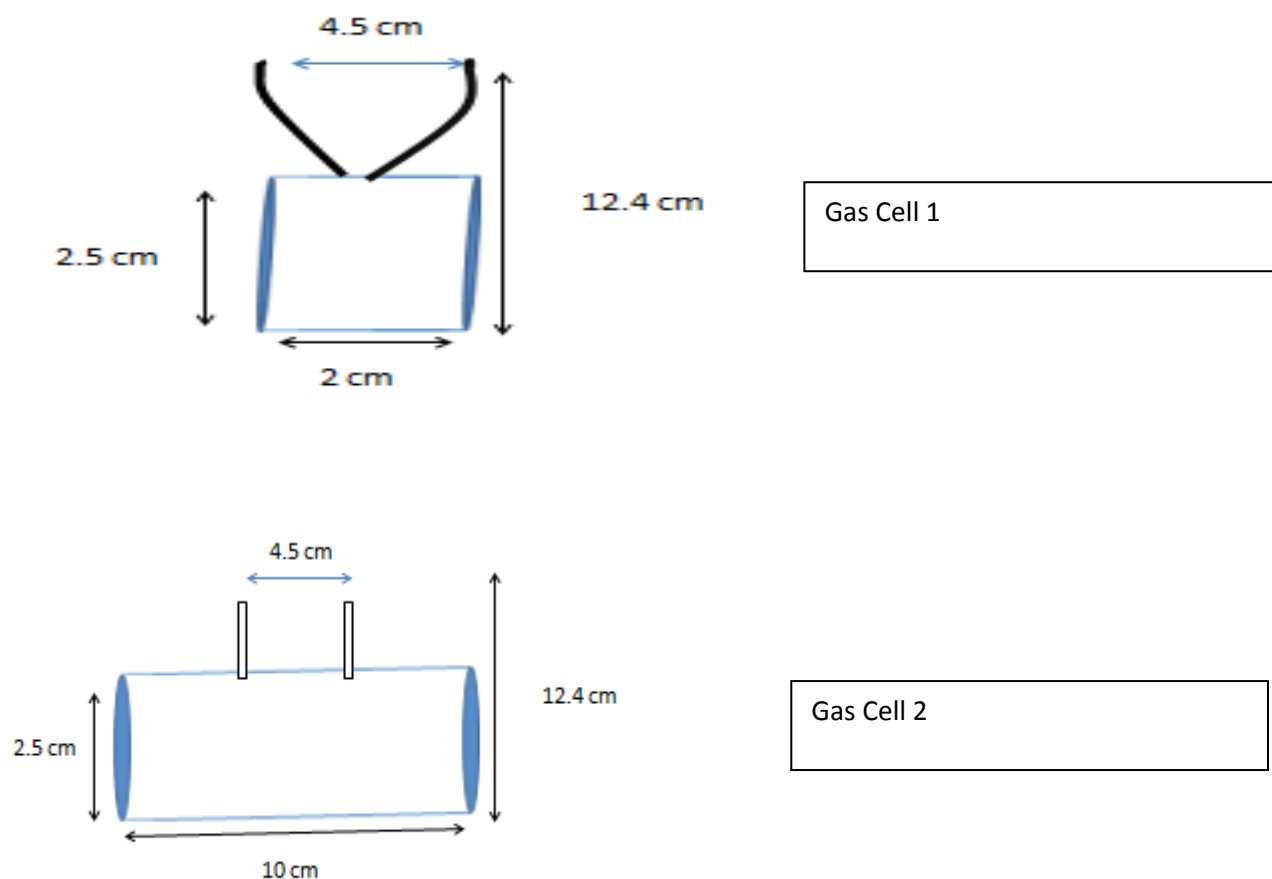


Figure 20 Gas Cell designs

Both gas cells connect in the flow system via $\frac{1}{4}$ " Cajon fittings with the only difference being the path length of the two cells. This controls the intensity of the signals in the infrared spectra. The gas cells body was made out of Pyrex. Gas cell 1 was only used with the infrared spectrometer and had KBr windows. Gas cell 2 design was used in both infrared and uv-visible spectrometer using KBr and quartz windows respectively. The windows were glued on to the gas cells using araldite. Two gas cells were used to avoid detection saturation of the detector and ensure the Beer-Lambert Law still applied. The system was periodically checked to ensure gas tightness.

2.2 Spectroscopy

2.2.1 Carbon monoxide (Infrared)

All infrared (Thermo Nicolet Is10i) spectra were taken as an average of 32 scans and an absorbance resolution of 4 cm^{-1} (47 s total scan time). Infra-red spectroscopy provides a sensitive method to identify phosgene formation and carbon monoxide consumption. The carbon monoxide is easy to follow by its C-O stretching mode which shows P and R¹⁹ branch characteristics at 2100 cm^{-1} . An example spectrum can be seen below²⁹

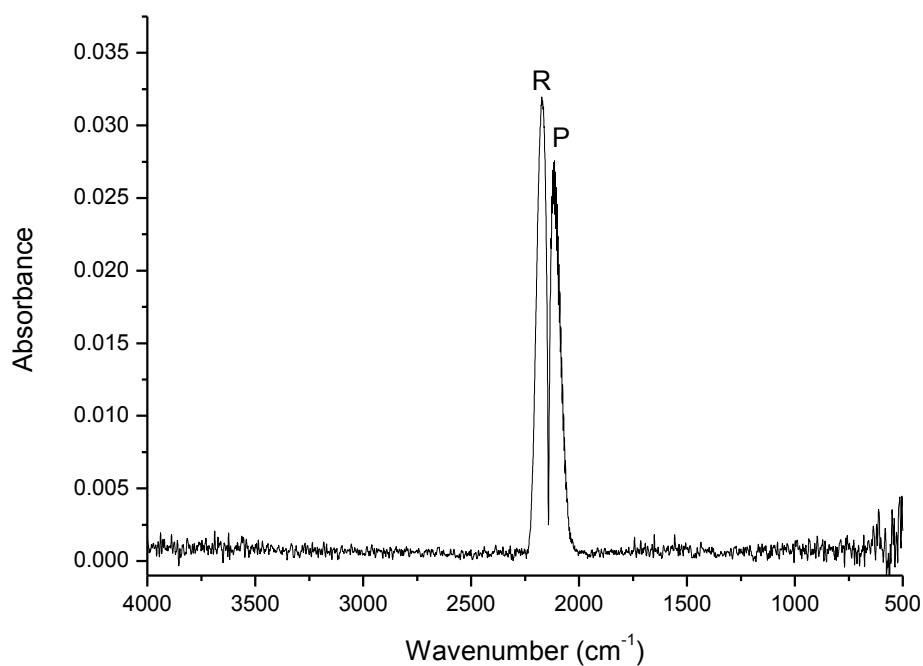


Figure 21 : Example spectrum taken at room temperature with a flow rate of CO of $5\text{ cm}^3\text{ min}^{-1}$ in a total flow of $159\text{ cm}^3\text{ min}^{-1}$, i.e. $5\text{ cm}^3\text{ min}^{-1}$ CO, $154\text{ cm}^3\text{ min}^{-1}$ N₂.

Table 4 Main band assignments for Fig. 21

Peak position cm^{-1}	Description
2169	C-O stretch (R-branch rotation)
2119	C-O stretch (P-branch rotation)

2.2.2 Chlorine (UV visible)

All UV (Shimadzu Uv-1800) measurements were made at a scan rate of 360 nm min^{-1} in the absorbance mode. An example UV- visible spectrum can be seen below. The chlorine signal is distinctive, with a broad peak with a λ_{max} of 330 nm for the $\pi^* \rightarrow \sigma^*$ transition²⁰

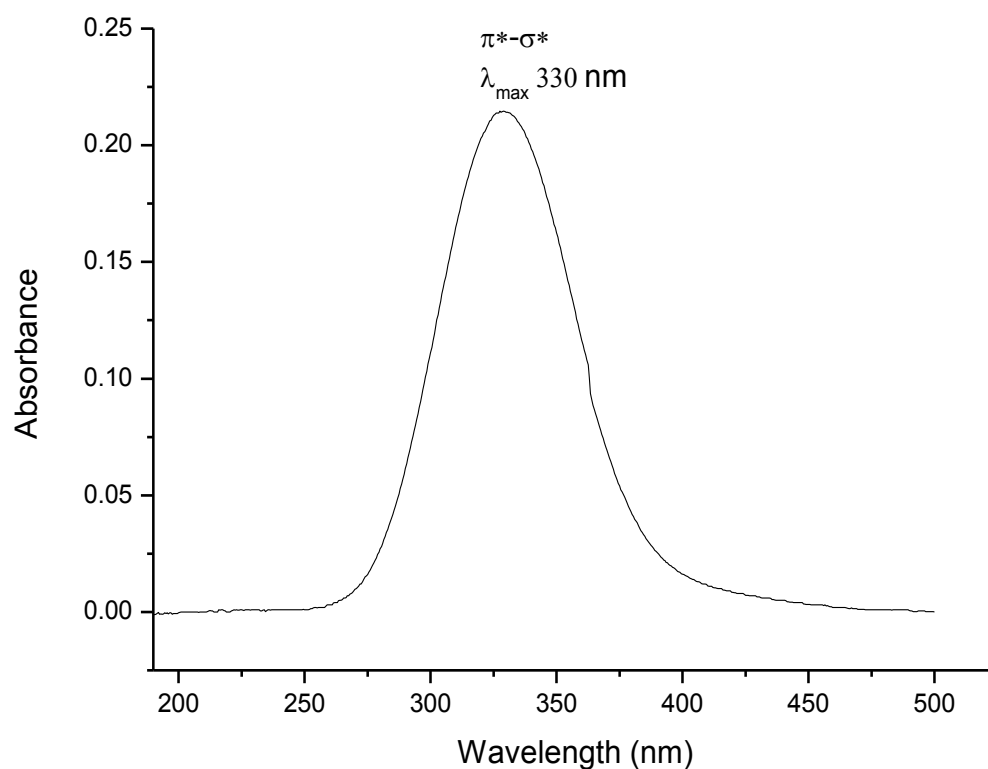


Figure 22 Example spectrum taken at room temperature with a flow rate of Cl_2 of $3 \text{ cm}^3 \text{ min}^{-1}$ in a total flow of $159 \text{ cm}^3 \text{ min}^{-1}$, i.e. $3 \text{ cm}^3 \text{ min}^{-1} \text{ Cl}_2$, $156 \text{ cm}^3 \text{ min}^{-1} \text{ N}_2$

2.2.3 Phosgene

Phosgene is a simple molecule that can be monitored easily spectroscopically and has a C_{2v} point group. Phosgene has distinct vibrations visible in the infrared region of the spectrum. The vibrations are shown below.

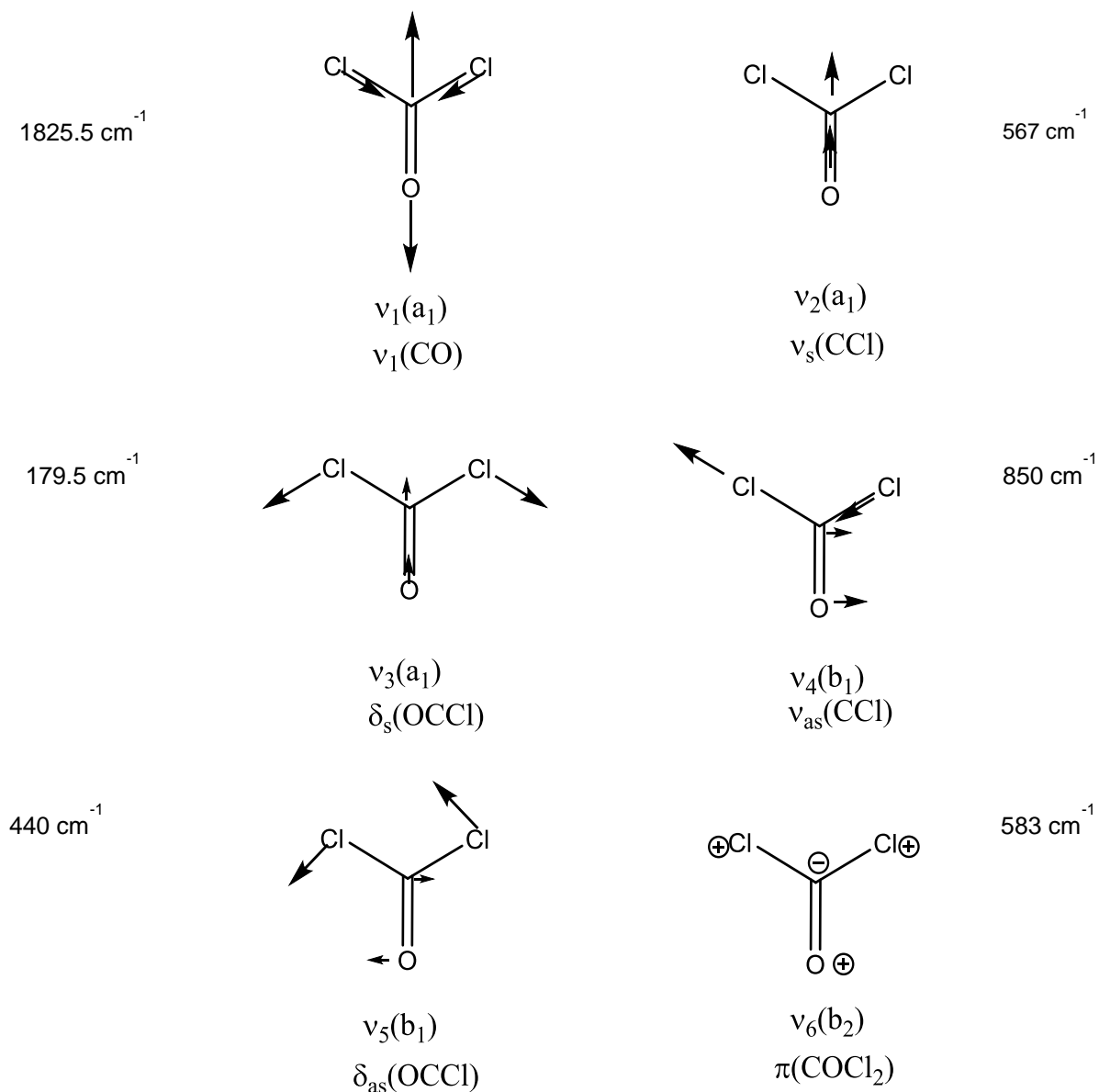


Figure 23 The fundamental vibrations of phosgene¹

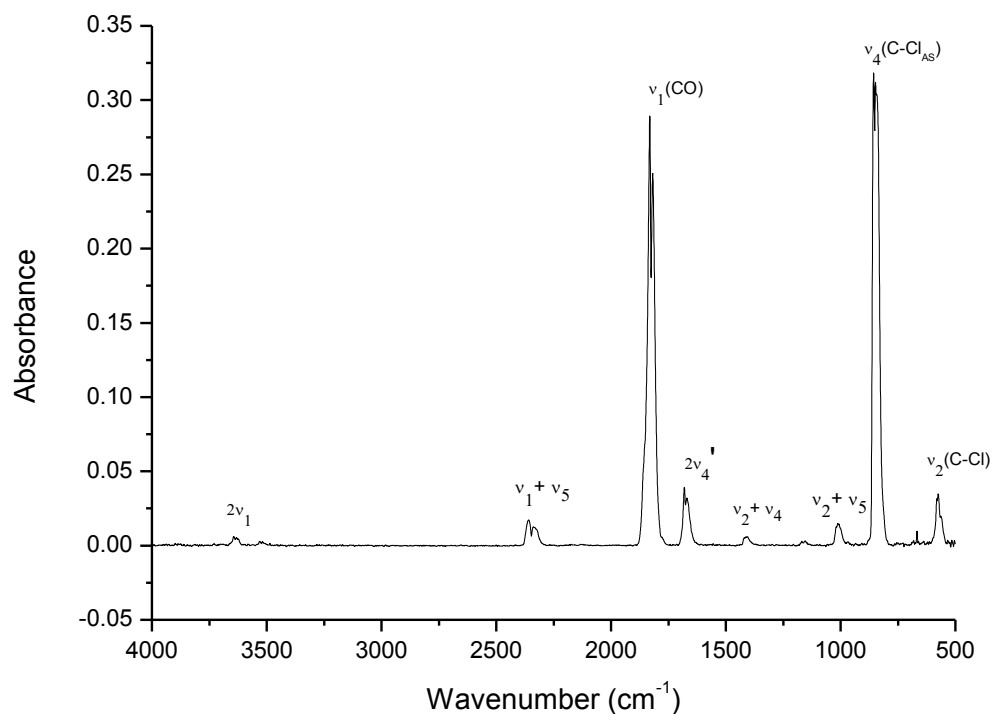


Figure 24 Example IR spectra of phosgene taken from calibrations at a phosgene flow of $4 \text{ cm}^3 \text{ min}^{-1}$ ^{1,29,72-74}, i.e. $3 \text{ cm}^3 \text{ min}^{-1}$ phosgene, $156 \text{ cm}^3 \text{ min}^{-1}$ N_2

Table 5 Peak assignments of Fig. 24^{1,29,72-75}

Peak position cm^{-1}	Description
1832, 1820	$\nu_1(a_1) \nu(\text{CO})$
843	$\nu_4(b_1) \nu(\text{C-Cl})$
576	$\nu_2(b_2) \nu(\text{COCl}_2)$
3627	$2\nu_1$
2360	$\nu_1+\nu_5$
1669	$2\nu_4$
1402	$\nu_2+\nu_4$
1011	$\nu_2+\nu_5$

Phosgene has a $\pi \rightarrow \pi^*$ transition^{29,76} which has a lambda max at 230 nm which is visible in the UV. An example spectrum is depicted below

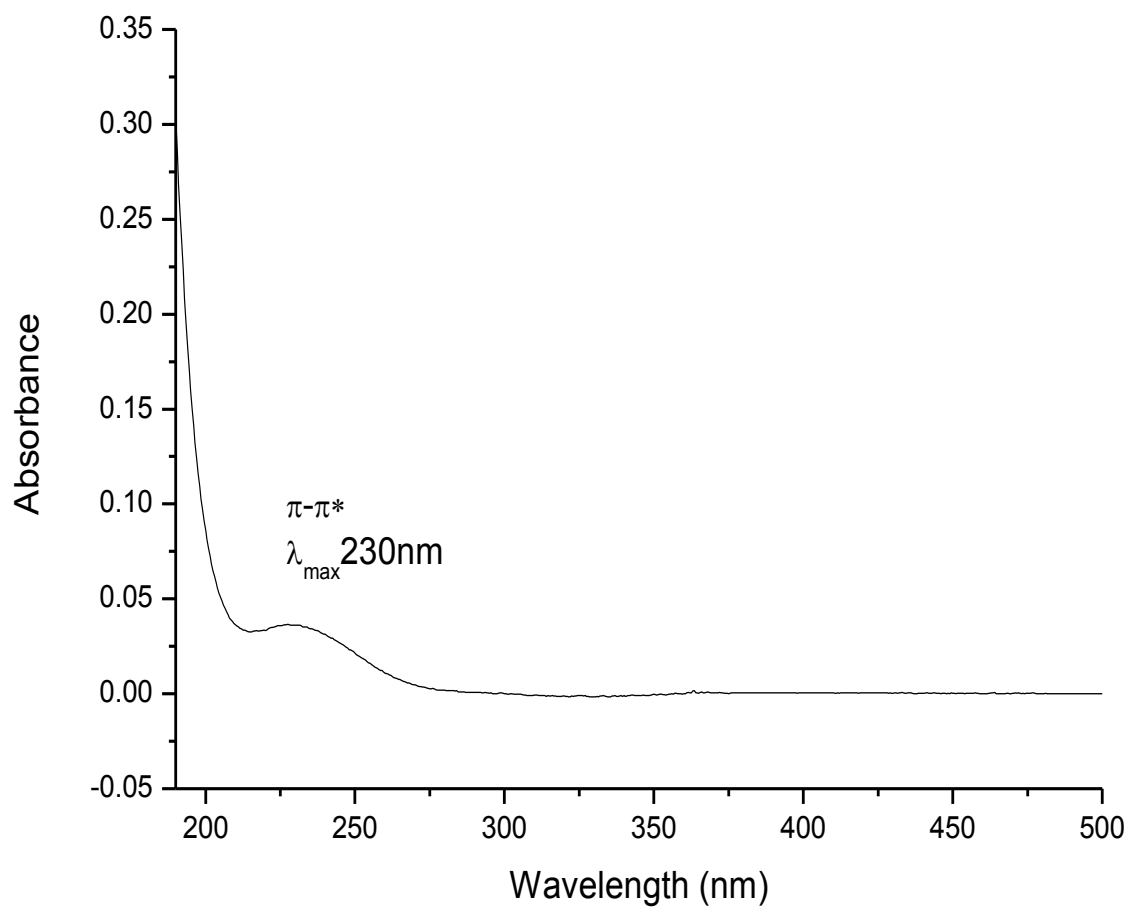


Figure 25 Example UV spectrum of phosgene taken from calibrations at a phosgene flow of $4 \text{ cm}^3 \text{ min}^{-1}$ ^{29,72-74}, i.e. $3 \text{ cm}^3 \text{ min}^{-1}$ phosgene, $156 \text{ cm}^3 \text{ min}^{-1} \text{ N}_2$

2.2.4 Calibrations

In order to make quantitative measurements the spectrometers have to be calibrated for each of the components of the reaction. The total flow was kept at a constant rate of $159 \text{ cm}^3 \text{ min}^{-1}$ (as used throughout for the reaction measurements, see chapters 4-7) for the reagents and nitrogen, and using the gas laws can be converted into the corresponding moles. The total flow was made up with $50 \text{ cm}^3 \text{ min}^{-1}$ drive flow and the addition of a $100 \text{ cm}^3 \text{ min}^{-1}$ dilution flow of nitrogen. However, the number of moles was calculated as per the flow rate through the reactor using standard temperature and pressure ($V_m = 22.4 \text{ L mol}^{-1}$). All measurements were made in triplicate. The excessive dilution used in these experiments (carrier gas + post reaction dilution) ensures that the gases conform to the ideal gas equation.

The carbon monoxide was calibrated for the infrared spectrometer by changing the flow rate between the ranges of $3\text{-}9 \text{ cm}^3 \text{ min}^{-1}$ in the constant flow. The peak area between $2260\text{-}2000 \text{ cm}^{-1}$ was integrated as a function of flow rate; this provides a way of converting the experimental peak area into moles²⁹. This allows the consumption of CO during the reaction to be followed in flow rates and converted into moles. Similarly to CO the $\nu_1(\text{CO})$ mode of phosgene was used to calibrate between $1\text{-}4 \text{ cm}^3 \text{ min}^{-1}$. Both gas infrared gas cells were calibrated for CO and COCl_2 . The $\nu_1(\text{CO})$ mode of phosgene was used rather than the stronger ν_4 band. This avoided problems with detector saturation at high COCl_2 concentrations. This latter matter was also avoided by use of a smaller path length cell for certain measurements.

The Cl_2 signal was calibrated in the UV-visible spectrometer by changing the flow rate from $2\text{-}5 \text{ cm}^3 \text{ min}^{-1}$ in the constant flow. The peak area between $275\text{-}474 \text{ nm}$ was integrated as a function of the flow rate and similarly converted into moles. This allows the Cl_2 consumption to be followed during the reaction. The response factor for all of reagents were calculated and are as follows:

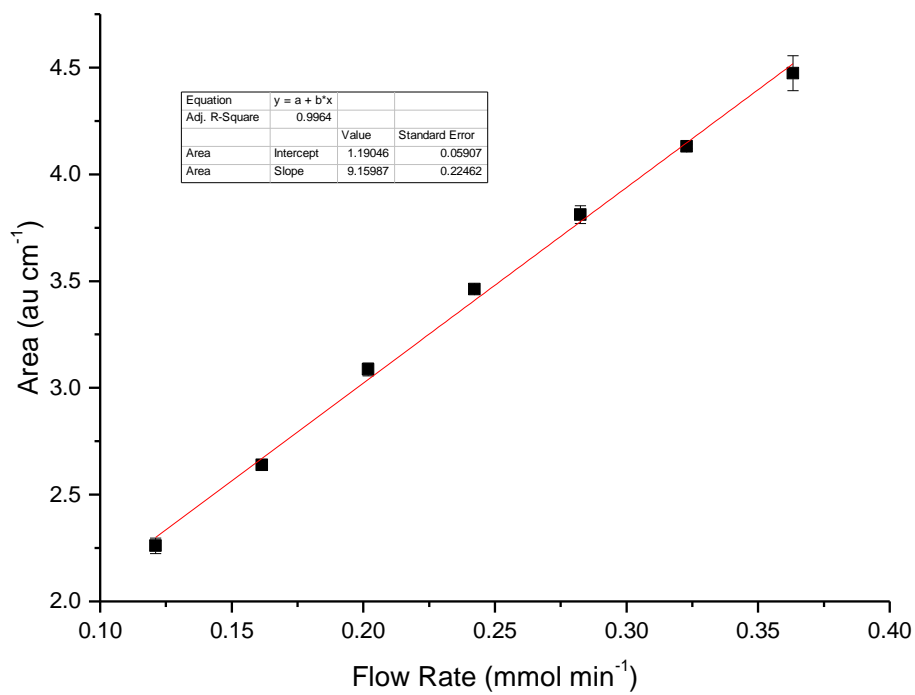


Figure 26 Calibration of CO gas cell 1

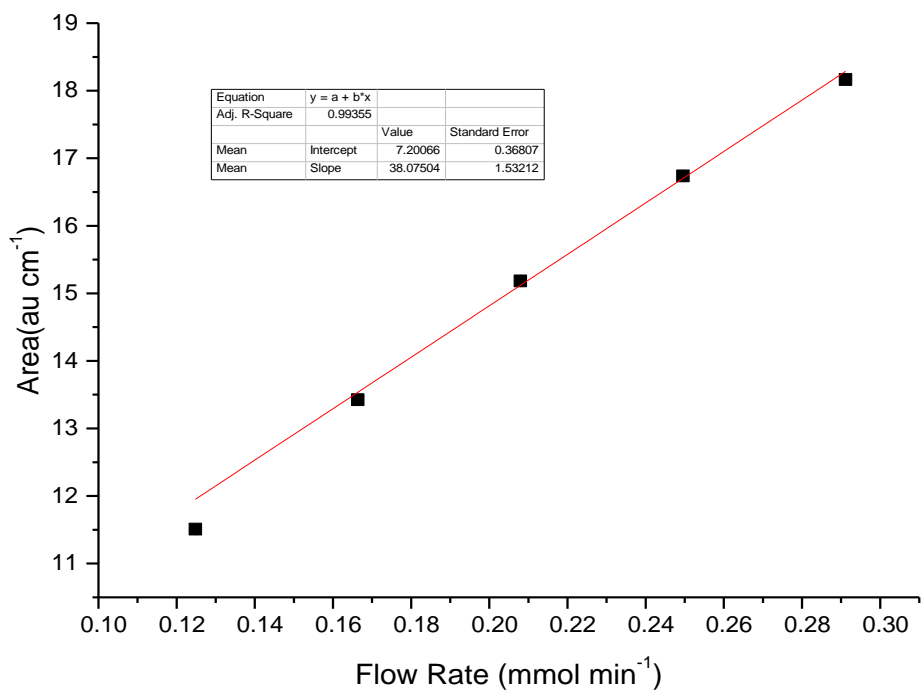


Figure 27 Calibration of CO gas cell 2

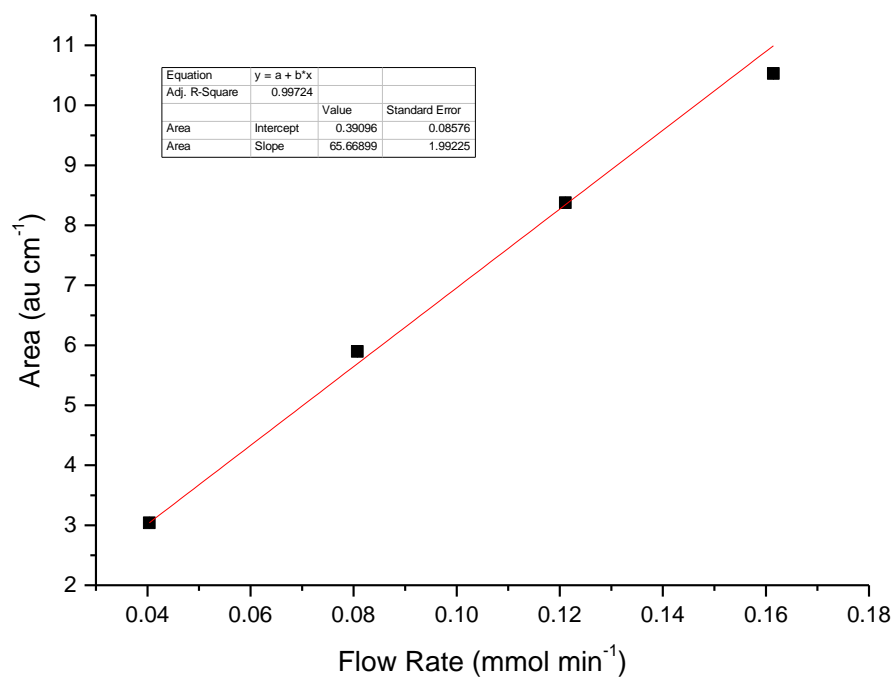


Figure 28 Calibration of Phosgene gas cell 1 (flow rate of phosgene in 10% phosgene in He)

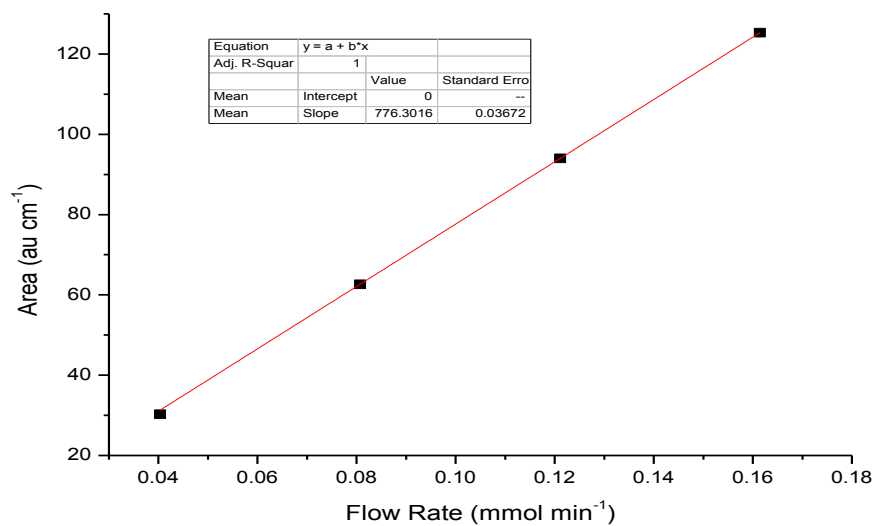


Figure 29 Calibration of phosgene gas cell 2 (flow rate of phosgene in 10% phosgene in He)

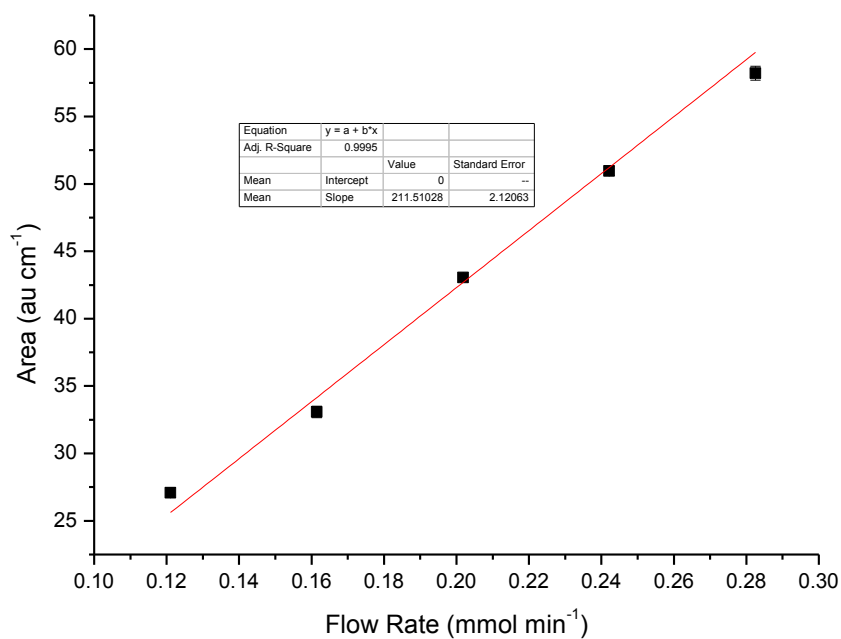


Figure 30 Calibration of chlorine

Table 6

	CO	Cl ₂	COCl ₂
Response factor au cm ⁻¹ (au cm ⁻¹ mmol min ⁻¹) ⁻¹ (gas cell 1)	9.16	211.51	74.48
Response factor au cm ⁻¹ (au cm ⁻¹ mmol min ⁻¹) ⁻¹ (gas cell 2)	38.08	N/A	776.58

2.1.6 Space velocity

For the vast majority of the measurements, the catalyst was loaded into the reactor as a ground powder. The catalyst was received as pellets; typically these were ground using a pestle and mortar then sieved through defined sieves so that the size fraction of 250-500 μm was utilised. Ground catalyst is used to minimise mass transport issues in the experiments.

The density of the catalyst was measured by filling a 5 cm^3 measuring cylinder to 2 cm^3 of ground catalyst and then was weighed. The density was found to be 0.805 g cm^{-3} . The space time (τ) is defined as the time to process one reactor at specific feed parameters. The space velocity is the inverse of the space time where it represents the number of reactor (catalyst) volumes processed per unit time²².

A representative catalyst charge is 0.1250 g. Corresponding space time and space velocity values are presented below

$$\text{Space time } \tau = \frac{\text{volume catalyst}}{\text{volume flow rate per minute}} / 60 \quad (23)$$

$$= \frac{\left(\frac{0.1250\text{g}}{0.805\text{ g cm}^{-3}}\right)}{59\text{ cm}^3\text{ min}^{-1}} / 60$$

$$= 4.39 \times 10^{-5}\text{ h}$$

$$\text{space velocity} = \frac{\text{Volume of flow rate}}{\text{volume of catalyst}} \quad (24)$$

$$\frac{59\text{cm}^3\text{min}^{-1}}{(0.1250\text{g}/0.8050\text{g cm}^{-3})} \times 60$$

$$= 22798\text{ h}^{-1}$$

2.1.7 Catalyst preparation

All measurements were performed on the Donau Supersorbon K40 catalyst. The reactor is usually charged with 120 mg of catalyst of size fraction 250-500 μm (Endcotts sieves) and dried overnight at 383 K in flowing nitrogen to remove any water. The catalyst is then exposed to reagents for 20 minutes before measurements are taken.

2.2 Bromine Co-feed Apparatus

There is industrial interest in establishing how small quantities of Br_2 impurity in the chlorine feed stream may affect COCl_2 production⁷⁷. This is a topic not covered in the literature that required a degree of development. The apparatus used for the conventional phosgene synthesis kinetics was modified to accommodate a bromine doser as a cylinder of diluted Br_2 proved to be unattainable. The bromine doser (Fig. 27) was constructed to only sample the vapour above solid bromine (Alfa Aeser, 99.8%).

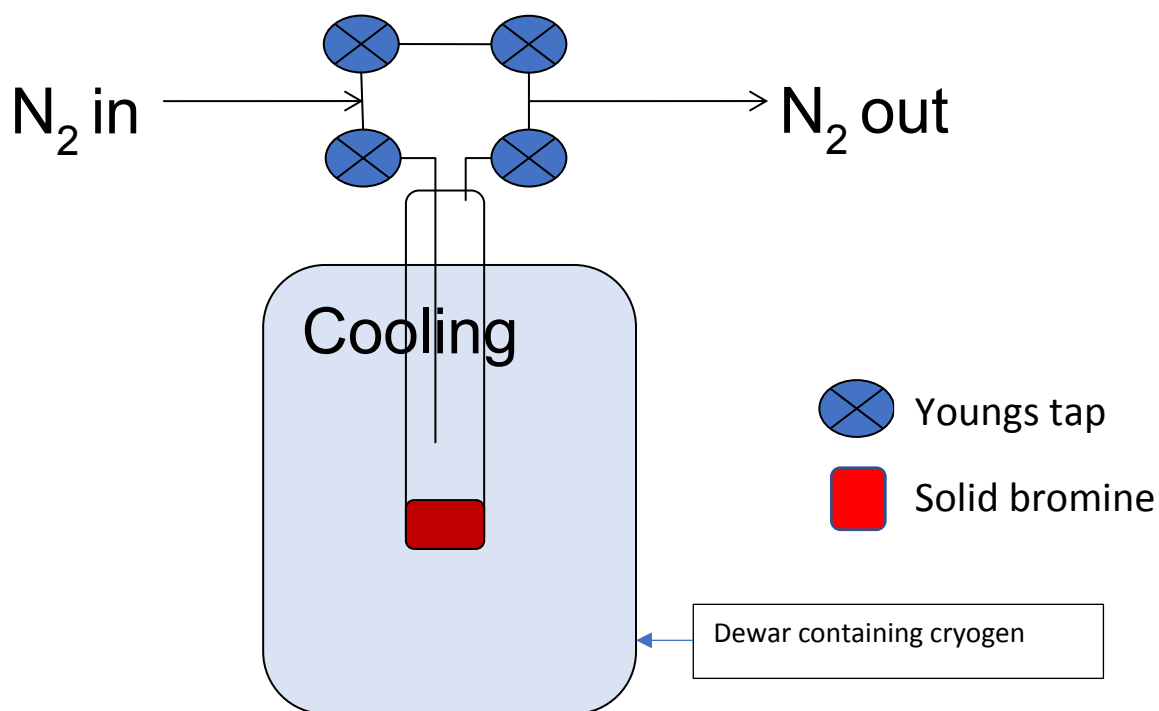


Figure 31 Bromine doser design

The design allows the flow to be switched easily between bypass (top two switches) and through the bromine vapour (bottom two switches). Fig. 32 shows how the bromine doser was fixed into the apparatus. The bromine (mp: 266 K, bp: 332 K) was maintained as a solid by using solvent cooling baths with either dry ice or liquid nitrogen contained with the Dewar flask. The temperature of the flask was monitored using a thermocouple (Hanna HI 935352).

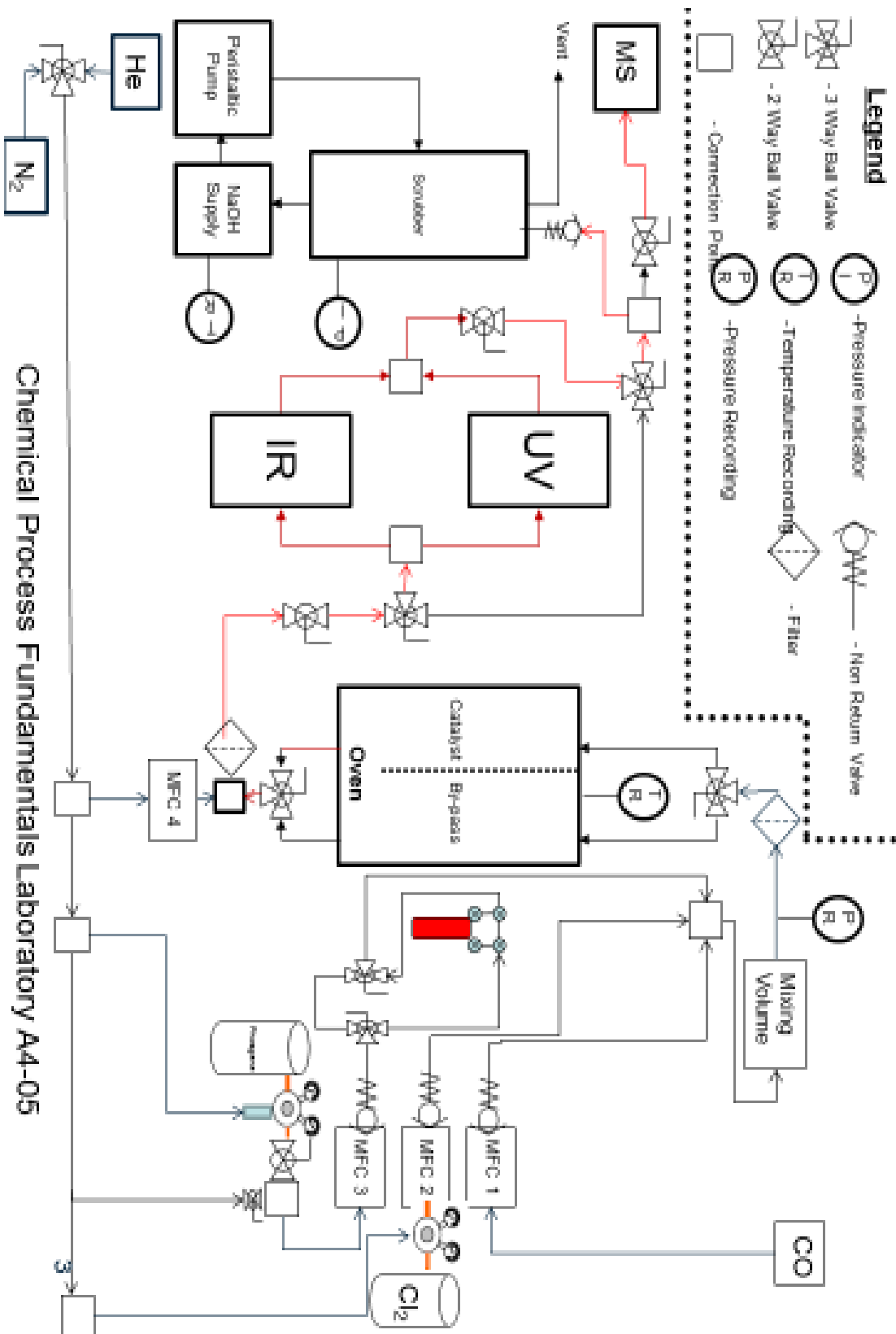


Figure 32 Apparatus design (the red box indicates solid bromine)

The quantity of dibromine in the co-feed is controlled by varying the temperature, at which, is itself controlled by varying the composition of the cooling bath. A plot of the vapour pressure as a function of temperature is shown in fig.33

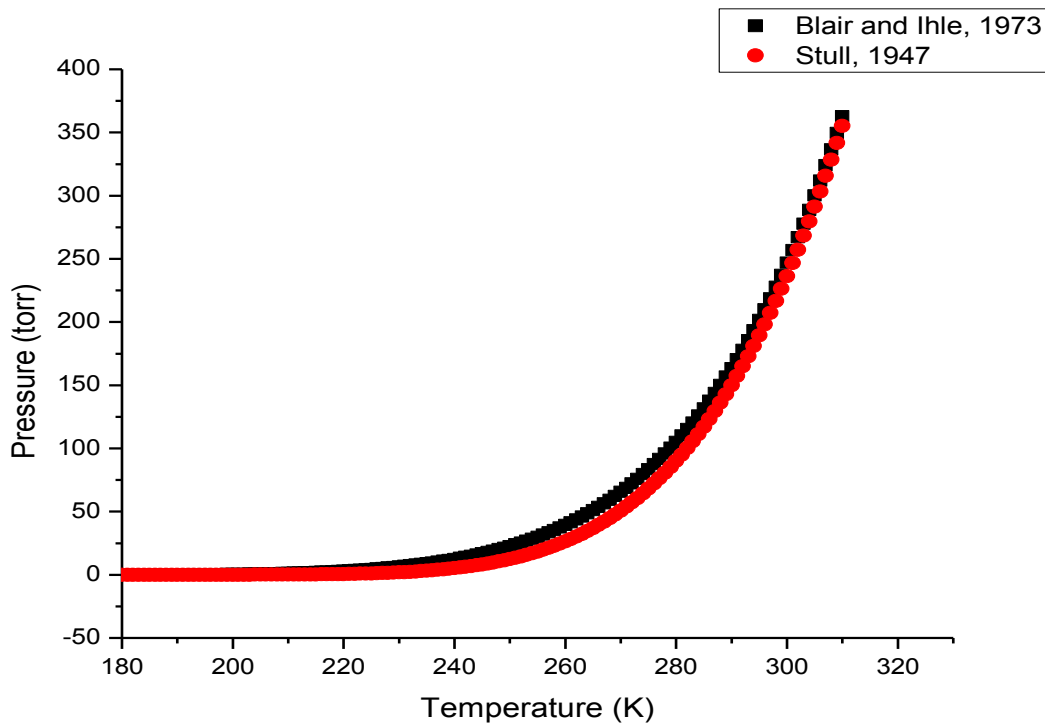


Figure 33 Theoretically calculated vapour pressure of bromine as a function of temperature⁷⁸

The vapor pressure was calculated using Antoine's law⁷⁹

$$\text{Log}_{10}(P) = A - \left(\frac{B}{T+C}\right) \quad (25)$$

Where the A, B and C are constants specific to bromine and T is the temperature in Kelvin

Table 7 Antoine's law data for Bromine

Reference	A	B	C
Blair and Ihle, 1973 ⁸⁰	4.703	1562.264	0.628
Stull, 1947 ⁸¹	2.945	638.258	-115.114

Similar to dichlorine, dibromine has a $\pi^* \rightarrow \sigma^*$ transition with a λ_{\max} at 415 nm as shown in Fig.

3

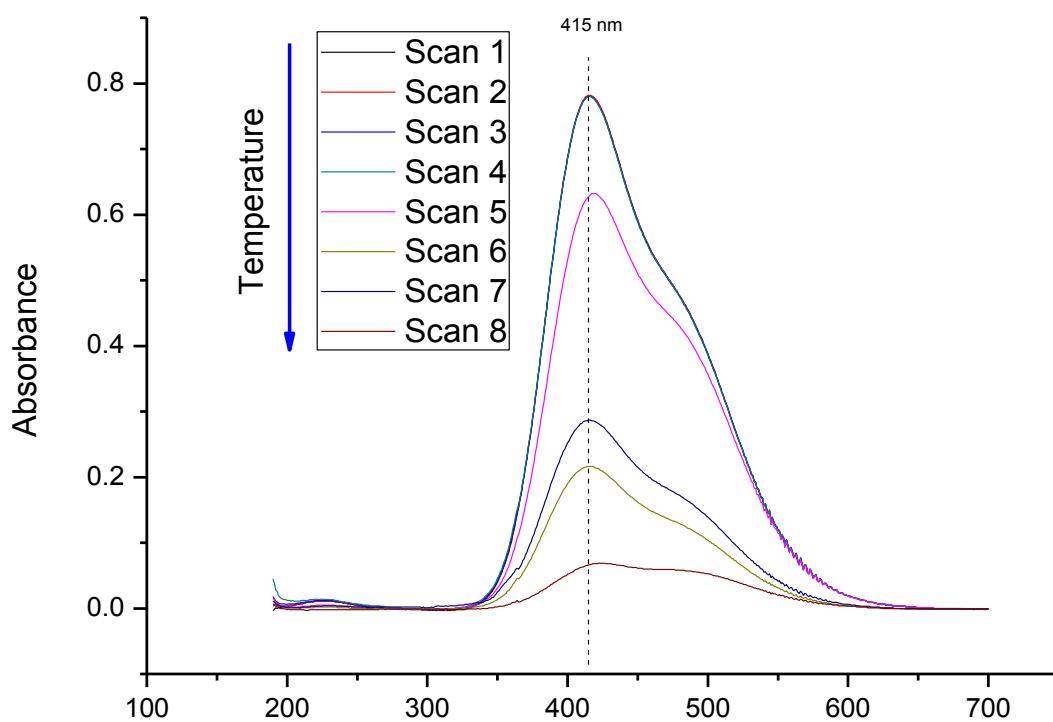


Figure 34 UV-visible spectrum of dibromine. The flow rate of bromine was varied by varying the temperature of the Dewar (allowing to cool from 298-77 K) in N_2 flow of $159 \text{ cm}^3\text{min}^{-1}$ (Drive $50 \text{ cm}^3\text{min}^{-1}$ and dilution $109 \text{ cm}^3\text{min}^{-1}$)

The spectrum of dibromine is more complicated than that of dichlorine due to to more electronic transitions accessible⁵⁴.

2.2.2 Quantification of bromine (Beer Lambert validation)

The dichlorine signal in the UV was monitored at different flow rates (4-8 cm³min⁻¹) in a fixed flow of 159 cm³min⁻¹(i.e. 155-151 cm³ min⁻¹ N₂). The concentration of dichlorine was calculated by taking the absorbance at 330 and using the extinction coefficient of 25.2 mol⁻¹ L cm⁻¹.⁵⁴ and this was compared with the concentration calculated by using the calibration factor (211.51 au(mmol min⁻¹)⁻¹ Section 7.6.2)

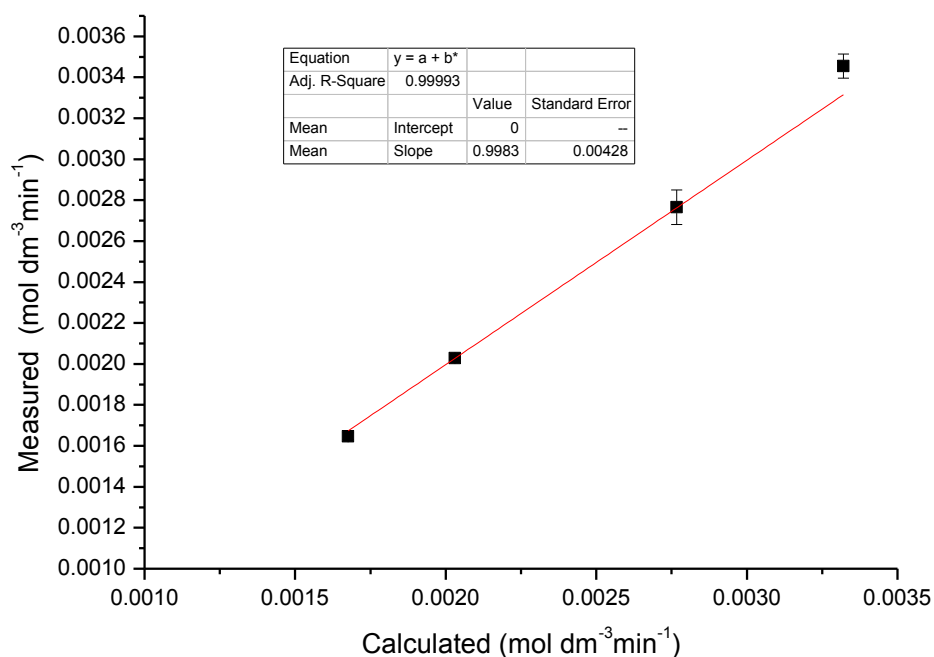


Figure 35 Chlorine calibration consistency check with measured concentration as a function of the calculated from the extinction coefficient at 330 nm

From the graph it is clear that there is good agreement with the concentrations calculated by the absorbance at a specific wavelength⁵⁴ and by the integrated area of the whole peak; slope= 0.9983 ± 0.00428 with the error representing the standard error in the fit. Thus, confirming that the literature molar extinction coefficient for Cl₂ and experimentally determined molar extinction coefficient are in good agreement for the quantification of a metered chlorine supply, the same approach was used to determine bromine flow rates. A calibration for dibromine by taking the absorbance at 420 nm and using the literature extinction coefficient⁵⁴ of 64.8 mol⁻¹L to calculate the molar flow rate and then plot that against the integrated area.

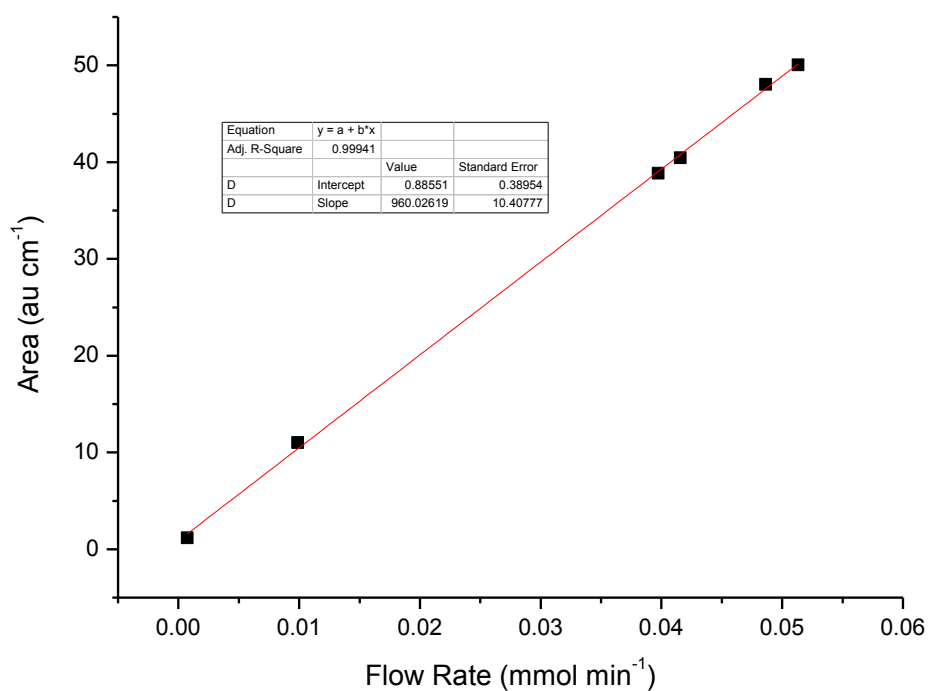


Figure 36 Calibration graph for dibromine (peak area against calculated flow)

It was possible to calibrate for dibromine in the UV spectrum. From figure 36 a response factor of 960.026 ± 10.408 (au cm⁻¹ mmol min⁻¹)⁻¹ is obtained. This can be used to determine Br₂ flow rate from the integrated area of Br₂ spectra for in-line measurements of a reacting system.

2.2.3 Mass spectrometric determination of Br₂

The bromine doser was maintained at room temperature and the total flow of 159 cm³ min⁻¹ (50 cm³ nitrogen front end drive and 109 cm³ min⁻¹ back end dilution). The mass spectrum of bromine shows that only the lower masses of the fragmented bromine are visible.

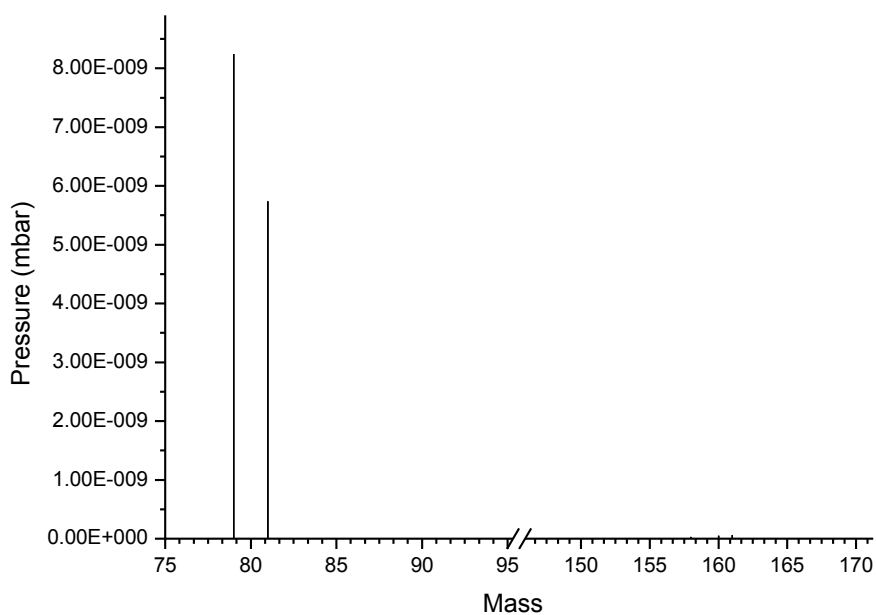


Figure 37 Mass spectrum of bromine at room temperature in a total flow of 159 cm³ min⁻¹

Mass 79 and mass 81 were used to follow bromine in the mass spectra. The molecular ion (158, 160, and 162 amu) is evidently not observed in the mass spectrometer. With respect to figure 37 and assuming that the irradiation cross-section of Cl₂ and Br₂ are similar, this is thought to occur due to the electronic ionisation process leading to the dissociation of Br₂

2.2.4 Baseline bromine content in the chlorine

The chlorine used throughout the thesis was checked for bromine content to establish baseline levels of bromine. The mass of 70 was used for dichlorine and the mass of 79 was used for dibromine.

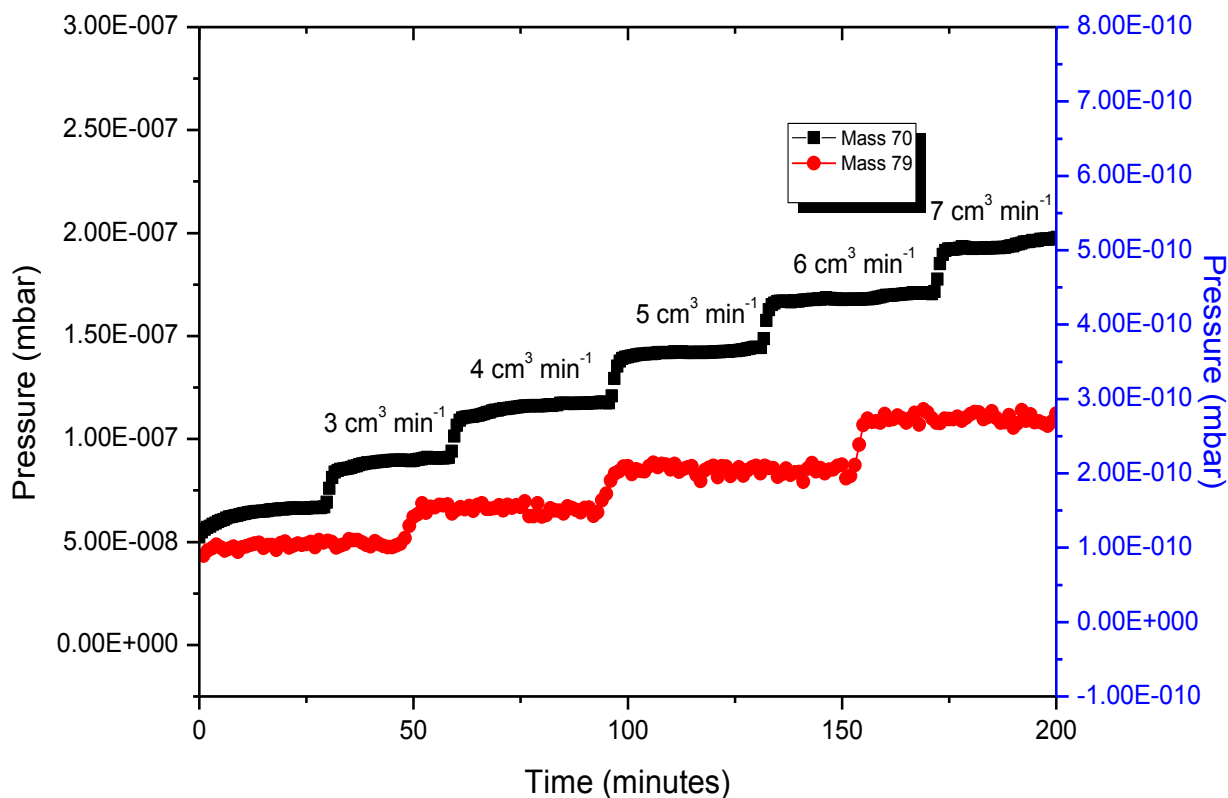


Figure 38 Mass spectra of chlorine at different flow rates of chlorine

The bromine signal to increase with increasing chlorine flow rate however, the obtained pressure for bromine is several orders of magnitude smaller than that of chlorine. With respect to figure 38, the bromine content of the chlorine used throughout the study contains $\leq 0.01\%$ bromine.

2.3 Summary

- An apparatus has been developed in the Chemical Process Fundamentals Laboratory that is capable of testing the kinetics of the gas phase reaction between CO and Cl₂ to form phosgene.
- The spectroscopic features of reagents and products have been described.
- The quantification of CO, COCl₂ and Cl₂ have been established allowing each species to be monitored simultaneously.
- The apparatus has been modified to accommodate a bromine doser.
- The quantification of bromine has been undertaken using electronic spectroscopy.
- Further modifications to the apparatus were made to investigate the oxychlorination process (Appendix 1). However, this is beyond the scope of the current investigation⁴⁶.

Chapter 3- Characterisation of the Donau K40 carbon catalyst

3.1 Introduction

This chapter examines the preliminary structural information of the commercial grade catalyst (Donau Supersorbon K40) by the application of four different analytical techniques to obtain separate information on various aspects of the catalyst. SEM(EDX) images were taken to estimate particle size and physical shape. Powder X-ray diffraction was used to gather structural information on crystal structure and to identify if the catalyst has any long range structural order. BET measurements were obtained to determine the surface area of the catalyst and the BJH method to estimate pore size. Raman spectroscopy of the catalyst was used to investigate the nature of the carbon material.

3.2 Scanning Electron Microscopy (SEM)

A set of SEM images were taken from a small quantity of the catalyst using a Philips XL30 ESEM. The instrument had an acceleration voltage of 25 kV.

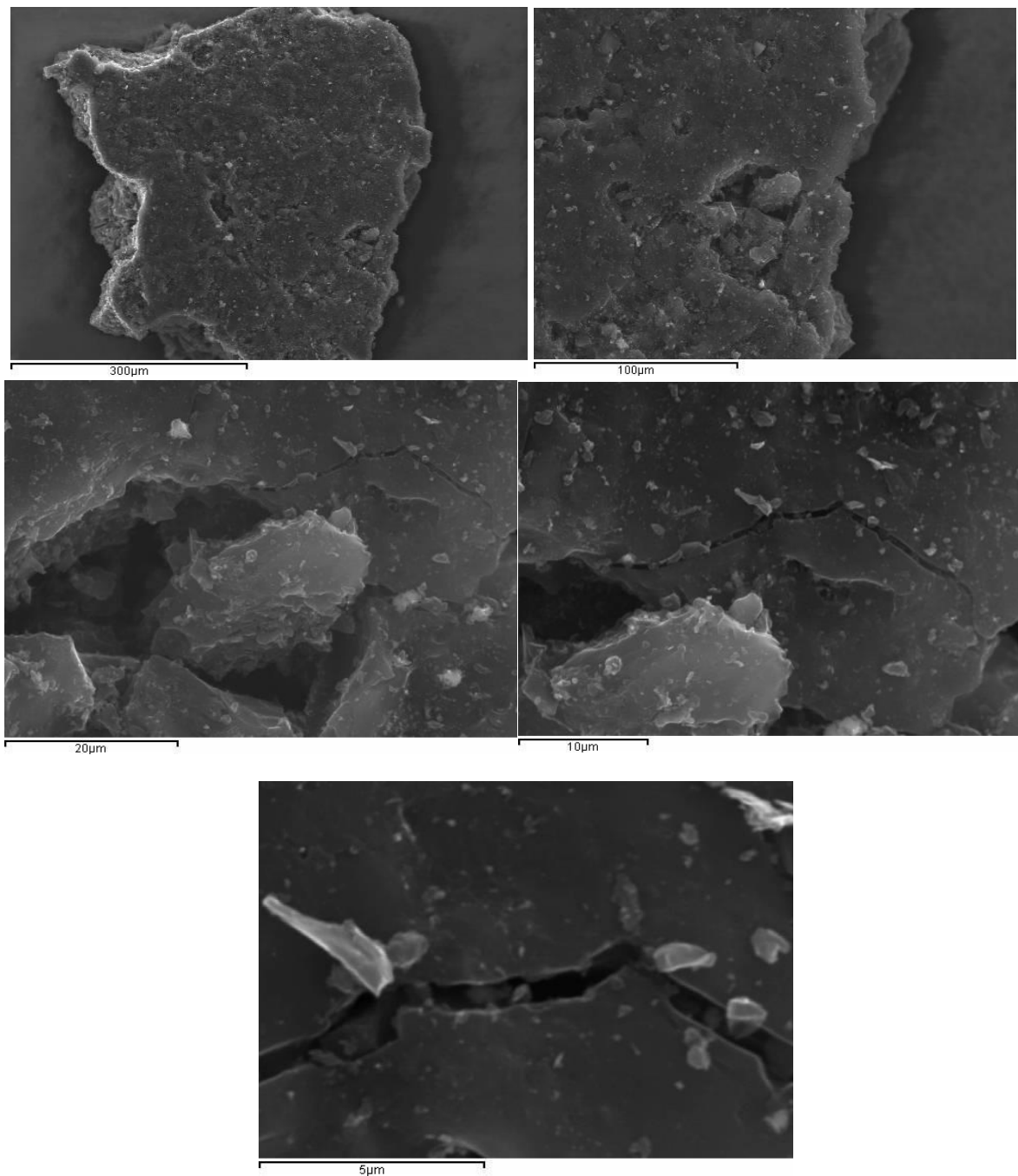


Figure 39 SEM Images of the Donau k40 catalyst (size indicated in the bar)

The SEM images established the carbon to be present as a plate-like structure. The catalyst was uniformly of this structure. Little further information can be gathered from the micrographs presented Fig 37. The SEM is further equipped with an energy dispersive X-ray spectrometry facility (EDX) (see sections 6.4 and 7.6). Fig 38 presents a representative spectrum of the as-received Donau Supersorbon k40 catalyst.

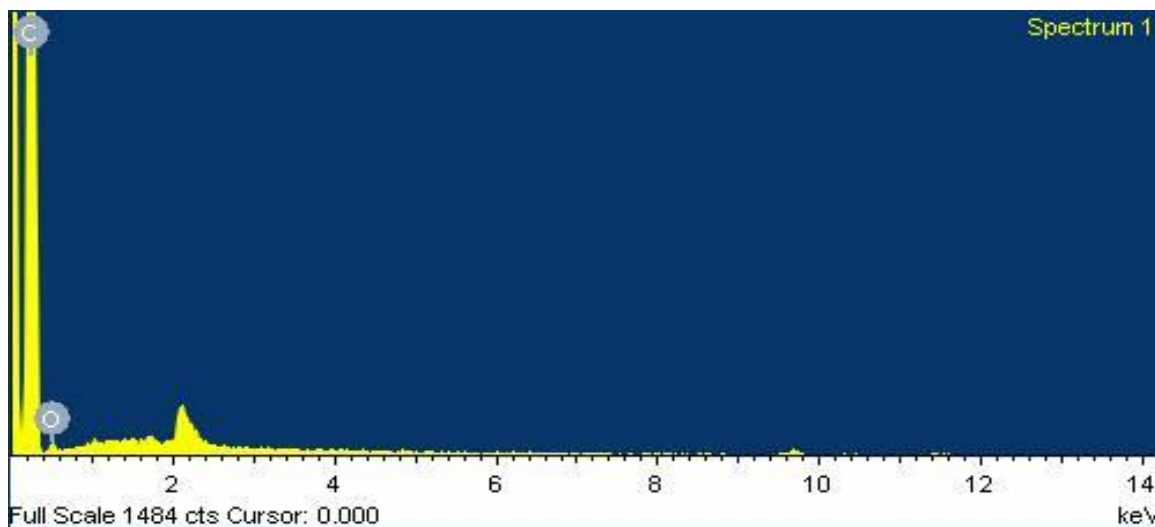


Figure 40 EDX of the fresh Donau catalyst

Table 8 EDX result of the as-received Donau Supersorbon K40 catalyst

Element	Weight %	Atomic %
Carbon	96.87	97.63
Oxygen	3.13	2.37
Totals	100	100

From the obtained spectra, the catalyst consists of mainly carbon and contains a small quantity of oxygen.

3.3 XRD

An X-ray diffraction pattern was taken of a small quantity of the catalyst using a PAN Analytic X'Pert Diffractometer. The wavelength used to scan the sample was 1.5418 \AA generated from a $\text{CuK}\alpha$ source. The sample was scanned through a $5 < \theta < 85$ angle at 0.017 degrees per second which generates the following diffraction pattern

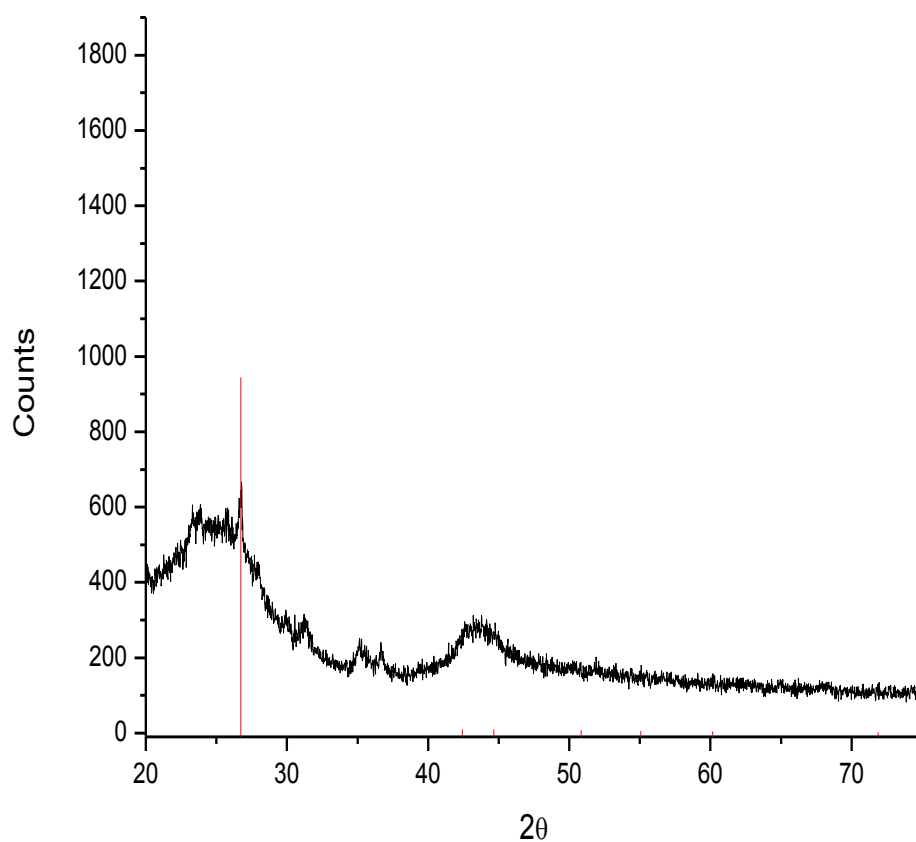


Figure 41 XRD of the fresh Donau K40 carbon catalyst (red line indicates the reflection of graphite⁴¹)

The diffraction pattern obtained indicates that the material is amorphous in nature but contains some graphitic character. No sharp features indicate the absence of any long-range order in the material.

3.4 BET

A BET surface area measurement was taken of the catalyst using a Quantachrome Quadrasorb evo, that allows the surface area to be calculated and pore size distribution to be determined. A small quantity of catalyst (0.09g) was placed in the sample vial and gaseous nitrogen passed over the sample for 16 hours. The measurement was performed in triplicate.

Table 9 BET results of the as received Donau Supersorbon K40 catalyst

Run	Surface Area (m ² /g)	Pore volume (cm ³ /g)
1	1267.0	0.578
2	1259.7	0.582
3	1234.0	0.578
Average	1253 ±17.3	0.579± 0.002

The errors represent the standard deviation of the triplicate measurements. The carbon appears to have a large surface area (1253±17.3 m²/g) and has a pore volume of 0.579±0.002 cm³/g. The values obtained are comparable to the values reported by Mitchell and co-workers(surface area :1200 m²/g and pore volume: 0.52 cm³/g).²

3.5 Raman Spectroscopy

Raman scattering was performed of the as-received Donau K40 catalyst using a Horiba Jobin Yvon LabRam HR confocal Raman microscope and a 532nm laser source at <20mW power. The spectra show three basic features, the D, and G bands around 1600, and 1350 cm^{-1} .

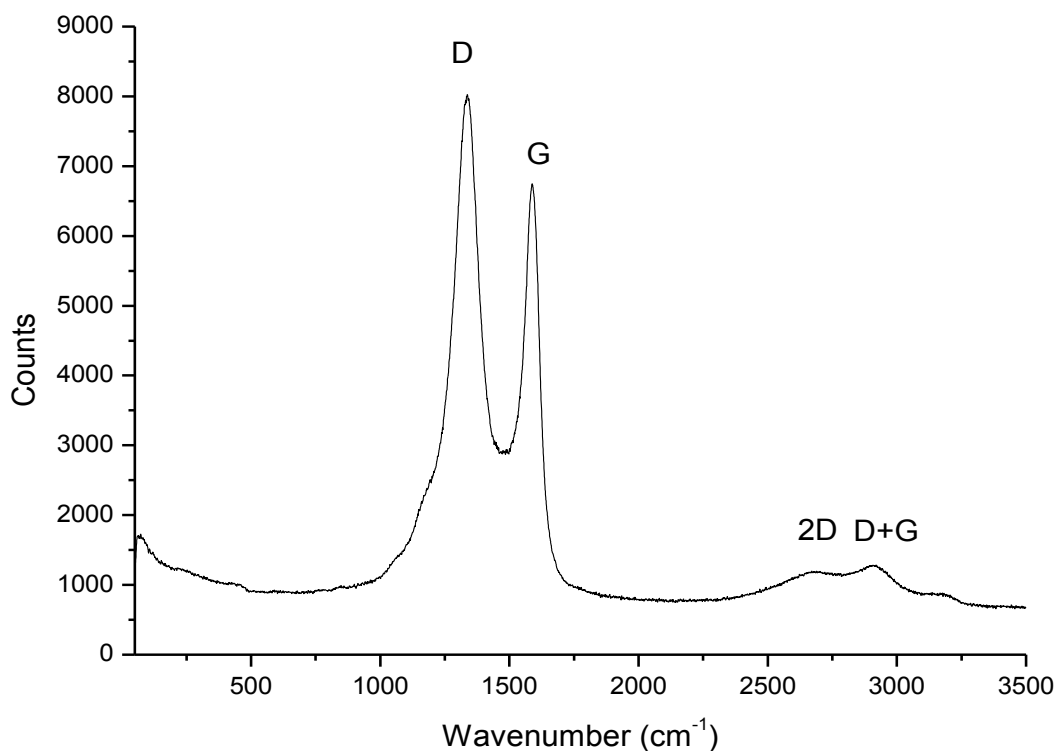


Figure 42 Raman spectrum of the fresh Donau K40 carbon catalyst

The G and D peaks are due to sp^2 sites only, the G peak is due to the bond stretching of all pairs of sp^2 sites in both rings and chains, and the D peak is due to the A_{1g} breathing mode of sp^2 atoms in a 6-fold aromatic rings. The G peak, is due to the stretching motion a pair of sp^2 sites, and is a good indicator of disorder^{66,67,69,82,83}. From the spectrum obtained the $I(D)/I(G)$ ratio is 0.9, which is consistent with amorphous sp^2 carbon.⁶⁹

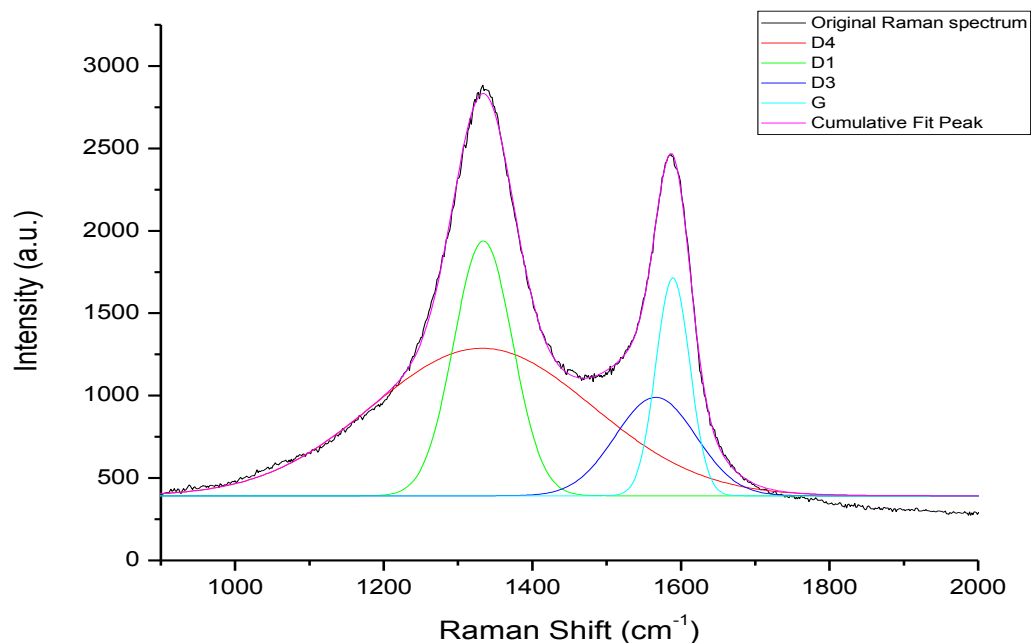


Figure 43 Multi-peak fitted Raman spectrum of the Donau Supersorbon K40 carbon

A number of workers have used Raman spectroscopy to characterize carbonaceous material,^{66,84,85} which have provided the necessary understanding for the interpretation of Raman spectra of carbonaceous materials.^{86,87} Following the approach of Sadezky et al⁸⁴, Figure 5 presents a multi-peak analysis for the Donau Supersorbon K40 carbon. The fitting procedure used the Origin Pro 8 software package. The cumulative fit of 5 separate peaks is well correlated with the experimental spectrum. Band assignments are outlined in Table 3. The D1, D3 and D4 bands were all accommodated within the fitting procedure.

Table 10 Band assignments for the Donau Supersotbon K40 carbon⁸⁸

Band	Raman Shift (cm ⁻¹)	Assignment
D4	1180	Disordered graphitic lattice
-	1250	Hydrogen-decorated carbon edge atoms
D1	1350	Disordered graphitic lattice
D3	1500	Amorphous carbon
G	1600	Graphitic lattice

The D1 band originates from a double resonant Raman scattering process consisting of a defect and an in-plane transverse optic phonon mode in the graphene lattice. The D3 Raman band is associated with amorphous carbon and the D4 Raman band is assigned to disordered graphitic lattice of an A_{1g} symmetry. The feature at 1250 cm⁻¹ that is tentatively assigned to hydrogen decorated carbon edge sites also positively contributes to the overall fit. A D2 mode observable at about 1620 cm⁻¹ is also reported,⁸⁴ that corresponds to a graphitic lattice mode with E_{2g} symmetry. However, in a similar manner to that described by McGregor *et al* in their analysis of coked dehydrogenation catalysts,⁸⁹ the inclusion of this band was somewhat arbitrary and therefore was omitted from the fitting procedure. The Raman spectrum of Figure 43 is consistent with carbonaceous materials. Due to the sensitivity of the resonance process to particle size and wavelength dependence⁶⁶ the authors are cautious in discerning a structural motif for the carbonaceous features of the Raman spectrum except to note a sizeable contribution of amorphous carbon, as evidenced by the D3 band

3.6 Summary

- From the SEM-EDX data it can be concluded that the Donau K40 carbon catalyst is consists mainly of carbon.
- The surface area and pore volume obtained are in good agreement with the literature.
- The XRD shows that there is no long-range order in the material and that the catalyst is amorphous.
- The Raman spectrum shows both the D and G bands, consistent with the presence of sp^2 carbons within the catalyst and that the structure is amorphous

Chapter 4- Kinetic measurements

4.1.0 Introduction

This chapter will describe fundamental kinetic measurements made on the Donau K40 activated carbon catalyst. These include the reaction as a function of time, temperature, determining the activation energy and rate law for the gas phase reaction. Also, included in this chapter is an experimental validation that the reaction is under kinetic control.

4.1.1 Temperature Studies

The reaction between CO and Cl₂ was observed as a function of temperature. The reaction flow was passed over the by-pass containing 0.1250 g ground quartz until stable signals were detected in the infrared and UV spectrometers; these were taken as the A₀ values for each reagent. The flow was then switched over to the catalyst and left for 20 minutes before samples were taken. The temperature was then increased in 20 degree steps from 298-433 K and the reaction was left 20 minutes to stabilise before any spectra were obtained. Following a procedure commonly used: in industry the feed stream of CO and Cl₂ utilised a slight excess of CO, *eg.* CO = 5 cm³ min⁻¹, Cl₂ = 4 cm³ min⁻¹. Chlorine is a most expensive reagent; having a small excess of CO ensures that all of the Cl₂ can in principle be incorporated into the (valuable) product

From the spectra obtained, the production of phosgene increases as a function of temperature and the reaction becomes limited by chlorine availability at high temperatures (Fig. 46).

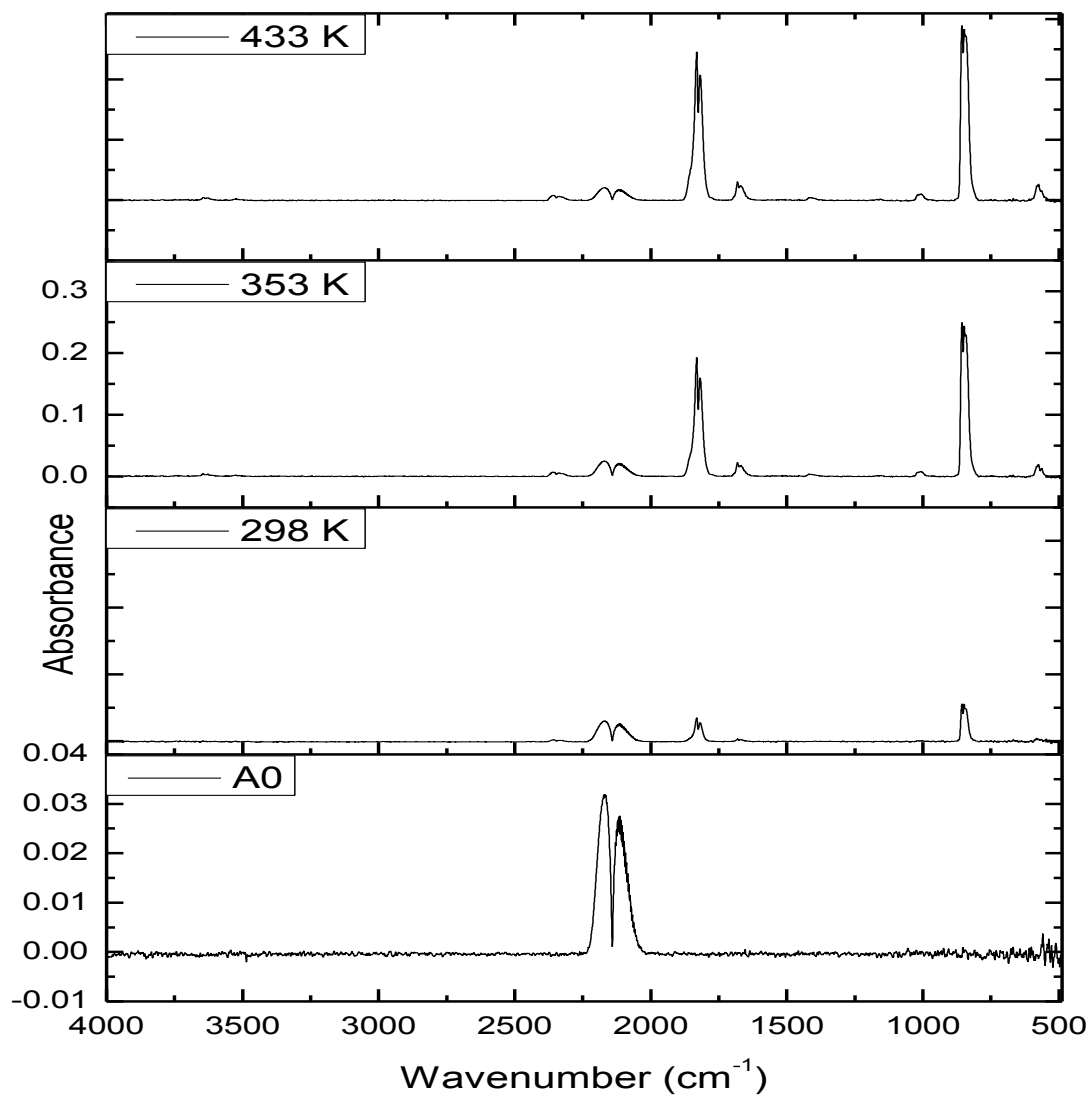


Figure 44 IR Spectra of reaction between CO and Cl₂ over the catalyst as a function of temperature with flow rates of 5 cm³ min⁻¹ and 4 cm³ min⁻¹ in a total flow of 159 cm³ min⁻¹, respectively, over a temperature range of 298-433K K (gas cell 1)

Table 11 Main peak assignments Fig.44^{1,29,72,74,75}

Peak position (cm ⁻¹)	Assignment
2174	ν (CO)
1830	ν_1 (CO) of COCl ₂
848	ν_4 asymmetric of COCl ₂ (C-Cl stretch)

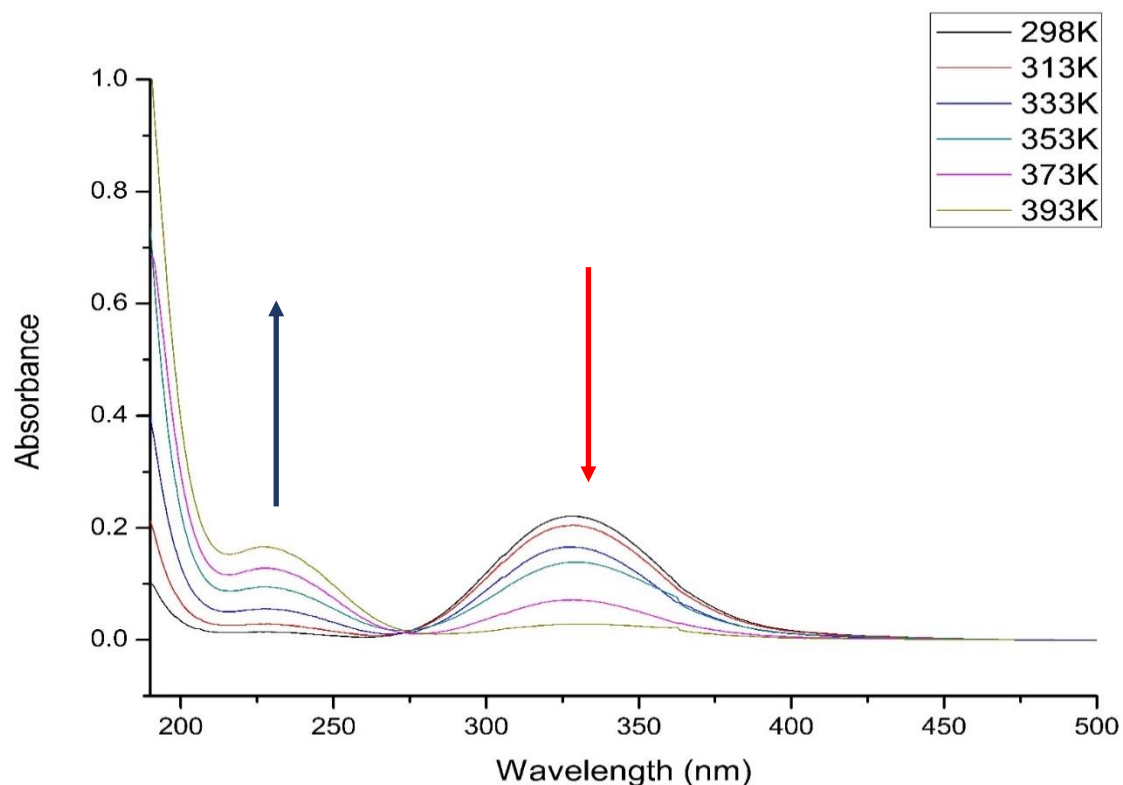


Figure 45 Overlay of UV Spectra of reaction between CO and Cl₂ over the catalyst as a function of temperature with flow rates of 5 cm³ min⁻¹ and 4 cm³ min⁻¹, respectively, over a temperature range of 298-433K

From the IR spectra (fig 44) obtained, it is clear that there is an increase in the band due to the ν_1 (CO) and the ν_4 asymmetric C-Cl stretch of COCl₂ and a decrease in the ν (CO) on increasing temperature. From the UV visible spectra (fig 45), there is a similar trend where there is an increase in COCl₂ production and chlorine consumption.

From the obtained spectra, there is a direct link between phosgene production and temperature. On increasing temperature, there is a clear increase in phosgene production and decrease in reactant concentration. Using previously described calibration procedures (Section 2.2.4) peak areas of reagents and product can be converted to flow rates.

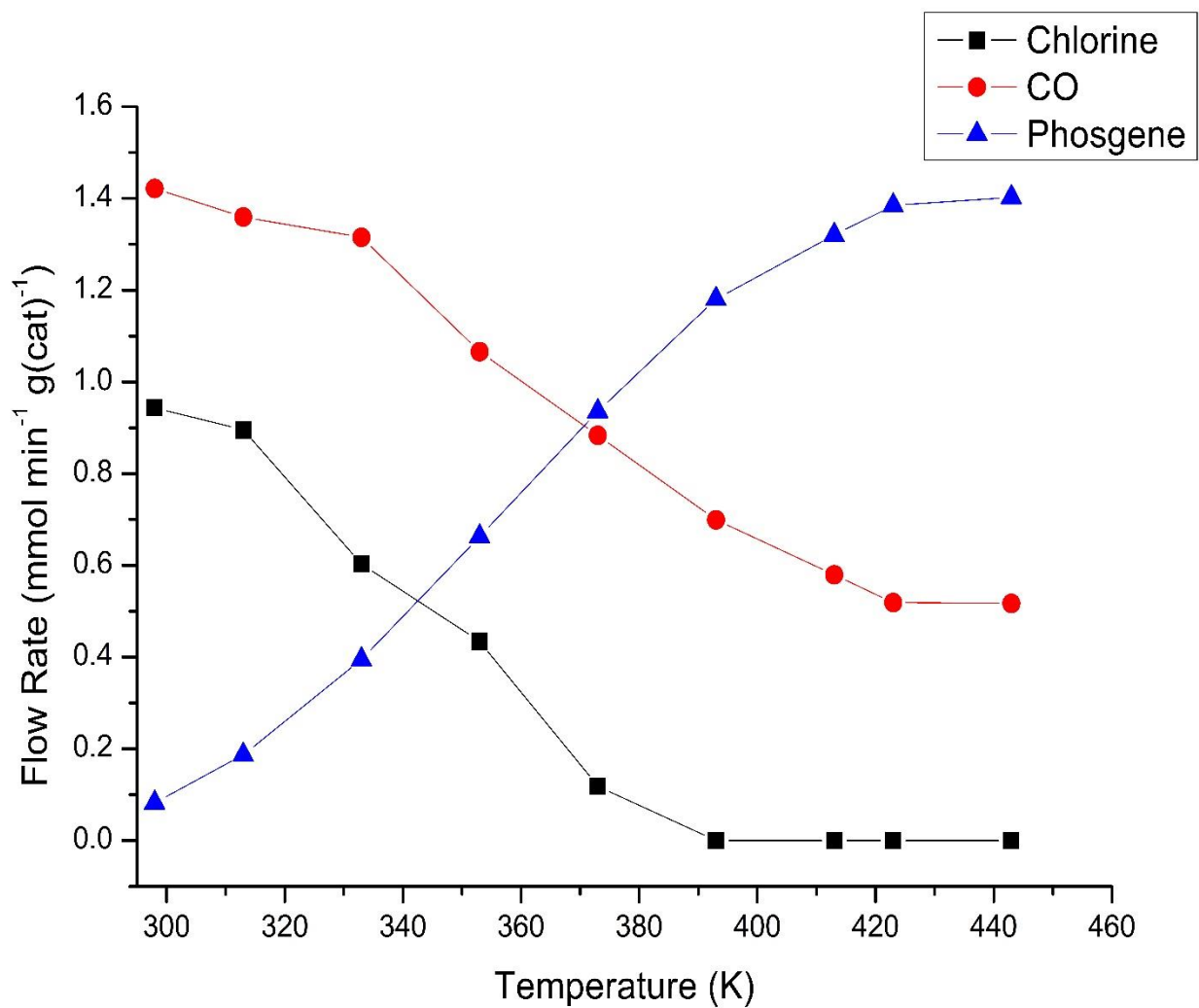


Figure 46 Temperature for the reaction of CO and Cl₂ over the catalyst with flow rates of 5 cm³ min⁻¹ and 4 cm³ min⁻¹, respectively, over a temperature range of 298-433K

From the reaction profile (Fig.46) the reaction rate increases as a function of increasing temperature. The reaction becomes limited by dichlorine availability at high temperatures.

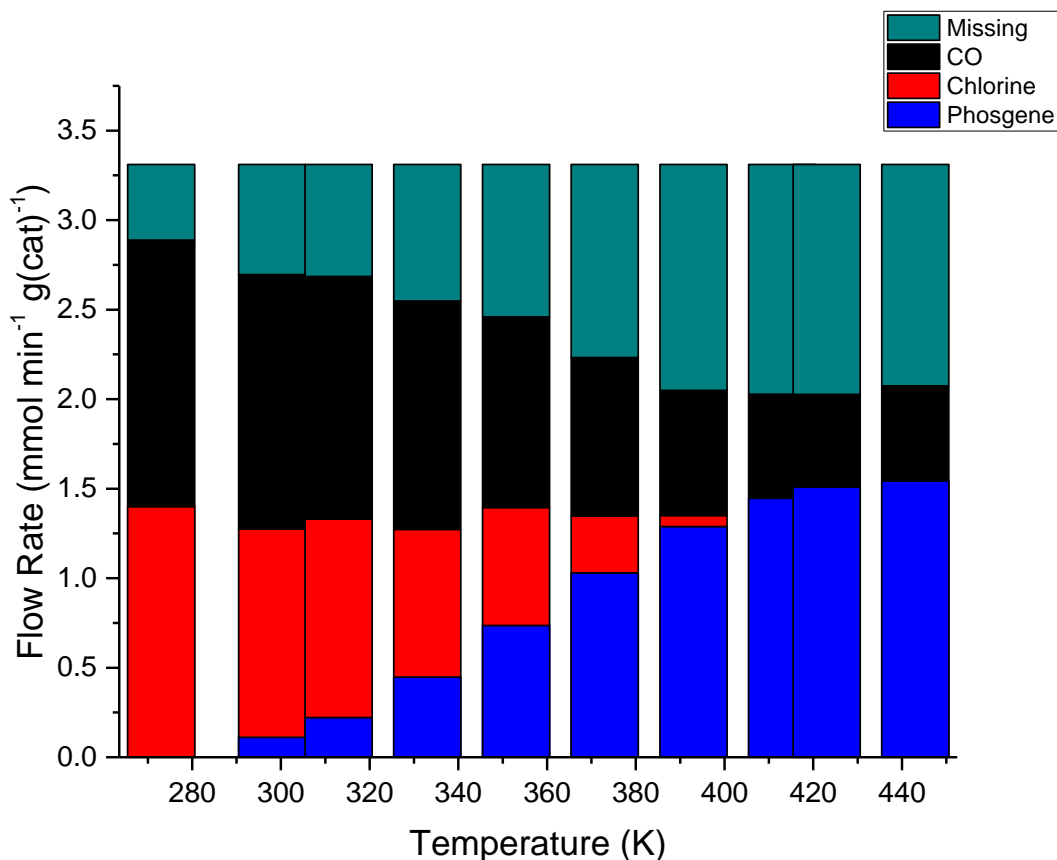


Figure 47 Mass balance for the reaction of CO and Cl₂ over the catalyst with flow rates of 5 cm³ min⁻¹ and 4 cm³ min⁻¹, respectively, over a temperature range of 298-433K

The reaction is operating under an open mass balance at all points throughout the profile with the missing mass attributed to chlorine (see section 4.5.2). At higher temperatures the reaction could be producing carbon tetrachloride². However, CCl_{4(g)} would be detected as the C-Cl⁹⁰ stretch of CCl₄ at 793 cm⁻¹ is different from the ν₄ band of phosgene at 848 cm⁻¹. No CCl₄ is detected in Fig. 44. Moreover, no chemical entities other than CO, Cl₂ and COCl₂ were spectroscopically observed. Therefore, phosgene is the only observable product throughout the whole temperature range *i.e* 100 % selectivity.

4.2 Homogeneous reaction

The reaction mixture was passed over 0.1250g of ground quartz to mimic reaction conditions and the flow was monitored using IR and UV spectroscopy as a function of temperature.

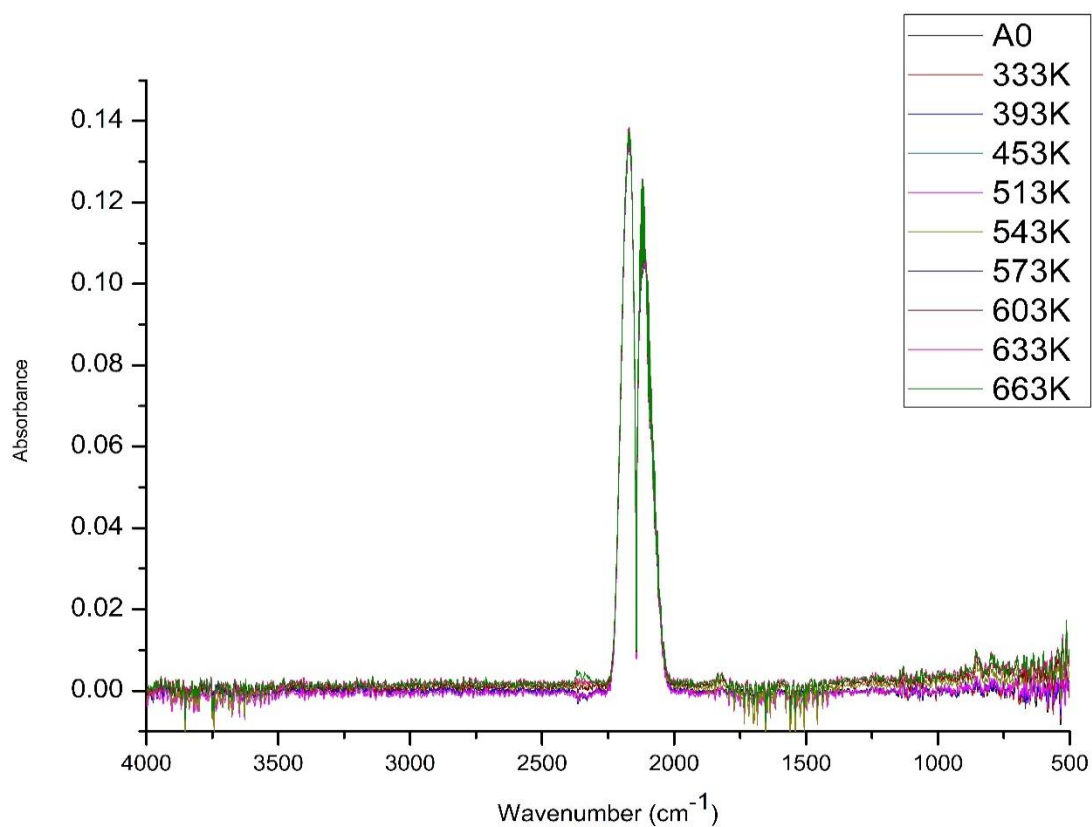


Figure 48 Overlay of IR Spectra of reaction between CO and Cl₂ over bypass as a function of temperature with flow rates of 5 cm³ min⁻¹ and 4 cm³ min⁻¹ over a temperature range of 298-663 K

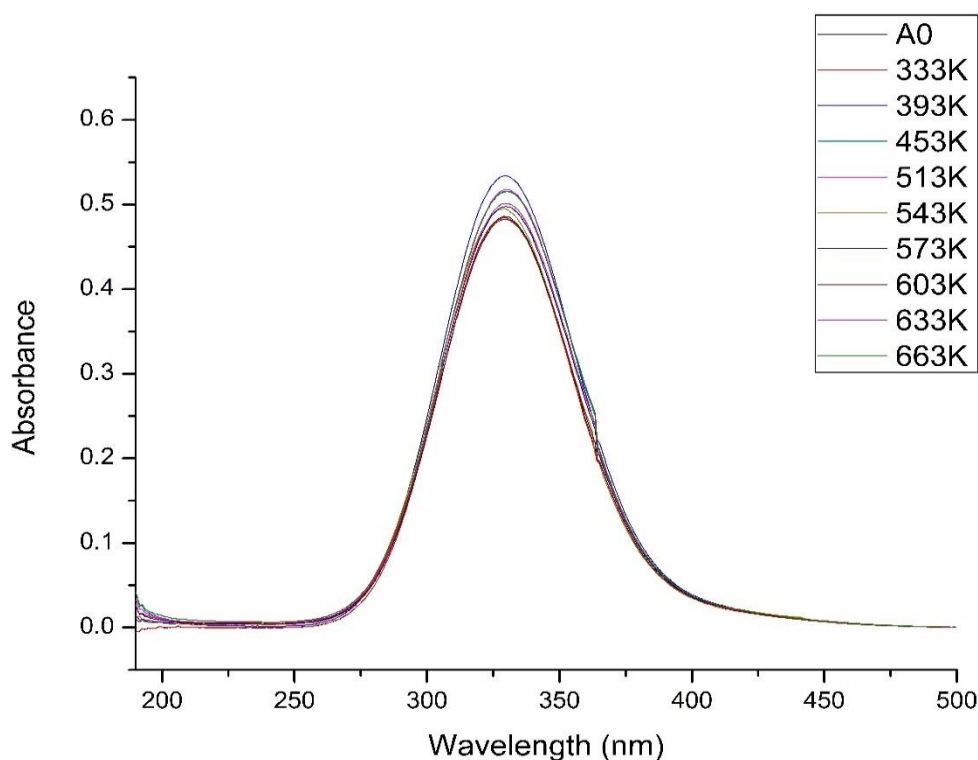


Figure 49 Overlay of UV Spectra of reaction between CO and Cl₂ over the bypass as a function of temperature with flow rates of 5 cm³ min⁻¹ and 4 cm³ min⁻¹ over a temperature range of 298-663 K

From the obtained spectra (Figures 48 and 49), there was no evidence of conversion under these flow conditions.

The contact time in the reactor was altered by decreasing the nitrogen drive flow (increasing residence time) and there is evidence that small quantities of phosgene are being formed.

The presence of the catalyst significantly decreases the energy required for this process. The temperature at which reaction is observed here is also consistent with literature as it is greater than 623 K¹. The dissociation energy of dichlorine is reported to be 242.58 kJ mol⁻¹ indicating that the energy of this process is significantly lowered with the presence of a catalyst.

Table 12 Phosgene production over ground quartz

Reaction conditions (663 K)	Space time (h)	Phosgene production (mmol min ⁻¹)
N ₂ (drive) 50 cm ³ min ⁻¹ N ₂ (dilution) 109 cm ⁻¹	4.39 x 10 ⁻⁵	0
N ₂ (drive) 20 cm ³ min ⁻¹ N ₂ (dilution) 139 cm ⁻¹	8.92 x 10 ⁻⁵	0.005

The standard flow conditions of total flow = $159 \text{ cm}^3 \text{ min}^{-1}$ is selected as it ensures detection linearity of detection of reacting species and product. Under these conditions there is effectively no contribution from homogeneous reaction. Thus, figures 48 and 49 show that at a standard flow rate (space time = $4.39 \times 10^{-5} \text{ h}$) no homogeneous reaction is induced. Decreasing the flow rate and increasing the space time to $8.92 \times 10^{-5} \text{ h}$ does induce very minor conversion. Phosgene production originates from heterogeneous catalysis.

4.3 Activation Energy

Similar to the temperature studies presented in section 4.1.1, the reactor was charged with 0.1236g of catalyst and the reaction of CO and Cl₂ were monitored between the temperature ranges of 298-323 K in 5 K steps. This measurement was performed in triplicate. The spectra obtained are shown in Fig. 50 and 51 and the same trend is observed.

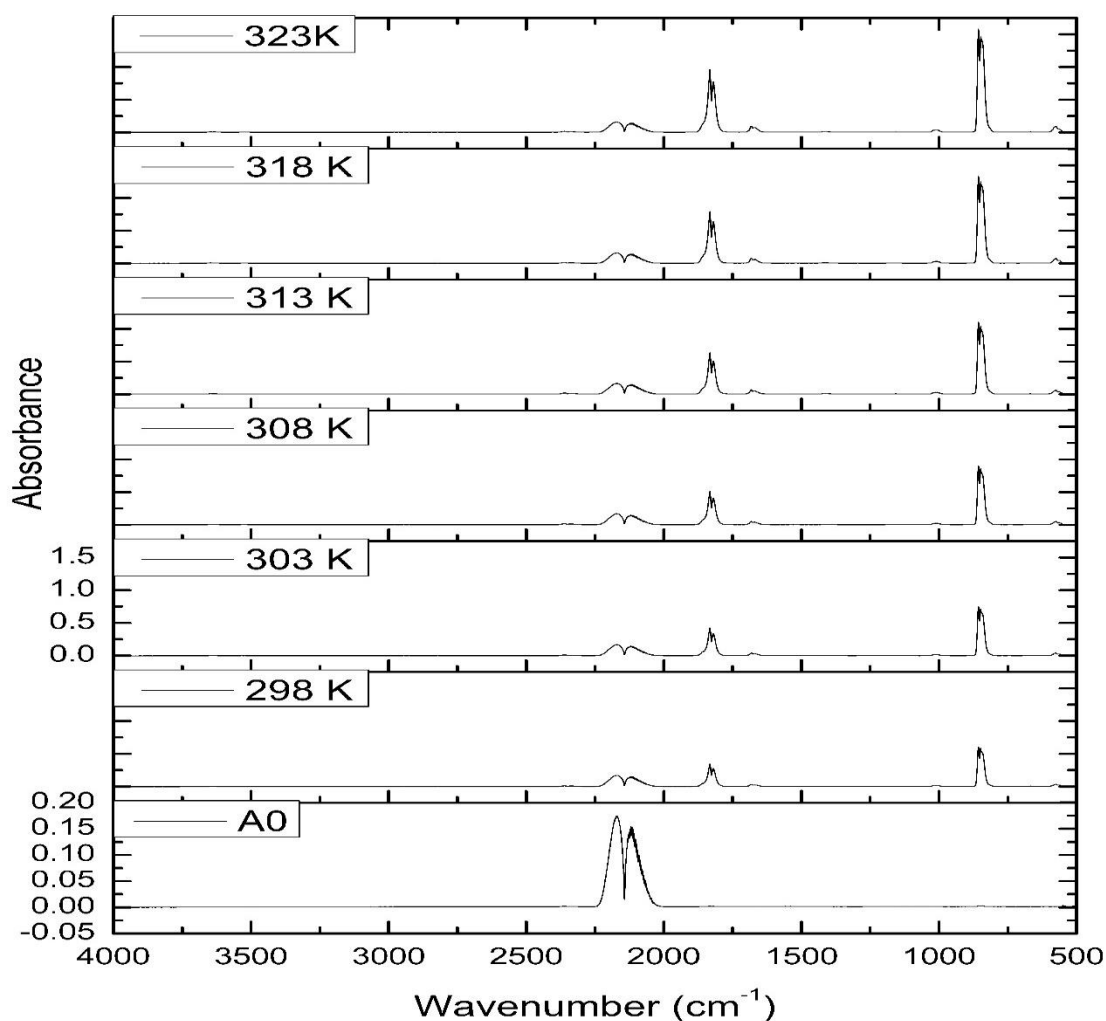


Figure 50 Infrared Spectra of the Arrhenius experiment for the reaction between CO and Cl₂ over the catalyst with flow rates of 5 cm³ min⁻¹ and 4 cm³ min⁻¹ over a temperature range of 298-323 (gas cell 2)

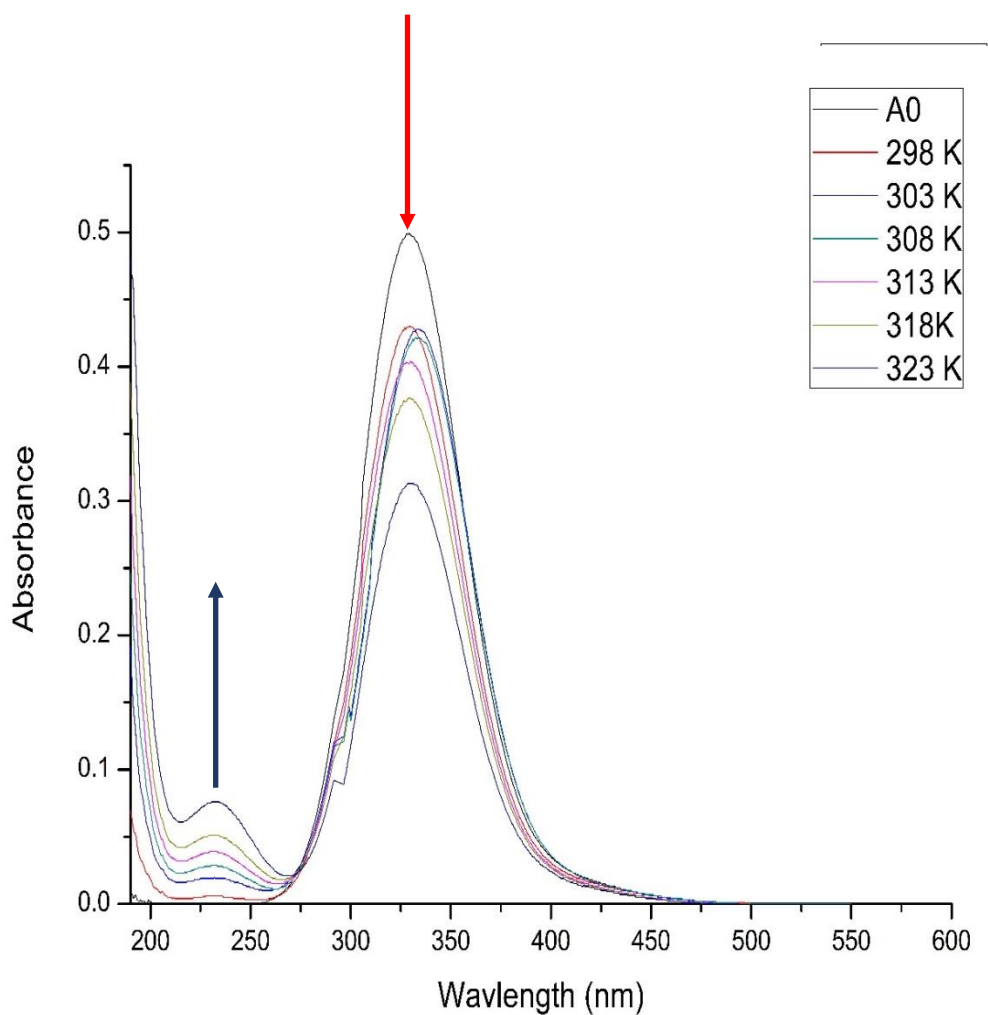


Figure 51 Overlay of UV spectra of the Arrhenius experiment for the reaction between CO and Cl₂ over the catalyst with flow rates of 5 cm³ min⁻¹ and 4 cm³ min⁻¹ over a temperature range of 298-323 K

From the IR spectra (Fig 50) obtained it is clear that there is an increase in the band due to the ν_1 (CO) and the ν_4 asymmetric C-Cl stretch of COCl₂ and a decrease in the ν (CO) on increasing temperature. From the UV visible spectra (Fig 51), there is a similar trend where there is an increase in COCl₂ production and chlorine consumption.

The reaction rate is a function of both temperature and reactant concentrations. The reaction rate is generally approximated to the product function of temperature and concentration⁵⁶.

$$v = k(T)xf(C_i) = Ae^{\frac{-E_a}{RT}}xf(C_i) \quad (26)$$

The concentration function $f(C_i)$ may be expressed in its simplest form as a product summation of the reactants and potential product molecules raised to the empirically determined exponents.

The Arrhenius law predicts an exponential increase in rate with increasing temperature⁵⁵. The dependence of temperature on rate is significantly greater than the other factors, particularly where E_a is large (i.e. greater than 30-50 kJ/mol) which is characteristic of a process in which chemical bonds are broken and/or formed such as in a catalyzed surface reaction⁵⁶. The reaction rate can be approximated to equation 27 to calculate the apparent activation energy.

The Arrhenius equation⁵⁸:

$$k = Ae^{\frac{-E_a}{RT}} \quad (27)$$

Where: k = rate constant

A = pre-exponential factor

E_a = activation energy (J mol⁻¹)

R = gas constant (J mol K⁻¹)

T = temperature (K)

Taking the natural log of both sides (equation 28):

$$\ln k = -\frac{E_a}{RT} + \ln A \quad (28)$$

Therefore, rearranging to give:

$$\ln k = \frac{-E_a}{R} \frac{1}{T} + \ln A_0 \quad (29)$$

Since rates of catalytic reactions have a temperature dependence in accordance with the Arrhenius law, it is customary to plot the log of the rate constant or of rate itself versus reciprocal temperature, the slope of which is $-E_a/R$ ^{55,56}. If rate constants can be calculated without ambiguity from rate data over a range of temperature, the plot of $\ln k$ versus $1/T$

provides a true activation energy; however, this is, only applicable to elementary reactions in the reaction-controlled regime. In most reaction systems the calculated rate constant is an ‘apparent’ rate constant, i.e. it is likely to be a product of constants for several elementary steps. Thus the ‘apparent’ activation energy is the sum or difference of several activation energies; only in unusually fortunate circumstances is it the activation energy for the rate determining step. Moreover, for heterogeneous catalytic reactions, the temperature dependence includes the temperature dependencies of equilibrium constants, which may be part of a complex Langmuir-Hinshelwood rate expression. Accordingly, even under reaction-controlled conditions, the calculated activation energy is generally an ‘apparent’ activation energy but one that nevertheless reflects the temperature dependence of the surface chemical process. It should be noted that Arrhenius plots involving apparent rate constants may not be linear over a wide range of temperature due to changes in heats of adsorption with temperature and/or shifts in the rate determining step. As a result of the difficulty of obtaining rate constants, it is common practice to plot $\ln(\text{rate})$ versus $1/T$ to obtain an ‘apparent’ activation energy⁵⁶. So by plotting rate, $\ln[\text{COCl}_2]/dt$ against $1/T$ the gradient, $-E_a/R$, gives (Fig. 52)

$$\ln \frac{[\text{COCl}_2]}{dt} = -\frac{E_a}{RT} + \ln A \quad (30)$$

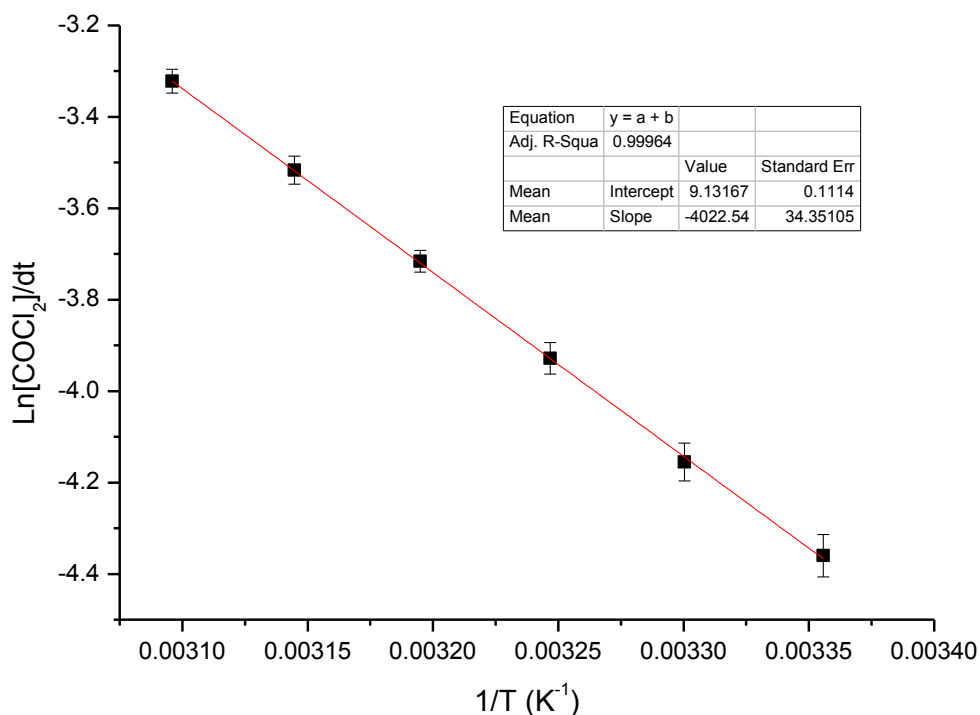


Figure 52 Arrhenius temperature dependence of phosgene formation (error bars represent standard deviation of three repeat experiments)

From Figure 52 the activation energy is calculated to be $34.1 \pm 0.2 \text{ kJ mol}^{-1}$ (error standard deviation of 3 repeat runs) which is slightly lower than that reported by Mitchell and co-workers² and comparable to a recent study⁹¹. This value i.e. $> 20 \text{ kJ mol}^{-1}$ indicates the reaction to be under kinetic control⁵⁶.

4.5.1 Time on Stream

The reaction flow was passed over the by-pass containing 0.1250 g ground quartz until stable signals were detected in the infrared and UV spectrometers; these were taken as the A_0 values for each reagent. The flow was then switched over to the reactor containing catalyst (0.1249g) and left for 20 minutes before samples were taken. The reaction was monitored at 323 K for 5 hours sampling every 30 minutes.

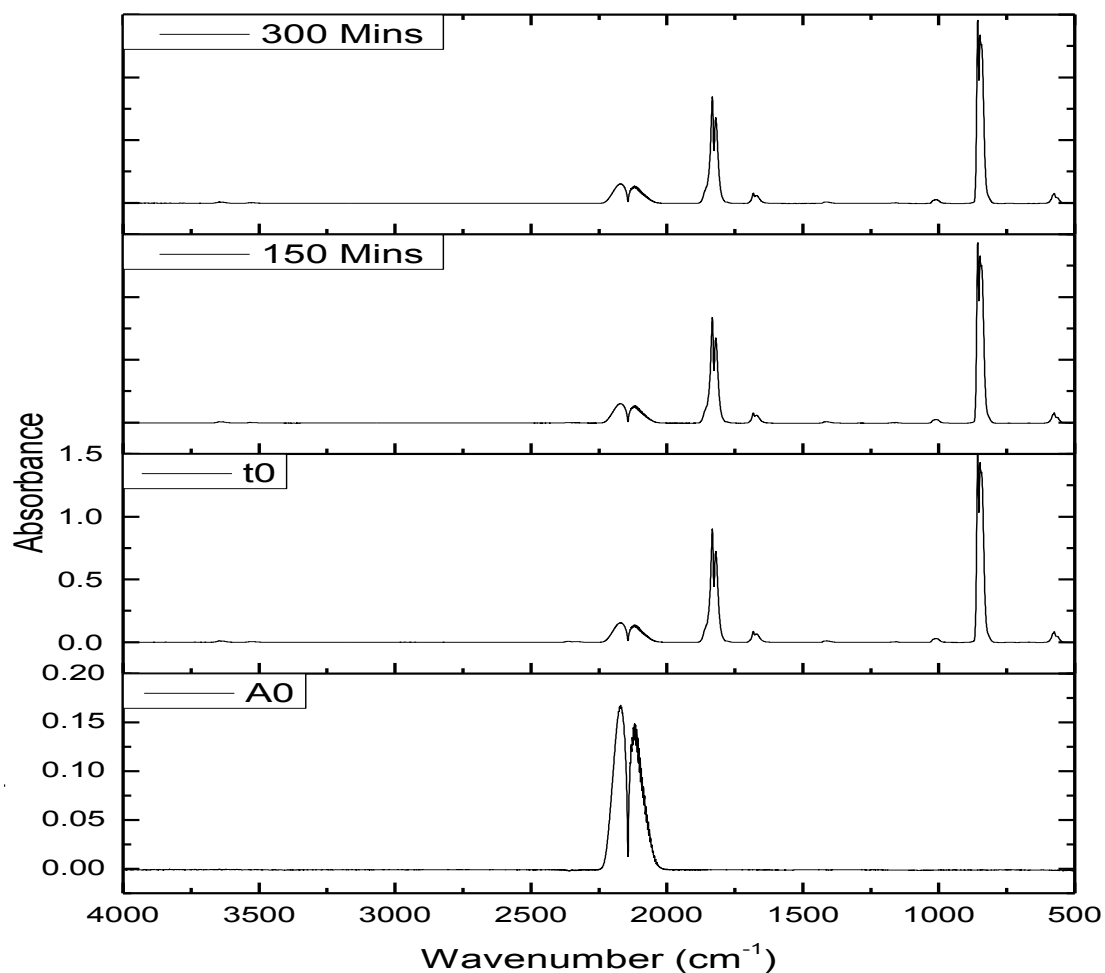


Figure 53 IR Spectra of reaction between CO and Cl₂ over the catalyst as a function of temperature with flow rates of 5 cm³ min⁻¹ and 4 cm³ min⁻¹ in a total flow of 159 cm³ min⁻¹ at 323 K over a period of 5 hours

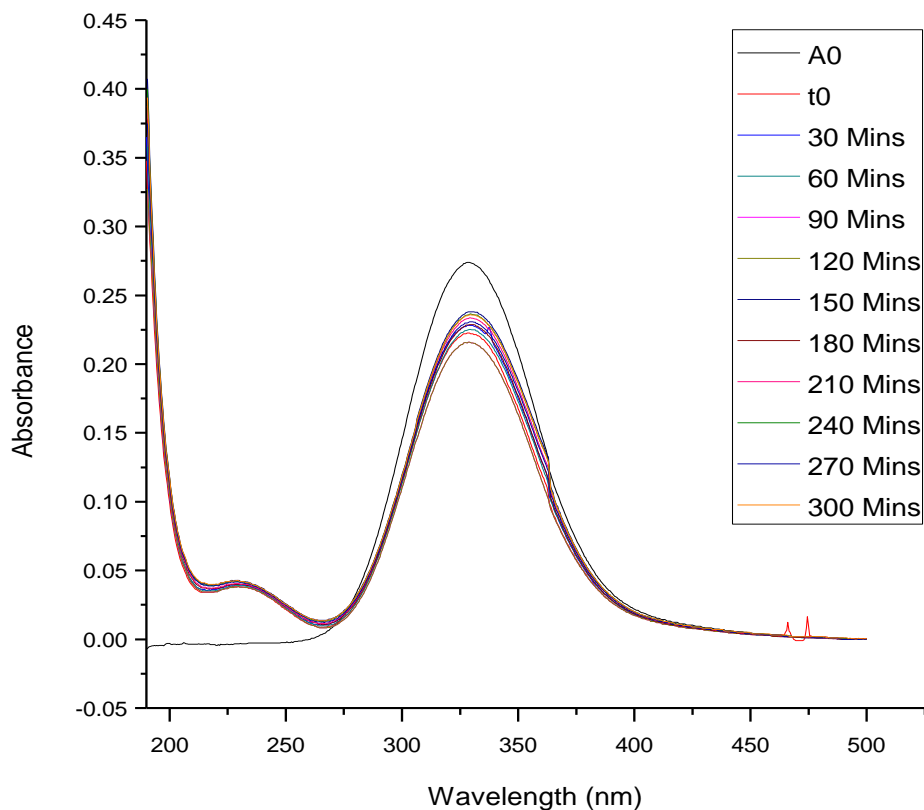


Figure 54 UV Spectra of reaction between CO and Cl₂ over the catalyst as a function of temperature with flow rates of 5 cm³ min⁻¹ and 4 cm³ min⁻¹ in a total flow of 159 cm³ min⁻¹ at 323 K over a period of 5 hours

From the obtained spectra, (Figure 53-54) there is little change in each of the reagents and product as a function of time over the 5 hour period. This indicates the reaction system to have stabilised and the apparatus to be stable and reproducible in performance over this time period.

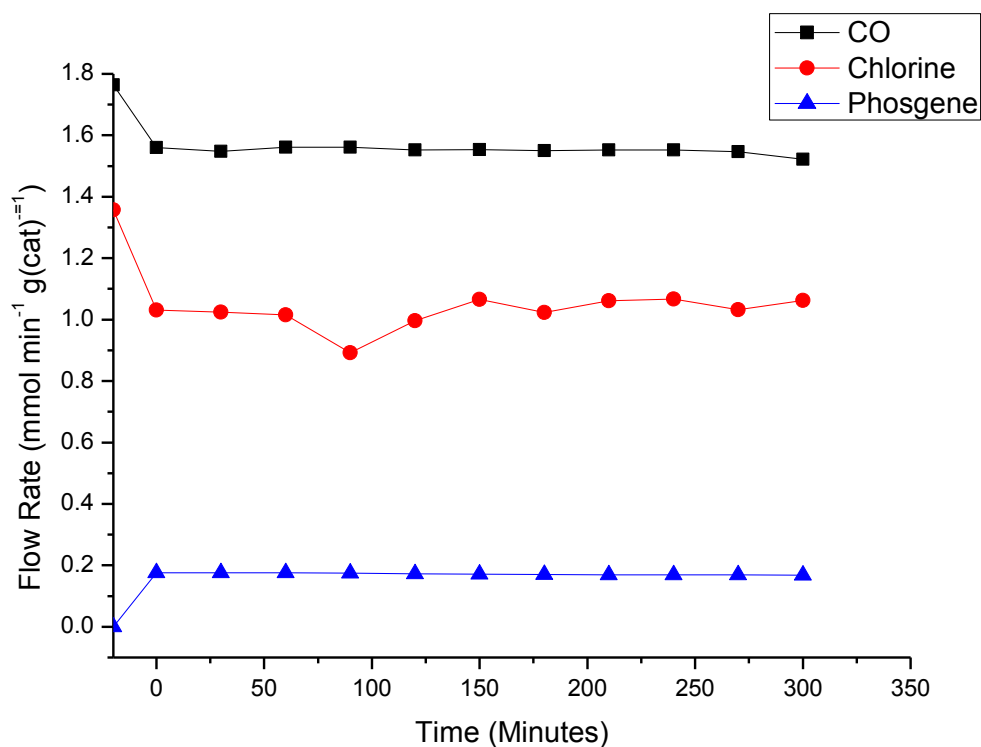


Figure 55 Reaction profile for the reaction between CO and Cl₂ over the catalyst as a function of temperature with flow rates of 5 cm³ min⁻¹ and 4 cm³ min⁻¹ in a total flow of 159 cm³ min⁻¹ at 323 K over a period of 5 hours

From the reaction profile in figure 55, the reaction operates under steady state with 100% selectivity to phosgene and low conversion (X_{CO} 12% and X_{Cl_2} 25%). The reaction always operates with an excess flow of CO, *i.e.* $[CO] > [Cl_2]$, 0.20 mmol min⁻¹ to 0.16 mmol min⁻¹. All the reagents are accessible in the gas phase and quantifiable allowing the construction of a reaction mass balance.

4.5.2 Mass Balance

The mass balance for the experiment was calculated providing information on how each reagent/product was distributed throughout the reaction coordinate. So the mass balance relationship

$$[CO]_{t=0} + [Cl_2]_{t=0} = [COCl_2]_t + [CO]_t + [Cl_2]_t \quad (31)$$

In terms of molar flow rate for CO

$$[CO]_{missing} = [CO]_{t=0} - [CO]_t + [COCl_2]_t \quad (32)$$

$$[Cl_2]_{missing} = [Cl_2]_{t=0} - [Cl_2]_t + [COCl_2]_t$$

And the mass balance relationship is calculated by

$$[CO]_{Total} = [CO]_t + [COCl_2]_t + [CO]_{Missing} \quad (33)$$

$$[Cl_2]_{Total} = [Cl_2]_t + [COCl_2]_t + [Cl_2]_{Missing}$$

The A_0 value was determined by the initial flow rate of each reagent over the ground quartz. The mass balance for each reagent (CO and Cl_2) are shown in Fig. 56 and 57

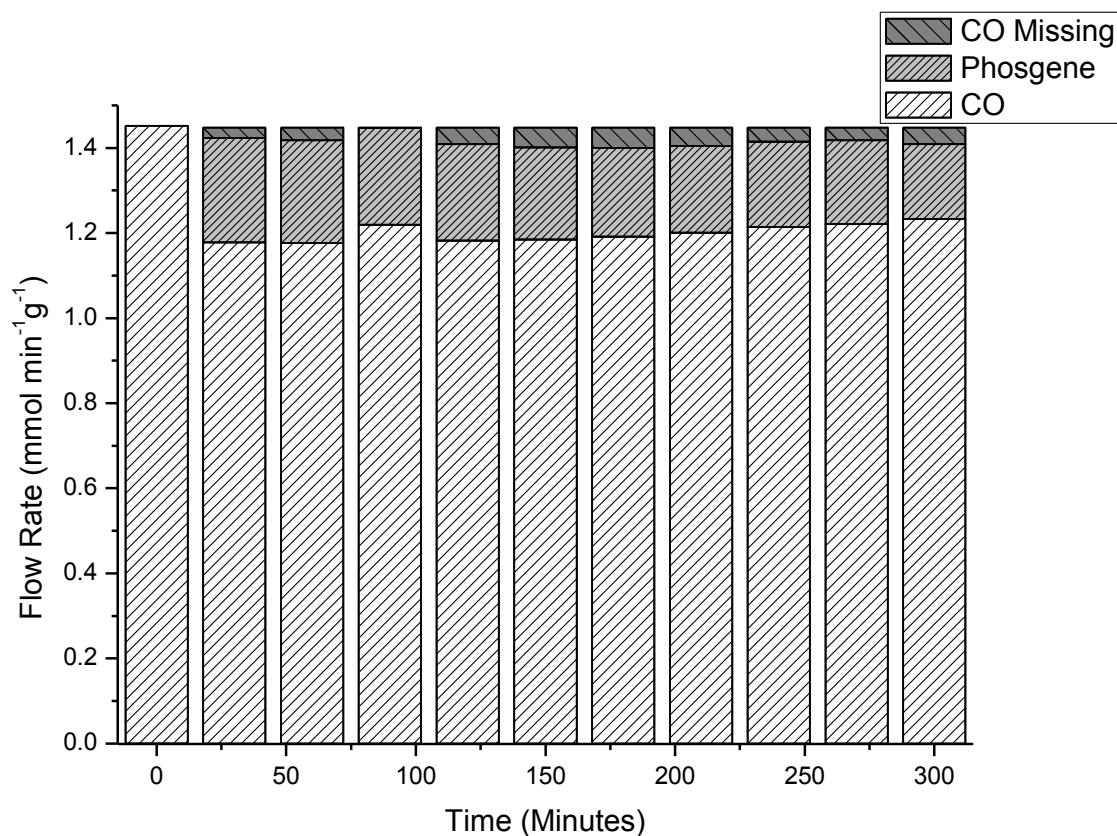


Figure 56 CO mass balance profile for the reaction between CO and Cl₂ over the catalyst as a function of temperature with flow rates of 5 cm³ min⁻¹ and 4 cm³ min⁻¹ in a total flow of 159 cm³ min⁻¹ at 323 K over a period of 5 hours

From the mass balance for CO there appears to be a mass imbalance of CO at steady state of 0.020 mmol min⁻¹ g⁻¹ *i. e.* very small missing mass (~2%). So for the reaction

$$\frac{-d[\text{CO}]}{dt} \approx \frac{d[\text{COCl}_2]}{dt} \quad (34)$$

So, all the CO can be effectively accounted for throughout the whole reaction coordinate as there is approximately complete incorporation of the CO to COCl₂. The small quantity of unaccounted CO evident in figure 56 is thought to be below the precision of the measurement at ~± 5%.

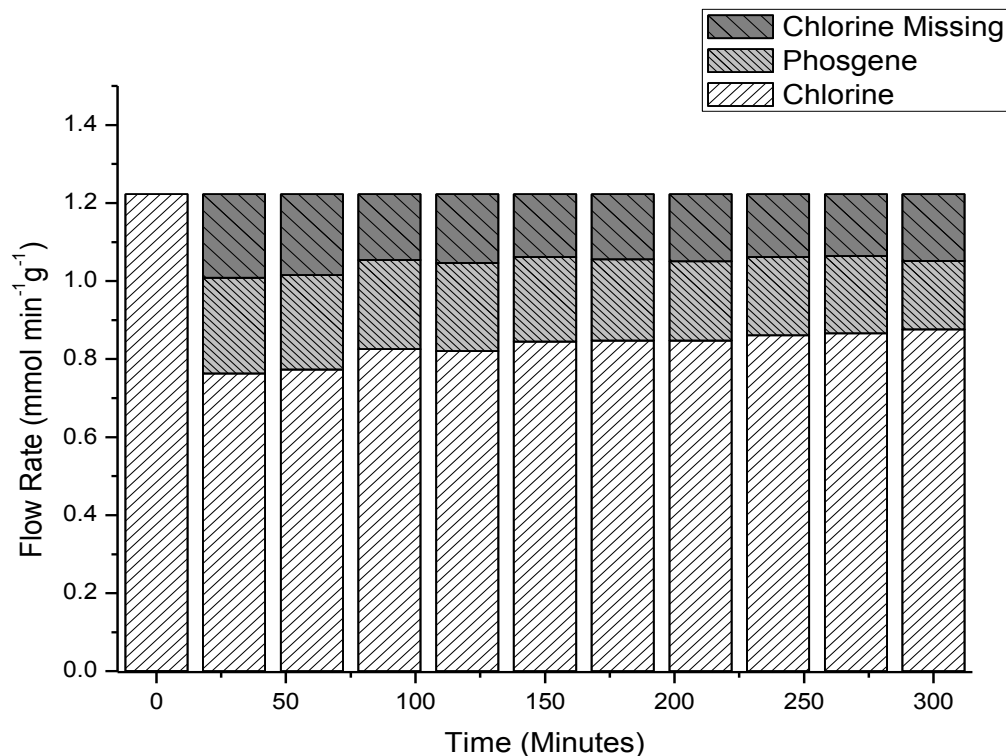


Figure 57 Cl₂ mass balance plot profile for the reaction between CO and Cl₂ over the catalyst as a function of temperature with flow rates of 5 cm³ min⁻¹ and 4 cm³ min⁻¹ in a total flow of 159 cm³ min⁻¹ at 323 K over a period of 5 hours

From the mass balance for Cl₂ there appears chlorine mass imbalance at steady state of 0.16 mmol min⁻¹ g⁻¹ missing mass so for the reaction

$$\frac{-d[Cl_2]}{dt} \neq \frac{d[COCl_2]}{dt} \quad (35)$$

This corresponds to a cumulative mass imbalance of 50.2 mmol Cl₂ min⁻¹ g⁻¹_{cat} over the 300 minute period that represents ~16.3 % of the total Cl₂ exposure over that period.

Thus, the missing mass is attributed to the retention of chlorine by the catalyst. The plot for the overall mass balance is presented in figure 57.

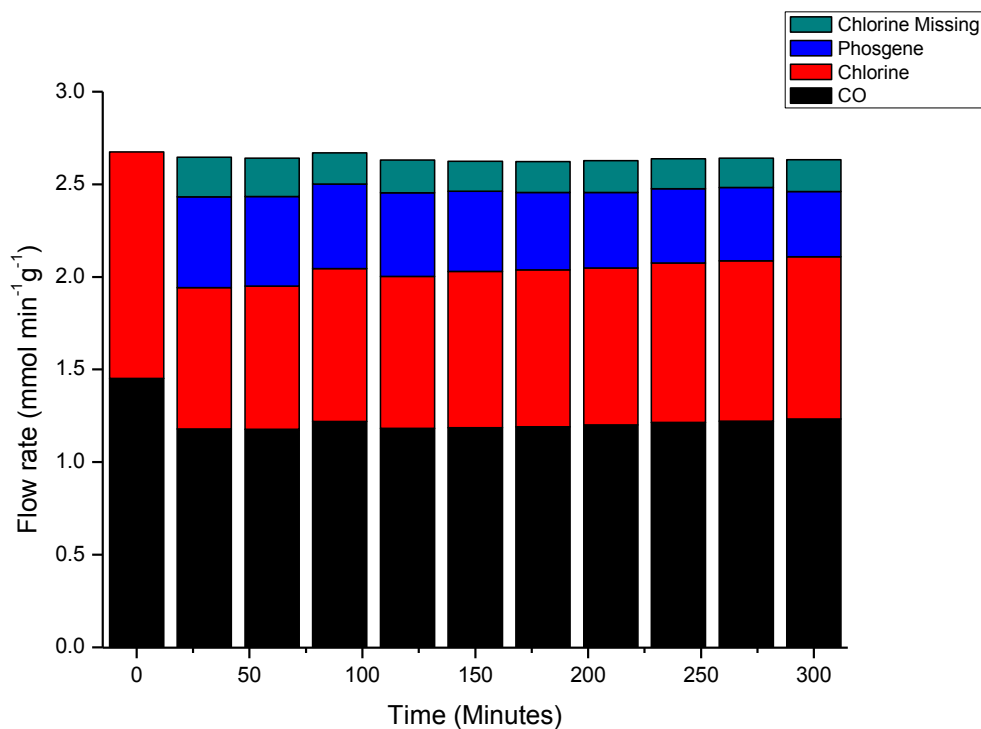


Figure 58 Overall mass balance plot profile for the reaction between CO and Cl₂ over the catalyst as a function of temperature with flow rates of 5 cm³ min⁻¹ and 4 cm³ min⁻¹ in a total flow of 159 cm³ min⁻¹ at 323 K over a period of 5 hours

From the reaction mass balance (Fig 58), there is a mass imbalance throughout the whole reaction coordinate. This can be attributed to retention of chlorine by the catalyst as there are no observable by-products throughout the reaction coordinate(See Section 4.1.1). However, there must be a limited capacity of retained material by the catalyst. This matter is further investigated in section 6.2 by monitoring the reaction over extended time periods.

4.6 Rate Law

The reactor was charged with 0.1250g of catalyst. The rate law was calculated by the isolation method⁵⁵ which involves following the reaction isothermally at 323 K and fixing one of the reagents concentration in large excess.

For the CO order dependence, the flow of Cl₂ was kept constant at 15 cm³ min⁻¹ and the nitrogen flow was changed with the varying CO so that the total flow going through the reactor was 59 cm³ min⁻¹(Fig. 59 and 60). For Cl₂ a comparable procedure was followed (Fig 61 and 62).

However, to determine the phosgene order dependence on the reaction, the flows of Cl₂ and CO were fixed at normal operational flows (CO 15 cm³ min⁻¹ and Cl₂ 15 cm³ min⁻¹). Once steady state phosgene production was established, COCl₂ was introduced to the feed stream in a controlled manner and the spectra periodically recorded. As the phosgene concentration was varied the CO signal in the infra-red was used to quantify the rate of formation of phosgene as:

$$\frac{-d[CO]}{dt} \approx \frac{d[COCl_2]}{dt} \quad (34)$$

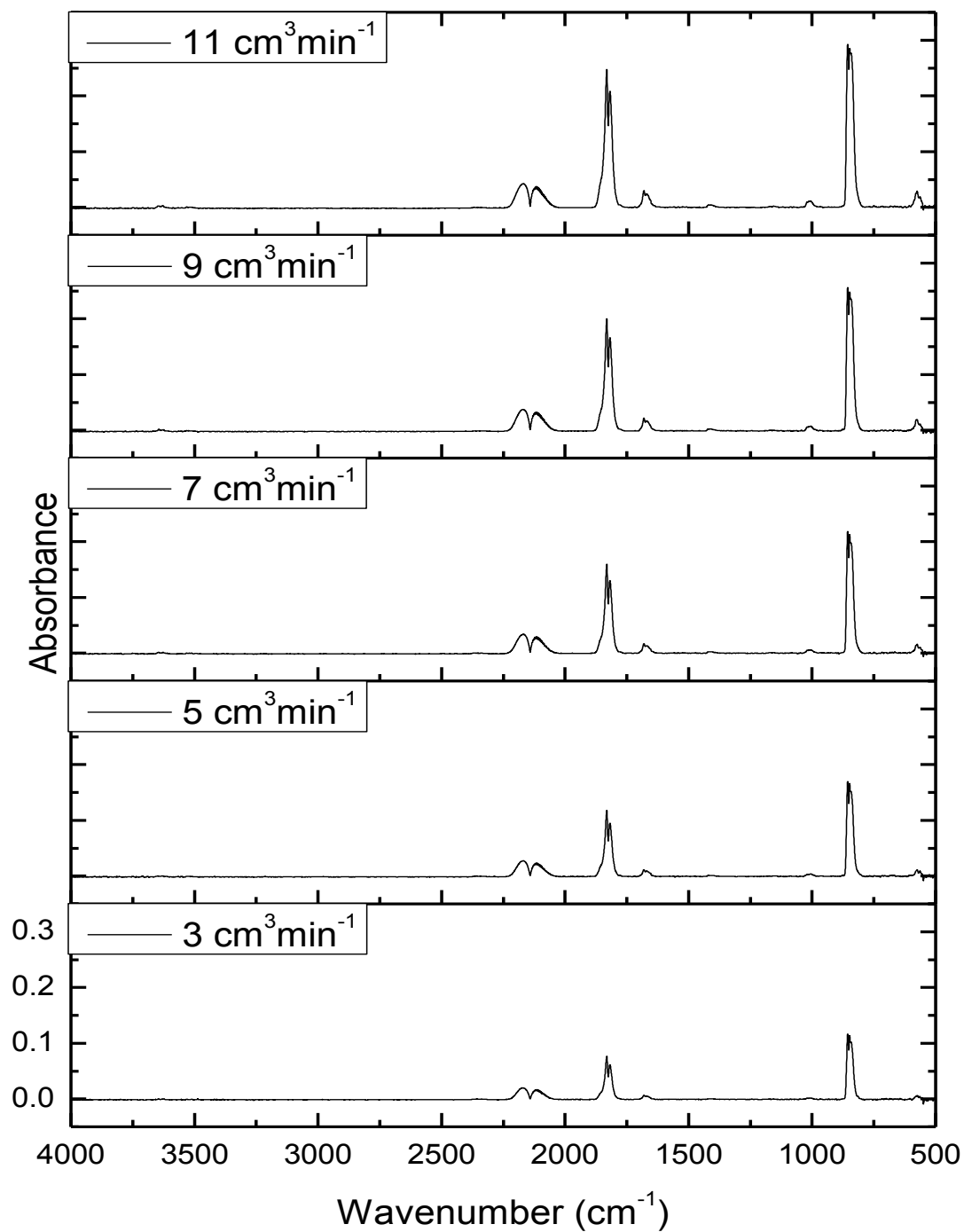


Figure 59 Infrared for the rate law determination with Cl₂ fixed at a flow rate of 15 cm³ min⁻¹ and the flow rate of the CO indicated in the box of each spectrum at 323 K gas cell 1

Table 13 Main peak assignments for Fig 59

Peak position (cm ⁻¹)	Assignment
2169, 2119	ν (CO)
1832, 1820	ν_1 (CO) of COCl ₂
848	ν_4 asymmetric (C-Cl stretch)

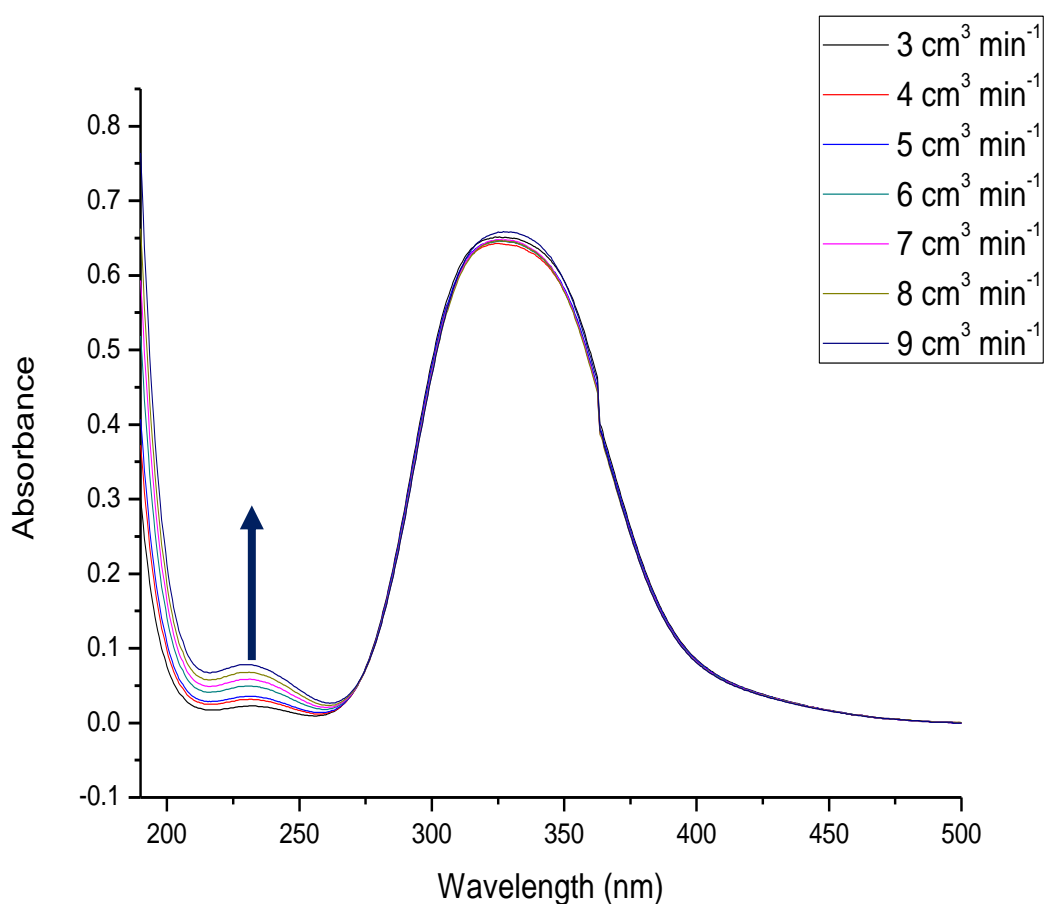


Figure 60 UV for the rate law determination with Cl₂ fixed at a flow rate of 15 cm³ min⁻¹ and the flow rate of the CO indicated in the box of each spectrum at 323 K

From the obtained spectra Figures 59-60, it is apparent that the reaction rate increases on increasing CO flow rate. From the IR spectra (fig 59) obtained it is clear that there is an increase in the ν_1 (CO) and the ν_4 asymmetric C-Cl stretch of COCl₂ and an increase in the ν (CO) on increasing the CO flow rate.

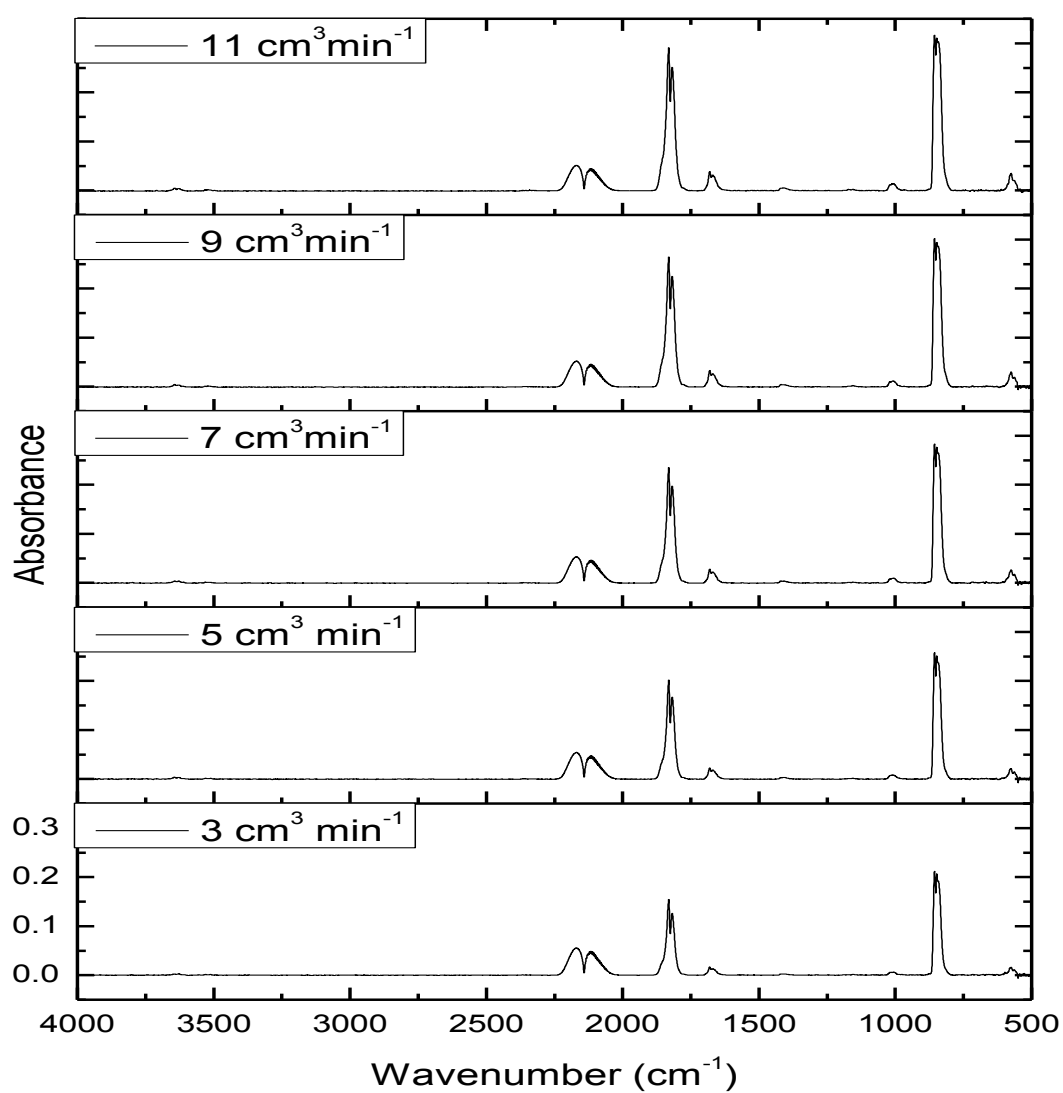


Figure 61 Infrared for the rate law determination with Cl_2 fixed at a flow rate of $15 \text{ cm}^3 \text{ min}^{-1}$ and the flow rate of the CO indicated in the box of each spectrum at 323 K gas cell 1

Table 14 Main peak assignments for Fig 61

Peak position (cm ⁻¹)	Assignment
2169, 2119	ν (CO)
1832, 1820	ν_1 (CO) of COCl ₂
848	ν_4 asymmetric (C-Cl stretch)

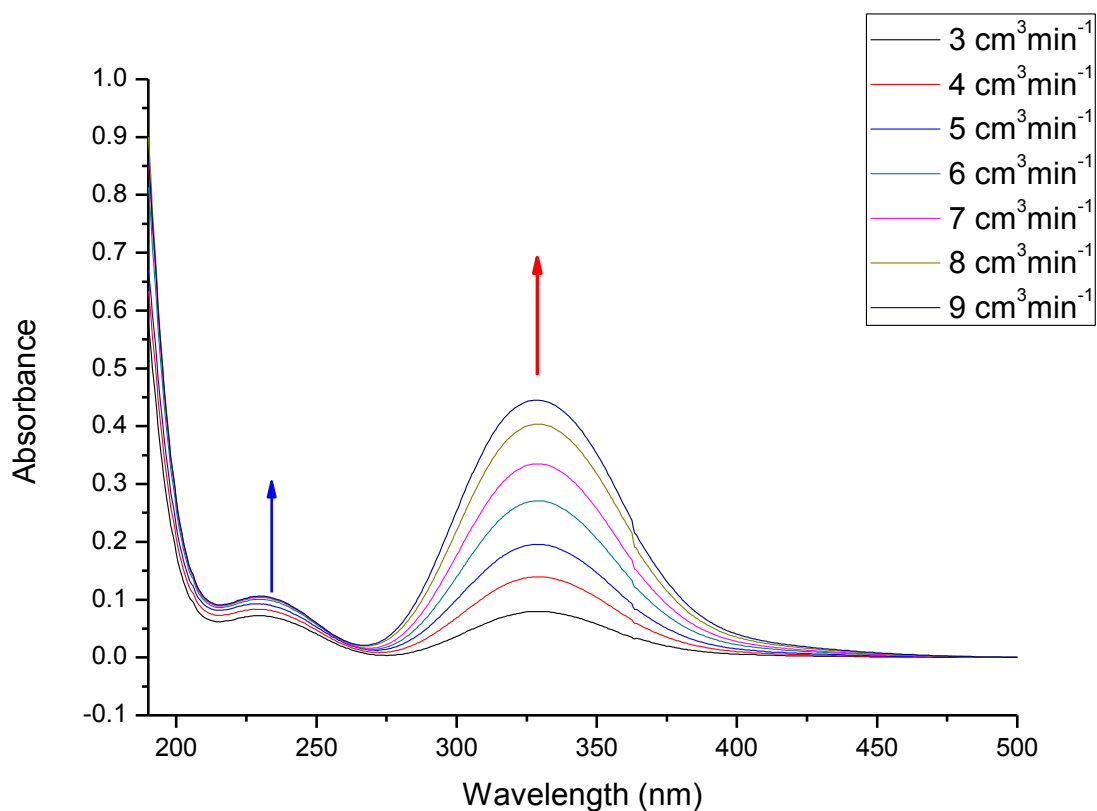


Figure 62 UV for the rate law determination with Cl₂ fixed at a flow rate of 15 cm³ min⁻¹ and the flow rate of the CO indicated in the legend at 323 K

From the obtained spectra Figures 61-62, it is apparent that the reaction rate increases on increasing Cl₂ flow rate. From the IR spectra (fig 61) obtained it is clear that there is an increase in the ν_1 (CO) and the ν_4 asymmetric C-Cl stretch of COCl₂ and an increase in the ν (CO) on increasing the Cl₂ flow rate. From the UV-visible spectra there is an increase in phosgene production and chlorine present on increasing the chlorine flow rate.

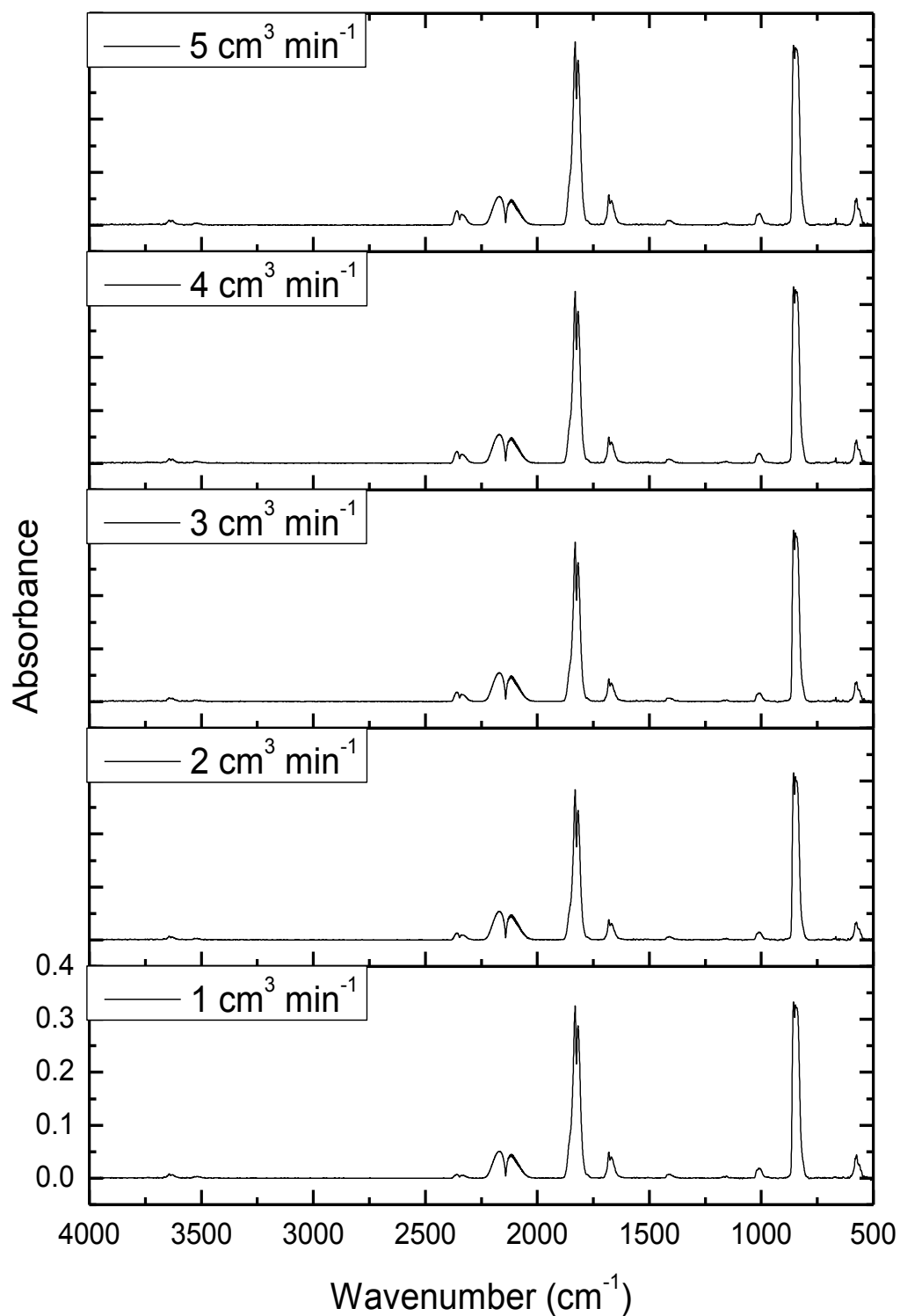


Figure 63 Infrared for the rate law determination of phosgene with CO and Cl_2 fixed at a flow rate of $15 \text{ cm}^3 \text{ min}^{-1}$ and the flow rate of the phosgene indicated in the box of each spectrum at 323 K (Gas Cell 1)

Table 15 Main peak assignments for Fig 63

Peak position (cm ⁻¹)	Assignment
2169, 2119	ν (CO)
1832, 1820	ν_1 (CO) of COCl ₂
848	ν_4 asymmetric (C-Cl stretch)

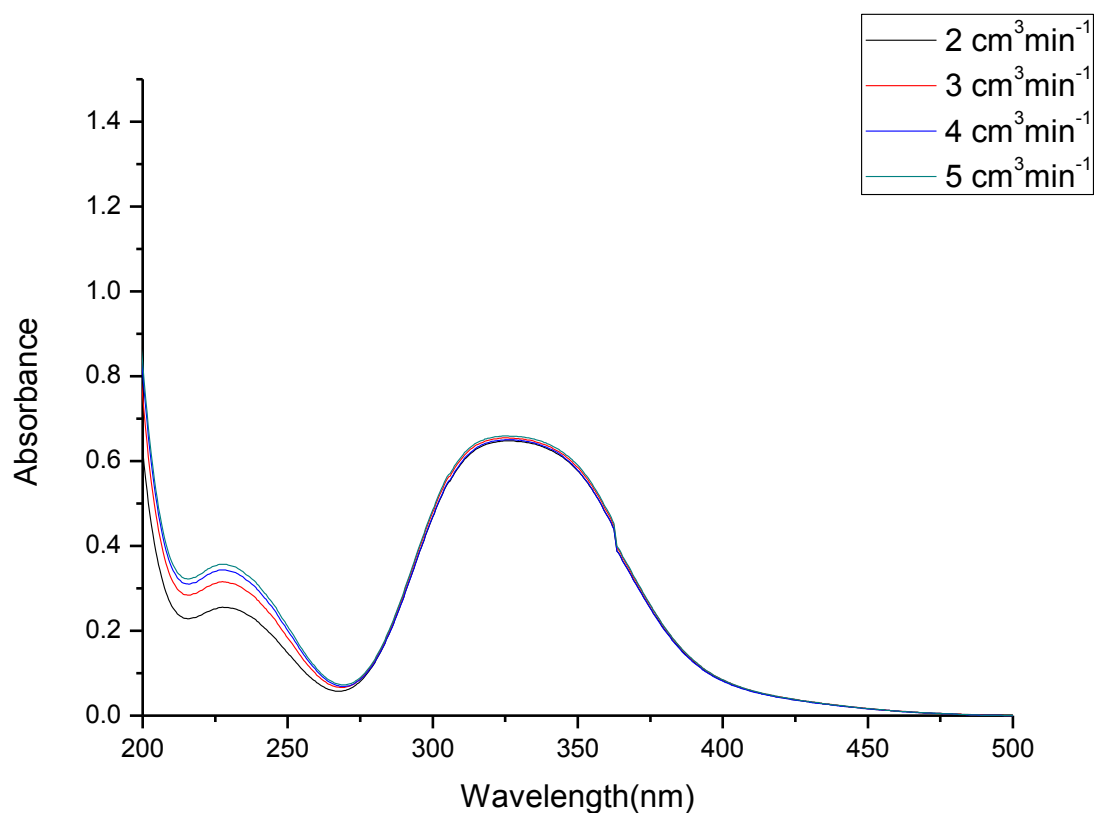


Figure 64 Infrared for the rate law determination of phosgene with CO and Cl₂ fixed at a flow rate of 15 flow rate of the phosgene indicated in the box of each spectrum at 323 K

From the obtained spectra Figures 63-64, it is apparent that the reaction rate is not affected on increasing COCl₂ flow rate. From the IR spectra (fig 63) obtained it is clear that there is an increase in the ν_1 (CO) and the ν_4 asymmetric C-Cl stretch of COCl₂ and an increase in the ν (CO) on increasing the COCl₂ flow rate. From the UV-visible spectra there is an increase in phosgene however, the chlorine remains constant on increasing the COCl₂ flow rate.

From the obtained spectra Figures 55-60, it is apparent that the reaction rate increases as the concentration of the limiting reagent increases. However, from Figures 57 it is clear that there is little change in the band due to $\nu(\text{CO})$ as a function of increasing phosgene concentration in the feed stream, indicating that the phosgene production rate is unaffected.

The rate of phosgene production (v) can be written as:

$$v = k[\text{CO}]^x[\text{Cl}_2]^y \quad (35)$$

where k is a rate constant

So, by fixing one of the reagent concentration the rate becomes.

$$v' = k'[\text{CO}]^x \text{ where } \frac{-d[\text{Cl}_2]}{dt} = 0 \quad (36)$$

when $[\text{Cl}_2] \gg [\text{CO}]$

So, by plotting the natural log of both sides gives the equation:

$$\ln[\text{COCl}_2] = x \ln[\text{CO}] + \ln k' \quad (37)$$

Where the gradient is the power as to which the reagent is raised in the rate law. To obtain the order dependence of phosgene, $[\text{COCl}_2]$ was varied and both $[\text{CO}]$ and $[\text{Cl}_2]$ were fixed. The consumption of $[\text{CO}]$ was used as the production of phosgene.

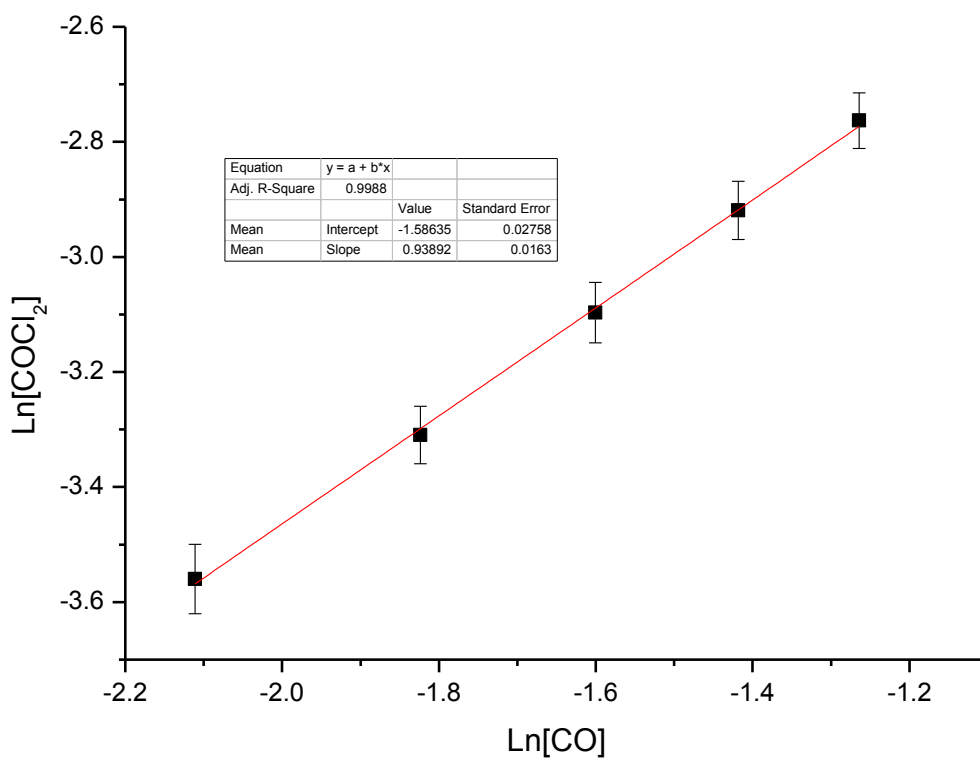


Figure 65 Plot of the log of the concentration dependence of CO on phosgene production

The dependence on the rate of [CO] can be written:

$$v = \frac{d[COCl_2]}{dt} \propto [CO]^{0.93 \pm 0.02} \quad (38)$$

The error is the standard error in the fit.

The reaction shows approximately first order dependence on [CO] which is consistent with early literature^{5,6}.

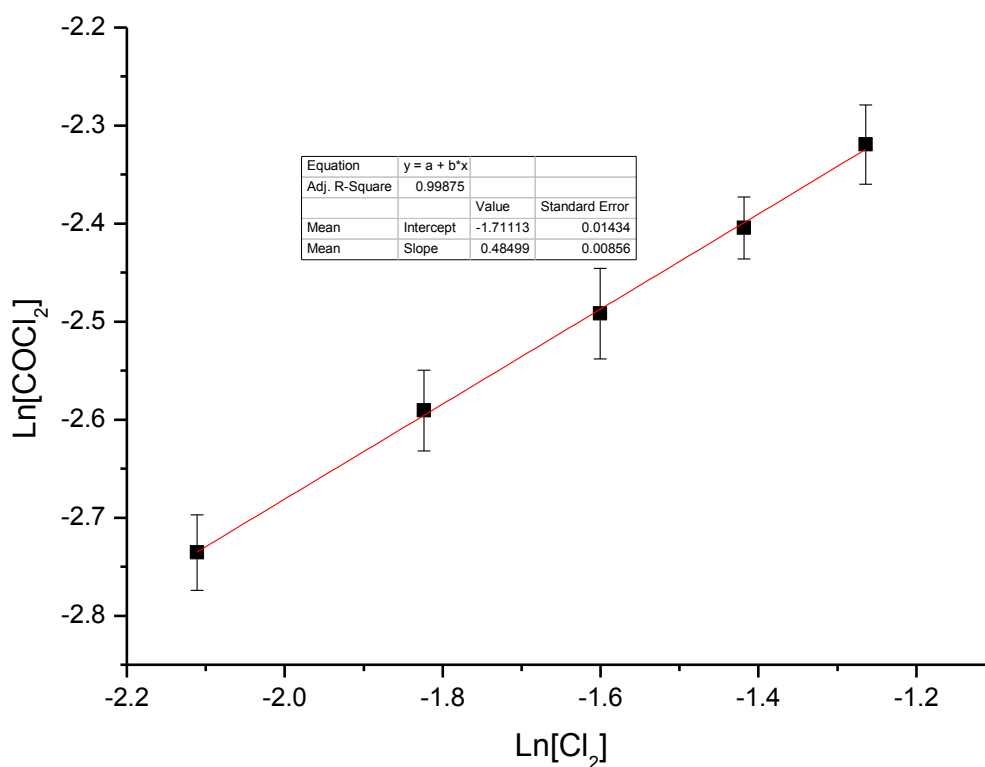


Figure 66 Plot of the log of the concentration dependence of Cl_2 on phosgene production

The dependence on the rate of $[\text{Cl}_2]$ can be written:

$$v = \frac{d[\text{COCl}_2]}{dt} \propto [\text{Cl}_2]^{0.48 \pm 0.01} \quad (39)$$

The error is the standard error in the fit.

The reaction shows approximately half order dependence on $[\text{CO}]$ which is consistent with early literature^{7,8}.

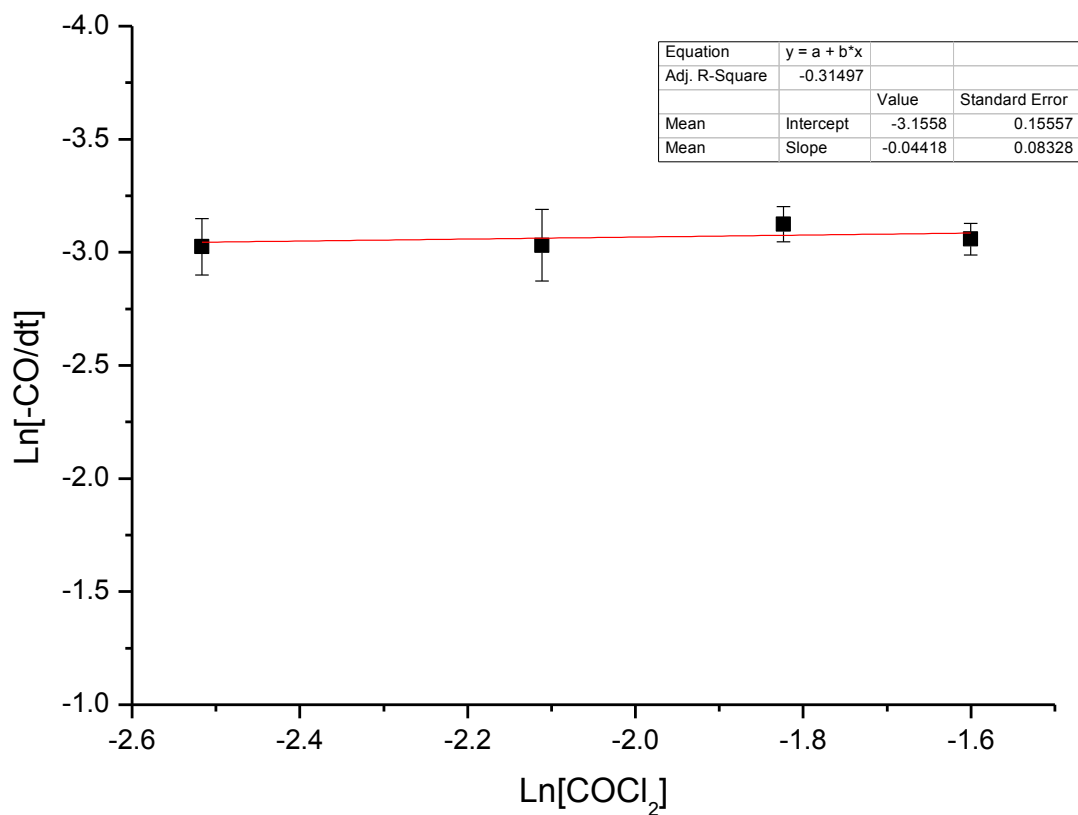


Figure 67 Plot of the log of the concentration dependence of COCl_2 on CO consumption

The dependence on the rate of $[\text{COCl}_2]$ can be written:

$$v = -\frac{d[\text{CO}]}{dt} \propto [\text{COCl}_2]^{-0.04 \pm 0.08} \quad (40)$$

The error is the standard error in the fit.

The reaction shows approximately zero order dependence on $[\text{COCl}_2]$.

So, the rate law for the formation of phosgene can be written as:

$$v = k[CO]^{0.93 \pm 0.02}[Cl_2]^{0.48 \pm 0.01}[COCl_2]^{-0.04 \pm 0.08} \quad (41)$$

where k represents a rate coefficient

The approximately half order dependence on chlorine indicates that the chlorine is reacting via dissociative adsorption mechanism.



The order dependence of both the CO and Cl₂ is consistent with the early work by Potter and Baron^{5,6}. The zero-order dependence of phosgene in the rate law indicates that phosgene does not affect, or even perturb the forward reaction. Thus, it appears that the presence of phosgene in the gas phase does not affect the catalytic turnover of CO and Cl₂

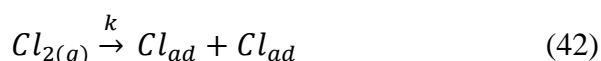
4.7 Summary

The reaction between CO and Cl₂ of the Donau K40 carbon catalyst is an efficient process which exhibits an activation of 34.1 ± 0.2 kJ mol⁻¹. Under the current flow regime, the homogeneous component does not play a role in the reaction chemistry over the catalyst. The rate law for phosgene formation over this catalyst can be written as:

$$v = k[CO]^{0.93 \pm 0.02} [Cl_2]^{0.48 \pm 0.01} [COCl_2]^{-0.04 \pm 0.08} \quad (41)$$

Where k represents a rate coefficient

The approximately half order in chlorine is suggestive that the chlorine is reacting via a dissociative adsorption mechanism.



The order dependence of both the CO and Cl₂ is consistent with the early work by Potter and Baron^{5,6}. The zero-order dependence of phosgene in the rate law indicates that the presence of phosgene does not affect the forward reaction chemistry. An awareness of the extent of reagent/product adsorption (Section 6.1) will allow for the form of the reaction mechanism to be deduced between Langmuir-Hinshelwood or Eley-Rideal.

Chapter 5-Kinetic validation- Mass transport considerations

5.1 Mass transport considerations

This chapter will examine the concept of mass transport and describe a series of tests which were used to validate that the reaction is under kinetic control and not limited by diffusion. The reaction was found to have an activation energy of 34.2 kJ mol⁻¹ which is large enough to be considered higher than that of external diffusion limitation⁵⁶. However, the reaction was subject to two tests that further evaluate whether intra and inter mass transport limitations play a role in the reaction chemistry. An effectiveness factor for the Donau K40 carbon catalyst was also determined.

5.2 Reynolds Numbers and Flow Regimes

Reynolds numbers are dimensionless numbers used in fluid mechanics to predict flow patterns in different flow regimes⁷⁹. A Reynolds number (Re) is a ratio of momentum forces against viscous forces and quantifies the relative importance of these forces in a given flow regime. Reynolds numbers are calculated by the following equation⁵⁶

$$Re = \frac{\text{inertial forces}}{\text{viscous forces}} = \frac{\rho VD}{\mu} \quad (43)$$

Where:

ρ is the fluid density (kg m⁻³)

V is the mean fluid velocity (m s⁻¹)

D is the pipe diameter (m)

μ is the fluid viscosity (Pa s)

Reynolds numbers are used to characterise the flow regime of which there are two different situations. At low Reynolds numbers ≤ 1000 the flow is described as Laminar where the viscous component of the flow is controlling the flow pattern so the flow is said to be smooth. At high Reynolds numbers ≥ 2000 the flow is controlled by momentum, so the flow is said to be turbulent where there is good mixing. Table 16 shows the calculated values for the flow rates of the experiment and the corresponding Reynolds number

Table 16 Reynolds numbers for different flowrates

Flow Rate of drive (cm ³ min ⁻¹)	Reynolds number
59	0.14
39	0.09
29	0.07

The flow regime in which the experiment operates is laminar flow as the values obtained are <1000. The low Reynolds numbers indicate that the flow is firmly in a laminar flow regime

5.2 Plug Flow Reactors

The reactor in which all experiments were performed operates under a plug flow reactor regime. A plug flow reactor (PFR) sometimes called a continuous tubular reactor (Figure 68) operates under the following assumptions⁹²:

1. Flow rate and fluid properties are uniform over any cross section of the reactor normal to the monition of the flow
2. There is negligible radial mixing –due to diffusion.

These assumptions hold when there is good radial mixing which is achieved at high flow rates ($Re > 10^4$) and when axial mixing may be neglected (when the length divided by the pipe diameter is ≥ 50).

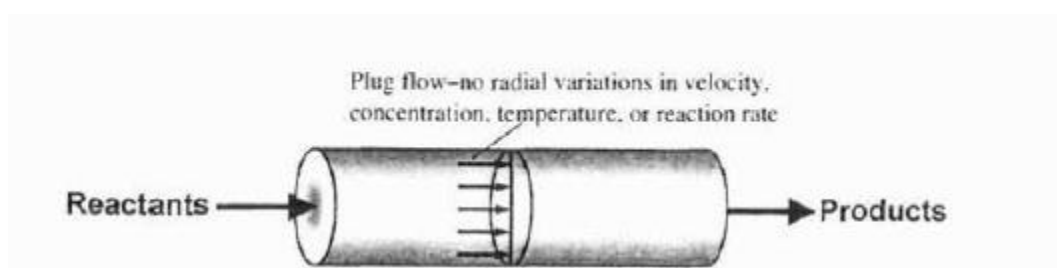


Figure 68 Plug flow (tubular) reactor⁹²

The flow in a plug flow reactor is assumed to be perfectly mixed as it moves through the reactor and will not exchange any material with the element in front or behind it. Another assumption

is that the reactor operates at steady state. This means that although reagent concentration varies on moving along the bed, however, at any given time the concentration at each point is constant⁶³.

5.4 Mass Transport

Mass transport plays a key role in catalytic reactions, which is the ability of reactants to diffuse onto the catalyst surface or within the catalyst pores. This is an important consideration when investigating reaction kinetics⁹³. There are three possible reaction regimes (Fig 69), 1. Kinetic - At low temperatures the effects due to diffusion will be insignificant so reaction kinetics will be observed; reactions at higher temperature have larger effects due to diffusion. 2. Internal mass transfer- pore diffusion plays an important role in controlling the rate of reaction. This is observed in the Arrhenius plot where the value obtained will be the average of the diffusion and the reaction and 3. External mass transfer- in this regime transport of material to the catalyst is limiting the reaction which can be observed by having low activation energy⁹³. The degree of diffusion limitation in the second regime is characterised by the “effectiveness factor”

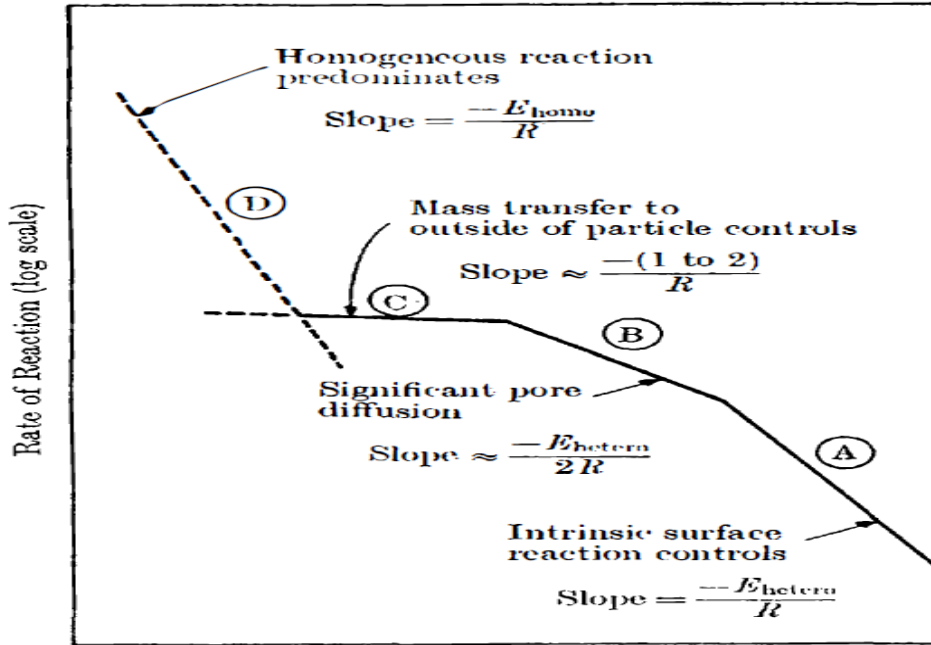


Figure 69 Possible reaction regimes for a gas phase reaction occurring on a porous solid catalyst. A is the reaction operating under kinetic control, B is the reaction operating with pore diffusion, C is the reaction limited by external diffusion and D is the homogeneous reaction⁵⁶

The catalyst effectiveness factor is a measurement of how the reaction rate is lowered by resistance to pore diffusion^{55,56,93,97} and is given by equation 1. The effectiveness factor is a measure of how much of the catalyst is being used.

$$\eta = \frac{\text{(reaction rate with diffusion)}}{\text{(reaction rate without diffusion)}} \quad (44)$$

The effectiveness factor can be measured by observing the reaction rate on several particle sizes under the same reaction conditions. The effectiveness factor approaches unity when no increase in reaction rate is observed on the subdivision of particle size. If data is available for finely divided particles having an effectiveness factor approaching unity, then the ratio of the reaction rate of the large particle to the reaction rate of the small particle is directly equal to the effectiveness factor of the larger particle.

5.5 Thiele Modulus

The Thiele modulus is a dimensionless number which is used to define the ratio between reaction rate and diffusion rate in porous catalysts (pellet). The Thiele modulus given is by the following equation⁵⁶:

$$\Phi_T = R \sqrt{\frac{k}{De}} \quad (45)$$

$$= \frac{\text{Rate of reaction}}{\text{Diffusion rate}}$$

Where Φ_T = Thiele modulus

De = effective diffusivity ($\text{m}^2 \text{s}^{-1}$)

R = Catalyst particle radius (m)

k = reaction rate constant (s^{-1})

The Thiele modulus is the inverse of the effectiveness factor and is given by the following equation:

$$\eta = \frac{1}{\Phi_T} \quad (46)$$

When a high value for the modulus occurs the reaction is said to be diffusion limited, whereas low values indicate the reaction is not limited by diffusion⁵⁶.

5.6 Methods for determining the presence of mass transport

There are a number of diagnostic tests⁹⁷ to determine whether there are interphase or intraphase mass transport limitations. There are a couple of diagnostic tests for the presence of interphase mass transport limitations. The tests are based on the principle that the space velocity (volume of catalyst /volume reactant per unit time) must be independent of the linear velocity. The external diffusion test (Fig.65) involves varying the catalyst volume and reagent flow while keeping their ratios constant.

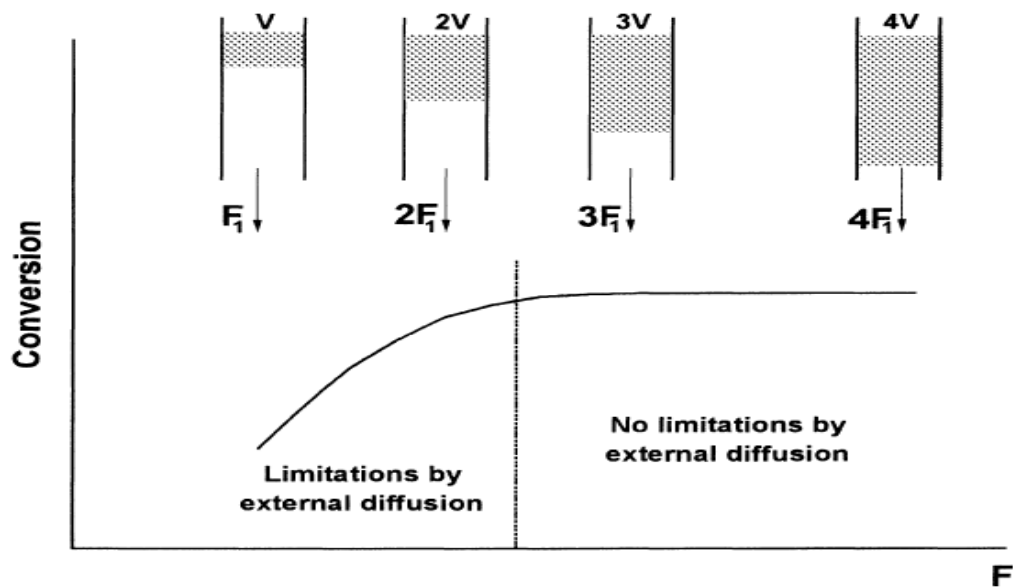


Figure 70 External diffusion test conversion vs flow rate. F is the flow rate and V is the volume of catalyst.⁹⁷

If there is no difference with respect to flow rate on conversion then it is possible to conclude that there is no interphase limitation. Figure 70 is another test for external diffusion is exactly the inverse of this by taking the space time ($1/\text{space velocity}$) and plotting two curves on two different volumes of catalyst and varying the space time. Plotting the two curves gives (Fig 71):

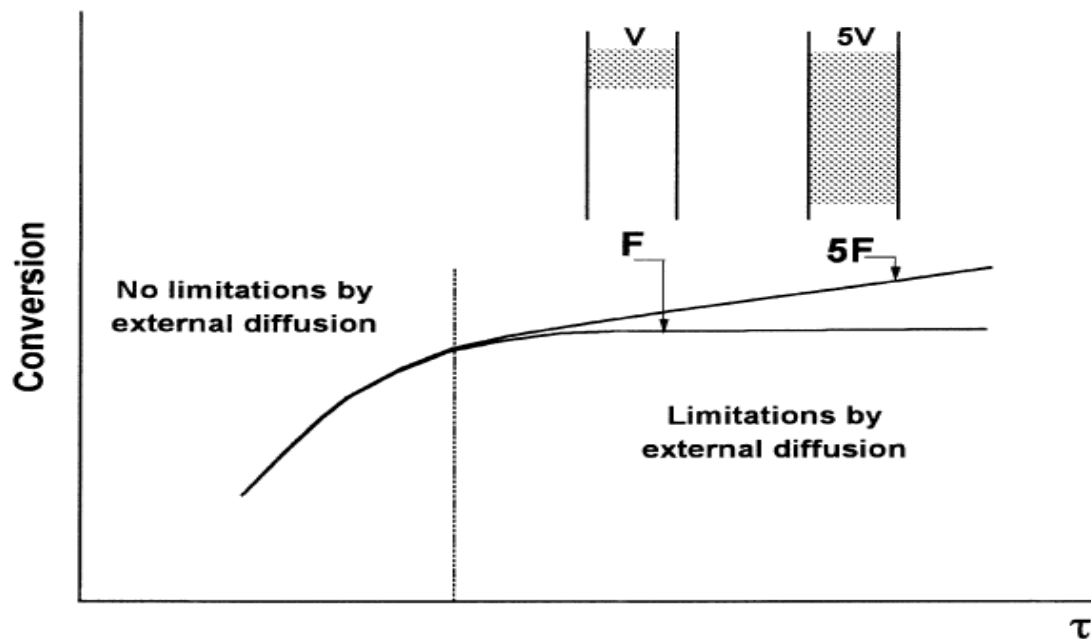


Figure 71 External diffusion test conversion vs space time. F is the flow rate, V is the volume of catalyst and τ is the space time.⁹⁷

If the two curves overlap illustrated in Fig 71 then the system is said to be under chemical kinetic control. For gas phase reactions it is possible to use the apparent activation energy as a means to detect interphase limitations if it has a value of $< 20 \text{ kJ mol}^{-1}$.⁵⁶

Intraphase limitations are harder to overcome. One of the ways to overcome this effect is to decrease particle size to as small as possible. A diagnostic test is to vary particle size while keeping a constant space velocity.

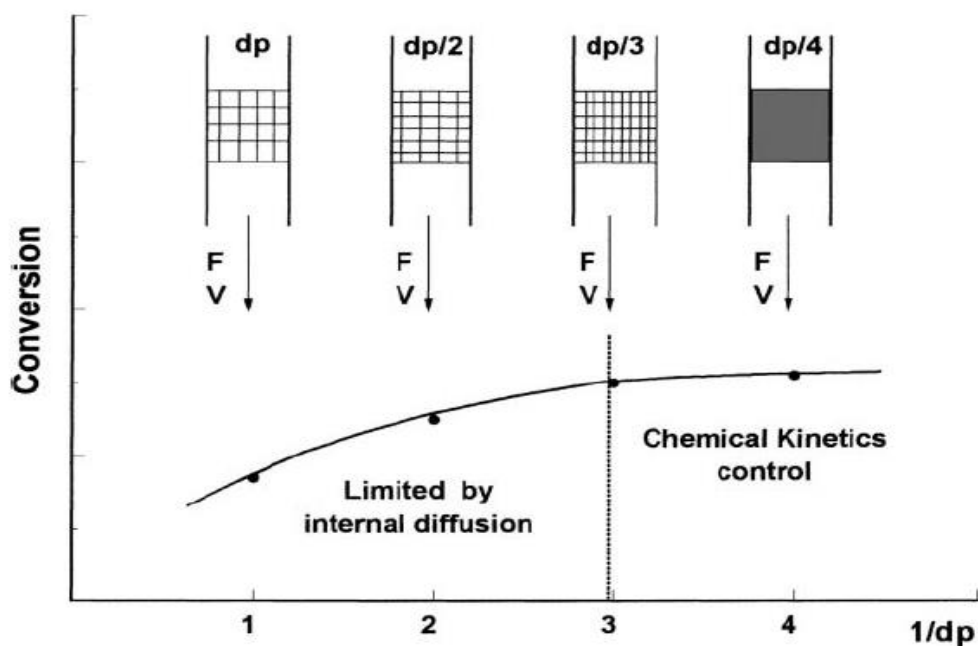


Figure 72 Evaluation of the influence of particle diameter on reaction rate. F is the flow rate, V is the volume of catalyst and dp is the particle size of the catalyst.⁹⁷

If the reaction rate remains constant on decreasing particle size then the reaction is under kinetic control and does not have any limitation by intraphase mass transport. The ratio of phosgene formation between powdered catalyst vs pellets was taken as a measure of relative catalyst effectiveness²

5.6.1 Intraphase Mass Transport Test Results

Different size fractions were prepared by grinding the Donau Supersorbon K40 catalyst through calibrated sieves (Endcots). Fig. 73 is the reaction rate of different size fractions and each point is the average value of monitoring the reaction under steady state at 323 K and sampling every 30 minutes for two hours. The size of particle was determined by physical sieving the catalyst and collecting at the various size fraction ranges (180-212, 212-250, 250-500, and 610-700 μm).

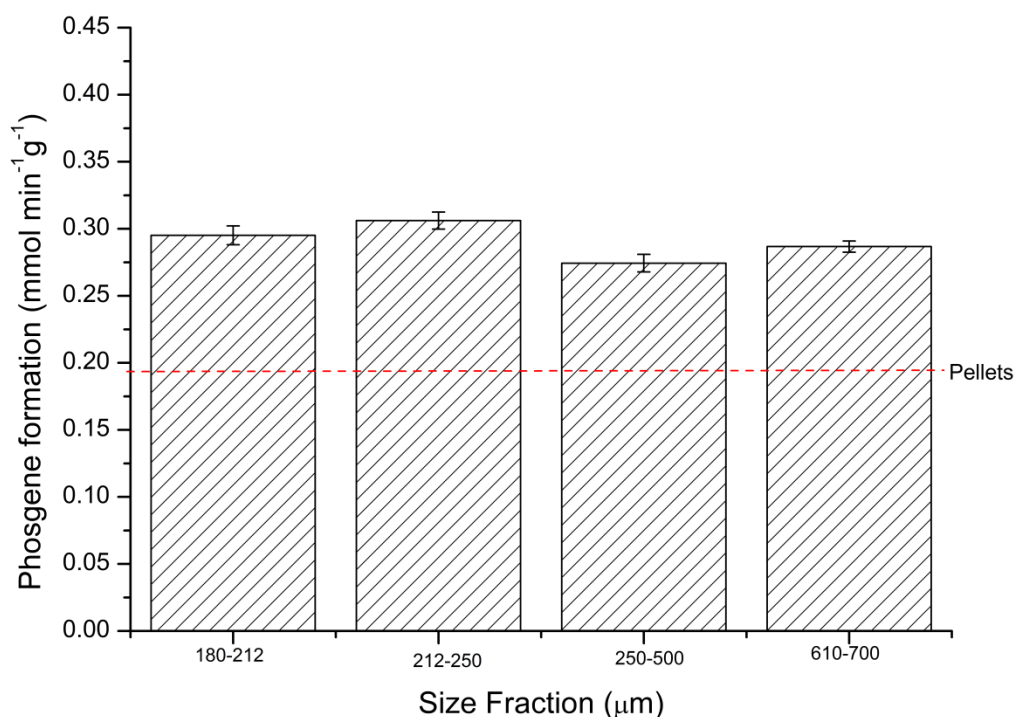


Figure 73 Reaction rate vs particle size at steady state for 2 hours a reaction temperature of 323 K in a total flow of $159 \text{ cm}^3 \text{ min}^{-1}$ (CO at $5 \text{ cm}^3 \text{ min}^{-1}$, Cl_2 at $4 \text{ cm}^3 \text{ min}^{-1}$ and N_2 at $150 \text{ cm}^3 \text{ min}^{-1}$). The dotted line represents phosgene production over the pelleted catalyst.

From Fig 73 comparing the different size fractions it is clear that there is very little difference in reaction rate relative to size fraction. This implies that the reaction is under surface kinetic control and is not intraphase mass transfer limited. However, there is a difference in reaction

rate between powder and pellet (Fig 74), which permits a relative effectiveness factor to be calculated

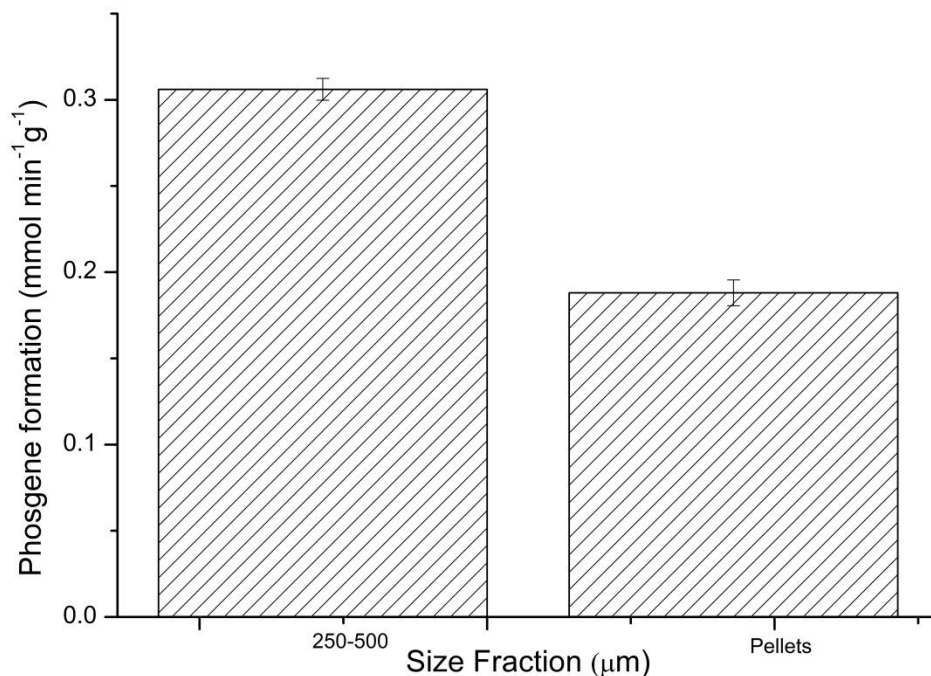


Figure 74 Reaction rate of powder vs at steady state for 2 hours a reaction temperature of 323 K in a total flow of 159 cm³min⁻¹(CO at 5 cm³ min⁻¹, Cl₂ at 4 cm³ min⁻¹ and N₂ at 150 cm³ min⁻¹).

$$\eta = \frac{\text{reaction rate pellet}}{\text{reaction rate powder}} \quad (50)$$

$$\frac{0.18 \text{ mmol min}^{-1} \text{ g}^{-1}}{0.27 \text{ mmol min}^{-1} \text{ g}^{-1}} = 0.70$$

The value is lower than the ratio reported in the literature for this catalyst which was 0.8². However, the experiment was performed at a higher temperature than that reported in the literature and the effectiveness factor decreases with increasing temperature ⁹³. The value obtained is high so the reaction is under chemical kinetic control as the barrier to diffusion is low.

5.6.2 Interphase Limitations

The reaction was monitored by changing the catalyst mass while keeping the flow conditions constant and following the reaction under steady state for two hours taking a sample every 30 minutes. The phosgene production rate as a function of space time is presented in Figure 75.

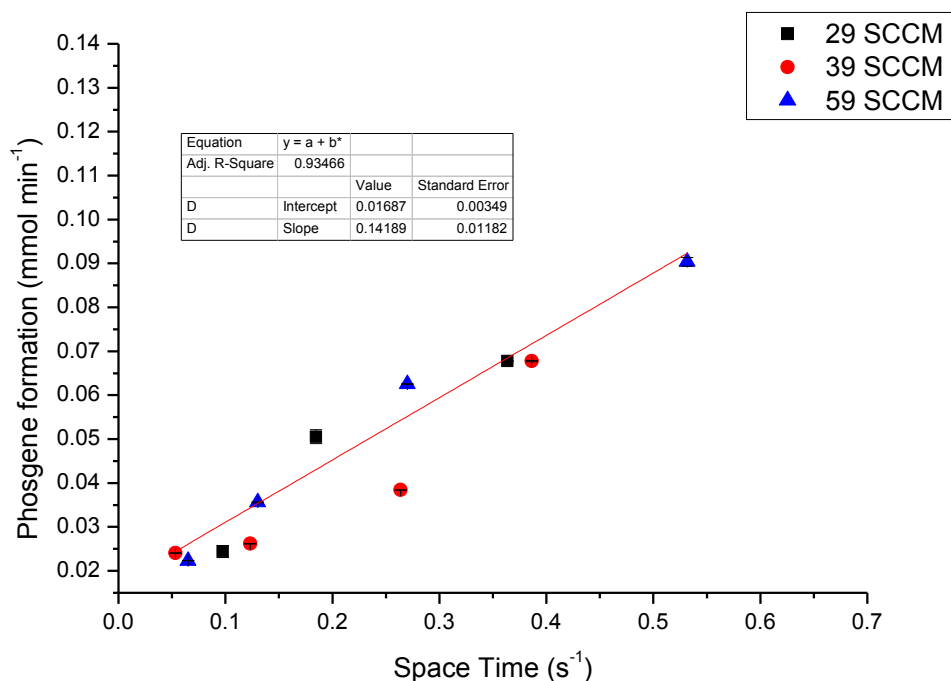


Figure 75 Phosgene production vs space time at 323 K. The squares are the drive flow at 20 cm³ min⁻¹, the circles are the drive flow at 30 cm³ min⁻¹, and the triangles are the drive flow at 50 cm³ min⁻¹ (CO at 5 cm³ min⁻¹, Cl₂ at 4 cm³ min⁻¹ and total N₂ at 150 cm³ min⁻¹).

$$\text{Slope} = 0.142 \pm 0.01 \text{ mmol min}^{-1}(\text{phosgene}) \text{ s}^{-1}$$

The error is the error in the fit

From figure 75 it is clear that the rate of phosgene production is directly proportional to the space time. All the points effectively lie on the same line, which indicates that the reaction is under chemical kinetic control and operates in the absence of interphase mass transfer.

5.7 Order dependence on changing catalyst mass

The order dependence of catalyst mass was determined by keeping the concentration of both carbon monoxide and chlorine constant so:

$$v_{[COCl_2]} = k[CO][Cl_2][Catalyst\ mass]^x \quad (51)$$

So by taking the natural log of both sides

$$\ln(v_{[COCl_2]}) = x \ln[catalyst\ mass] + \ln k' \quad (52)$$

where k' is a rate constant

The reaction was monitored isothermally at 323 K with one exception of a measurement at 298 K

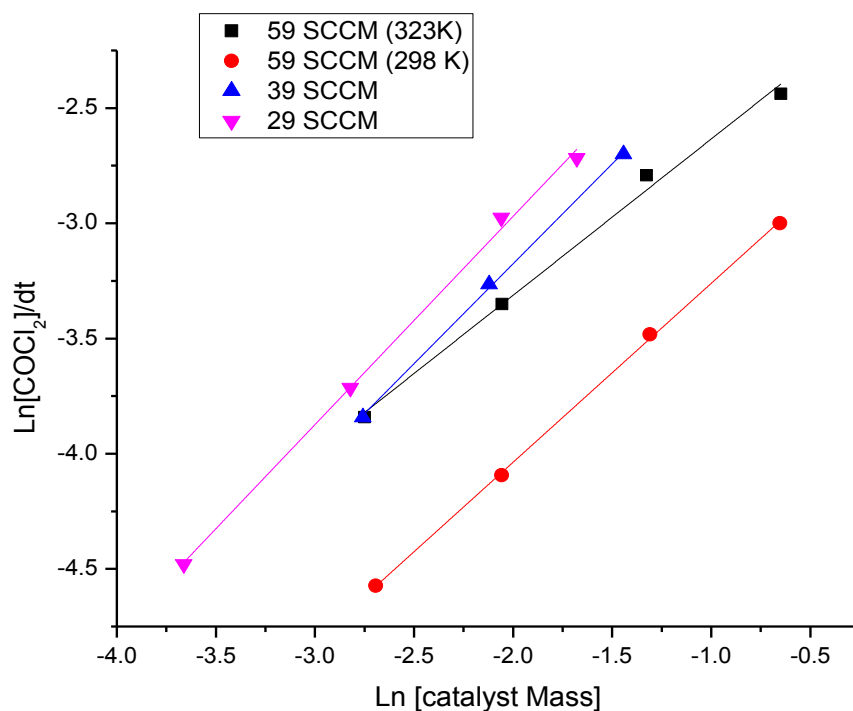


Figure 76 Plot of the log of the catalyst mass dependence of CO on phosgene production (CO at 5 cm³ min⁻¹, Cl₂ at 4 cm³ min⁻¹ and total N₂ at 150 cm³ min⁻¹).

Table 17 Order dependencies of catalyst mass

Flow rate through the reactor (cm ³ min ⁻¹)	Order dependence
59	0.68
59 (303 K)	0.78
39	0.86
29	0.90

From the results, it is clear that at slower flow the greater the rate of phosgene production and the order dependence is approaching unity at the slower flow rates (*i.e.* longer residence times). This could indicate that the residence time is too short at the standard flow rate of 59 cm³ min⁻¹ to get the full use of the reagents in the reactor and therefore at a reduced flow rate the experiment would operate under ideal flow conditions. The reaction conditions were selected to ensure detection linearity and allow for reliable quantification of reagent/product in both infrared and UV visible spectroscopy (Section 2.2.4). Reducing the flow rate/ increasing the residence time of the gases over the catalyst will lead to higher conversions, for a fixed temperature. However, this could compromise the applicability of the Beer-Lambert law used in our detection strategies. On this basis maintenance of the flow rate of 59 cm³ min⁻¹ was deemed more acceptable.

5.8 Discussion

The results indicate that the system operates under kinetic control in the absence of mass transfer limitations. From the experimentally determined activation energy of $34.1 \pm 0.3 \text{ kJ mol}^{-1}$ which is above the threshold for gas phase reactions to be limited by diffusion ($< 25 \text{ kJ mol}^{-1}$). This in combination with the size fraction experiments shows little change on reaction rate with smaller particle sizes so the reaction is not limited by internal diffusion. The effectiveness factor for the catalyst was found to be 0.7 which is close to the recent literature value calculated for this catalyst². The effectiveness factor signifies that the Thiele modulus has a low value of 1.42, which indicates that the reaction is under kinetic control.

The reaction rate was found to increase with increasing space time. The order dependence on changing catalyst mass also increases and tends towards first order at slower flow rates. However, the dilute conditions and the ability to experimentally obtain steady concentrations of reagents suggest that the experiment is operating under ideal plug flow conditions where there is good mixing. From Figure 75, all points lie on the same line which indicates the absence of external mass transfer.

It is acknowledged that the flow regime is not optimised to give optimal rates but operating under dilute conditions avoid exotherms and ensures detection linearity. When the flow conditions are slowed through the reactor the order dependence tends towards unity so there is a direct link between phosgene production and catalyst mass

Chapter 6- Mechanistic Studies

6.0 Introduction

This chapter will describe further kinetic measurements made on the Donau K40 activated carbon catalyst that allow the reaction mechanism to be deduced. These include adsorption, desorption and extended time on stream measurements. This builds on the current understanding to be able to describe the physio-chemical process operate over the Donau catalyst.

6.1 Breakthrough Measurements

Breakthrough measurements are a method to determine the adsorption capacity by the catalyst^{98,99}. The breakthrough is a measurement in a continuous flow system to determine the adsorption of reagents by the catalyst and is a measure of the return to initial concentration after switching from bypass to catalyst as a function of time. The breakthrough measurement was carried out using a two-reactor system (Figure 77) switching from position 1 to 2 on both valves.

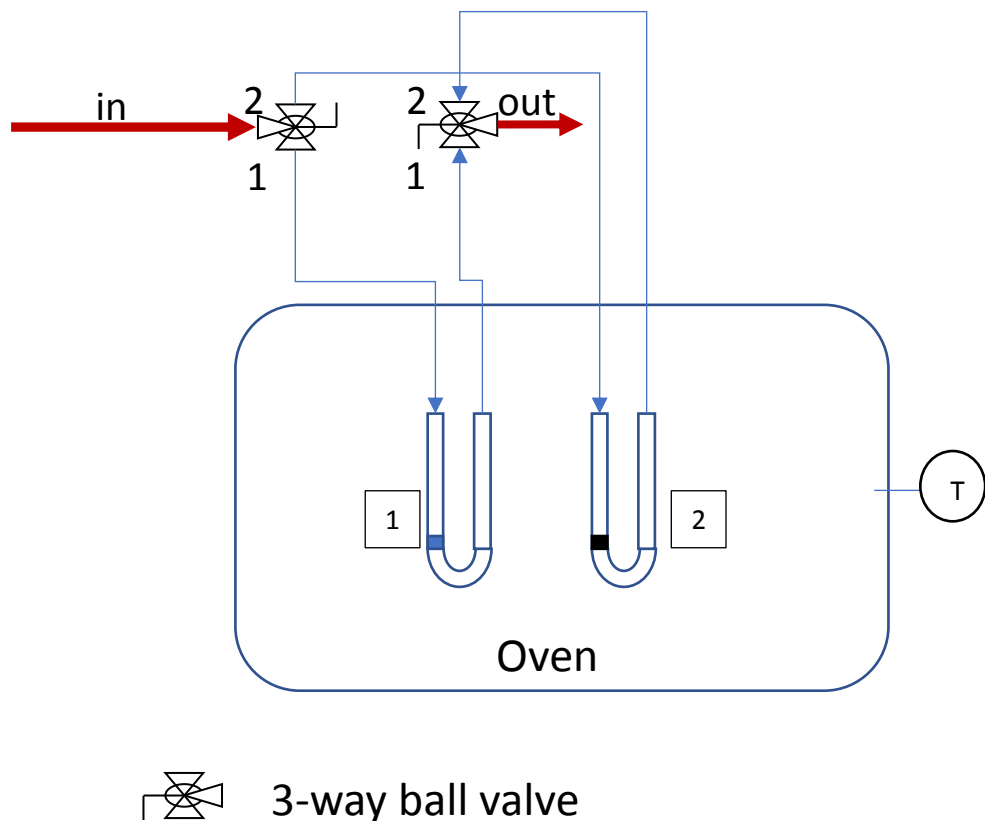


Figure 77 Schematic of 2-reactor system. Reactor 1 contains ground quartz and reactor 2 contains the catalyst

Both reactors were charged with comparable masses of catalyst and ground quartz and the flow of each reagent ($\text{CO } 5 \text{ cm}^3 \text{ min}^{-1}$, $\text{Cl}_2 4 \text{ cm}^3 \text{ min}^{-1}$ and $\text{COCl}_2 3 \text{ cm}^3 \text{ min}^{-1}$) in the total flow of $159 \text{ cm}^3 \text{ min}^{-1}$ was first started in the bypass. The flow was then switched over to the second reactor and the time response for each signal to return to its initial value was measured. This was then subtracted from the integrated area under the curve for each reagent for the time response to limit the signal loss due to physical switching. After each run the flow was stopped and a temperature ramp was run from 323-673 K in steps of 5 K min^{-1} until the temperature reached 673 K and was held a for 2 hours before repeating the process. It is noted that these measurements were performed on fresh catalyst in each instance, therefore each breakthrough measurements reflect the adsorption characteristics over the as-received catalyst. It is acknowledged that adsorption over an aged catalyst may be different.

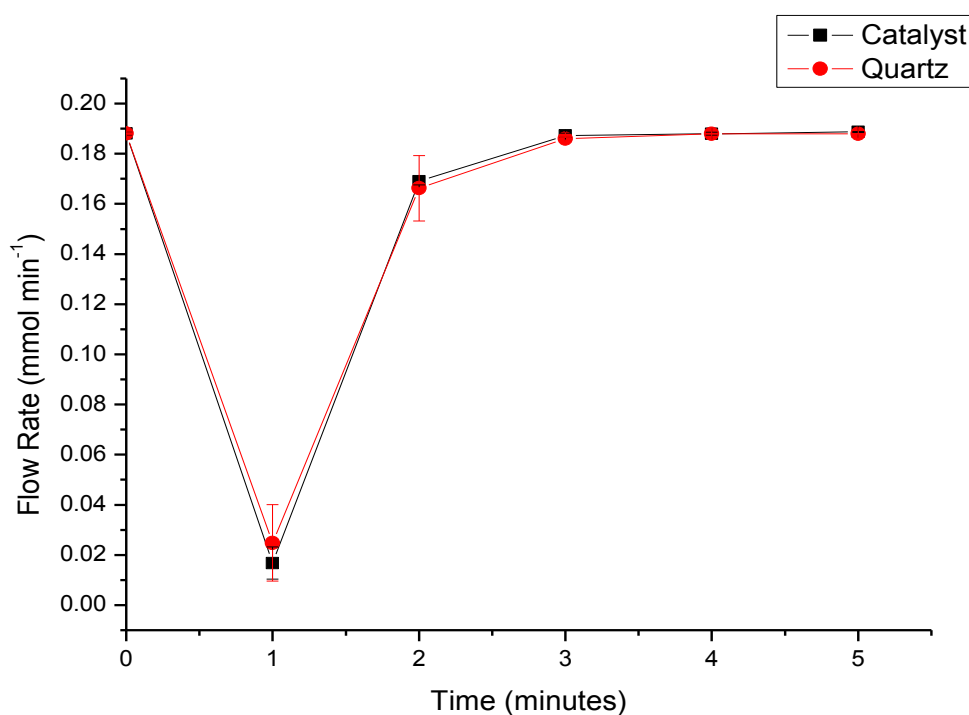


Figure 78 Time response of switching the flow of CO over the catalyst at 323 K in a total flow of $159 \text{ cm}^3 \text{ min}^{-1}$

Figure 78 is the molar flow profile of physical switching between the quartz to quartz (black) and quartz to catalyst (red). The initial drop in molar flow rate is caused by the empty reactor being filled after which it is a measure of adsorption. The quartz to quartz was subtracted from the catalyst run to remove the effect of physical switching. The profiles are very similar indicating a small adsorption coefficient

for carbon monoxide by the catalyst ($0.008 \text{ CO mmol g}^{-1}\text{cat}$). Somewhat surprisingly, Figure 78 indicates that CO is not absorbing on the catalyst under the conditions studied. No chemisorption of this reagent indicates that it cannot be directly contribute to a Langmuir-Hinshelwood mechanism. However, it is entirely possible that it could contribute via an Eley-Rideal step. This outcome is consistent with an early review by Satterfield where it is stated that phosgene synthesis operates within a collisional regime.⁹³ This important matter will be explored further in Section 6.5.

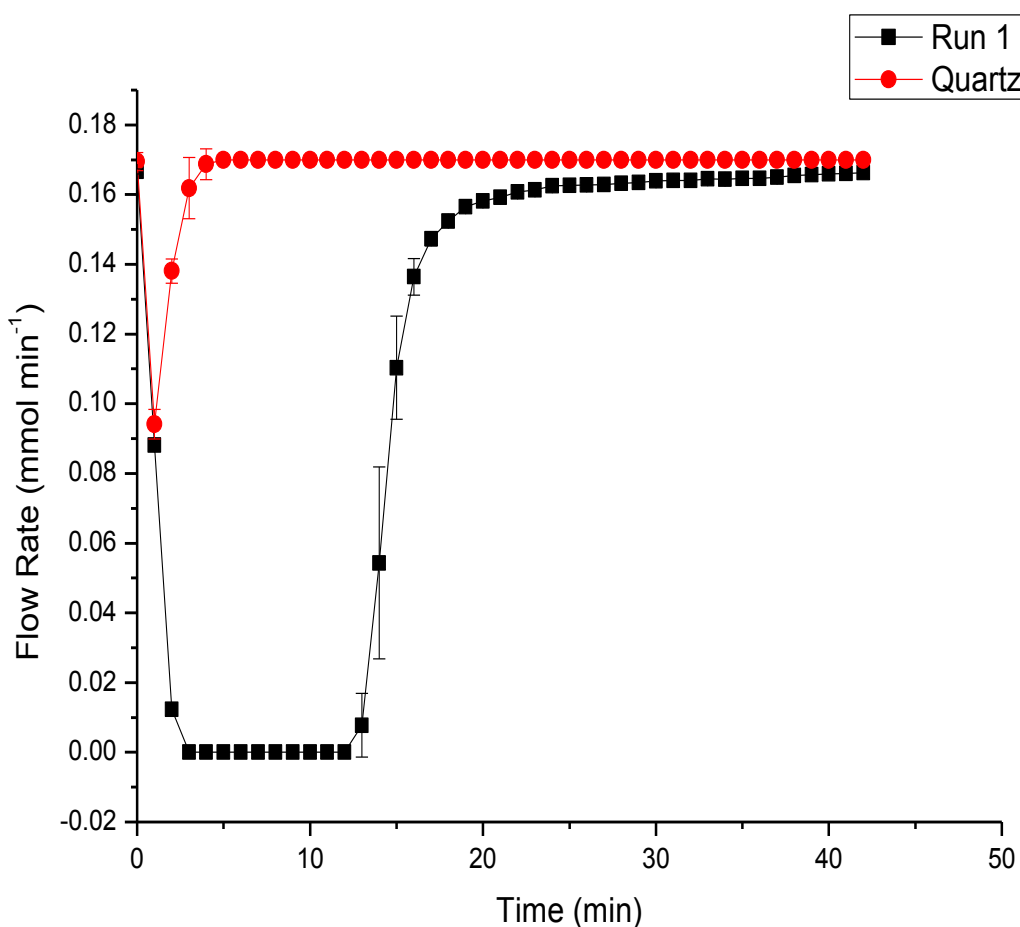


Figure 79 Time response of Switching the flow of chlorine over the catalyst at 323 K in a total flow of $159 \text{ cm}^3 \text{ min}^{-1}$

In contrast to Figure 78, Figure 79 shows significant adsorption of chlorine by the catalyst to be observed. Integrating the area under the curve and subtracting from the curve for ground quartz it was found that $4.27 \text{ mmol Cl}_2 \text{ g}^{-1}\text{cat}$ was adsorbed. After the first measurement, the reactor was heated to 673 K and left for 2 hours the reactor was then cooled to 323 K and the process was repeated.

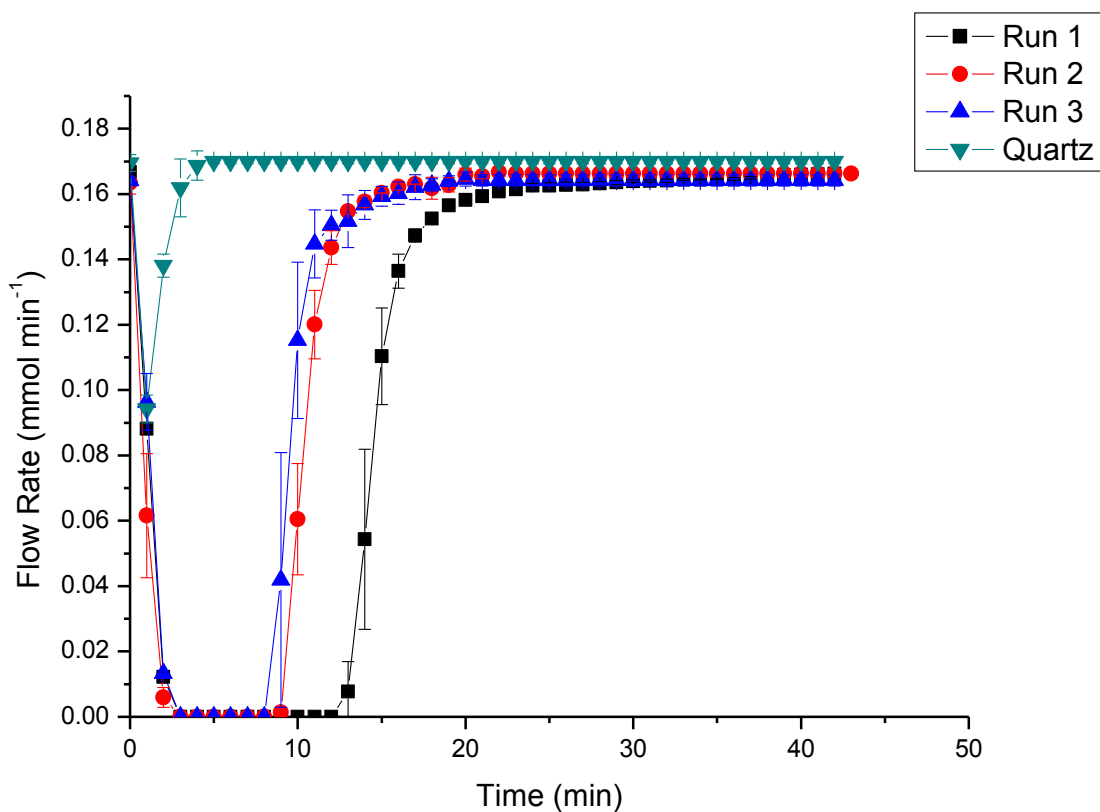


Figure 80 Time response of Switching the flow from quartz to catalyst of repeated chlorine at 323 K in a total flow of $159 \text{ cm}^3 \text{ min}^{-1}$

From Fig. 80 the time response from run 1 is significantly different from runs 2 and 3 indicating that the catalyst is not regenerated back to its original state. However, runs 2 and 3 have similar adsorption profiles which is indicative of a reaction mechanism that requires 2 sites of adsorption on the catalyst, namely a strong and a weak site.

Table 18 Chlorine adsorption on repeated runs

Run	Chlorine adsorbed ($\text{mmol Cl}_2 \text{ g}^{-1}_{\text{cat}}$)
1	4.27
2	2.79
3	2.71

Heating the catalyst to 673 K (2 h) is thought to be insufficient to desorb all the retained Cl. The chlorine retained after this treatment represents strongly bound Cl_(ad). In contrast, the take up post desorption represents less strongly bound Cl_(ad).

From the values in Table 18 it is possible to estimate the relative populations of Cl_{ad} on the strong and weak binding sites.

$$Cl_{total} = 4.27 \text{ mmol Cl}_2 \text{ g}^{-1} \text{ cat} \quad (53)$$

$$Cl_{strong} = Cl_{total} - Cl_{weak} = 4.27 - 2.79 = 1.48 \text{ mmol Cl}_2 \text{ g}^{-1} \text{ cat}$$

$$Cl_{weak} = Cl_{total} - Cl_{strong} = 4.27 - 1.48 = 2.79 \text{ mmol Cl}_2 \text{ g}^{-1} \text{ cat}$$

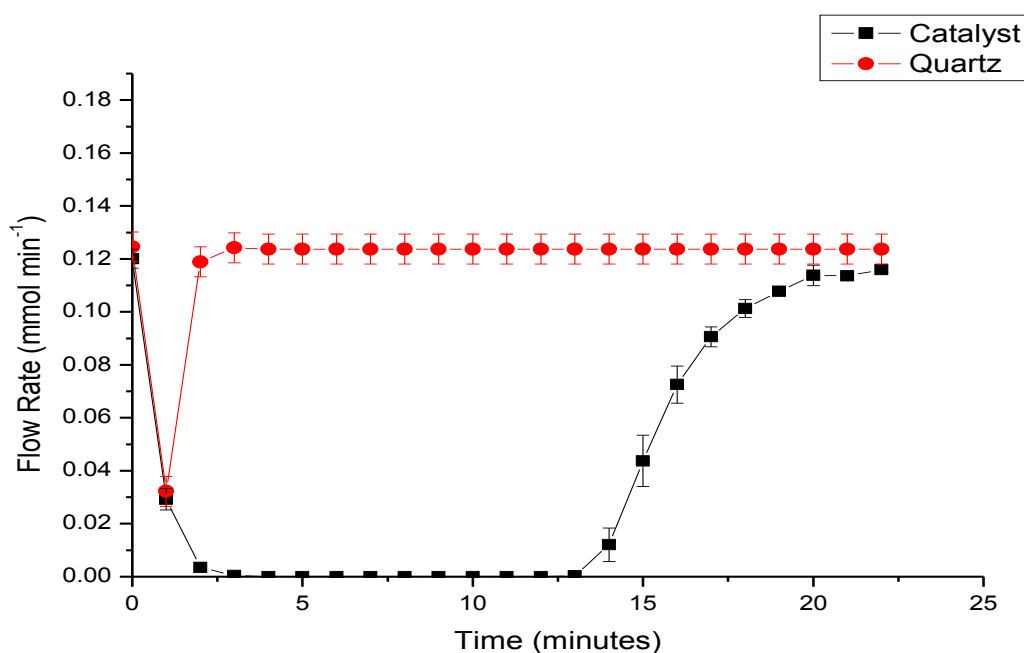


Figure 81 Time response of Switching phosgene flow between quartz to catalyst at 323 K in a total flow of 159 cm³ min⁻¹

Fig. 77 shows the time response of phosgene over the catalyst. From the graph it is clear that there is significant adsorption of phosgene on the catalyst. The catalyst has a capacity of 3.25 COCl₂ mmol g⁻¹ cat.

From the breakthrough measurements the order of the adsorption coefficients is as follows:

$$K_{Cl} > K_{COCl_2} \gg K_{CO}$$

with the adsorption coefficient of chlorine being greater than phosgene. In a competitive environment, chlorine would be the dominant surface species which is consistent with the rate law. With reference to Figure 76 it is apparent that there is a significant difference in the enthalpy of adsorption of chlorine on the catalyst between the two sites of adsorption. In order to describe this phenomenon, the following nomenclature will be utilised.

Cl_{ad}^* = weak

Cl_{ad}^{**} = Strong

6.2 Time on Stream (extended)

These measurements were made to investigate the mass balance over extended time periods to see if the mass imbalance observed (section 4.5.1) returns the system to a closed mass balance. The reaction flow was passed over the bypass containing 0.1250 g ground quartz until stable signals were detected in the infrared and UV spectrometers. These were taken as the A_0 values for each reagent. The flow was then switched over to the catalyst and left for 20 minutes before samples were taken. The reaction was monitored at 353 K (Fig. 82) and 323 K (Fig.83) for 74 and 54 hours respectively, sampling every 2 hours.

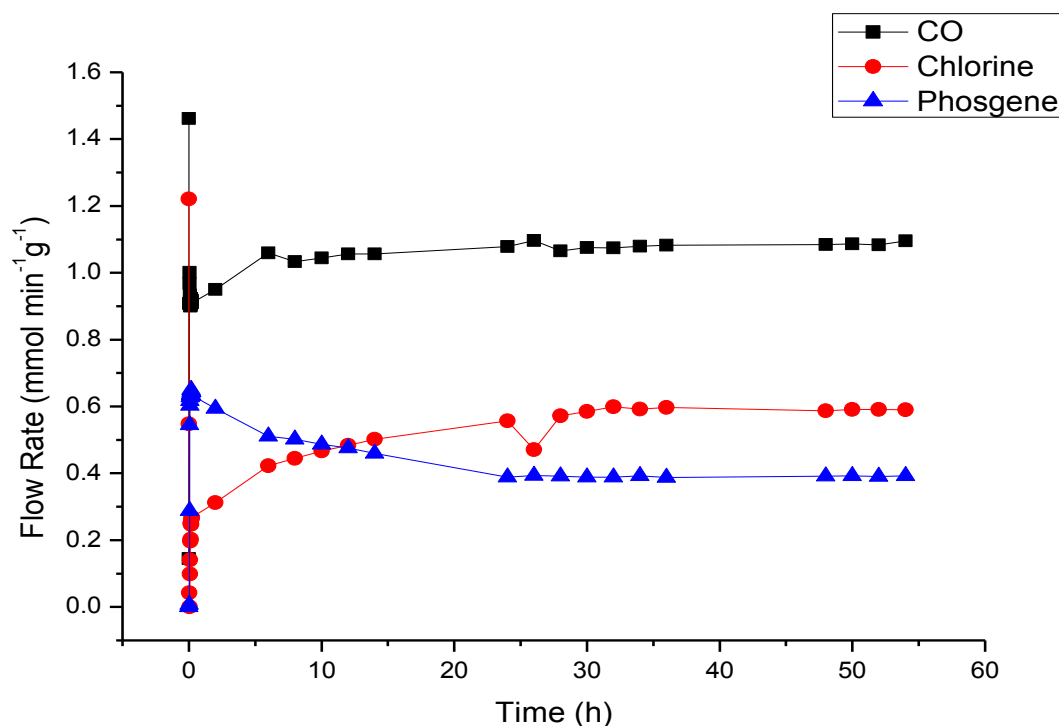


Figure 82 Concentration profile for the reaction between CO and Cl₂ over the catalyst as a with flow rates of 5 cm³ min⁻¹ and 4 cm³ min⁻¹ in a total flow of 159 cm³ min⁻¹ over a period of 54 hours at 353 K

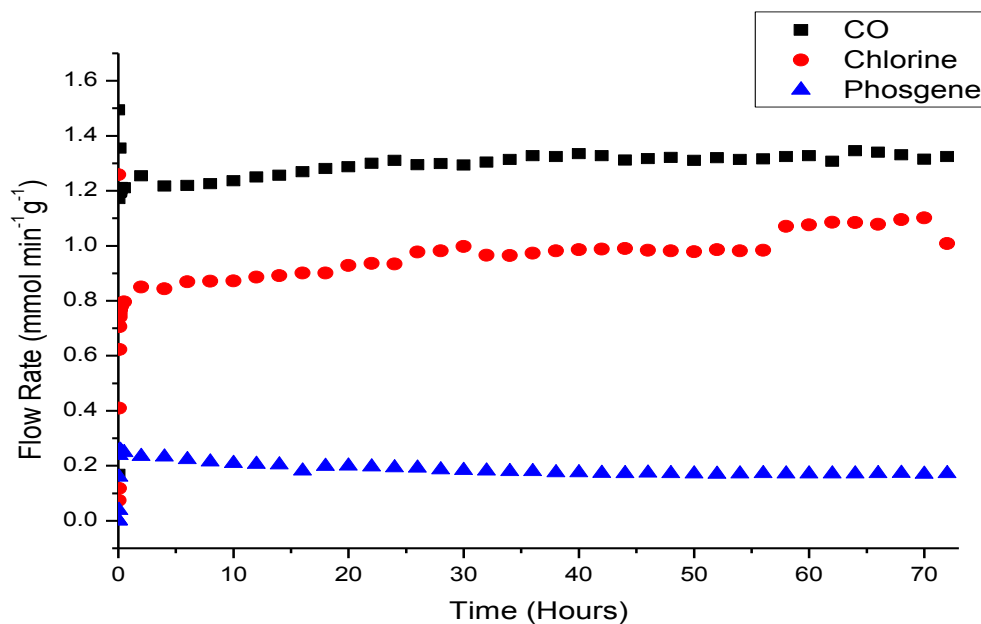


Figure 83 Concentration profile for the reaction between CO and Cl₂ over the catalyst with flow rates of 5 cm³ min⁻¹ and 4 cm³ min⁻¹ in a total flow of 159 cm³ min⁻¹ a period of 74 hours at 323 K over

From the reaction profiles, as evidenced by Figure 78 ($X_{CO}= 12\%$, $X_{Cl}= 25\%$ and $S_{COCl_2}= 100\%$) and 79 ($X_{CO}= 26\%$, $X_{Cl}= 54\%$ and $S_{COCl_2}= 100\%$) it is clear that there is a slight deactivation over the first 24 hours before the reaction reaches steady-state. Thereafter no deactivation is apparent.

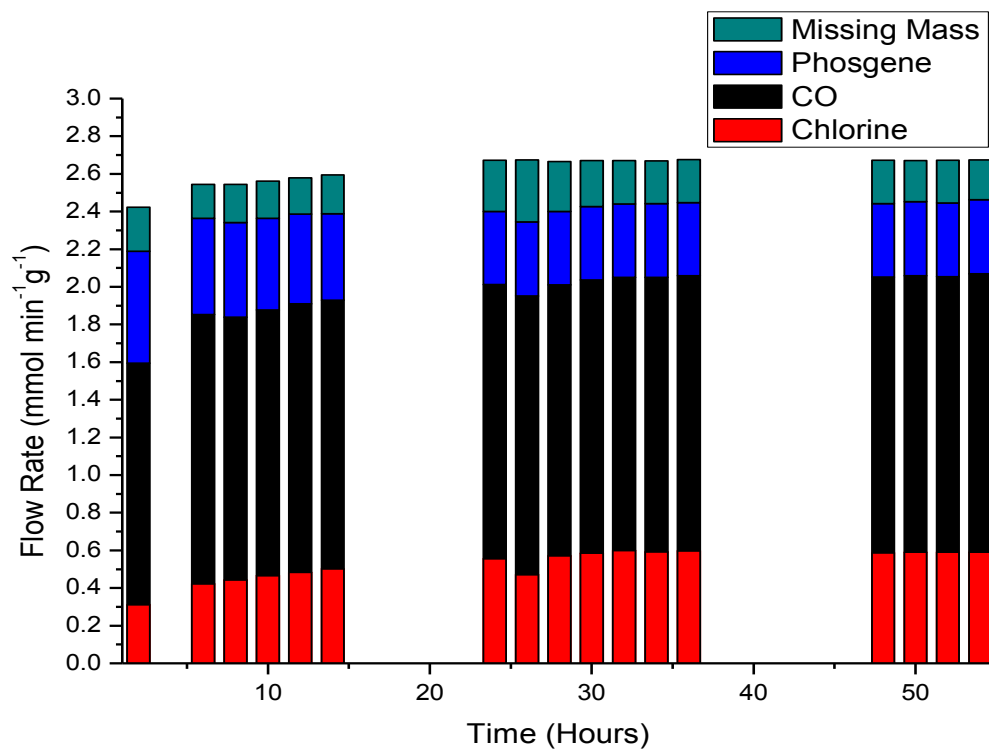


Figure 84 Overall mass balance plot for the reaction at 353 K for 54 Hours

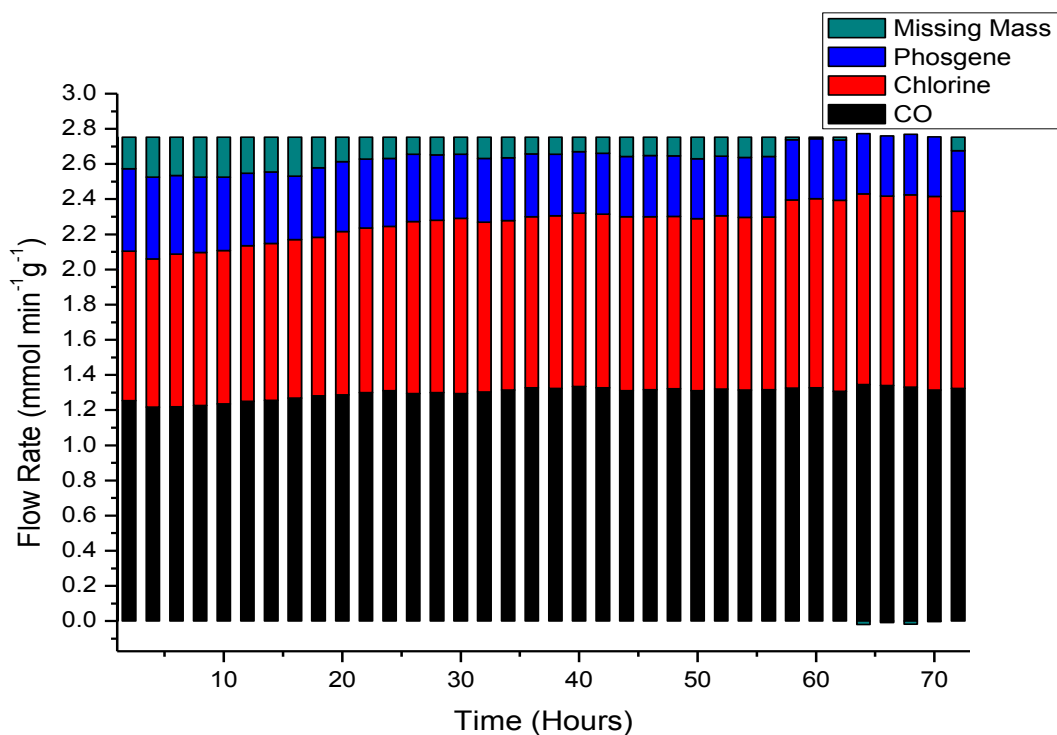


Figure 85 Overall mass balance plot for the reaction at 323 K for 74 Hours

There is some variation between Figs 84 and 85 but the longer run indicates that over a period of ca. 2-3 days continuous phosgene production and the degree of chlorine retention by the catalyst diminishes. Figure 85 and 86 indicate a closed mass balance to be attained after ca. 62 h T-o-S. This occurs due to a finite capacity (large) for contained chlorine. Once that capacity is reached, no additional chlorine is retained by the catalyst. Indeed Figure 86 indicates a loss of retained chlorine from the catalyst surface during the period 60-70 h. At no point throughout the reaction coordinate is $\text{CCl}_{4(g)}$ observed. The adsorbed chlorine is thought to be surface bound to the carbon through the carbon-carbon double bonds²³.

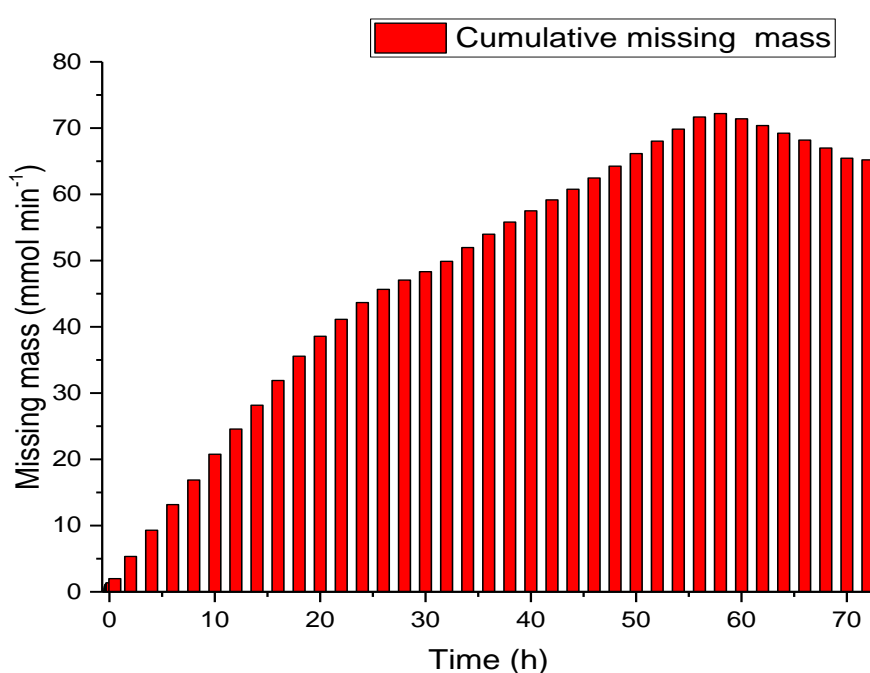


Figure 86 Cumulative missing mass as a function of time at a reaction temperature of 323 K (from fig 85)

From Fig 86 the cumulative missing mass at 50 h is $437.6 \text{ mmol Cl}_2 \text{ g}^{-1}_{\text{cat}}$ (323 K). The equivalent value for 353 K (Figure 84) is $637.6 \text{ mmol Cl}_2 \text{ g}^{-1}_{\text{cat}}$. These values exceed the chlorine capacity determined by the breakthrough measurements ($4.27 \text{ mmol Cl}_2 \text{ g}^{-1}_{\text{cat}}$, Section 6.1). However, the breakthrough measurements were not performed under the same conditions used for phosgene production, *i.e.* single chemisorption versus active competitive adsorption and reaction. Fig 14 also shows that during the first 20 hours of reaction the chlorine retention rate ($0.0316 \text{ mmol min}^{-2}$) is greater than between 20 and 58 h ($0.0146 \text{ mmol min}^{-2}$). From Fig 86, after 58 hours the catalyst has reached capacity at $577.6 \text{ mmol Cl}_2 \text{ g}_{\text{cat}}^{-1}$ and thereafter the

reaction begins to return some of the missing chlorine to the gas phase. It is therefore deduced that the driving force for chlorine retention appears to be greater under phosgene synthesis conditions compared to simple exposure of chlorine.

To assess the chlorine capacity, one could consider a specific coverage²³, *i.e.* chlorine coverage with respect to BET surface area. The respective coverage of chlorine to the carbon catalyst for the two temperatures (at 50 h) 0.56 (353 K) are and 0.40 (323 K) mmol Cl₂ m⁻²_{cat}. However, as noted by González et al²³ (section 1.1.2) BET is not an appropriate indicator when considering chlorine adsorption on activated carbon. BET surface area will not be representative of the carbon active surface area and therefore the resulting specific coverages (mmol Cl₂ m⁻²_{cat}) will not be considered further. Instead, it is preferred to rationalise differences in chlorine capacity as indicated by the chlorine mass imbalance of the extended runs (cumulative = 437.6 mmol Cl₂ g⁻¹_{cat} after 50 h at 323 K, Section 6.2) with the capacity indicated by the breakthrough measurement (4.3 mmol Cl₂ g⁻¹_{cat}, Section 6.1). This discrepancy of two orders of magnitude is attributed to additional chlorine transport within the carbon matrix during extended time on stream compared to the concept of solely chlorine adsorption on clean activated carbon.

The exchange mechanism for this chlorine transport/storage is thought to be the interchange between weakly (Cl*_{ad}, Site 1) and strongly (Cl**_{ad}, Site 2) adsorbed chlorine. Cl*_{ad} being available for reaction at these temperatures, and Cl**_{ad} retained throughout the catalyst surface, equation 54.



K is an equilibrium constant.

Thus, the chlorine chemisorption measurement over clean activated carbon (Section 6.1) underestimates the actual chlorine capacity of the carbon during reaction conditions (Section 6.2). Under actual reaction conditions involving competitive adsorption there appears to be a progressive interchange from chlorine atoms bound at Site 1 to move across to Site 2. Figure 86 indicates that at 323 K saturation of Site 2 is complete after 58 h at a cumulative value of 577.6 mmol Cl₂ g_{cat}⁻¹.

6.3.1 Desorption post-reaction

This purpose of this experiment is to examine what species are adsorbed after a 2-hour reaction. The reaction flow was passed over the bypass containing ground quartz until stable signals were detected in the mass spectrometer. The flow was then passed over 0.1250 g of catalyst and the reaction was monitored for 2 hours at 298 K (Figure 83)

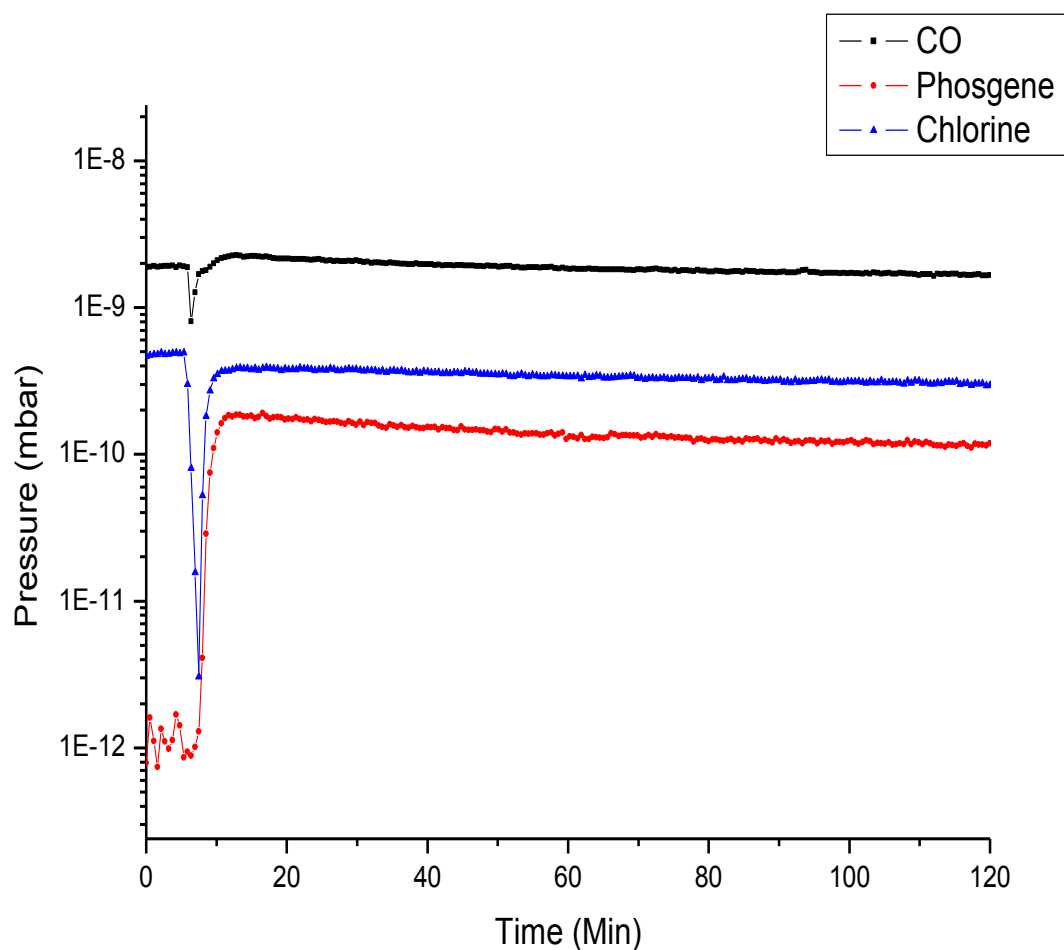


Figure 87 Reaction profile for reaction at 298 K for 120 mins using a mass spectrometer with flow rates of CO and Cl₂ of 5 cm³ min⁻¹ and 4 cm³ min⁻¹ in a total flow of 159 cm³ min⁻¹

Figure 87 shows the reaction profile where the flow was switched from the bypass to catalyst at 5 minutes. There is a drop in the signals of CO and chlorine before the production of phosgene was observed. The reaction then proceeds steadily for 2 hours.

After the reaction, had completed (2 hours), the flows of each reagent were switched off and the reagent signals were allowed to drop down to minimum levels. A temperature ramp 298-633 K in 5 K min⁻¹ steps was run and each ion channel was monitored.

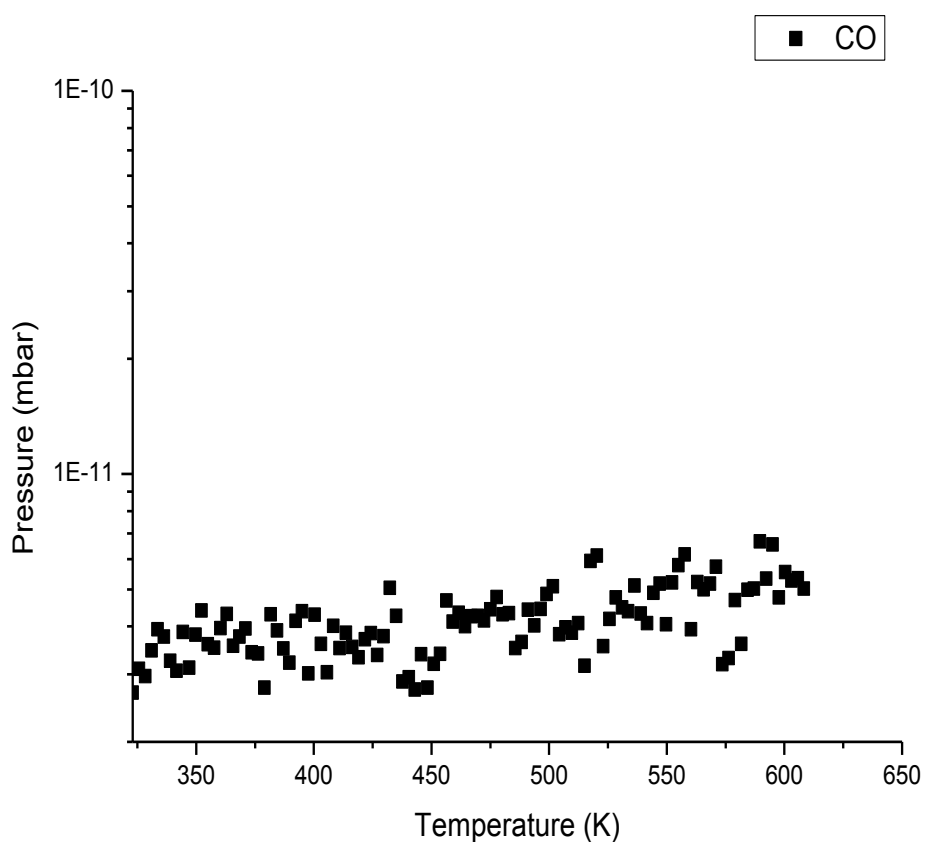


Figure 88 Temperature ramp 298-633 K in 5 K steps post reaction monitoring mass 28 for CO (159 cm³ min⁻¹ He)

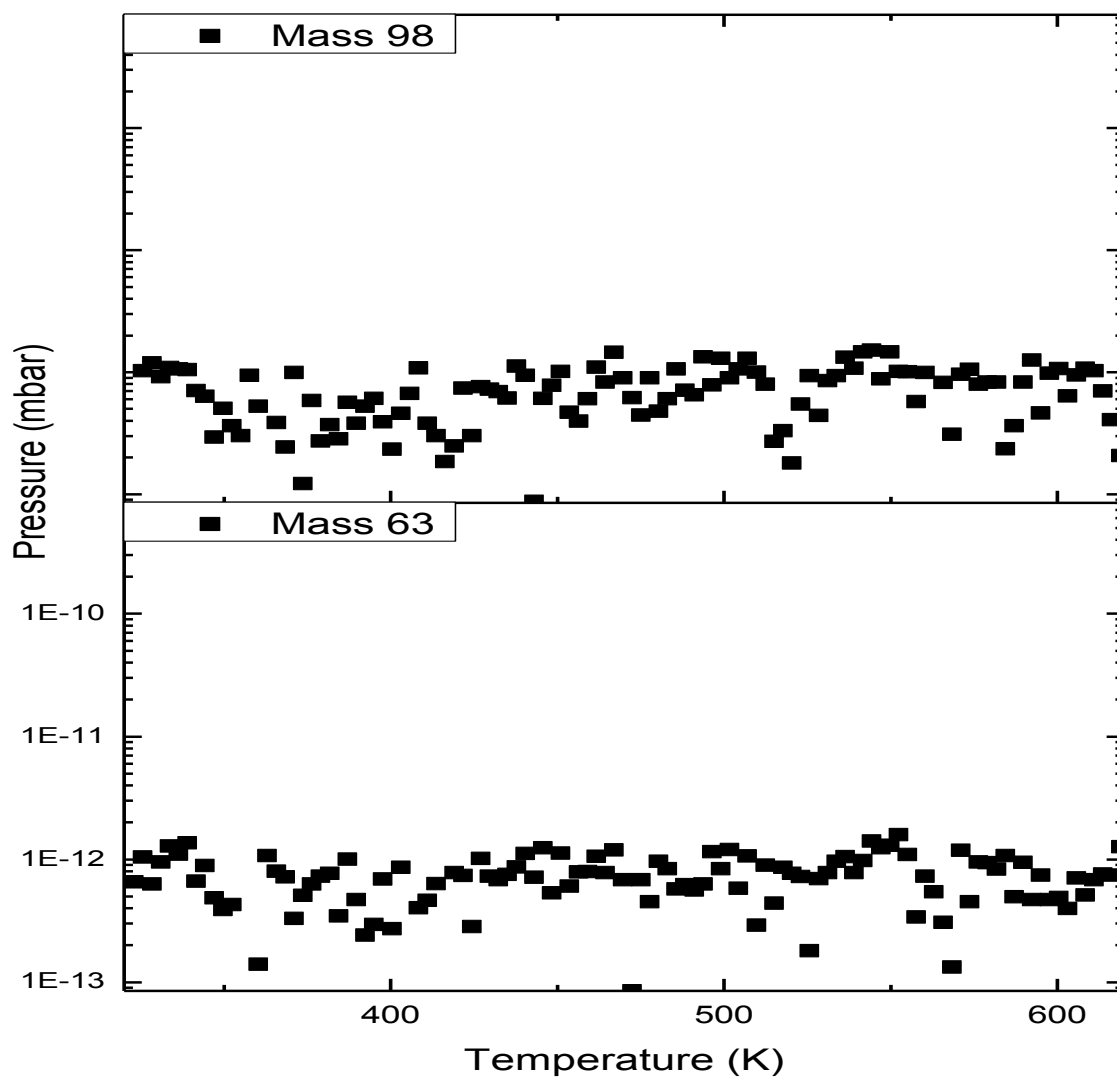


Figure 89 Temperature ramp 298-633 K in 5 K steps post reaction monitoring mass 63 and 98 for COCl_2 ($159 \text{ cm}^3 \text{ min}^{-1}$ ^1He)

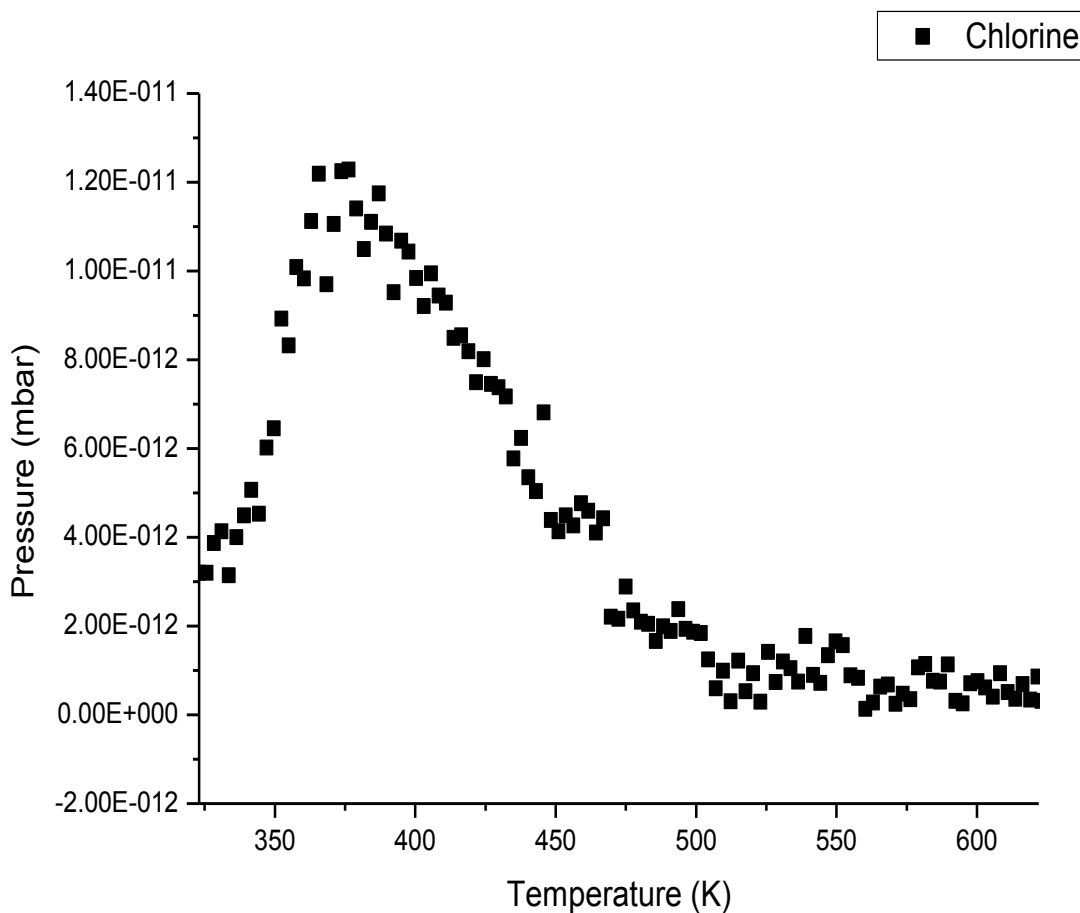


Figure 90 Temperature ramp 298-633 K in 5 K steps post reaction monitoring mass 70 for Cl₂(159 cm³ min⁻¹ He)

From Figure 88 and Figure 89, there is no desorption of either CO and COCl₂ from the catalyst post reaction. However, from Figure 90 there is desorption of chlorine as Cl₂ from the catalyst surface indicating that under reaction conditions the surface is dominated predominantly by chlorine. This is consistent with the deduced relative magnitudes of the adsorption coefficients for the reagents/product.

6.3.2 Desorption fresh catalyst

This purpose of this experiment is to examine which reagents were adsorbed on exposure to the fresh catalyst. All reagents were passed (CO , Cl_2 , and COCl_2) over 0.125 g of fresh catalyst for 10 minutes and monitored using the mass spectrometer. The flows of CO ($5 \text{ cm}^3 \text{ min}^{-1}$), Cl_2 ($4 \text{ cm}^3 \text{ min}^{-1}$) and COCl_2 ($3 \text{ cm}^3 \text{ min}^{-1}$) in a total flow of $159 \text{ cm}^3 \text{ min}^{-1}$ at 298 K and then the reagent flow was switched off. A temperature ramp 298-673 K in 5 K steps was run once the reagent signal had dropped to its original value and the mass spectrometer used to continually monitor the exit stream.

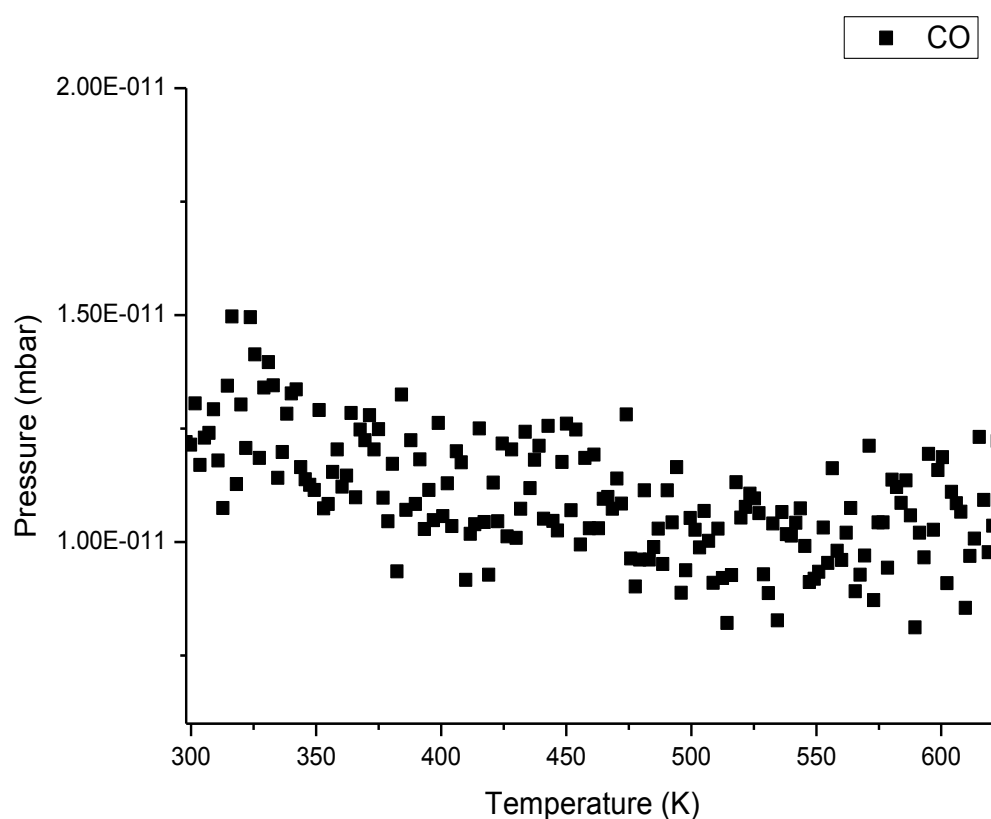


Figure 91 Temperature ramp 298-633 K in 5 K steps on fresh catalyst monitoring mass 28 for CO ($159 \text{ cm}^3 \text{ min}^{-1}$ He)

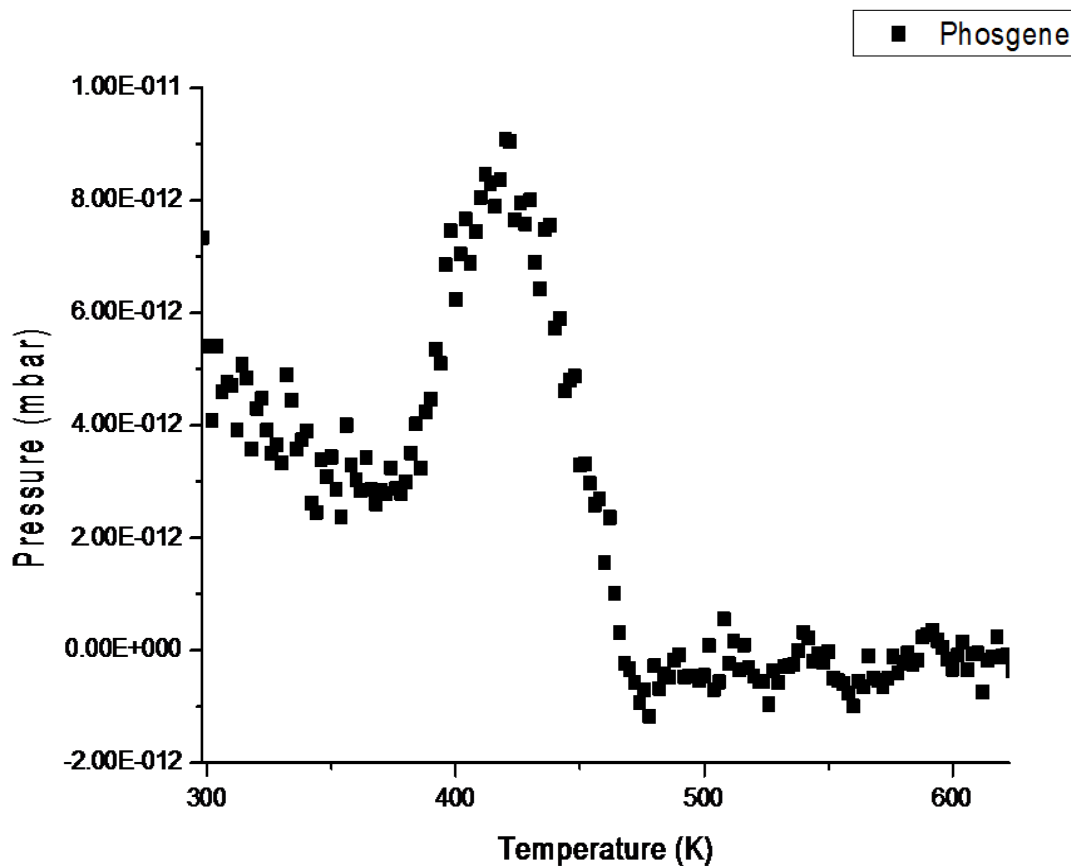


Figure 92 Temperature ramp 298-633 K in 5 K steps on fresh catalyst monitoring mass 98 for COCl_2 ($159 \text{ cm}^3 \text{ min}^{-1} \text{ He}$)

From Figure 92 phosgene is desorbed from fresh catalyst indicating that phosgene is adsorbed onto the surface. This is entirely consistent with the breakthrough measurements. From the T_{max} at 425 K it can be assumed that the phosgene is adsorbed onto the weaker energy binding site. Phosgene shows a zero-order dependence in the rate law. Therefore, in a competitive adsorption regime, chlorine would be the dominant surface species as illustrated in Figs 87-90.

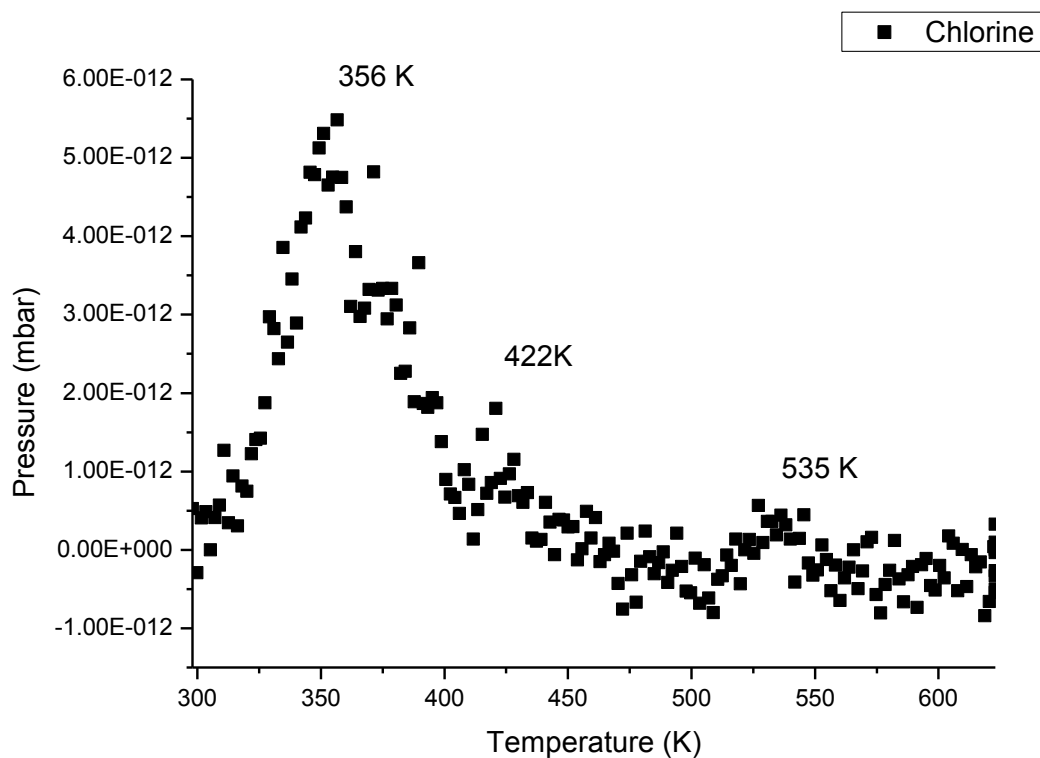


Figure 93 Temperature ramp 298-633 K in 5 K steps on fresh catalyst monitoring mass 70 for Cl₂ (159 cm³ min⁻¹ He)

From Figure 93, chlorine is desorbed from fresh catalyst indicating that chlorine is adsorbed onto the surface. This is entirely consistent with the breakthrough measurements. From the desorption profile, there is clear desorption with a T_{\max} at 356 K. There are peaks seen at 422 and 535 K. It is possible that further bound chlorine could be present beyond the temperature range. However, these are out with the maximum temperature of the Shimadzu (GC14A) oven which has a maximum temperature of 673 K.

Table 19 T_{\max} desorption temperatures of reagents over the fresh catalyst (159 cm³ min⁻¹ He)

Species	T_{\max} Desorption (K)
CO	N/A
COCl ₂	422
Cl ₂	356, 422, 535

6.4 Post reaction catalyst analysis

This purpose of this experiment is to examine the catalyst surface after a 4-hour reaction ($\text{CO} + \text{Cl}_2$ at 323 K). The reaction flow was passed over the by-pass containing ground quartz until stable signals were detected in both the infrared and UV-Visible spectrometers. The flow was then passed over 0.1250 g of catalyst and the reaction was monitored for 4 hours at 323 K. The reaction was then terminated by switching the flow over the bypass and the flow of reagents was switched off leaving only nitrogen flowing. The catalyst reactor was purged for 16 hours at 323 K and a catalyst sample was extracted from the reactor. This sample was then analysed by SEM and EDX.

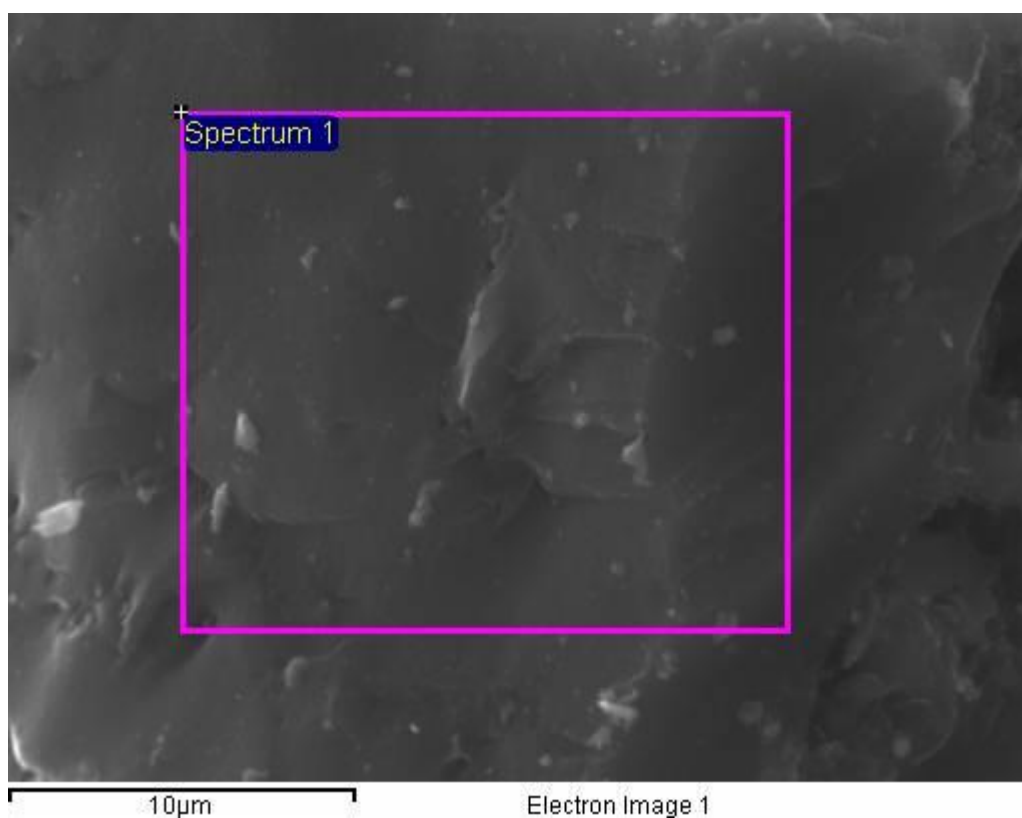


Figure 94 SEM image of the Donau Supersorbon K40 catalyst post reaction (4 hours at 323 K, $\text{CO } 5 \text{ cm}^3 \text{ min}^{-1}$ and $\text{Cl}_2 \text{ cm}^3 \text{ min}^{-1}$) showing the area of which an EDX was taken

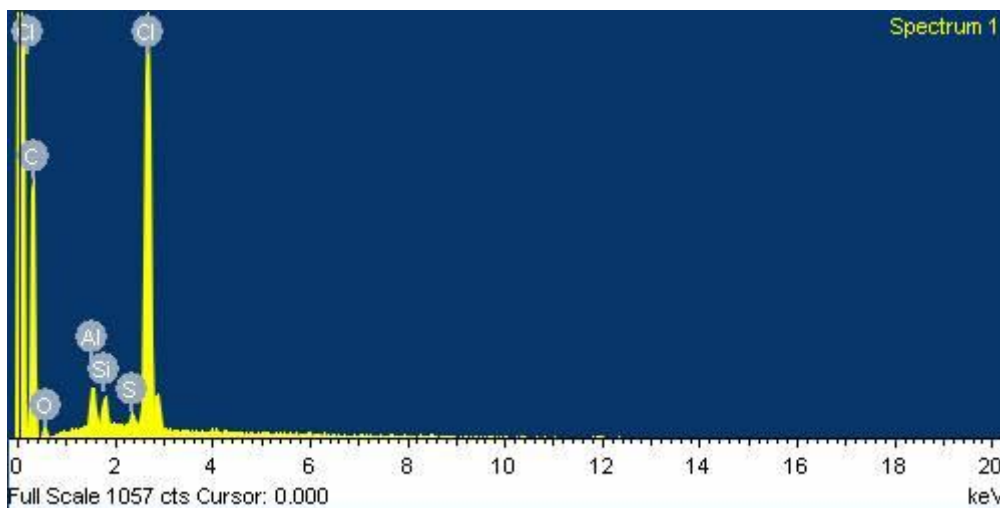


Figure 95 EDX of the Donau Supersorbon K40 catalyst (4 hours at 323 K, CO 5 cm³ min⁻¹ and Cl₂ 4 cm³ min⁻¹)

Table 20 EDX results from Figure 95

Element	Weight %	Atomic %
Carbon	80.36	97.63
Oxygen	3.87	2.37
Aluminium	0.82	0.41
Silicon	0.36	0.31
Chlorine	13.94	5.32

From the EDX spectrum of the catalyst after 4 hours (Figure 95), it is clear that chlorine has been adsorbed on to the catalyst surface. This is entirely consistent with breakthrough and desorption measurements, as well as the proposed mechanism (section 6.5)

6.5 Summary

The breakthrough measurements show that the order of the adsorption capacity is as follows:

$$K_{Cl} > K_{COCl_2} \gg K_{CO}$$

In a competitive environment, chlorine, will be the dominant surface species. Two distinct binding sites for chlorine on the catalyst are proposed

Cl_{ad}^* = weak

Cl_{ad}^{**} = Strong

From the extended time on stream measurements (Figs 84-85, Section 6.2), it appears that there is missing mass across the reaction coordinate. That may be attributed to retained chlorine atoms. This suggests that interchange between Cl_{ad}^* and Cl_{ad}^{**} is possible

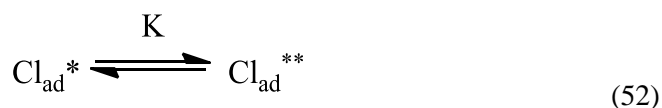


Fig 81 shows greater chlorine retention at elevated temperature. This could arise from increasing the concentration of Cl_{ad}^{**} . At $t= 50h$ $Cl_{retained} = 437.6 \text{ mmol } Cl_2 \text{ g}^{-1}_{cat}$ (323 K) and $637.6 \text{ mmol } Cl_2 \text{ g}^{-1}_{cat}$ (353 K). It is possible that increased temperature overcomes a diffusional barrier for retained chlorine atoms, nudging equation 52 to the right-hand side.

The desorption measurements show when fresh catalyst is exposed to each of the reagent ($Cl_2 + COCl_2$) both chlorine and phosgene are retained (Figures 90-93). However, post reaction the only species desorbed from the catalyst is chlorine.

6.5 Discussion

The rate law for phosgene formation over this catalyst can be written as:

$$v = k[CO]^{0.93 \pm 0.02} [Cl_2]^{0.48 \pm 0.01} [COCl_2]^{-0.04 \pm 0.08} \quad (39)$$

where k is a rate constant

The approximately half order in chlorine indicates that the chlorine is reacting via dissociative adsorption mechanism^{5,6,94}.



The order dependence of both the CO and Cl₂ is consistent with the early work by Potter and Baron^{5,6}. The half order dependence of the chlorine suggests that the chlorine is binding to the carbon material, probably via double bonds present on the activated carbon.^{40,100} The zero-order dependence of phosgene in the rate law indicates that phosgene does not affect the forward reaction.

From the breakthrough measurements the order of the adsorption coefficients is as follows:

$$K_{Cl} > K_{COCl_2} \gg K_{CO}$$

In a competitive environment chlorine will be the dominant surface species. From the different relative magnitude of the adsorption coefficient for repeat runs obtained for chlorine, the catalyst after exposure is not regenerated to its original state after desorption. This is suggestive of at least two populations of adsorbed chlorine on the catalyst surface.

Cl_{ad}* = weak, Site 1

Cl_{ad}** = Strong, Site 2

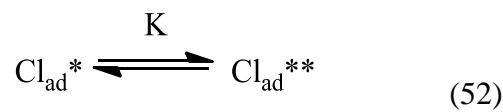
There is a significant difference in the enthalpy of adsorption of chlorine on the catalyst between two sites of adsorption. The catalyst is thought to activate the chlorine-chlorine bond and therefore lowering the energy required for the process.

The time on stream experiment (Section 4.5.1, Figure 58) highlights that there is a mass imbalance attributed to missing chlorine as

$$\frac{-d[\text{CO}]}{dt} \approx \frac{d[\text{COCl}_2]}{dt} \quad (30)$$

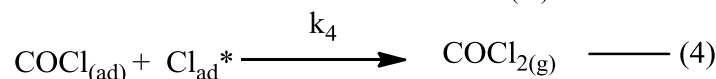
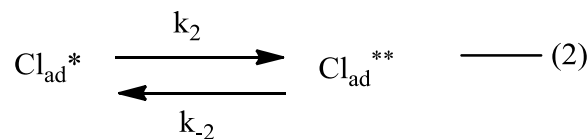
$$\frac{-d[\text{Cl}_2]}{dt} \neq \frac{d[\text{COCl}_2]}{dt} \quad (31)$$

The reaction operates under a modest mass imbalance even over extended time periods which, unless there is interchange between the two adsorption sites, would otherwise exceed the capacity determined by the breakthrough measurements.

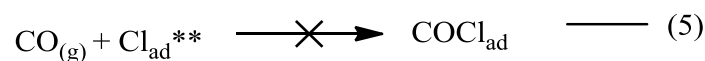


This is also consistent with the desorption after reaction where the only species observed desorbing is chlorine (no phosgene detected in desorption experiments post-reaction, Section 6.3.1, Figure 81).

With reference to Section 6.1 CO breakthrough measurements on the clean catalyst indicated no effective CO chemisorption. This excludes CO from a Langmuir-Hinshelwood elementary stage, although CO could contribute via an initial Eley-Rideal stage. The following two-site model reaction mechanism is proposed



Chlorine adsorbed on site 2 is not available for reaction which is consistent with the mass imbalance.



Step 1 involves dissociative adsorption of dichlorine. Adsorbed chlorine atoms then partition between two sites: site 1 is weakly adsorbed and site 2 is strongly adsorbed. A degree of exchange is possible between Cl residing in these two sites which is thought to be hindered by a diffusional barrier.

Gaseous CO impinging on Cl atoms residing on site 1 conforms to an Eley-Rideal stage that leads to the formation of COCl_{ad} . This species then reacts with a further adsorbed chlorine atom residing in site 1 via a Langmuir-Hinshelwood to form $\text{COCl}_{2(\text{ad})}$. It is assumed that $\text{COCl}_{2(\text{ad})}$ rapidly desorbs on formation. Conversely, gaseous CO collision with a chlorine atom bound at site 2 leads to no reaction.

In summary, the overall reaction is a combination of dissociative adsorption, an Eley-Rideal stage followed by a Langmuir-Hinshelwood process. Figure 91 shows a schematic for the proposed reaction mechanism.

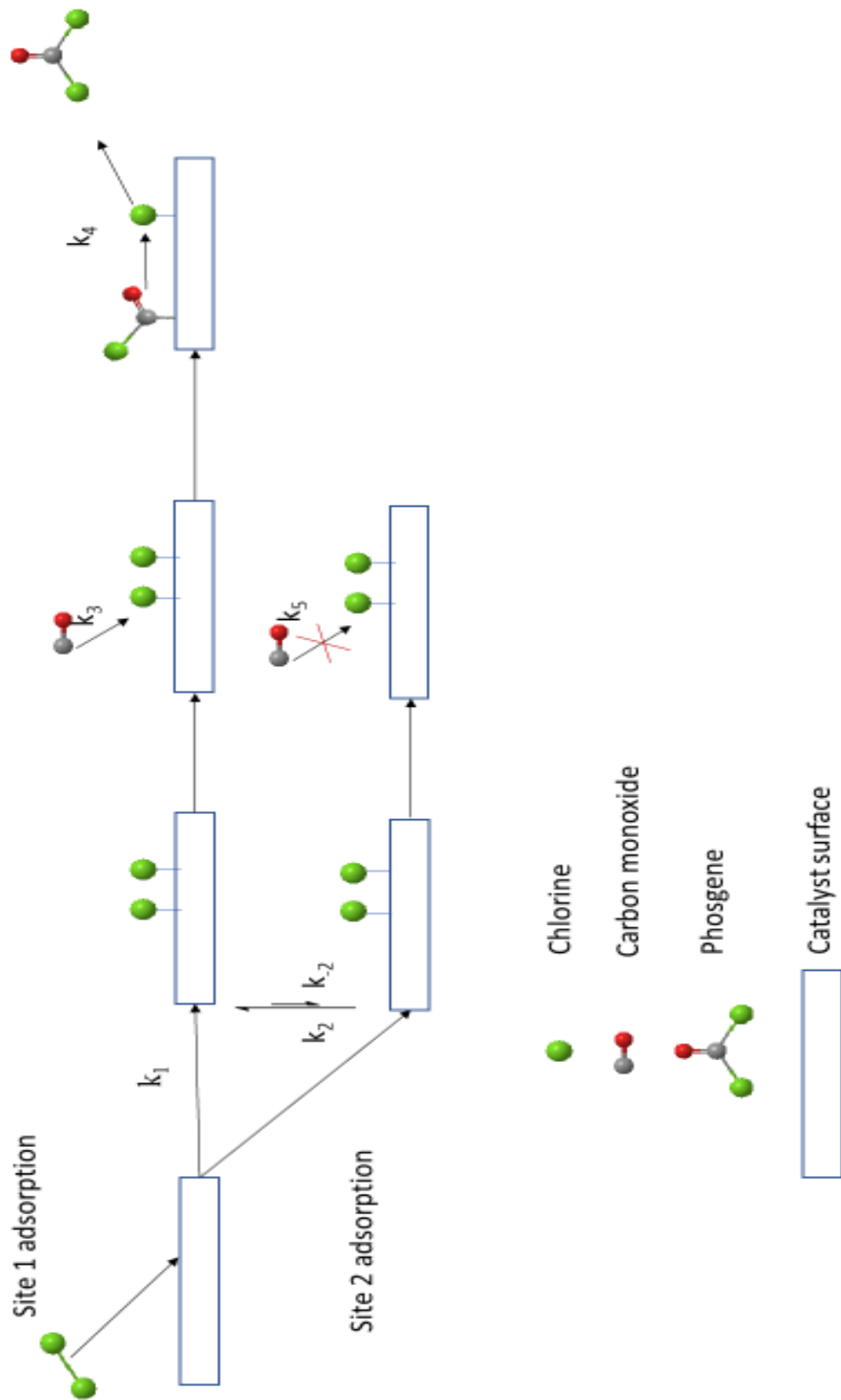


Figure 96 Proposed reaction mechanism for phosgene production over the Donau Supersorbon K40 catalyst

where:

k_1 = dissociative adsorption of Cl_2

k_2 = interchange of Cl_{ad}^* into the strong binding site Cl_{ad}^{**}

k_{-2} = interchange of Cl_{ad}^{**} into the weak binding site Cl_{ad}^*

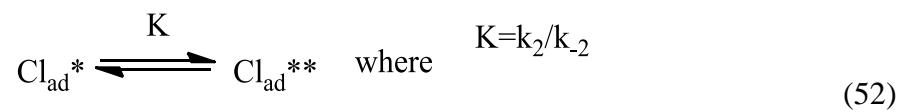
k_3 = Collisional reaction between surface adsorbed Cl_{ad}^* and CO

k_4 = reaction of $COCl_{ad}$ and Cl_{ad}^* to produce phosgene

k_5 = Collisional reaction between surface adsorbed Cl_{ad}^{**} and CO

k_6 = reaction of $COCl_{ad}$ and Cl_{ad}^{**} to produce phosgene

The interchange Cl_{ad}^* into the strong binding site Cl_{ad}^{**} is defined by K



Equation here for K, k_2 , k_{-2}

Chapter 7- Influence of bromine on the reaction kinetics

7.1 Introduction

There is industrial interest into the observed effects of small quantities of a bromine impurity in the feed stream on the reaction chemistry for the production of phosgene⁷⁷. The apparatus was modified to accommodate a bromine co-feed and the quantification procedures are described in section 2.2.2. There were however, issues connected with co-feeding the two halogens simultaneously.

This chapter will explain the issues/ complications/ challenges associated with the co-feed and describe the modified procedures to quantify the bromine under these conditions. The reaction chemistry with a bromine co-feed was tested under various reaction conditions. These include varying reaction temperature and bromine concentration. The reaction without chlorine was tested to show whether it is possible to form COBr_2 and compare it to phosgene formation. Desorption measurements were used to determine whether the catalyst was retaining bromine similarly to chlorine.

The final part of this chapter will rationalise the observations with respect to the deduced reaction mechanism for phosgene formation. This allows the deduced phosgene synthesis mechanism to be tested considering a new component

7.2.1 Spectroscopic Issues

The following spectra were obtained when co-feeding dibromine (bromine doser temp=293 K) and dichlorine ($4 \text{ cm}^3 \text{ min}^{-1}$) over ground quartz in the normal flow regime ($159 \text{ cm}^3 \text{ min}^{-1}$ total flow).

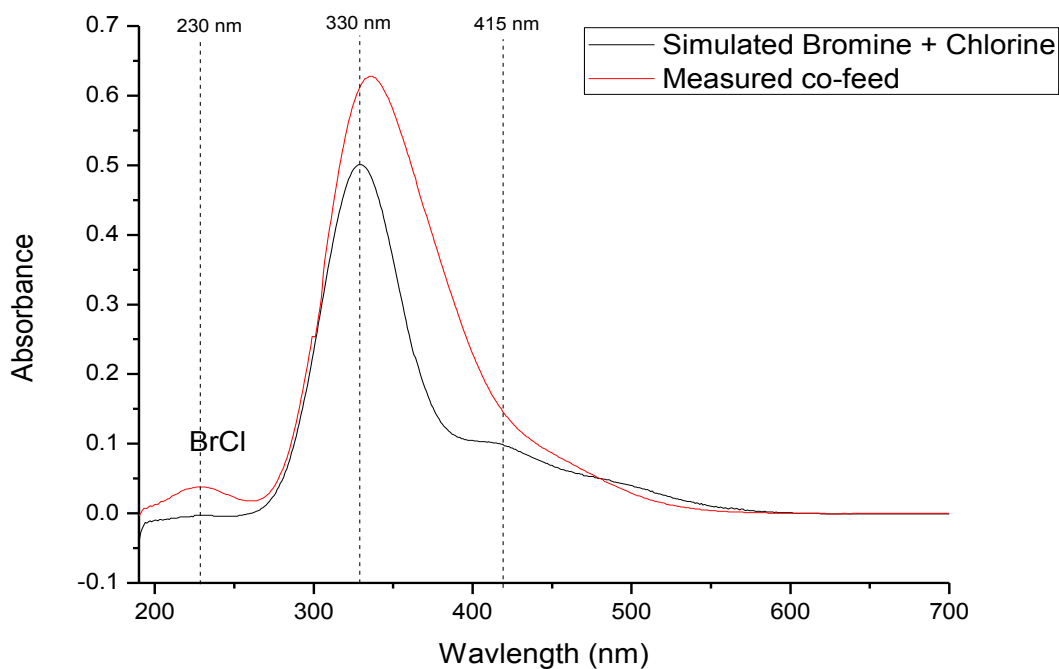


Figure 97 UV -visible spectrum of dibromine co-fed with dichlorine (bromine doser at room temperature) and chlorine at $4 \text{ cm}^3 \text{ min}^{-1}$ at a fixed flow $159 \text{ cm}^3 \text{ min}^{-1}$ (The red line shows obtained spectrum and the black line shows the linear addition of the spectra of following (i) Cl_2 and (ii) Br_2).

The black spectrum is the addition of a chlorine spectrum and bromine spectrum recorded individually. The red spectrum is the measured UV-vis spectrum when co-feeding diluted Cl_2 and diluted Br_2 . From the obtained spectra there appears to be an extra component at 230 nm that is associated with the formation of BrCl . The spectra of the individual components are shown in Fig.98

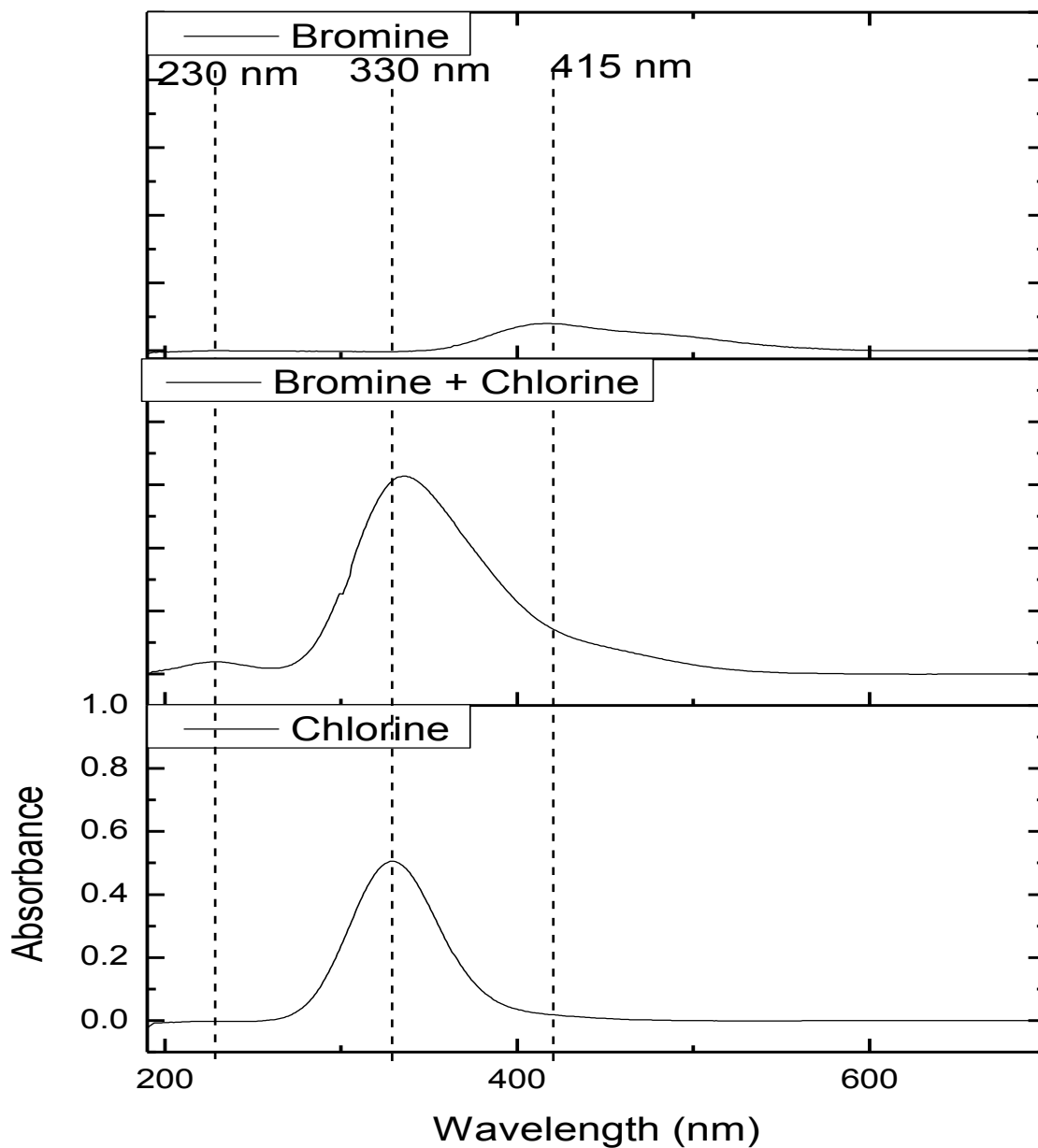
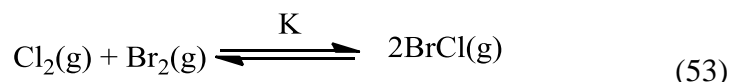


Figure 98 Example UV of Cl₂, Br₂ and BrCl.

The chlorine and bromine peaks overlap and the spectra are complicated due to the absorbance due to a BrCl species at 230nm at high bromine levels^{54,101}. The methodology has been modified to distinguish absorption bands and refine quantification procedures, specifically due to the symmetric Gaussian shape of the Cl₂ peak, this can be subtracted from the skewed Br₂ peak.

7.2.2 Calculating the bromochloride equilibrium constant

There is a literature precedence that the following reaction between chlorine and bromine occurs^{53,101,102}:



The flow of chlorine was started at $2.5 \text{ cm}^3 \text{ min}^{-1}$ in a total flow of $159 \text{ cm}^3 \text{ min}^{-1}$ and the flow was maintained until stable signals in the UV were obtained. The UV of flowing bromine vapour (doser at room temperature) was recorded and the flow of chlorine was started and left for 20 minutes. The flow was then switched over the line bypass to maintain the gas static in the gas cell and spectra was recorded for 30 minutes, *i.e.* this represents a stopped flow measurement.

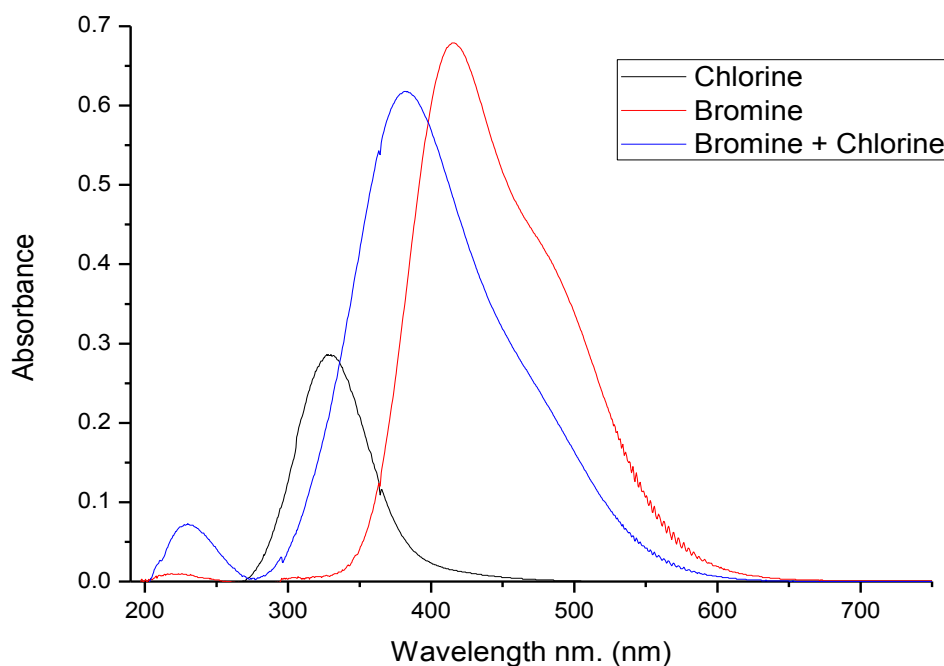


Figure 99 UV visible spectra of bromine doser at 293 K, chlorine at 4 cm min and both halogens isolated simultaneously in the gas cell after 30 minutes, *i.e.* spectra not acquired under flow conditions.

From the obtained spectra, it is possible to estimate the equilibrium constant for this reaction.

Table 21

Material	Molar adsorption coefficient ⁵⁴ (mol ⁻¹ L cm ⁻¹)	Wavelength (nm)	Initial concentration (mol l ⁻¹)	Equilibrium concentration (mol l ⁻¹)
BrCl	6.0	230	N/A	1.17x10 ⁻³
chlorine	25.2	330	9.78 x10 ⁻⁴	3.93 x10 ⁻⁴
Bromine	64.1	410	9.72 x10 ⁻⁴	3.87 x10 ⁻⁴

$$K = \frac{[BrCl]^2}{[Cl_2][Br_2]} \quad (54)$$

$$K = \frac{[1.17 \times 10^{-3}] (mol\ l^{-1})^2}{[3.93 \times 10^{-4}] (mol\ l^{-1}) [3.87 \times 10^{-4}] (mol\ l^{-1})}$$

$$K_{293} = 8.9$$

The equilibrium constant at 293 K is determined to be 8.9 which is close to the literature value of 9.1.⁵³ The reaction always favours the interhalogen species so when bromine and chlorine are co-fed the reactive species BrCl will present.

7.2.3 Determining BrCl in the Flow

The formation of BrCl was monitored as a function of varying chlorine concentration in the normal reaction flow regime ($159 \text{ cm}^3 \text{ min}^{-1}$). The bromine concentration was maintained constant by keeping the bromine doser temperature constant at 298 K; this corresponds to a Br_2 flow rate of $0.12 \text{ mmol min}^{-1}$ (see experimental). The flow of chlorine varied between $2.0\text{--}5 \text{ cm}^3 \text{ min}^{-1}$ and were left for 20 minutes before spectra was recorded.

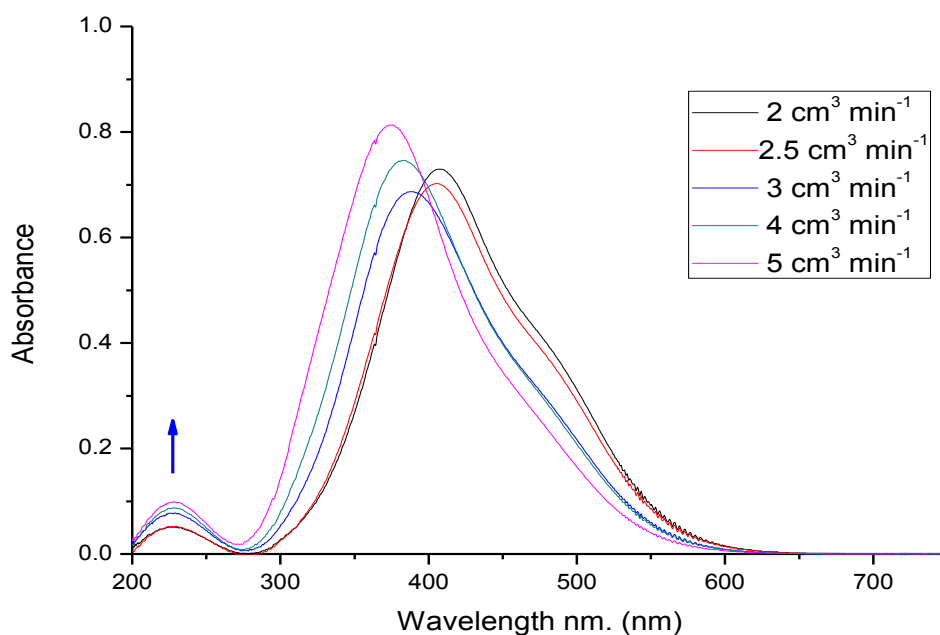


Figure 100 UV Vis Spectra of bromine at room temperature and varying chlorine flow in a total flow of $159 \text{ cm}^3 \text{ min}^{-1}$ at a reaction temperature of 298 K (bromine doser at room temperature at an estimated flow rate of $0.12 \text{ mmol min}^{-1}$)

From the obtained spectra, it is clear that BrCl is present, as indicated by the peak at 230 nm and increases with increasing chlorine flow rate *i.e.* concentration. The peak position of the Br_2

shifts because of the addition of the chlorine contribution to the peak as the reaction becomes limited in bromine.

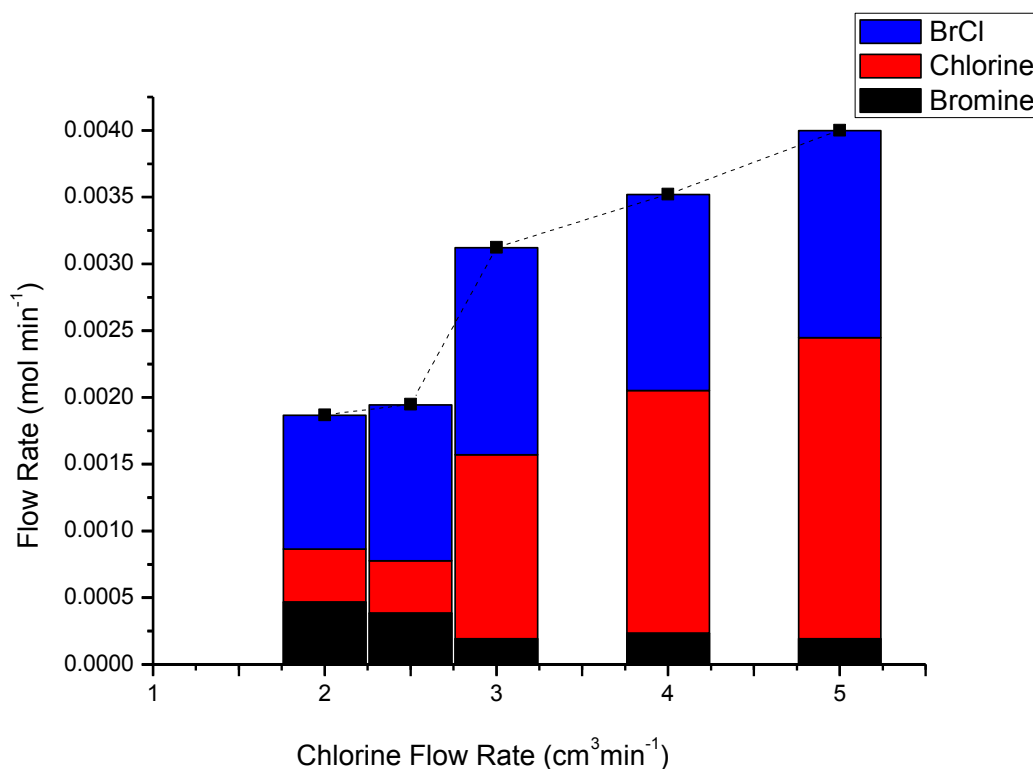


Figure 101 Mass balance for the reaction of Cl₂ and Br₂, the Br₂ flow was kept constant at room temperature and the flow rate of chlorine was varied 2-5 cm³ min⁻¹ in a total flow rate of 159 cm³ min⁻¹

The reaction returns a closed mass balance. The majority of the dibromine co-fed with chlorine exists as BrCl in the reaction flow.

7.3.1 Preliminary Bromine Experiments

The reactor was charged with 0.1285 g of Donau K40 carbon catalyst. The reaction was performed at 353 K for 1 hour before introducing the bromine. A flow rate of 0.0016 mmol min⁻¹ (195 K doser temperature) was introduced and the reaction was monitored using IR and UV-vis spectroscopy.

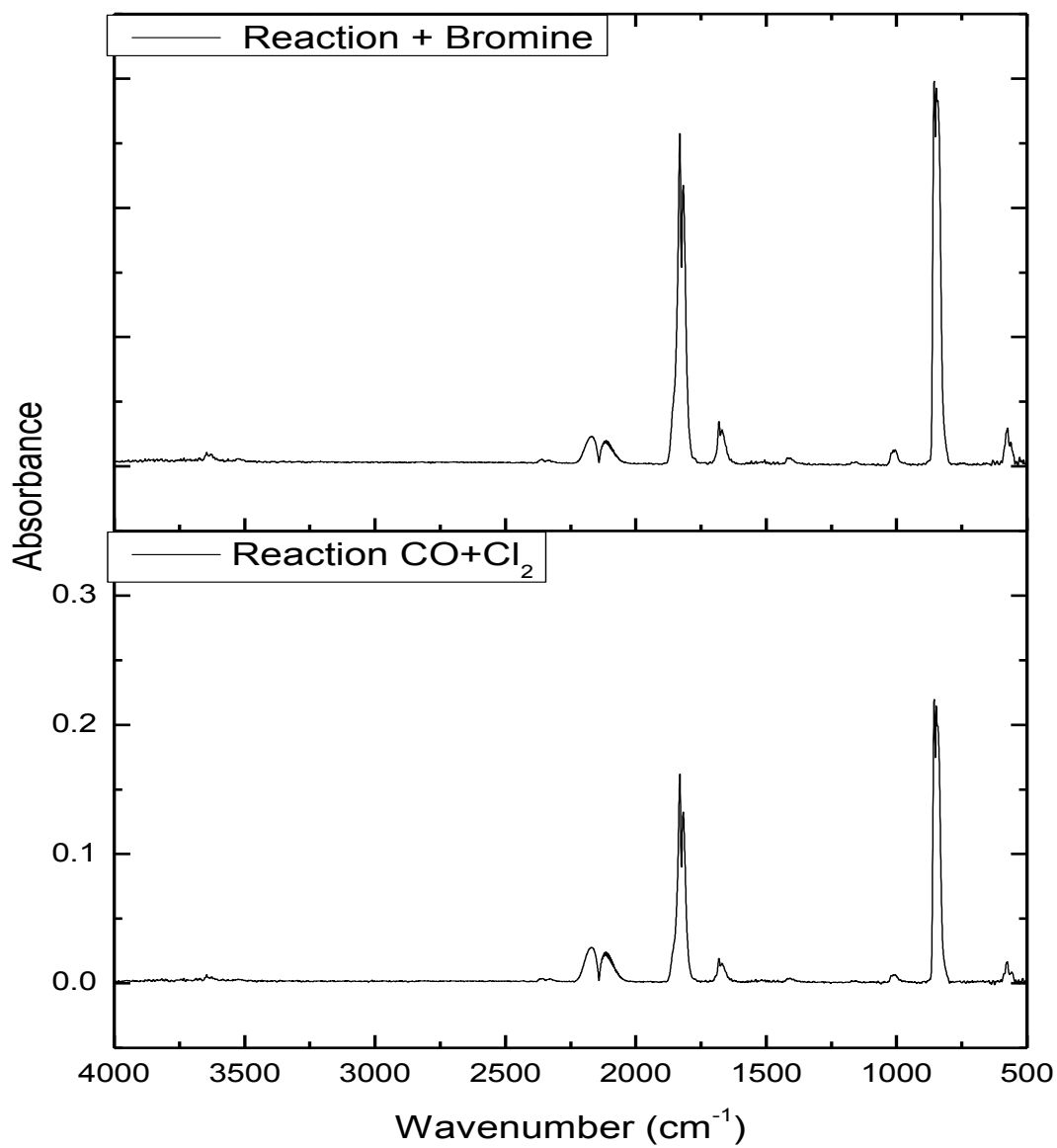


Figure 102: IR spectra for the reaction of CO and Cl introducing the bromine co-feed($0.0016 \text{ mmol min}^{-1}$) over the catalyst with flow rates of $5 \text{ cm}^3 \text{ min}^{-1}$ and $4 \text{ cm}^3 \text{ min}^{-1}$ over at a temperature of 353 K

Table 22 Main assignments for Fig.102

Peak position (cm ⁻¹)	Assignment
2169, 2119	ν (CO)
1832, 1820	ν_1 (CO) of COCl ₂
848	ν_4 asymmetric of COCl ₂ (C-Cl stretch)

From Fig. 102 phosgene is the only product observed on the introduction of Br₂. However, the rate at which phosgene is produced has increased following the introduction of Br₂. This preliminary experiment indicates Br₂ may influence phosgene formation. The Figure 99 summarises the initial observation.

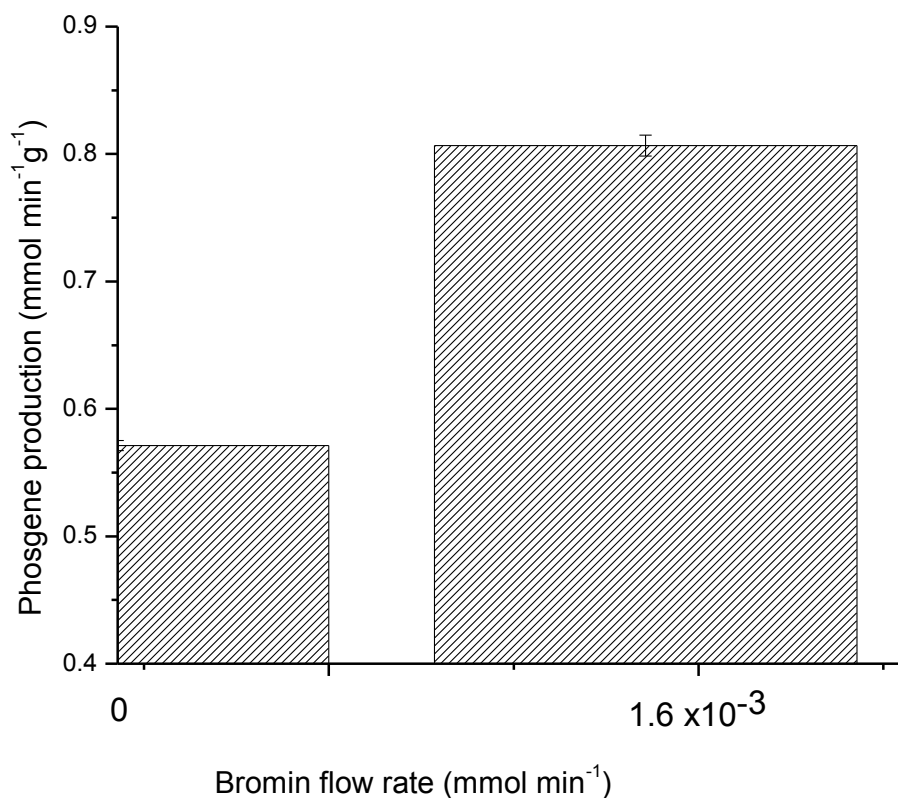


Figure 103 Phosgene production rate at 353 K as a function of reaction conditions (i) normal reaction (CO+Cl₂) and (ii) normal reaction with bromine present (0.0016 mmol min⁻¹, doser temperature of 195 K)

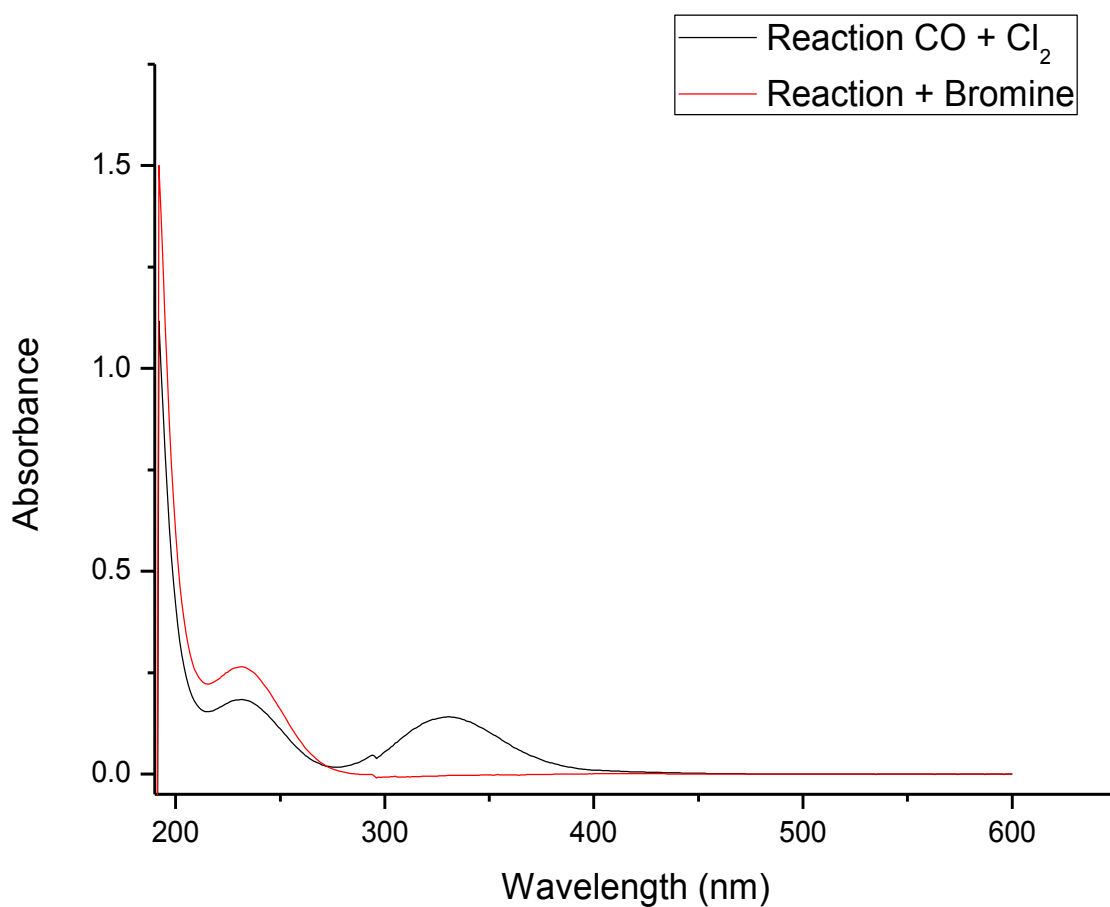


Figure 104 UV-vis spectra for the reaction of CO and Cl₂ introducing the bromine (bromine doser temperature of 195K, 0.0016 mmol min⁻¹) over the catalyst with flow rates of 5 cm³ min⁻¹ and 4 cm³ min⁻¹ respectively over at a temperature of 353 K

Table 23

Peak position (nm)	Assignment
330	$\pi^* \rightarrow \sigma^*$ of chlorine
230	$\pi \rightarrow \pi^*$ of COCl ₂

In both the infrared and UV vis there is a clear increase in phosgene production and consumption of dichlorine. However, the band for phosgene in the UV at 230 nm cannot be used to monitor phosgene as it overlaps with the BrCl band. The IR spectrum shows no formation of by-products infrared under these reaction conditions.

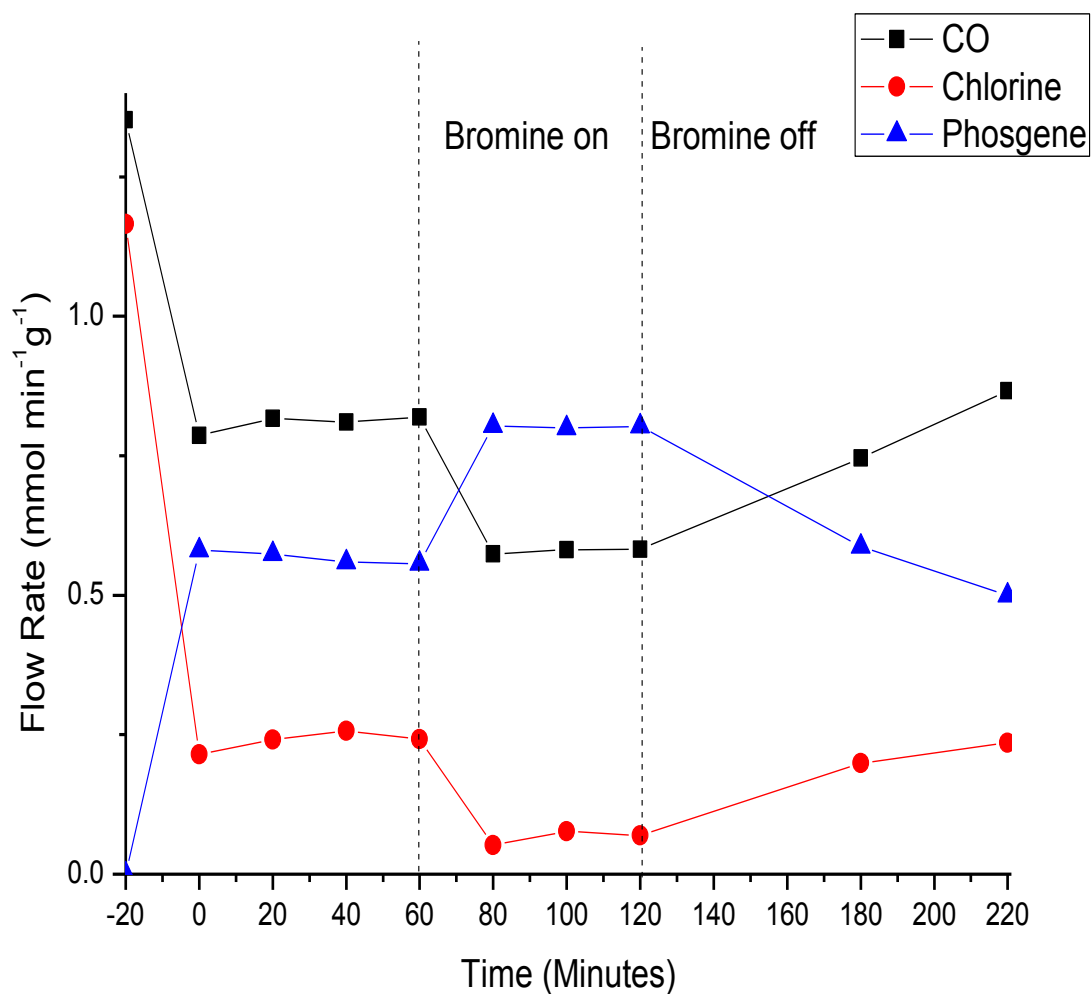


Figure 105 Reaction profile for the reaction of CO and Cl₂ over the catalyst with flow rates of 5 cm³ min⁻¹ and 4 cm³ min⁻¹, over at a temperature of 353 K with bromine co-feed (bromine doser at 195 K, 0.0016 mmol min⁻¹)

On the introduction of bromine (Figure 105), the reaction rate is enhanced phosgene and the reaction rate reaches steady state. The original activity is resumed when the bromine is switched off. Small quantities of Br₂ co-feed improve the phosgene yield and there is a fast response of the chemical system to the presence of Br₂. From the reaction profile (Figure 105) the effects due to the Br₂ are reversible.

7.3.2 Reaction with Br₂ and CO

The reactor was charged with 0.1225g of fresh catalyst and the reactor and bromine doser were maintained at room temperature (9.72×10^{-3} mmol min⁻¹). The reaction was tested under standard operating conditions. From the infrared spectrum, it can be observed that COBr₂ is formed. On increasing the temperature ($T > 323$ K) carbonyl bromide breaks down into CO and Br₂ as it is not thermodynamically stable under these conditions¹ There is a relatively low CO conversion at 10%; *i.e.* COBr₂ only partial (as well as being meta-stable)

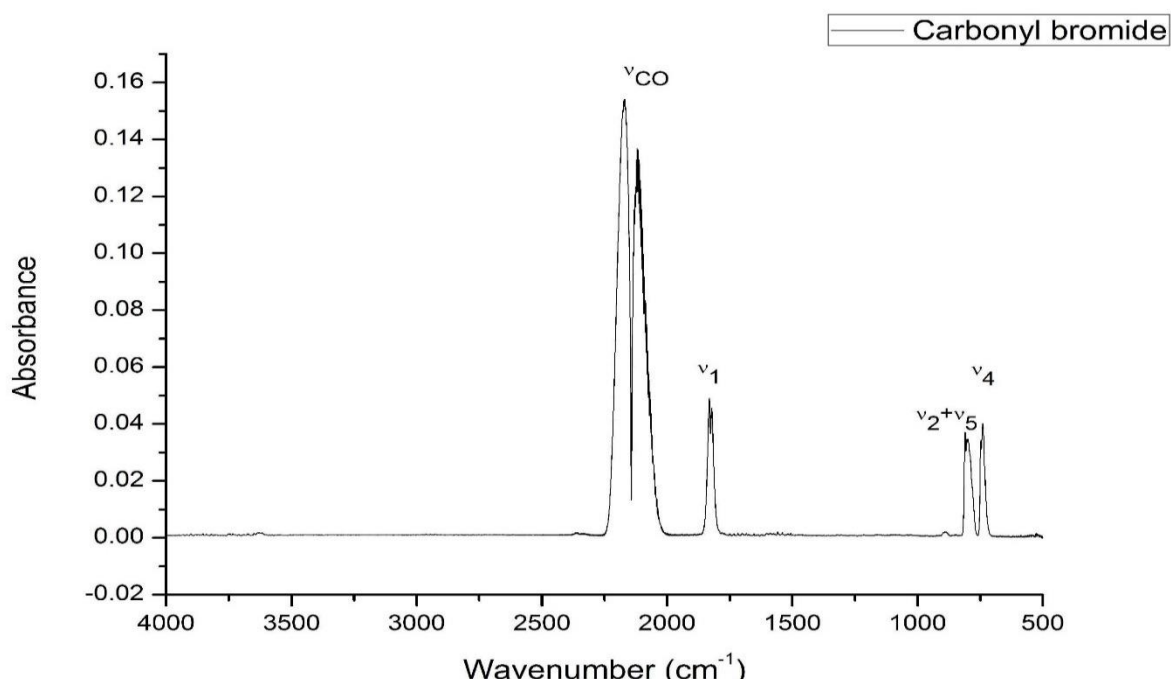


Figure 106 Example IR spectra of carbonyl bromide at a reaction temperature of 298 K, bromine doser at room temperature

Table 24 Main assignments of man bands seen in Fig. 106^{1,72,74}

Peak position (cm ⁻¹)	Assignment
2169, 2119	ν (CO)
1832, 1820	ν_1 (CO) of COBr ₂
757	ν_4 asymmetric of COBr ₂ (C-Br stretch)
779	ν_{2+} ν_5

7.3.3 Reaction with varying concentration of Bromine at a reaction temperature of 303 K

The reactor was charged with 0.1235g of catalyst and the reaction was operated at 303 K for 2 hours under normal operating conditions ($\text{CO } 5 \text{ cm}^3 \text{ min}^{-1}$, $\text{Cl}_2 4 \text{ cm}^3 \text{ min}^{-1}$ and $\text{N}_2 150 \text{ cm}^3 \text{ min}^{-1}$) before introducing bromine at different doser temperatures. The reaction is operating at low chlorine conversion $\chi_{\text{Cl}} \sim 10 \%$. To measure the bromine concentration, the reaction flow was then switched over bypass the chlorine flow was then stopped before introducing the bromine. Three different temperatures of bromine (temperature of cooling bath) were tested for 2 hours. The reaction rate was found to increase as a function of increasing the temperature of the bromine doser, *i.e.* on increasing the concentration of Br_2 in the feed stream using temperature of the doser as a control.

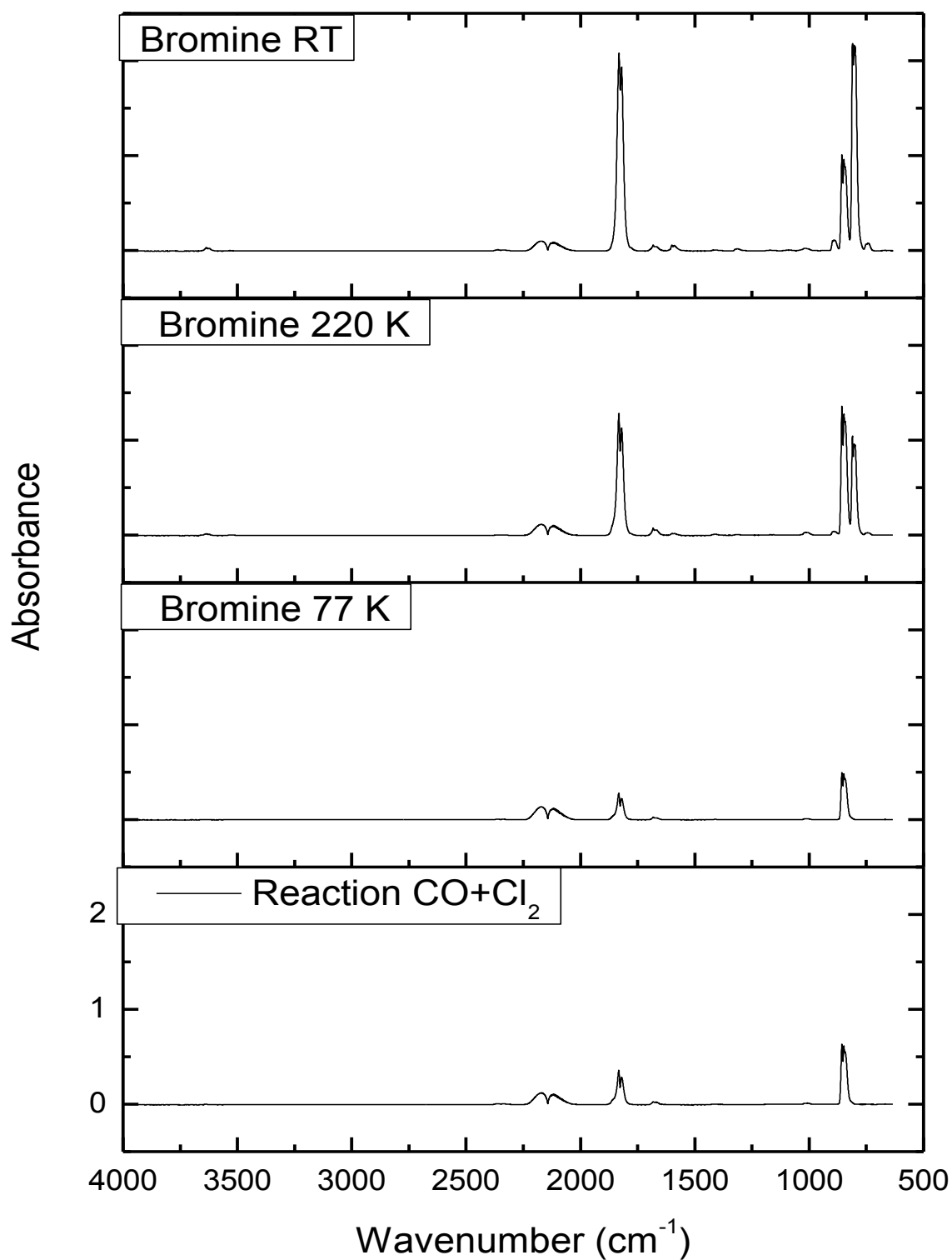


Figure 107 IR spectra for the reaction of CO and Cl₂ introducing the bromine cofeed over the catalyst with flow rates of 5 cm³ min⁻¹ and 4 cm³ min⁻¹ over at a temperature of 303 K

Table 25 Main band assignments seen in Fig.107

Peak position (cm ⁻¹)	Assignment	Species
2169, 2119	v (CO)	CO
1832, 1820	v ₁ (CO)	COCl ₂
848	v ₄ asymmetric (C-Cl stretch)	COCl ₂
744	v ₄ asymmetric (C-Br stretch)	COBr ₂
810	v ₄ asymmetric (C-ClBr stretch)	COClBr

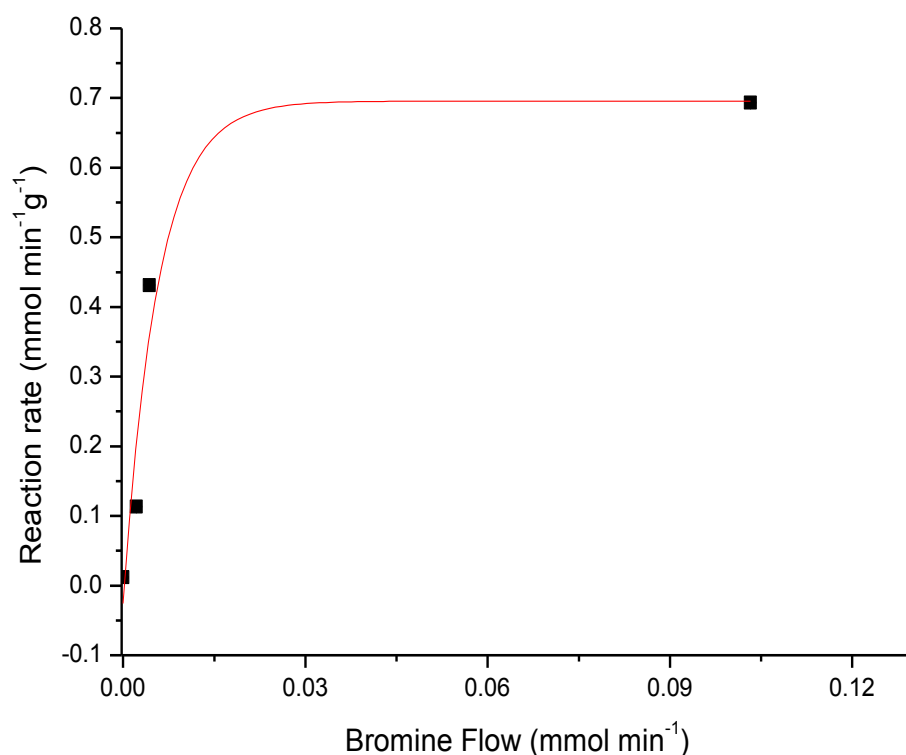


Figure 108 Reaction rate as a function of bromine flow rate calculated based on the v₁ mode of phosgene, COClBr, and COBr₂

From the infrared spectrum taken with the bromine doser at room temperature (Figure 108), COClBr appears to be present, then phosgene, and COBr₂. The extent of reaction with the bromine doser at room temperature (Br₂ flow rate ~0.1 mmol Br₂ min⁻¹) is limited by chlorine availability.

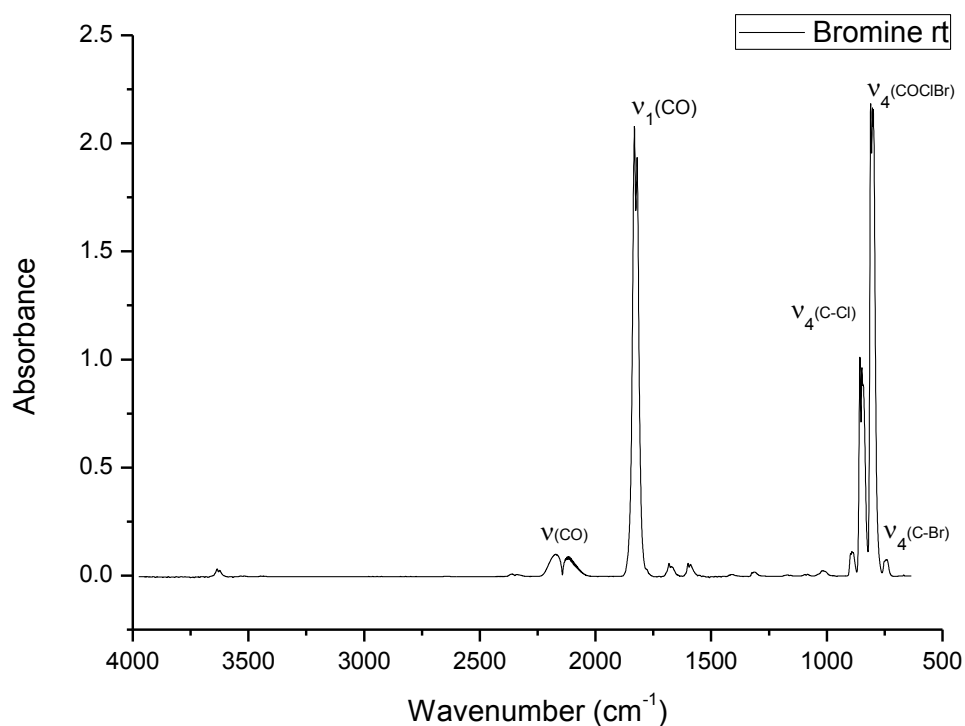


Figure 109 IR spectra for the reaction of CO and Cl introducing the bromine at room temperature co-feed over the catalyst with flow rates of 5 cm³ min⁻¹ and 4 cm³ min⁻¹ over at a catalyst temperature of 303 K

Figure 109 is a reproduction of the top frame of Fig 103 but utilising an expanded y coordinate. At high Br₂ flow rates *ca* 0.1 mmol min⁻¹ it is apparent that COClBr, COCl₂ and COBr₂ are present at a catalyst temperature of 303 K. However, this is indicating that there is an active role for BrCl in the reaction chemistry. At high bromine concentrations, the reaction to form BrCl in the feedstream is significant. The reaction of BrCl over the catalyst would result in all of the observed products being formed at low temperature.

In order to provide information on how reaction temperature may influence the presence of reacting species the temperature was increased to 353 K, and compared to the reaction over the catalyst at 303 K

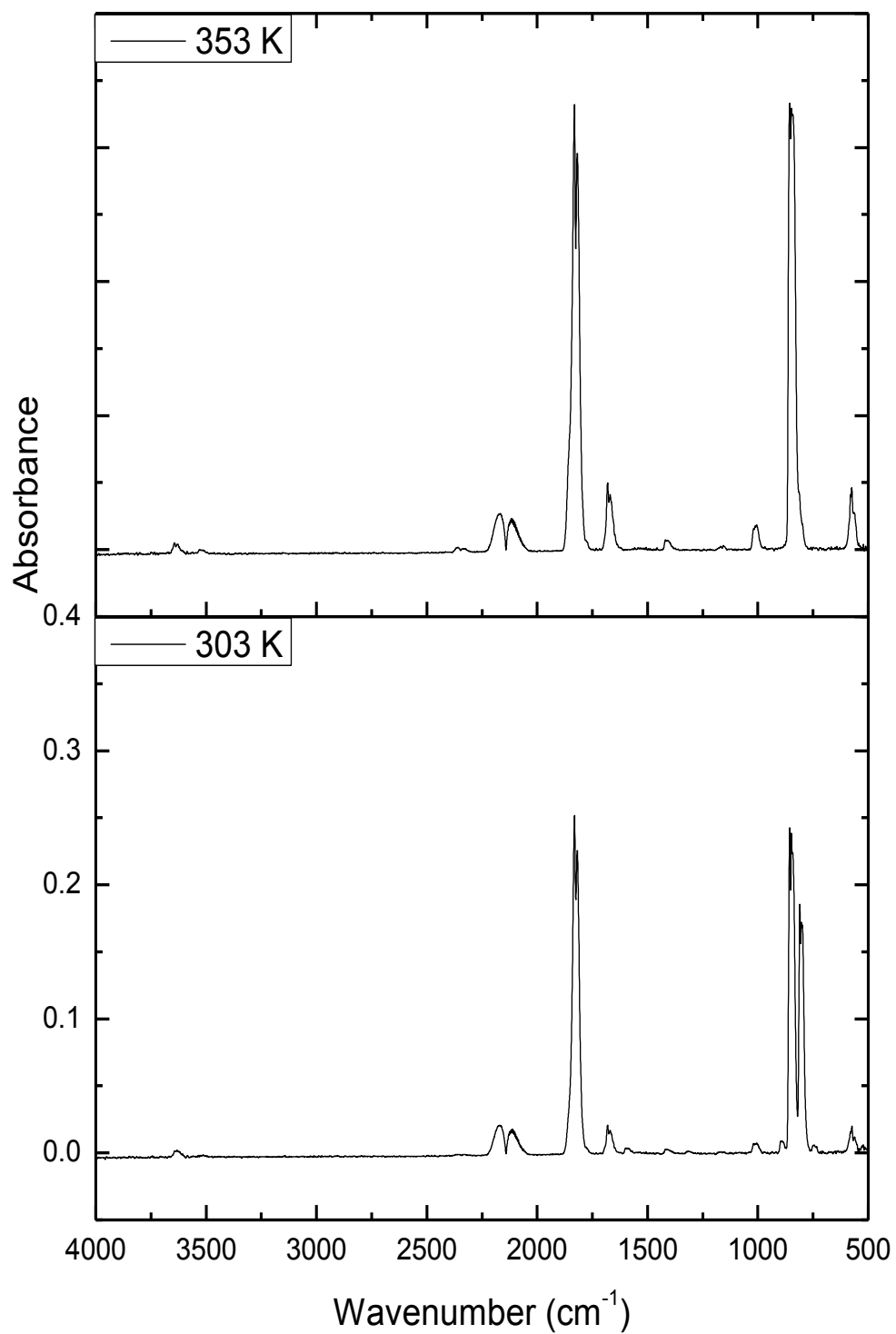


Figure 110 : IR spectra for the reaction of CO and Cl₂ introducing the bromine cofeed over the catalyst with flow rates of 5 cm³ min⁻¹ and 4 cm³ min⁻¹, respectively, over increasing the temperature from 303 K to 353 K

Table 26 Main assignments form Fig.110

Peak position (cm ⁻¹)	Assignment	Species
2169, 2119	ν (CO)	CO
1832, 1820	ν_1 (CO)	COCl ₂
848	ν_4 asymmetric (C-Cl stretch)	COCl ₂
744	ν_4 asymmetric (C-Br stretch)	COBr ₂
810	ν_4 asymmetric (C-ClBr stretch)	COClBr

At the higher reaction temperature, the reaction returns only phosgene, whereas at the lower reaction temperature it returns a mixture of products (COCl₂, COBr₂ and COClBr)

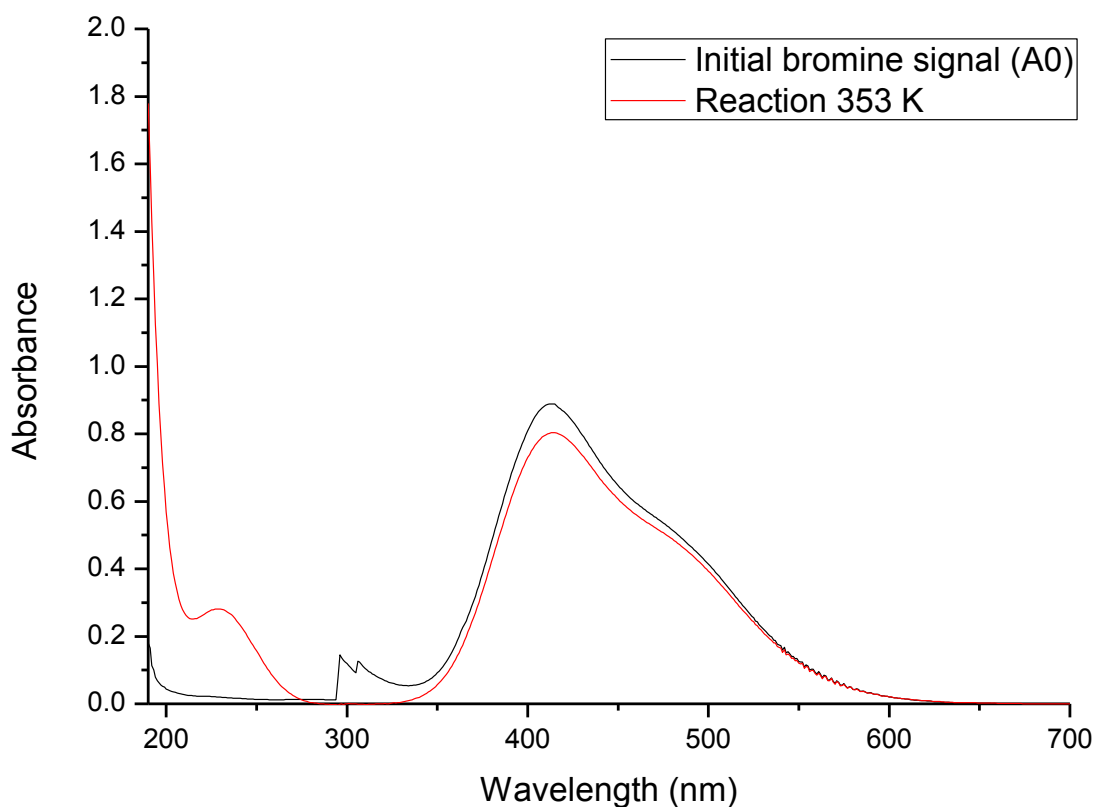


Figure 111 Initial bromine signal obtained over the bypass and signal on increasing the reaction temperature to 353 K in a total flow of 159 cm³ min⁻¹

The clips at 300 nm are due to the lamps switching (W/D₂) in the spectrometer. The reaction at the higher temperature almost returns the initial dibromine concentration and there is a clear switch in the IR from COBrCl, COBr₂ to only phosgene due to the relative thermal stabilities of these moieties (COCl₂ > COBrCl >> COBr₂).

For the reaction at low temperature, COClBr and COBr₂ are observed in the IR spectrum along with COCl₂. This is indicative that the reaction to form BrCl in the feedstream is occurring and is playing a role in the reaction chemistry. However, on increasing the temperature the reaction returns COCl₂ and Br the latter as evidenced by UV-vis (Figure 111), consequently, COClBr and COBr₂ are identified as being intermediary species. Interestingly, Figure 111 shows the bromine to be almost completely returned from the reaction, so it could be considered catalytic.

7.4.1 Reactions at 323 K with varying dibromine concentration

These experiments are an elaboration following on from section 7.3.1 which investigated the influence of a small bromine concentration on the rate of formation of phosgene. The concentration of dibromine was controlled using different cooling baths at different temperatures (improvement of method). The reaction (CO + Cl₂) was performed at 323 K. The reaction was operated for 1 hour before introducing the bromine. The chlorine was switched off to allow quantification of a steady flow of bromine before restarting the flow. Four different dibromine flow rates (concentrations) were investigated.

Table 27 Bromine in the feedstream

Cooling Bath	Br source temperature (K)	Dibromine flow rate (mmol Br ₂ min ⁻¹)	$\frac{[Br_2]}{[Cl_2]}$ %	ppm Br ₂ in Cl ₂
Liquid N ₂ + isopentane	113	3.66E-4	0.24	2400
Liquid N ₂ + pentane	143	6.90E-4	0.40	4000
Dry Ice + Acetone	196	0.0016	1.05	10500
Dry Ice + Acetonitrile	223	0.0024	1.61	16100

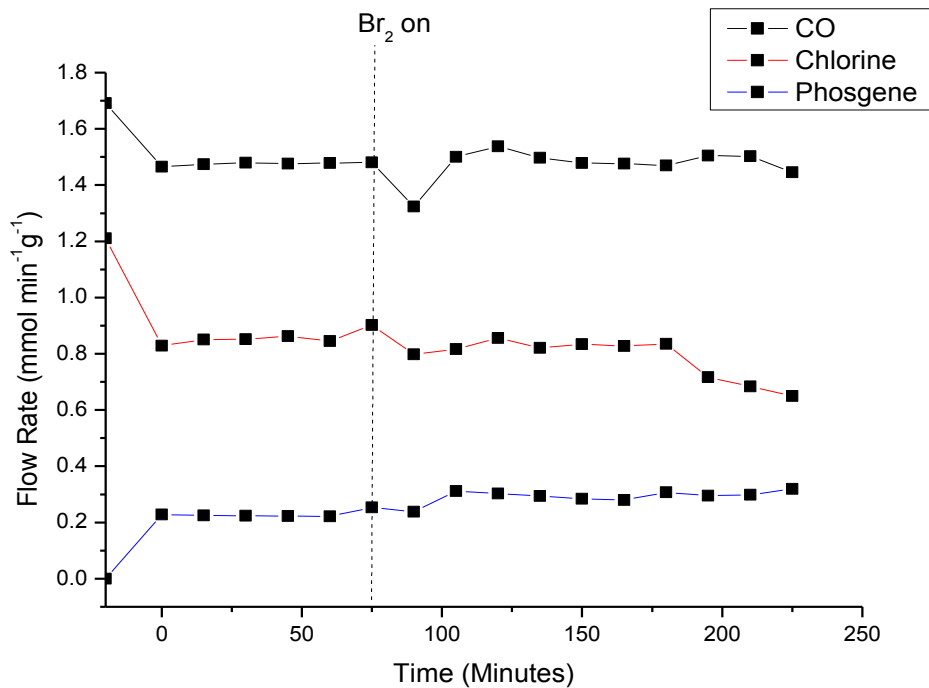


Figure 112 Reaction profile of the reaction between CO and Cl₂ at 323 K with a bromine flow rate of 3.6×10^{-4} mmol min⁻¹ (Br₂ doser T = 113 K) at 1 hour

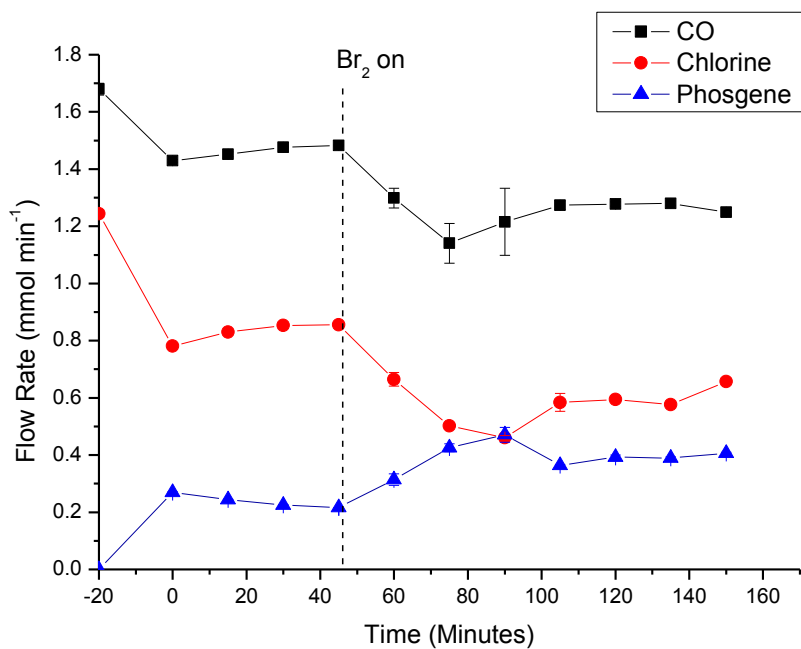


Figure 113 Reaction profile of the reaction between CO and Cl₂ at 323 K with a bromine flow rate of 6.9×10^{-4} mmol min⁻¹ (Br₂ doser T = 143 K) at 1 hour (error bars are the standard deviation of 3 spectra)

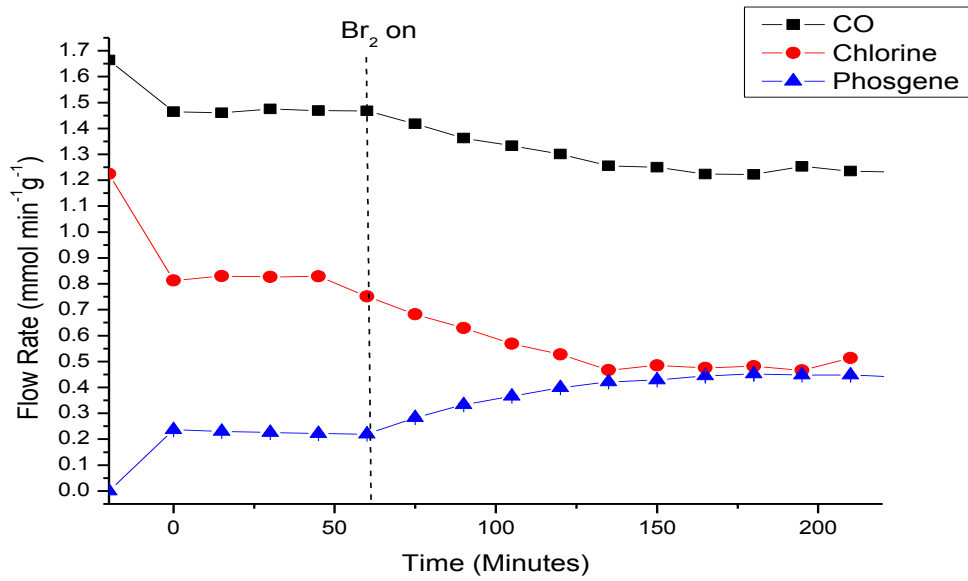


Figure 114 Reaction profile of the reaction between CO and Cl₂ at 323 K with a bromine flow rate of⁴ 0.0016 mmol min⁻¹ (Br₂ doser T = 196 K) at 1 hour

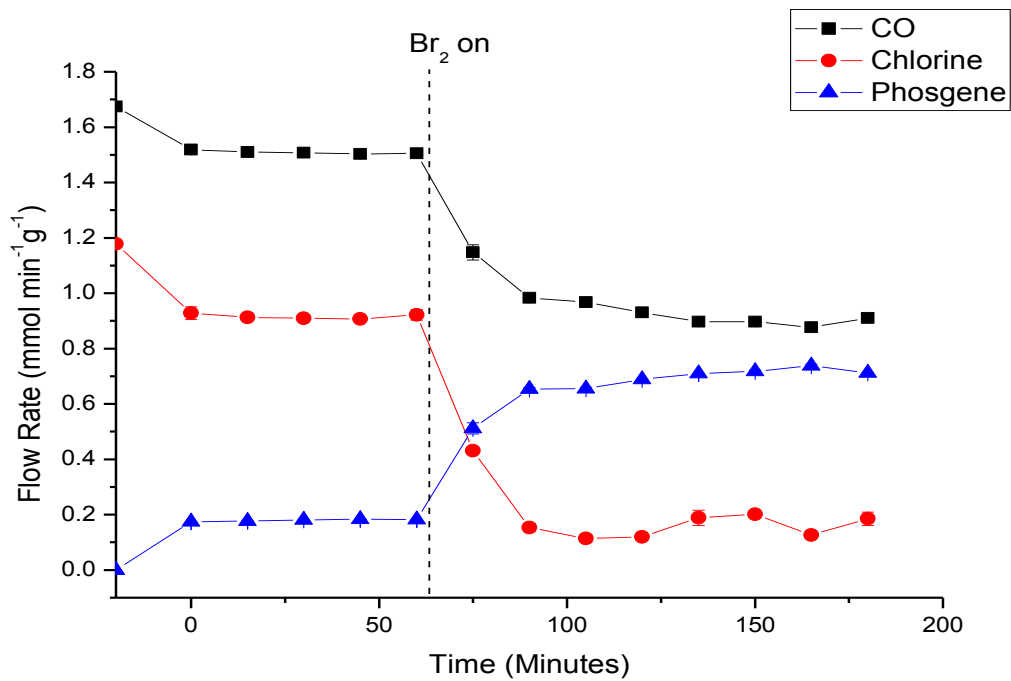


Figure 115 Reaction profile of the reaction between CO and Cl₂ at 323 K with a bromine flow rate 0.0024 mmol min⁻¹ (Br₂ doser T = 223 K) at 1 hour

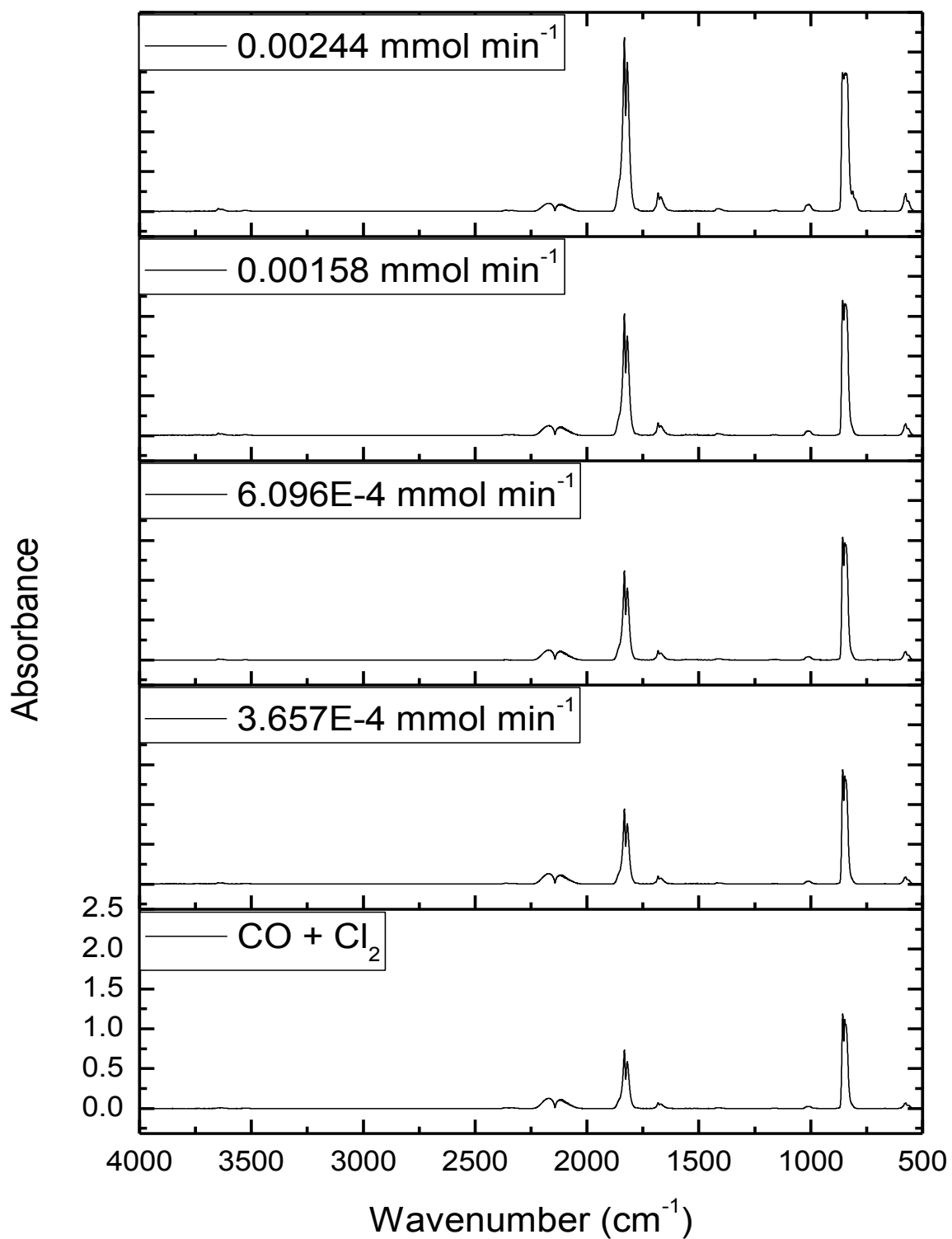


Figure 116 Infrared Spectra of the reaction between CO and Cl₂ operating at 323 K at different bromine flow rates

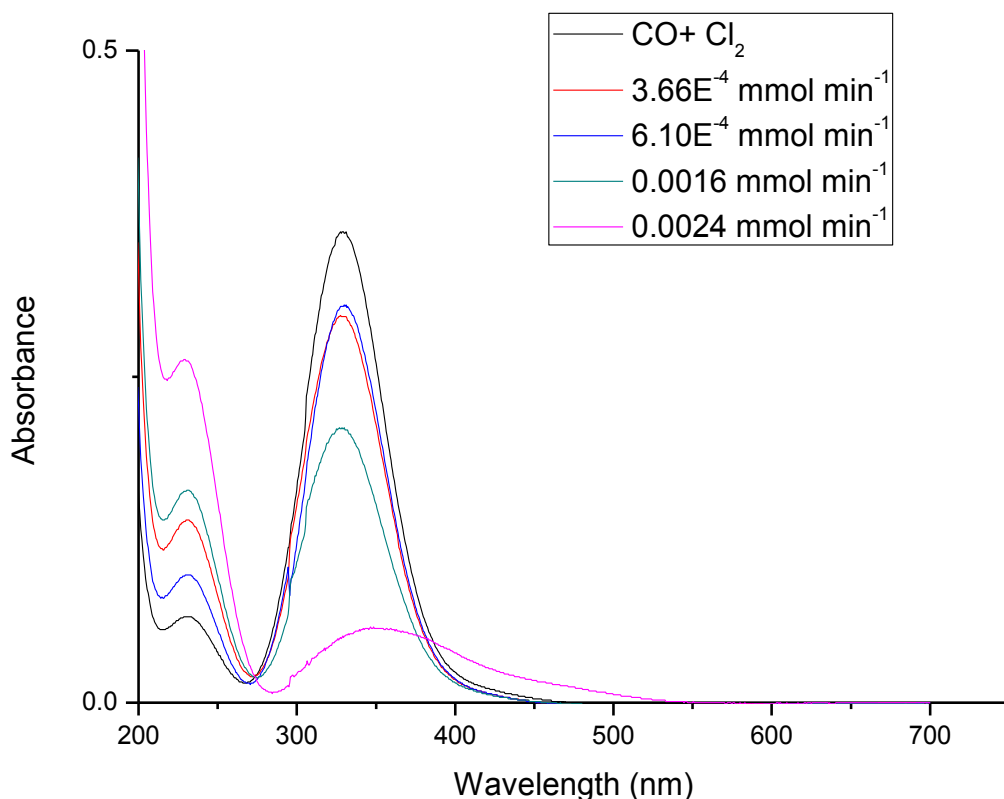


Figure 117 UV-Vis Spectra of the reaction between CO and Cl₂ operating at 323 K at different bromine flow rates

Figures 108-111 present the reaction profiles on increasing Br₂ flow rates whilst the catalyst is maintained at 323 K. The corresponding IR and UV-vis spectra are respectively presented in Figures 112-113. Even for the lowest exposure Br₂ of $3.65 \times 10^{-4} \text{ mmol min}^{-1}$ Br₂, a slight increase in COCl₂ production is noted. Inspection of the $\nu_1(\text{CO})$ band of COCl₂ at 1832 and 1820 cm^{-1} shows increasing Br₂ substantially increases rate of formation of COCl₂.

The only product observed in the infrared spectra (Figure 116) is phosgene, indicating the by-products COBr₂ and COBrCl to be unstable for reaction temperatures $\geq 323 \text{ K}$. Although the intensity of the 230 nm feature in the UV-vis spectra (Figure 117) is complicated by contributions from COCl₂ and BrCl (see Section 7.2.1), the chlorine is seen to be consumed but, interestingly, as evidenced by the tail $\geq 400 \text{ nm}$, Br₂ is being observed in the product stream at a Br₂ flow rate of $2.4 \times 10^{-3} \text{ mmol Br}_2 \text{ min}^{-1}$. It is possible that the thermal decomposition of COBr₂ and COClBr are contributing to the Br₂ pool.

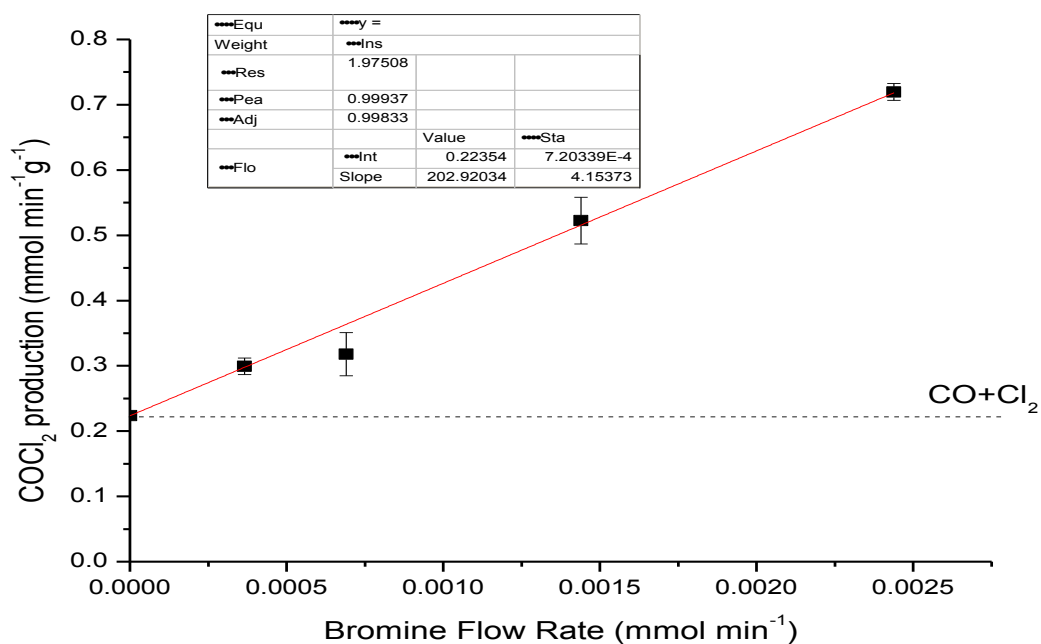


Figure 118 Phosgene production as a function of bromine flow rate in the feedstream. The dotted line is the reaction operating with only CO and Cl₂. The error bars represent the standard deviation of the reaction operated at steady state for 2 hours. The red line represents a linear fit to all five data points [slope= 202.92 ± 4.15 mmol COCl₂ min⁻¹g⁻¹cat(mmol Br₂ min⁻¹)⁻¹]

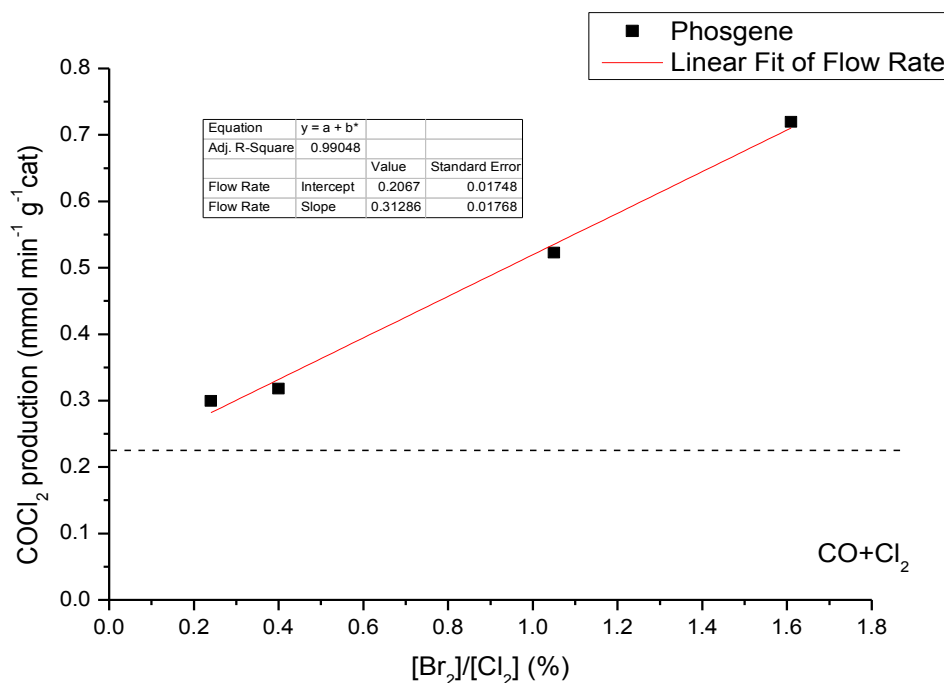


Figure 119 Phosgene production as a function of % bromine in the feedstream. The dotted line is the reaction operating with only CO and Cl₂. The red line represents a linear fit to all five data points [slope= 0.313 ± .018 mmol COCl₂ min⁻¹g⁻¹cat(% Br₂/Cl₂)⁻¹]

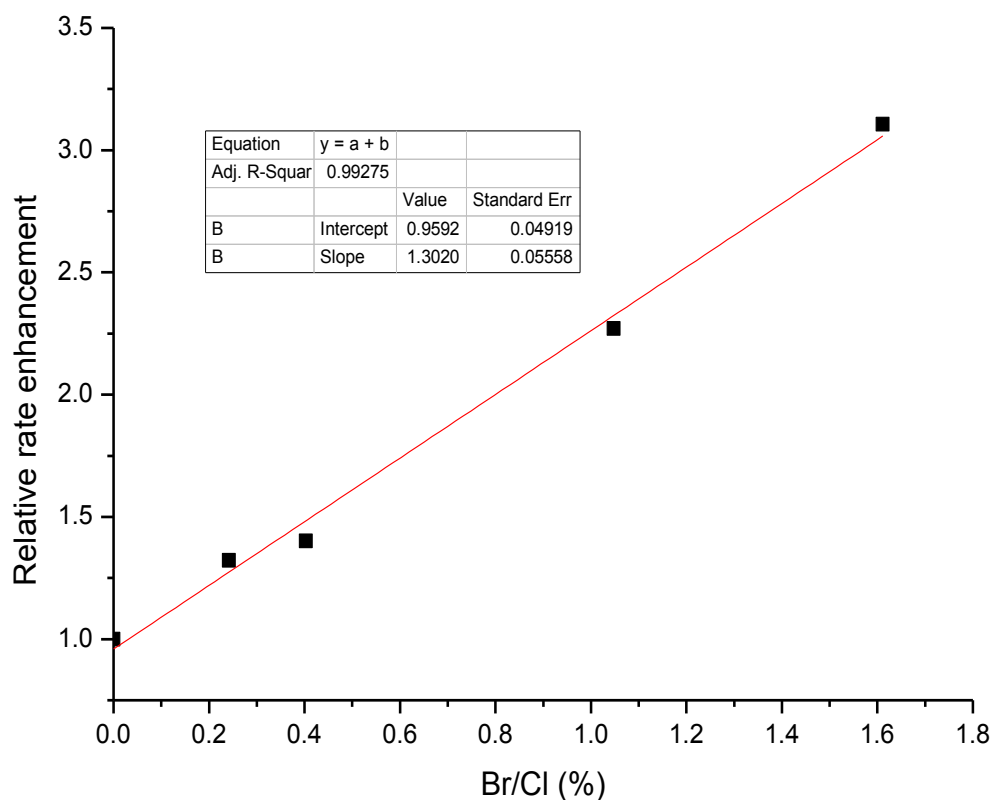


Figure 120 Relative enhancement in phosgene production rate as a function of % bromine in the feedstream. The dotted line is the reaction operating with only CO and Cl₂. The red line represents a linear fit to all five data points [slope= 1.30 ± 0.06 enhancement(% Br/Cl₂)⁻¹]

From the Fig.114 it is clear that there is a direct relationship between the bromine content in the feed stream and the rate of phosgene formation. The intercept is the rate of formation of COCl₂ under normal reaction conditions (without bromine in the feedstream). With *ca* 1% bromine/chlorine in the feedstream the reaction rate doubles (Figs. 118-120).

7.5 Bromine Desorption

The reactor was charged with 0.1225g of catalyst. The bromine doser was maintained at 195 K ($0.0016 \text{ mmol min}^{-1}$) and reactor were kept at room temperature. The total flow was kept at $159 \text{ cm}^3 \text{ N}_2 \text{ min}^{-1}$ and UV spectra was used to follow the bromine signal until stable signals were obtained, at which point the flow was then switched over the catalyst. The bromine was passed over the catalyst until the initial signal (A_0) was returned and the flow of bromine was stopped.

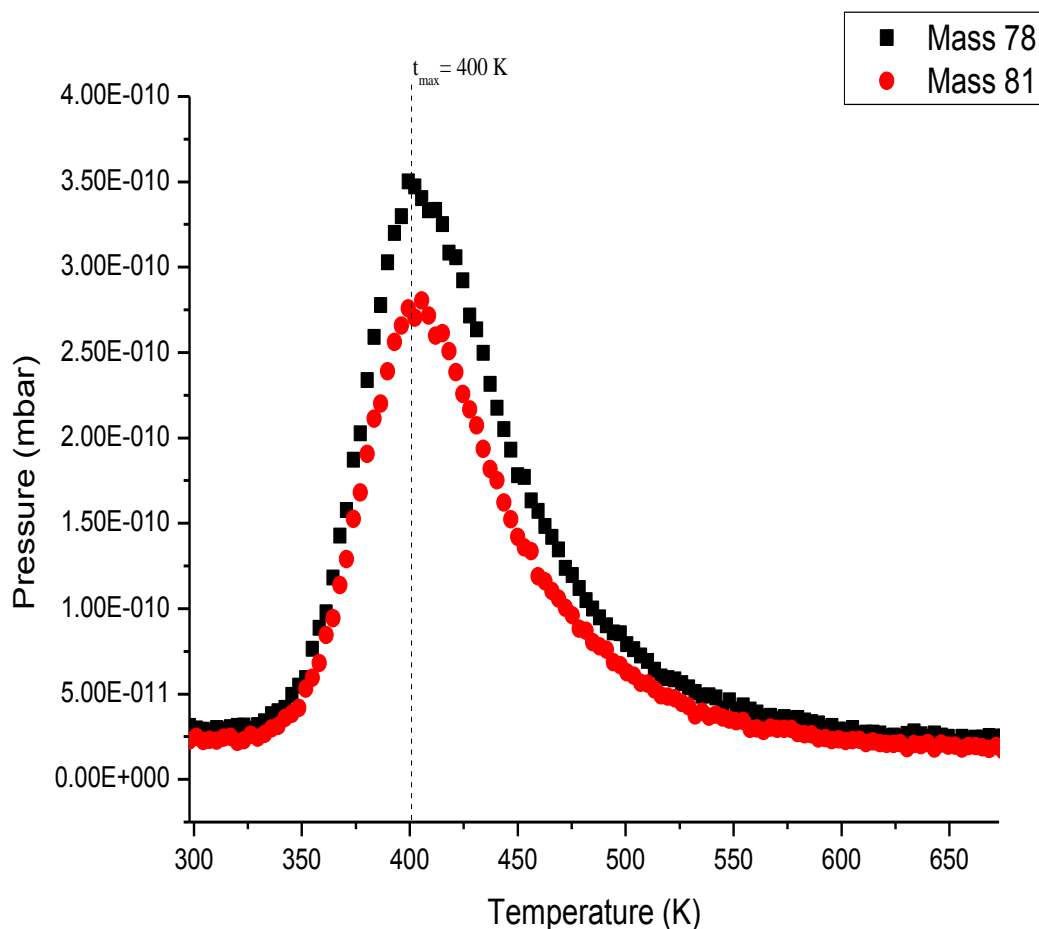


Figure 121 Bromine desorption from the fresh Donau k40 catalyst with a temperature ramp 298-673 K at 5 K/min in a total flow of $159 \text{ cm}^3 \text{ min}^{-1}$

There is clear signal due to desorption from the catalyst with a T_{max} of 400 K which is similar to that of chlorine ($T_{\text{max}}= 356 \text{ K}$, Section 6.3.2). This is evidence for Br_2 retention by the catalyst. With respect to the experimental section (Section 2.2.3), it is thought that the mass

spectrometer signal corresponds to the recombinative desorption of Br atoms, *i.e.* Br₂ is the detected species and not Br ·.

7.6 Post reaction catalyst analysis (bromine)

This purpose of this experiment is to examine the catalyst surface after a 4-hour reaction (3 hours of CO + Cl₂ and 1 hour with bromine doser at 195 K (0.0016 mmol min⁻¹ bromine in the feed-stream)) to determine if there was any interchange at the surface with chlorine and bromine. The reaction flow was passed over the bypass containing ground quartz until stable signals were detected in both the infrared and UV-Visible spectrometers. The flow was then passed over 0.1250 g of catalyst and the reaction was monitored for 3 hours at 323 K before introducing the bromine into the reaction feed. The reaction was then terminated by switching the flow over the bypass and the flow of reagents was switched off leaving only nitrogen flowing. The catalyst reactor was purged and an SEM/EDX was taken of the catalyst sample.

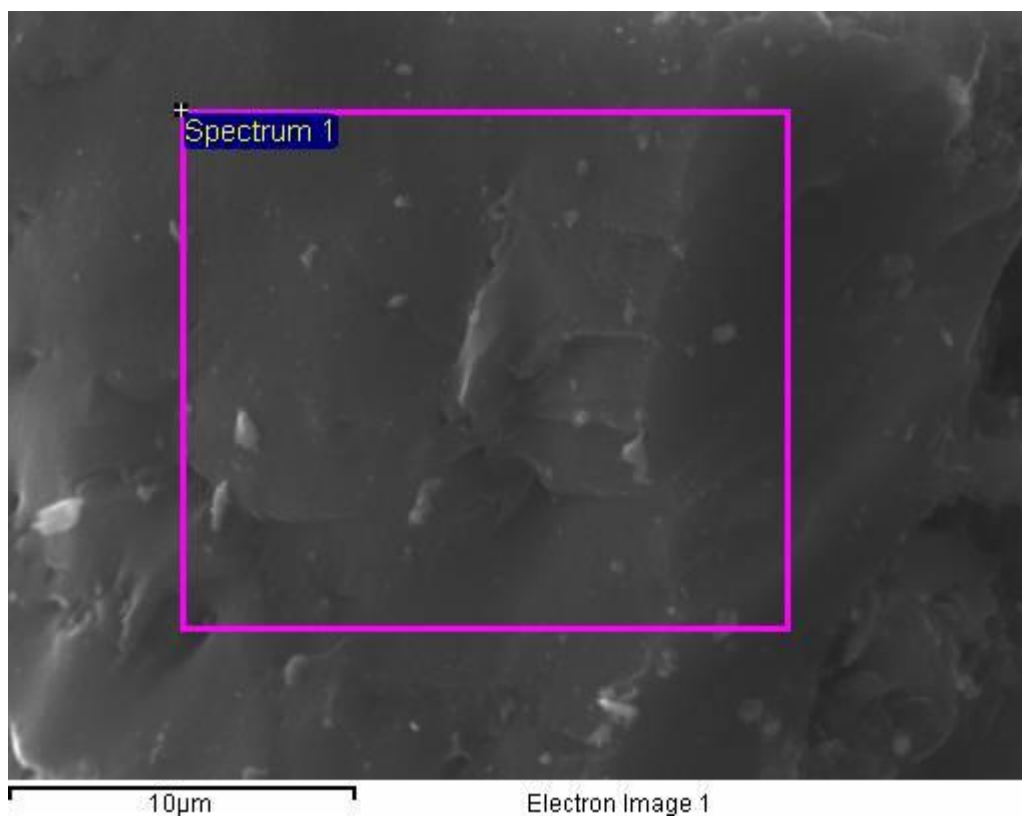


Figure 122 SEM image of the Donau Supersorbon K40 catalyst post reaction (4 hours at 323 K) showing the area of which an EDX was taken

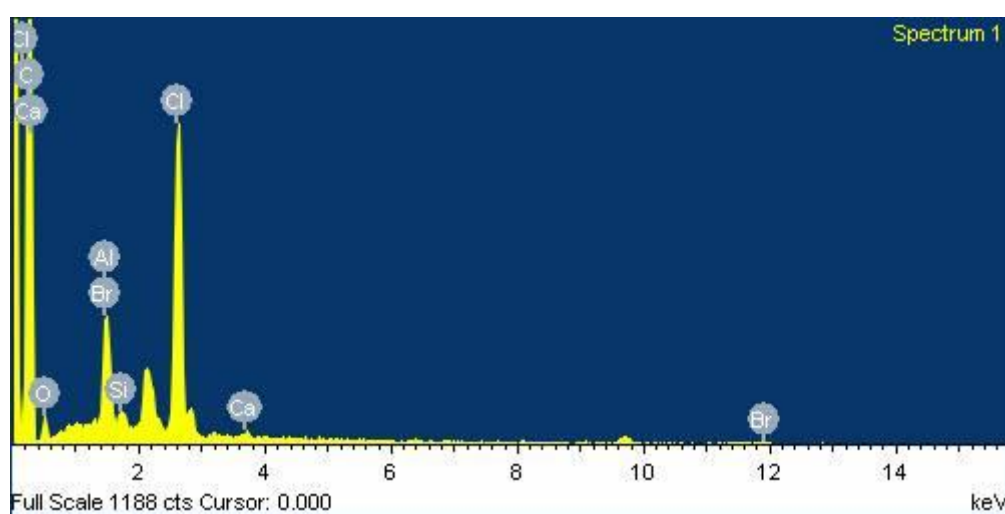


Figure 123 EDX of the Donau Supersorbon K40 catalyst after 4 hours of reaction at 323 K (3 hours + 1 hour with bromine)

Table 28 EDX result for Fig 123

Element	Weight %	Atomic %
Carbon	84.34	92.37
Oxygen	5.02	4.13
Aluminium	0.47	0.23
Silicon	0.23	0.11
Chlorine	7.26	2.69
Calcium	0.17	0.06
Bromine	2.51	0.41

From the EDX taken of the catalyst after 3 hours and 1 hour with bromine, it is clear that chlorine and bromine have been adsorbed on to the catalyst surface. However, the catalyst appears to have a significant quantity of bromine on the surface relative to the exposure time and concentration of bromine(1.05 % of bromine/chlorine content).

7.7 Summary

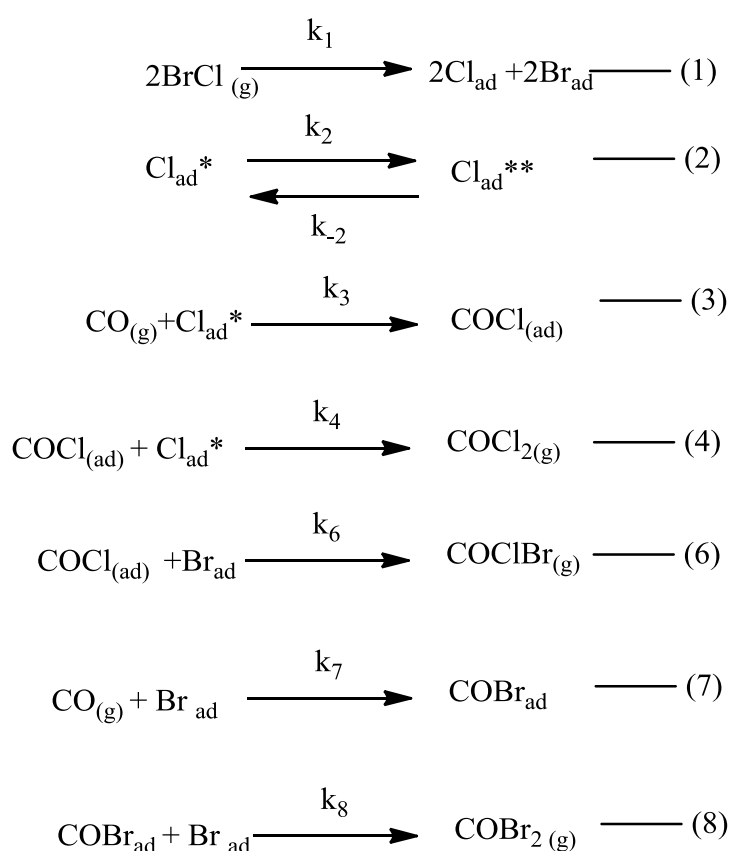
- The interhalogen species BrCl readily forms when co-feeding bromine and chlorine.
- The reaction rate of phosgene production increases with increasing bromine flow rate.
- At low temperature ($T \leq 303$ K), by-products are observed (COBrCl and COBr₂) indicating an active role for BrCl in the reaction chemistry.
- At high reaction temperature ($T \leq 303$ K), the only product observed is the desired phosgene at an accelerated rate and the reaction returns bromine as Br₂.
- The catalyst adsorbs bromine and has a similar T_{\max} to retained chlorine in the desorption measurements. This indicates comparable adsorption enthalpies which, in a competitive adsorption regime, will lead to a competition for active sites for halogen species.

7.8 Discussion

The gas phase reaction between bromine and chlorine to produce bromine chloride is observed.



A high bromine concentration and low temperature the reaction mechanism with respect to the presence of BrCl becomes:



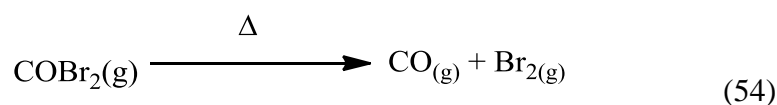
Chlorine adsorbed on site 2 is not available for reaction which is consistent with the previously described mass imbalance (Section 6.5).



Fig. 111 clearly shows that small quantities of Br₂ in the co-feed lead to an enhanced COCl₂ formation. One possible avenue for this is that Br co-adsorption shifts the Cl_{ad}* ⇌ Cl_{ad}** equilibrium (equation 2) to the left-hand side, making more Cl_{ad}* available for reaction at

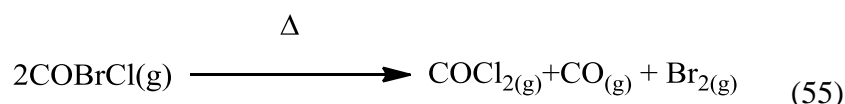
particular temperature thereby facilitating elevated COCl_2 synthesis. Such a scenario is consistent with the postulated COCl_2 reaction mechanism over carbon (section 6.5). Thus, Br_2 is thought to be catalysing the COCl_2 synthesis reaction by increasing the population of Cl_{ad}^* via perturbation of reaction 2.

At higher temperatures (323K and above), Figures 116 and 117 show that the reaction returns only phosgene and bromine (or BrCl depending on whether there is unreacted chlorine). There is unfortunately very little structural information on $\text{COClBr}^{1,103,104}$ but the bromine returned could arise from thermal decomposition of COBr_2 .



Almost complete decomposition of COBr_2 is reported under mild heat conditions¹.

The disappearance of the COClBr species at the higher temperature would require further investigation. However, the reaction might be analogous to the disproportionation of COFBr to COBr_2 and COF_2 where the reaction is reported to be catalysed by activated carbon¹. The reaction is not at equilibrium due to the thermal decomposition of COBr_2 . So, the following reaction is proposed.



Further investigation is required to conclusively determine the reaction mechanism in the presence of bromine. Nevertheless, this work has shown that small quantities of bromine result in a significant increase in the rate of production of phosgene. At lower temperatures, the formation of COBr_2 and COClBr are observed.

It is possible that Br_2 is acting catalytically. Given that the Br sinks decompose at temperatures ≥ 323 K. Equations 54 and 55 shows that this process releases Br_2 which is then available via Equation 53 to form BrCl . This moiety can be dissociatively adsorbed and shift the equilibrium described by Equation 2 to the left-hand side favouring COCl_2 production by a relatively increased quantity of Cl residing in Site 1. In this way Br does not appear in the product, the thermodynamic sink of COCl_2 . Figure 124 shows a schematic for the proposed reaction mechanism in the presence of bromine.

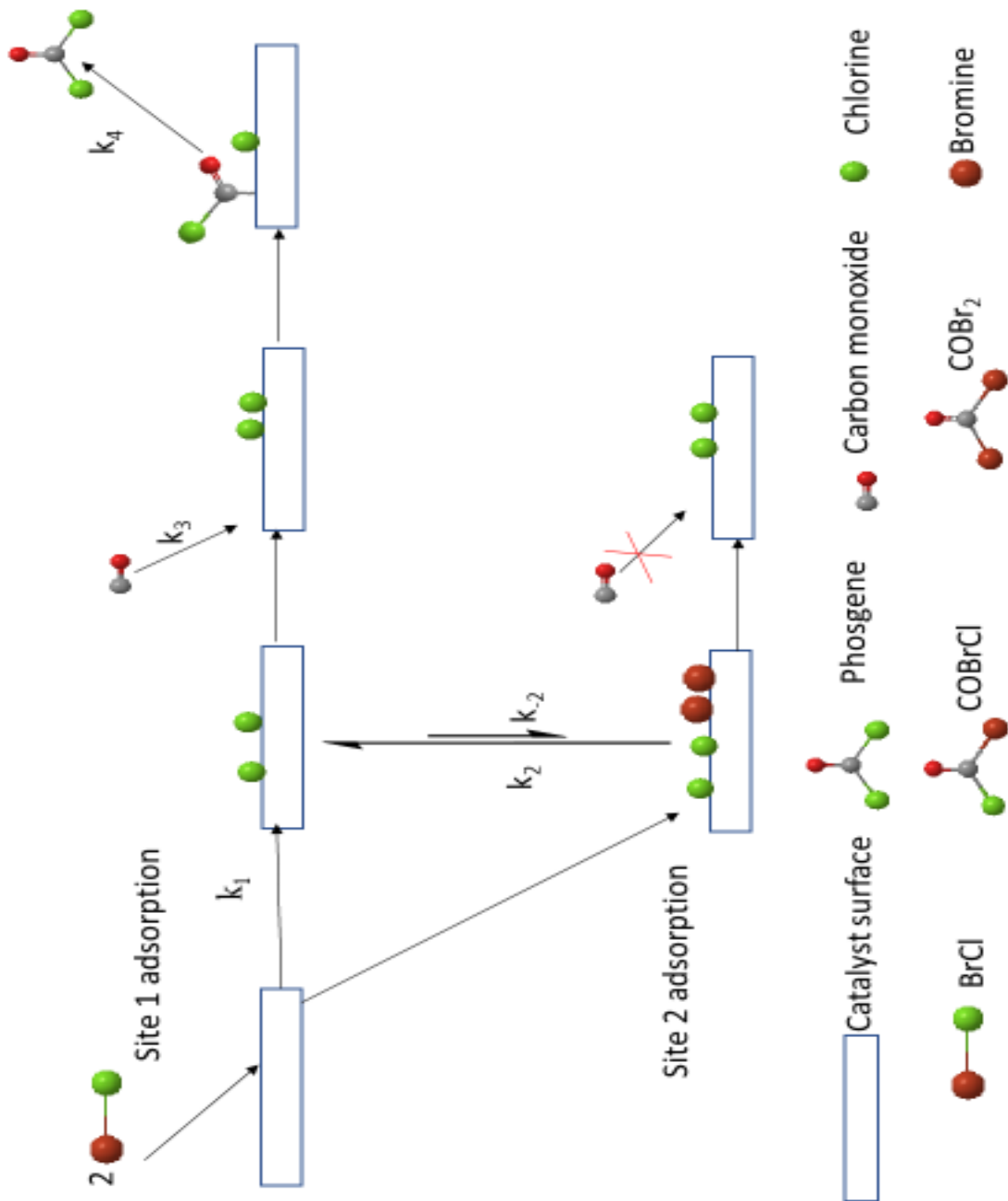


Figure 124 Schematic for the proposed reaction mechanism in the presence of bromine

Chapter 8 –Conclusions

8.1 Conclusions

An apparatus has been developed to test the kinetics for the gas phase reaction between CO and Cl₂ to form phosgene over carbon catalysts. The reaction between CO and Cl₂ over the Donau K40 carbon catalyst is an efficient process which exhibits an activation energy of 34.1±0.2 kJ mol⁻¹. Under the current flow regime, the homogeneous reaction component does not play a role in the observed reaction chemistry over the catalyst. The rate law for phosgene formation over this catalyst can be written as:

$$v = k[CO]^{0.93 \pm 0.02} [Cl_2]^{0.48 \pm 0.01} [COCl_2]^{-0.04 \pm 0.08}$$

where k is a rate coefficient

There is a mass imbalance for reaction runs ≤ 2 days. This can be attributed to retention of chlorine by the catalyst as there are no observable by-products. On extended reaction time (≥ 2.5 days) the mass imbalance is reduced.

The system operates under kinetic control in the absence of mass transfer limitations. The effectiveness factor for the pelleted catalyst is 0.7. The order of the adsorption coefficients is as follows:

$$K_{Cl} > K_{COCl_2} \gg K_{CO}$$

There are at least 2 sites of adsorption for chlorine on the catalyst. A reaction mechanism for phosgene formation over the Donau Supersorbon K40 carbon is proposed. The reaction probably takes place on the double bonds of the activated carbon and chlorine is bound to catalyst surface.^{40,100}

Bromine co-fed with chlorine results in the formation of BrCl. The presence of bromine in the co-feed results in an increase of rate for phosgene formation at high temperatures. At low temperatures ($T \leq 303$ K) (COBrCl and COBr₂) are observed by-products indicating that BrCl plays an active role in the reaction chemistry in the production of phosgene.

8.2 Future work

This study has investigated the kinetics of phosgene formation and is limited to one commercially available carbon catalyst. To progress the understanding of this process and the proposed kinetic scheme. The phosgene synthesis reaction should be investigated over different commercial catalysts.

The reaction kinetics in the presence of bromine are certainly worthy of further investigation. The catalyst also needs to be characterised pre and post reaction to relate reaction chemistry to structural features. This would assist future catalyst optimisation strategies.

References

- 1 T. A. Ryan, E. A. Seddon, K. R. Seddon and C. Ryan, *Phosgene: And Related Carbonyl Halides*, Elsevier Science, 1996.
- 2 C. J. Mitchell, W. van der Borden, K. van der Velde, M. Smit, R. Scheringa, K. Ahrika and D. H. Jones, *Catal. Sci. Technol.*, 2012, 2, 2109.
- 3 J. Davy, *Philos. Trans. R. Soc. London*, 1812, 102, 144–151.
- 4 Schützenberger P., *Comptes rendus Chim.*, 1868, 747–8.
- 5 C. Potter and S. Baron, *Chem. Eng. Prog.*, 1951, 47, 473–481.
- 6 S. Baron, Columbia University, 1950, PhD Thesis, 'The kinetics of the catalytic fotation of phosgene' .
- 7 D. Randall and S. Lee, *The Polyurethanes Book*, Wiley-Blackwell, 2003
- 8 H. Marsh, *Activated carbon*, Elsevier Science & Technology Books, 2006.
- 9 A. Cabiac, T. Cacciaguerra, P. Trens, R. Durand, G. Delahay, A. Medevielle, D. Plée and B. Coq, *Appl. Catal. A Gen.*, 2008, 340, 229–235.
- 10 C. Y. Yin, M. K. Aroua and W. M. A. W. Daud, *Sep. Purif. Technol.*, 2007, 52, 403–415.
- 11 M. S. Shafeeyan, W. M. A. W. Daud, A. Houshmand and A. Shamiri, *J. Anal. Appl. Pyrolysis*, 2010, 89, 143–151.
- 12 A. Bhatnagar, W. Hogland, M. Marques and M. Sillanpää, *Chem. Eng. J.*, 2013, 219, 499–511.
- 13 P. Chingombe, B. Saha and R. J. Wakeman, *Carbon N. Y.*, 2005, 43, 3132–3143.
- 14 L. Liu, S. (Johnathan) Tan, T. Horikawa, D. D. Do, D. Nicholson and J. Liu, *Adv. Colloid Interface Sci.*, 2017, 250, 64–78.
- 15 Douglas M. Ruthven, *Principles of Adsorption and Adsorption Processes*, Wiley, 1984.
- 16 K. Kinoshita, *Carbon Electrochemical and Physicochemical Properties*, Wiley, 1988.
- 17 M. Domingo-García, F. J. López-Garzón and M. Pérez-Mendoza, *J. Colloid Interface Sci.*, 2000, 222, 233–240.
- 18 A. S. da C. Lopes, S. M. L. de Carvalho, D. do S. B. Brasil, R. de A. Mendes and M. O. Lima, *Am. J. Anal. Chem.*, 2015, 6, 528–538.
- 19 R. R. A. Rios, D. E. Alves, I. Dalmázio, S. F. V. Bento, C. L. Donnici and R. M. Lago, *Mater. Res.*, 2003, 6, 129–135.
- 20 A. Aburub and D. E. Wurster, *J. Colloid Interface Sci.*, 2006, 296, 79–85.

- 21 S. J. Park and Y. S. Jang, *J. Colloid Interface Sci.*, 2002, 249, 458–463.
- 22 H. L. Chiang, C. P. Huang and P. C. Chiang, *Chemosphere*, 2002, 47, 257–265.
- 23 J. González, M. C. Del Ruiz, A. Bohé and D. Pasquevich, *Carbon N. Y.*, 1999, 37, 1979–1988.
- 24 C. Hall and Holmes RJ, *Carbon N. Y.*, 1992, 30.
- 25 D. M. Pasquevich, *Thermochim. Acta*, 1990, 167, 91–98.
- 26 T. H and A. Soffer, *Carbon N. Y.*, 1985, 23.
- 27 G. Sennyey, *Spec. Chem.*, 1990, 364.
- 28 E. K. Gibson, University of Glasgow, 2007, PhD Thesis, 'Amine hydrochloride salts: a problem in polyurethane synthesis'.
- 29 G. Herzberg, *Molecular Spectra and Molecular Structure Volume II Infrared and Raman Spectra of Polyatomic Molecules*, 1945.
- 30 M. Bodenstein, *Z. Phys. Chem.*, 1927, 130.
- 31 M. Bodenstein, *Helv. Chim. Acta*, 1935, 18.
- 32 M. Bodenstein, *Chem. Rev*, 1930, 7.
- 33 M. Bodenstein, S. Lenher and C. Wagner, *Z. Phys. Chem., Abt. B*, 1929, 3.
- 34 J. A. N. A. Dahlberg, V. O. Christiansen and E. A. Eriksson, 1973, 16, 41–46.
- 35 K. Ryan, T. Anthony; Ryan, Christine; Seddon, Elaine A.; Seddon, Phosgene and Related Carbonyl Halides, 1996.
- 36 E. N. Shapatina, V. L. Kuchaeve and M. I. Tempkin, *Kinet. Catal.*, 1977, 18, 968–972.
- 37 E. N. Shapatina, V. L. Kuchaeve and M. I. Tempkin, *Kinet. Catal.*, 1978, 20, 972–976.
- 38 E. N. Shapatina, V. L. Kuchaeve, B. E. Pen'kovi and M. I. Tempkin, *Kinet. Catal.*, 1976, 17, 559–566.
- 39 G. E. Rossi, University of Glasgow, 2014, Masters Thesis, 'Experimental arrangements suitable for evaluating heterogeneous catalysts for phosgene formation'.
- 40 N. K. Gupta, A. Pashigreva, E. A. Pidko, E. J. M. Hensen, L. Mleczko, S. Roggan, E. E. Ember and J. A. Lercher, *Angew. Chemie - Int. Ed.*, 2016, 1728–1732.
- 41 N. K. Gupta, B. Peng, G. L. Haller, E. E. Ember and J. A. Lercher, *ACS Catal.*, 2016, 6, 5843–5855.
- 42 T. Zhang, C. Troll, B. Rieger, J. Kintrup, O. F. K. Schlüter and R. Weber, *Appl. Catal. A Gen.*, 2009, 365, 20–27.
- 43 T. Zhang, C. Troll, B. Rieger, J. Kintrup, O. F. K. Schlüter and R. Weber, *J. Catal.*, 2010, 270, 76–85.

- 44 F. Cavani, *Catal. Today*, 2010, 157, 8–15.
- 45 T. Zhang, C. Troll, B. Rieger, J. Kintrup, O. F. K. Schlüter and R. Weber, *Appl. Catal. A Gen.*, 2009, 357, 51–57.
- 46 EPSRC UK Catal. Hub, Environ. Theme, Ex. Proj. 2 "Towards closing chlorine cycle large-scale Chem. Manuf. Process. EP/K014854/1, August 2014 - December 2017.
- 47 L. Cotarca and H. Eckert, *Phosgenations: A Handbook*, Wiley, 2006.
- 48 J. Callison, University of Glasgow, 2010, PhD Thesis, ' The investigation of a side reaction leading to colour formation in a polyurethane production chain'.
- 49 *Top. Inorg. Gen. Chem.*, 1996, 24, 223–266.
- 50 P. Schitzenberger, *Compt. Rend*, 1868, 66.
- 51 W. I. Awad, Y. A. Gawargious and S. S. M. Hassan, *Microchim. Acta*, 1967, 55, 847–851.
- 52 P. Atkins, T. Overton, J. Rourke, M. Weller and F. Armstrong, *Shriver & Atkins Inorganic Chemistry 4th Edition*, 2006.
- 53 J. Tellinghuisen, *J. Phys. Chem. A*, 107, 753–757.
- 54 S. Hubinger, *Photochem. Photobiol.*, 1995, 86, 1–7.
- 55 P. Atkins and J. De Paula, *Atkin's Physical Chemistry 9th Edition*, .
- 56 C. . H. Bartholomew and R. J. Farrauto, *Fundamentals of industrial catalytic processes*, Wiley, Second Edi., 2006, vol. 2006.
- 57 P. R. Griffiths and J. a. de Haseth, *Fourier Transform Infrared Spectrometry. Second Edition*, 2007.
- 58 P. Atkins and J. De Paula, *The Elements of Physical Chemistry*, 2006.
- 59 M. Heidelberger and H. P. Treffers, *J. Gen. Physiol.*, 1942, 25, 523–531.
- 60 Y. Leng, *MATERIALS Introduction to Microscopic and Spectroscopic Methods*, 2008.
- 61 B. J. Wuensch, *Zeitschrift für Krist.*, 1970, 131, 159–160.
- 62 A. Lazzarini, A. Piovano, R. Pellegrini, G. Leofanti, G. Agostini, S. Rudić, M. R. Chierotti, R. Gobetto, A. Battiato, G. Spoto, A. Zecchina, C. Lamberti and E. Groppo, *Catal. Sci. Technol.*, 2016, 6, 4910–4922.
- 63 J. R. Anderson and K. C. Pratt, *Introduction to Characterization and Testing of Catalysis*, 1985.
- 64 K. Sing, *Colloids Surfaces A Physicochem. Eng. Asp.*, 2001, 187–188, 3–9.
- 65 D. J. Shaw, *Intoduction to Colloid & Surface Chemistry*, Butterworth-Heineman, Fourth Edi., 1992.

- 66 M. A. Pimenta, G. Dresselhaus, M. S. Dresselhaus, L. G. Cançado, A. Jorio and R. Saito, *Phys. Chem. Chem. Phys.*, 2007, 9, 1276–1290.
- 67 A. C. Ferrari and J. Robertson, *MRS Proc.*, 1999, 593, 299–304.
- 68 F. Tuinstra and J. L. Koenig, *J. Chem. Phys.*, 1970, 53, 1126–1130.
- 69 A. C. Ferrari and J. Robertson, *Phys. Rev. B*, 2000, 61, 14095–14107.
- 70 A. Eckmann, A. Felten, A. Mishchenko, L. Britnell, R. Krupke, K. S. Novoselov and C. Casiraghi, *Nano Lett.*, 2012, 12, 3925–3930.
- 71 R. Juárez, P. Concepción, A. Corma, V. Fornés and H. García, *Angew. Chemie - Int. Ed.*, 2010, 49, 1286–1290.
- 72 B. Schneider and J. Stokr, *Collect. Czechoslov. Chem. Commun.*, 1961, 26, 1221–1230.
- 73 S. Yamamoto, *J. Mol. Spectrosc.*, 1984, 13, 299–313.
- 74 M. J. Hopper, J. W. Russell and J. Overend, *J. Chem. Phys.*, 1968, 48, 3765–3772.
- 75 R. J. Jakobsen, *Spectrochim. Acta*, 1965, 21, 433–442.
- 76 M. R. J. Hachey and F. Grein, *Chem. Phys.*, 1997, 224, 19–31.
- 77 R. H. Carr, Personal Communication, Everberg, Belgium, 2014.
- 78 D. R. Lide, *Handb. Chem. Phys.*, 2003, 53, 2616.
- 79 B. R. Munson and D. F. Young, *Fundamentals of Fluid Mechanics, Fourth.*, 2002.
- 80 A. Blair and H. Ihle, *J. Inorg. Nucl. Chem.*, 1973, 35, 3795–3803.
- 81 D. R. Stlll, *Ind. Eng. Chem.*, 1947, 39, 518–536.82 A. C. Ferrari and J. Robertson, *Phys. Rev. B*, 2001, 64, 75414.
- 83 A. C. Ferrari and D. M. Basko, 2013, 1–26.
- 84 A. Sadezky, H. Muckenhuber, H. Grothe, R. Niessner and U. Pöschl, *Carbon N. Y.*, 2005, 43, 1731–1742.
- 85 R. Saito, M. Hofmann, G. Dresselhaus, A. Jorio and M. S. Dresselhaus, *Adv. Phys.*, 2011, 60, 413–550.
- 86 J. McGregor, Z. Huang, E. P. J. Parrott, J. A. Zeitler, K. L. Nguyen, J. M. Rawson, A. Carley, T. W. Hansen, J. P. Tessonier, D. S. Su, D. Teschner, E. M. Vass, A. Knop-Gericke, R. Schlögl and L. F. Gladden, *J. Catal.*, 2010, 269, 329–339.
- 87 M. Knauer, M. E. Schuster, D. Su, R. Schlögl, R. Niessner and N. P. Ivleva, *J. Phys. Chem. A*, 2009, 113, 13871–13880.
- 88 A. R. McFarlane, I. P. Silverwood, R. Warringham, E. L. Norris, R. M. Ormerod, C. D. Frost, S. F. Parker and D. Lennon, *RSC Adv.*, 2013, 3, 16577–16589.

- 89 J. McGregor, Z. Huang, E. P. J. Parrott, J. A. Zeitler, K. L. Nguyen, J. M. Rawson, A. Carley, T. W. Hansen, J. P. Tessonnier, D. S. Su, D. Teschner, E. M. Vass, A. Knop-Gericke, R. Schlögl and L. F. Gladden, *J. Catal.*, 2010, 269, 329–339.
- 90 T. Chakraborty and A. L. Verma, *Spectrochim. Acta - Part A Mol. Biomol. Spectrosc.*, 2002, 58, 1013–1023.
- 91 S. K. Ajmera, M. W. Losey, K. F. Jensen and M. A. Schmidt, *AIChE J.*, 2001, 47, 1639–1647.
- 92 I. S. Metcalfe, *Chemical Reaction Engineering*, Oxford University Press, 1997.
- 93 C. N. Satterfield, *Mass Transfer in Heterogeneous Catalysis*, M.I.T Press, vol. 1970.
- 94 C. N. Satterfield, *Heterogeneous catalysis in industrial practice*, Krieger Publishing Company, Reprint Ed., 1996.
- 95 J. Wiley, K. Hepburn and O. Levenspiel, *Chemical Reaction Engineering*, 1964, vol. 19.
- 96 K. B. Bischoff, *Fundamentals of Chemical Reaction Engineering (Brotz, Walter)*, 1966, vol. 43.
- 97 C. Perego and S. Peratello, *Catal. Today*, 1999, 52, 133–145.
- 98 A. Rezaee, H. Rangkooy, A. Khavanin, A. Jonidi-jafari and R. D. Cheshma, 2011, 2, 2–6.
- 99 H. Aljamaan, R. Holmes, V. Vishal, R. Haghpanah, J. Wilcox and A. R. Kovsky, *Energy and Fuels*, 2017, 31, 1193–1207.
- 100 H. Sahin and S. Ciraci, *J. Phys. Chem. C*, 2012, 116, 24075–24083.
- 101 D. Maric, J. P. Burrows and G. K. Moortgat, *J. Photochem. Photobiol. A Chem.*, 1994, 83, 179–192.
- 102 T. X. Wang, M. D. Kelley, J. N. Cooper, R. C. Beckwith, D. W. Margerum and R. June, *Inorg. Chem.*, 1994, 33, 5872–5878.
- 103 M. J. Parkington, T. A. Ryan and K. R. Seddon, *J. Chem. Soc. Dalt. Trans. Inorg. Chem.*, 1997, 251–256.
- 104 M. J. Parkington, K. R. Seddon and T. A. Ryan, *J. Chem. Soc. Chem. Commun.*, 1989, 1823.

Appendix 1

The apparatus was modified to accommodate an HCl and oxygen feed to study the oxy-chlorination and Deacon chemistry. The HCl flow is controlled by an additional mass flow controller and control box. The oxygen flow is controlled by a 200 SCCM rotameter.

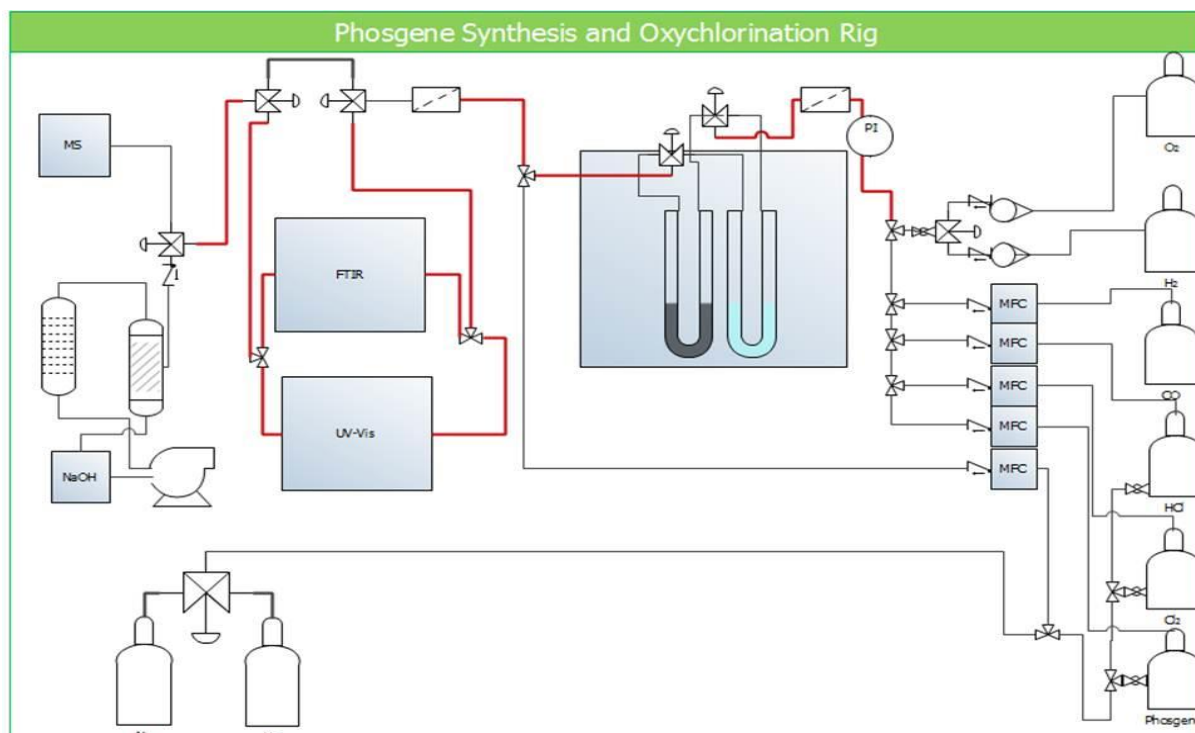


Figure A1 Phosgene synthesis and oxy-chlorination apparatus

This modification to the apparatus was undertaken in collaboration with Dr. Shaoliang Guan of the University of Cardiff

The following figures were taken using gas cell 2 and the signals were considered too large, so might have deviated from the Beer-Lambert law. Figures A2-5 used CaF₂ windows on the gas cell so the full spectral range is not observed. Figures A6 and 7 were initial experiments from Chapter 7.

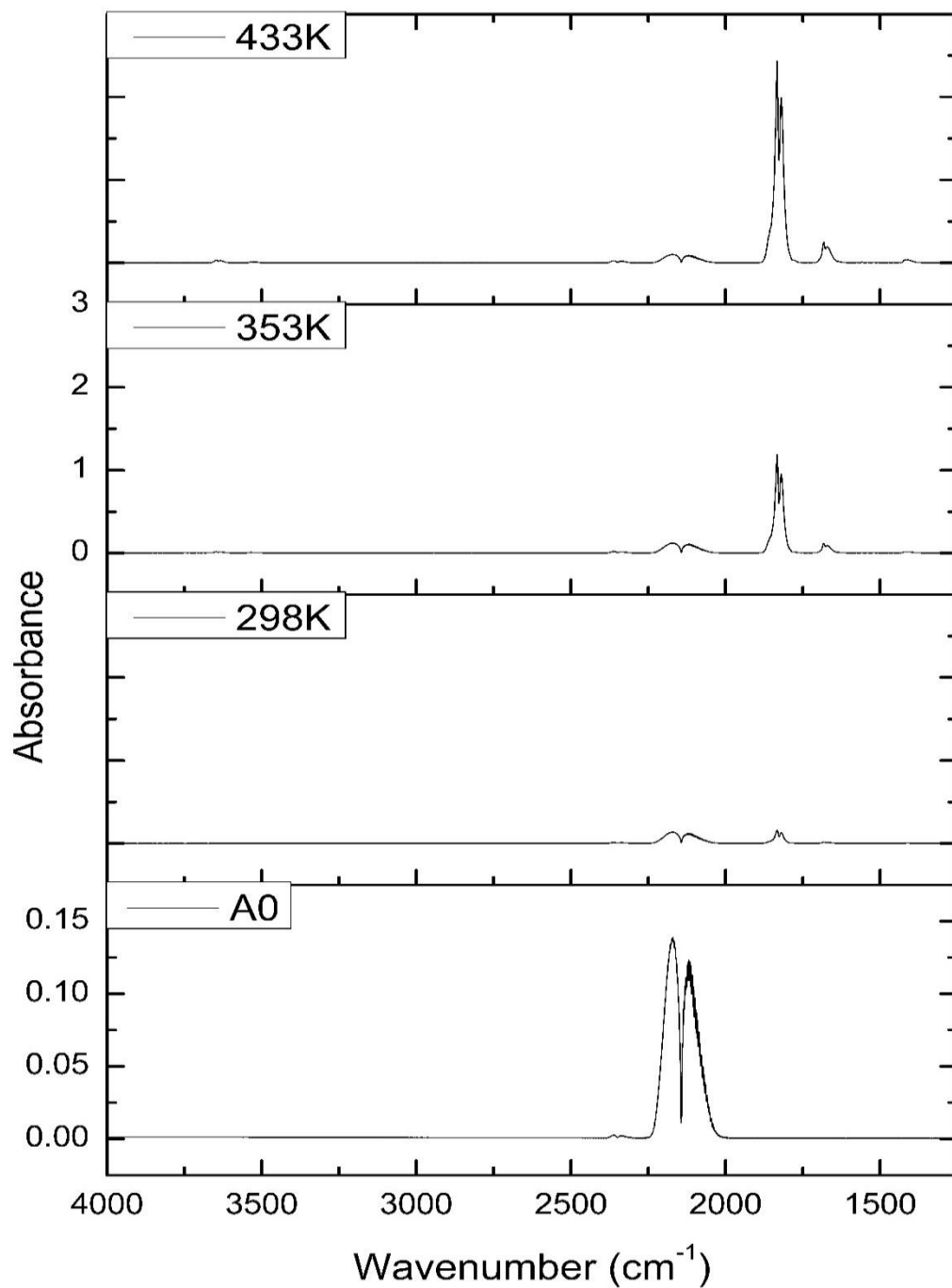


Figure A2 IR Spectra of reaction between CO and Cl₂ over the catalyst as a function of temperature with flow rates of 5 cm³ min⁻¹ and 4 cm³ min⁻¹ in a total flow of 159 cm³ min⁻¹ over a temperature range of 298-433 K (CaF₂ gas cell 2)

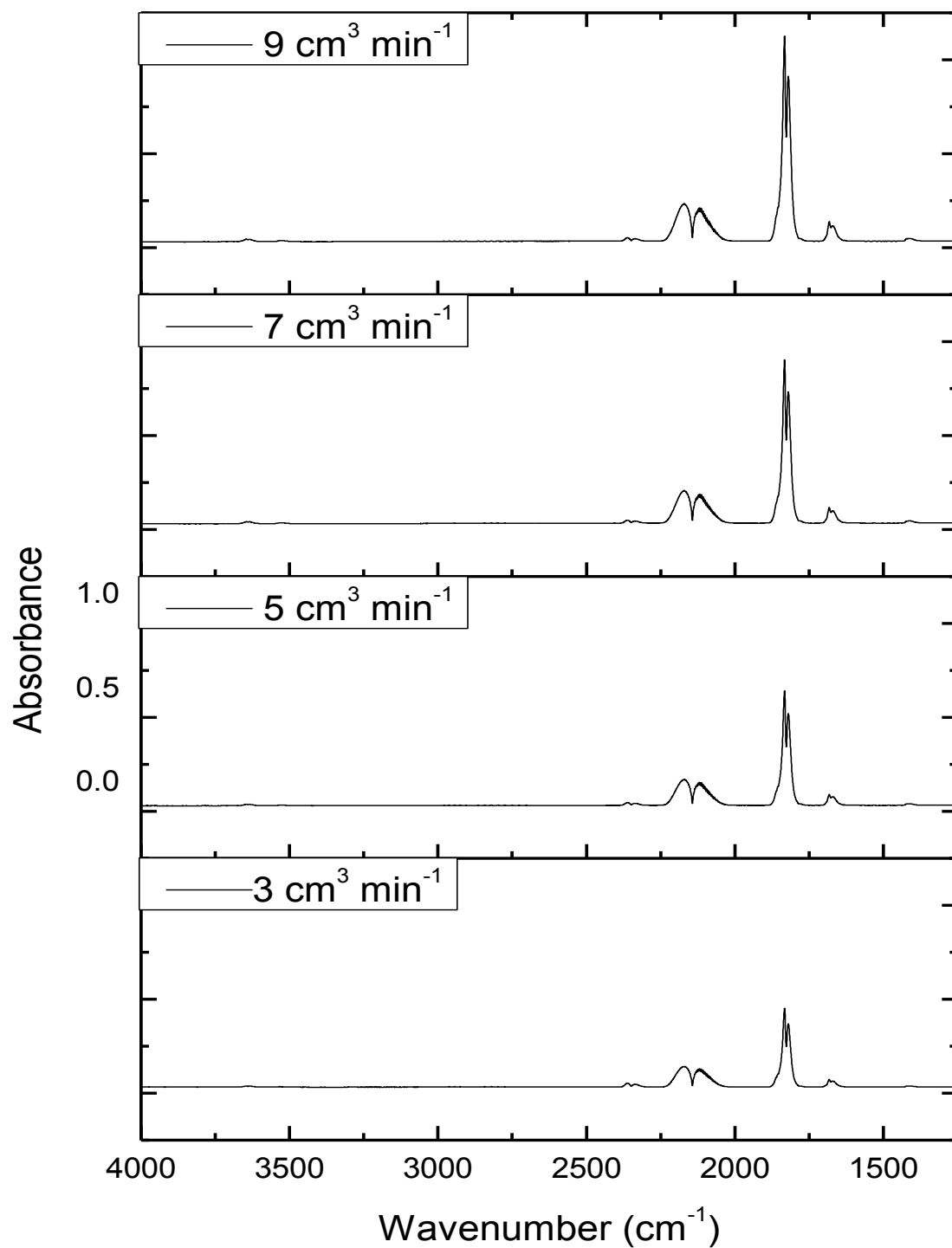


Figure A3 Infrared for the rate law determination with Cl₂ fixed at a flow rate of 15 cm³ min⁻¹ and the flow rate of the CO indicated in the box of each spectrum at 323 K (CaF₂ windows)

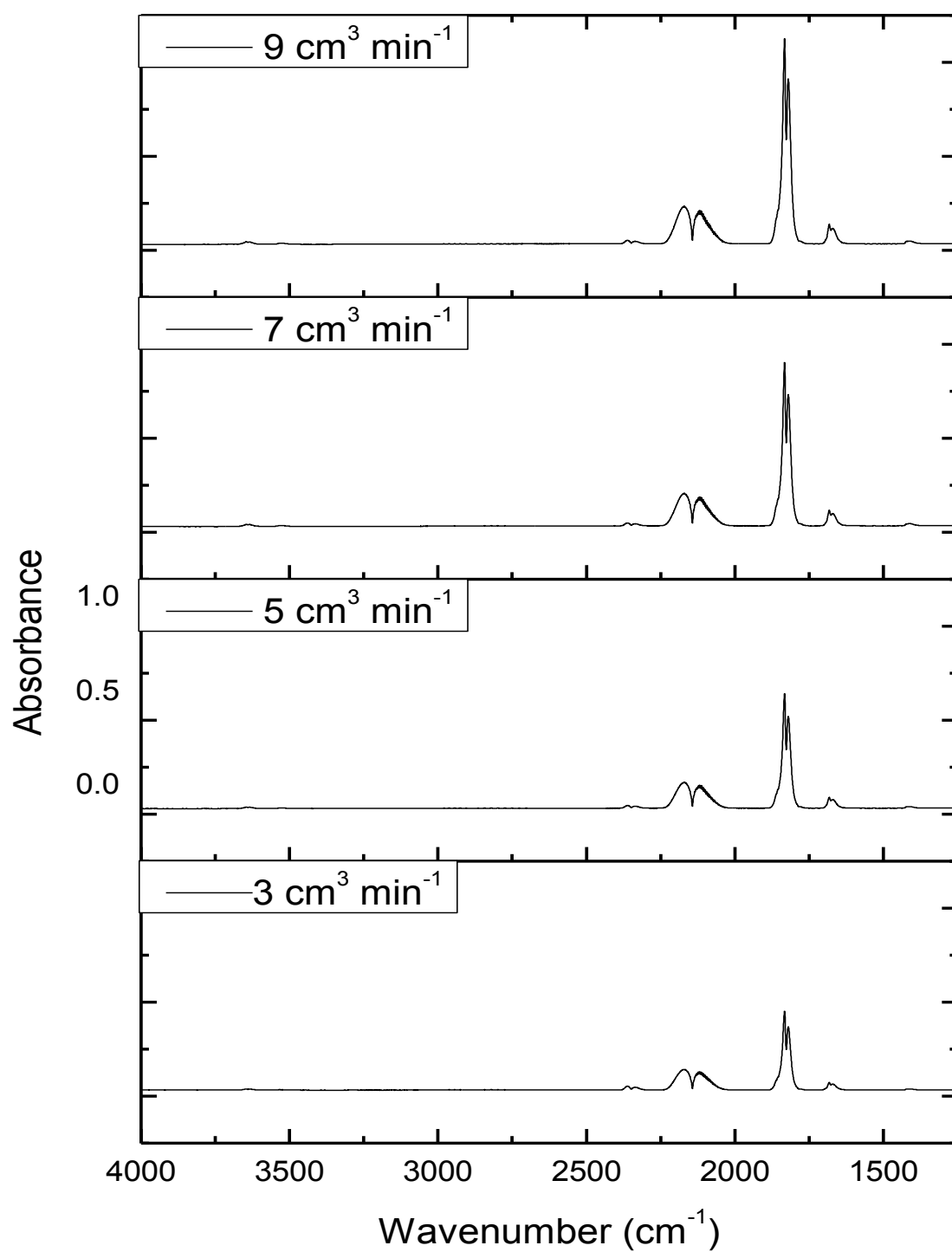


Figure A4 Infrared for the rate law determination with Cl_2 fixed at a flow rate of $15 \text{ cm}^3 \text{ min}^{-1}$ and the flow rate of the CO indicated in the box of each spectrum at 323 K (CaF_2 windows)

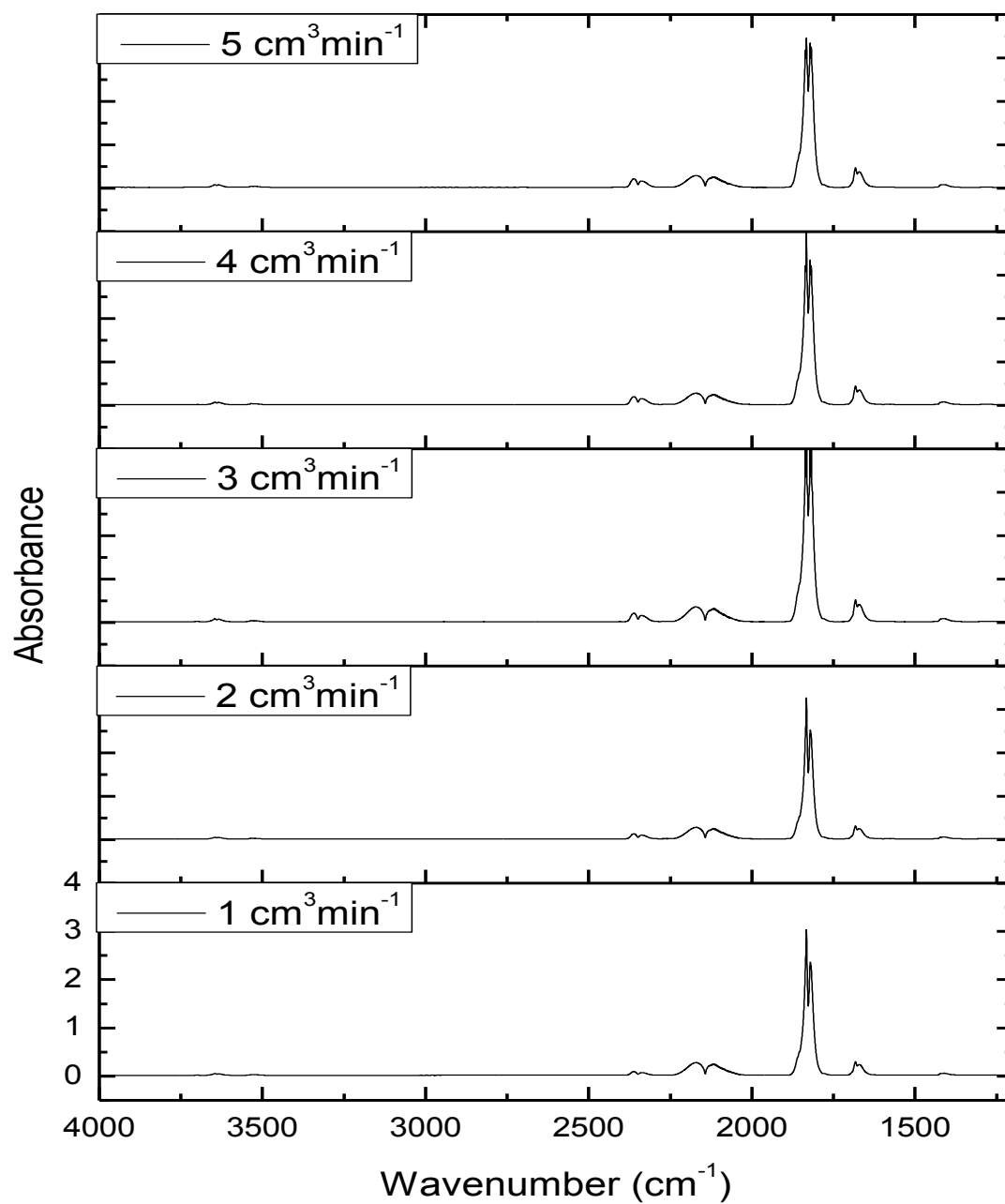


Figure A5 Infrared for the rate law determination with CO and Cl_2 fixed at a flow rate of $15 \text{ cm}^3 \text{ min}^{-1}$ and the flow rate of the COCl_2 indicated in the box of each spectrum at 323 K (CaF_2 windows)

The trends in section 4.6 are also observed in the spectra in this section. The same values for the rate law are obtained

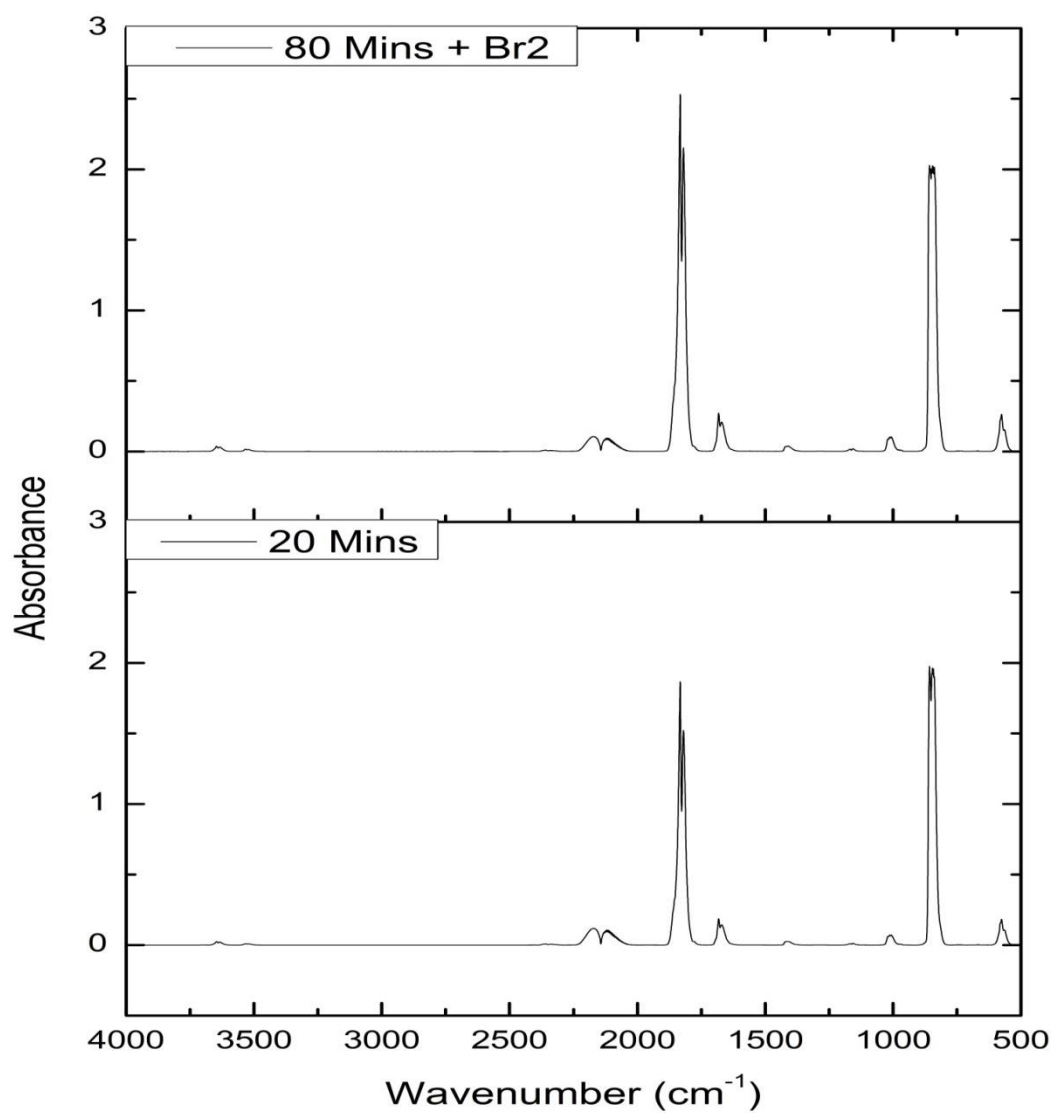


Figure A6 Infrared spectra for the reaction of CO and Cl₂ introducing the bromine over the catalyst with flow rates of 5 cm³ min⁻¹ and 4 cm³ min⁻¹ over at a temperature of 353 K

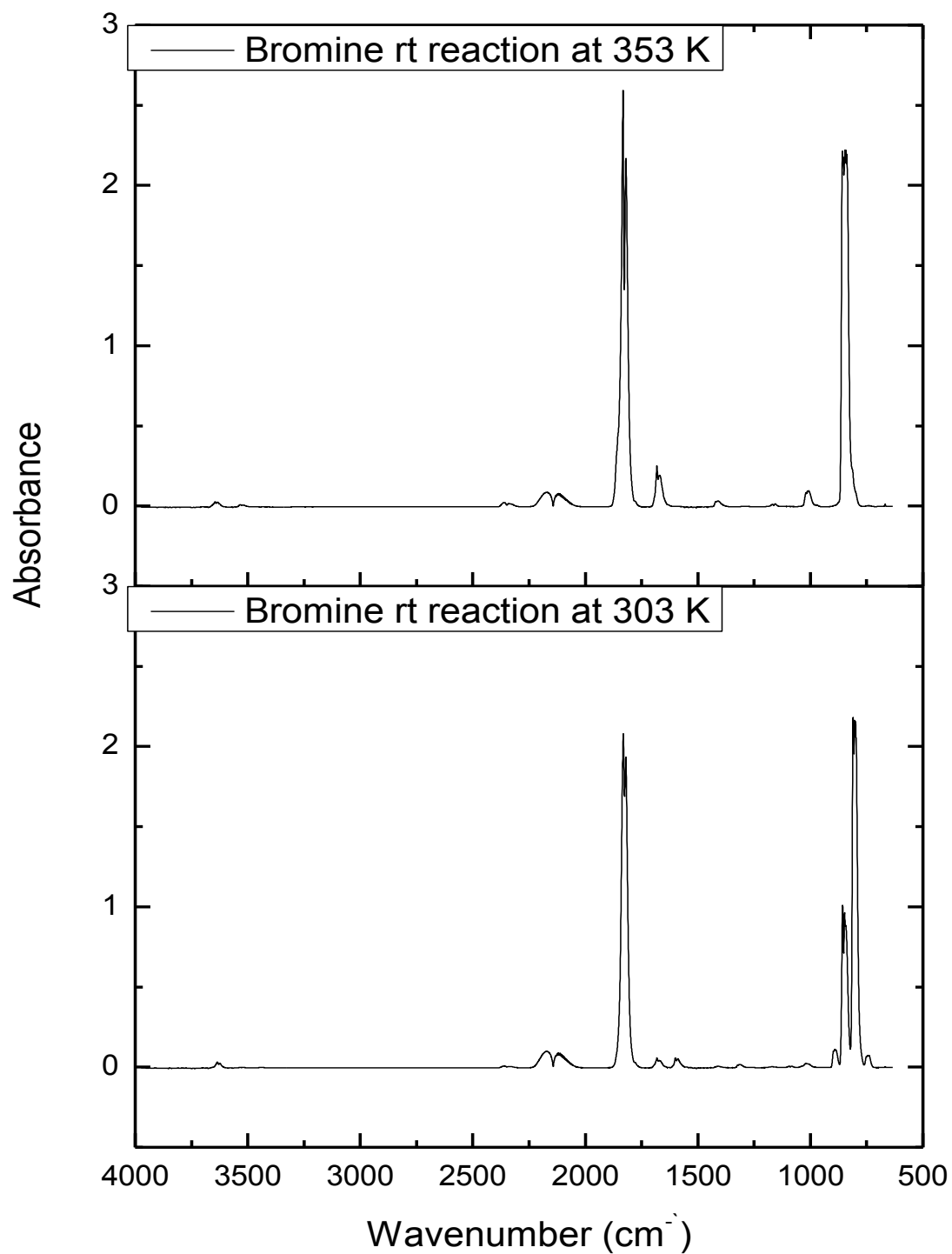


Figure A7 Infrared spectra for the reaction of CO and Cl₂ introducing the bromine over the catalyst with flow rates of 5 cm³ min⁻¹ and 4 cm³ min⁻¹ increasing the temperature of 303K to 353 K